CREEP FRACTURE IN SOME LOW-ALLOY STEELS

By

ROBIN GEORGE STANLEY, B.Met.

A thesis presented in fulfilment of the requirements for the degree of Doctor of Philosophy in the Faculty of Materials, University of Sheffield.

April, 1978.

SUMMARY

The processes involved in the high temperature creep deformation and fracture of low alloy steels have been extensively reviewed.

The fracture behaviour of two series of alloy steels, 2¼Cr 1Mo and ½Cr ½Mo ¼V, has been investigated over a range of temperature extending from the ambient to that experienced under typical power plant operating conditions. The effect of prior heat treatment, stress state and presence of tramp elements on the accumulation of creep damage has also been studied.

In a heavily tempered condition, the 2¼Cr 1Mo alloy steels exhibited a high ductility and similar rupture mode over a wide temperature range. The sliding of adjacent prior austenite and bainite plate boundaries contributed to the overall creep strain. The presence of wide precipitate free zones suppressed the nucleation of grain boundary cavities and the dominant mechanism of damage accumulation involved decohesion, after large plastic strains, at the interface of coarse $M_{23}C_6$ particles and the matrix. Growth of such damage occurred by a viscous process that was inhibited by the introduction of a hydrostatic compressive component of stress. Additions of Sn had no effect on creep life or ductility over the range explored.

The simulated heat affected zone structure of the ½Cr ½Mo ¼V alloy steel possessed extremely limited ductility at typical power plant operating temperatures. Failure occurred by the nucleation, growth and interlinkage of cavities at the prior austenite grain boundaries. A nucleation mechanism has been invoked, involving the interaction of matrix dislocations and grain boundary precipitates.

Growth of cavities probably occurred by vacancy transport. Detailed quantitative fractography has yielded empirical laws governing the nucleation and growth of such cavities which show some similarities to those suggested for the phenomenon in single phase materials. It was demonstrated that remaining creep life was a function of the previous stress history of the material.

CONTENTS

CHAPTER I

INTRODUCTION

Low alloy ferritic steels are extensively used for components operating at elevated temperatures and low stresses, particularly in the power generating industry for piping and pressure vessel applications. The properties which make this range of steels appropriate for this task are: the low alloy content makes them relatively inexpensive, they are readily weldable, they are tough and ductile at low temperatures and exhibit excellent creep resistance in the temperature range 500 - 700^{o}C.

Despite this versatility, these materials are susceptible, when subject to the constraints of applied stresses, prior heat treatment and the presence of certain tramp elements, to premature failure after very small creep extensions. These constraints are most prevalent in the heat-affected zones of weldments, where they are more difficult to control, and consequently, it is in these regions that catastrophic failures tend to occur. The problem is particularly worrying in that the failure process is mechanically very efficient, occurring in situations where the stress is relatively low and the strain to fracture is minimal. Also, because the creep strain is often so small and the final fracture process is rapid, on-site detection of suspect components and prediction of creep life is difficult.

It is commonly recognized that the phenomenon responsible for this type of failure is the nucleation and growth of grain boundary

cavities which eventually link up to provide an intergranular fracture path. Such creep damage is also found to lead to the premature failure of some simpler materials such as Cu, Mg and α - Fe. Much work has been done on these "model" materials and some of the factors affecting cavitational damage have been isolated and their mutual interaction established - although the whole story is far from complete. However, with more complex engineering materials, such as ferritic and austenitic steels, it has been demonstrated that transformation structure and precipitation characteristics introduce further parameters which influence the nature and severity of this type of creep damage.

Clearly, there is a need to determine the precise role of such features and to devise some means of controlling them to render these materials less susceptible to cavitational damage. Further, the studies of creep cavitation in the simple "model" materials have shown that by monitoring the accumulation of damage throughout creep life, some progress can be made in predicting failure under non-steady conditions of temperature and stress. A similar approach adopted with low alloy ferritic steels should enable accurate assessment of component life, which has great potential value, not only from a safety, but also from an economic standpoint.

CHAPTER 2

CREEP DEFORMATION IN METALS AND ALLOYS

2.1. General Features of Creep

Creep, is the deformation attributable to plastic flow that occurs in materials when subjected to a continuing stress over a prolonged period of time. Experiments have shown that the process can occur at all temperatures above absolute zero. However, it is only creep at elevated temperatures (i.e. above about 0.5 Tm, where Tm is the melting point) that is of technological importance.

The creep properties of individual materials may be identified by monitoring the progress of plastic deformation with time under known conditions of constant stress (or more usually, constant load), temperature and atmospheric environment. The elongation /time curve produced usually has four characteristic stages:- instantaneous, primary, secondary and tertiary. Instantaneous creep strain is the intial extension produced immediately upon application of the load. This is followed by the primary and transient stage where the creep rate decreases with time until it reaches a constant value in the secondary creep stage. This steady state phase then gives way to a tertiary stage of accelerated creep, often associated with localized necking and the formation of cavities or cracks. These structural instabilities lead, finally, to fracture.

At temperatures in the range 0.5 to 0.7 Tm, in which creep resistant materials are mainly used, diffusion rates are such as to allow the motion of dislocations and vacancies under the influence

of an applied stress. Such movement is achieved by thermally activated mechanisms that enable the forces, from work hardening obstacles resisting dislocation glide, to relax continually. Thus, a steady state is achieved where there is a balance between work hardening and thermal softening. The influence of stress, temperature and microstructural parameters on the secondary creep stage has provided the basis for deducing the various mechanisms responsible for intergranular deformation in metals and creep resistant alloys.

2.1.1. Stress Dependence

Extensive studies have shown that, subject to testing conditions, the steady state creep rate, $\dot{\varepsilon}_s$, can exhibit a variety of stress dependent behaviour (Sherby and Burke, 1967). The stress sensitivity varies widely between high and low stresses, however, the data may be generalized in a relation of the form:

$$\dot{\varepsilon}_s = A\,\sigma^n \qquad \text{.....(1)}$$

where A is a temperature dependent constant, σ is the applied stress and n is the stress exponent. As the stress is varied, the changing stress dependence may be conveniently represented in terms of changing values of n.

This behaviour has been interpreted as one in which the controlling creep mechanism changes as a function of stress. A diversity of such changes has been proposed to account for the various characteristic n values and some uncertainty remains regarding the controlling process within a given stress range.

At extremely low stresses, particularly at high temperatures, $n = 1$ in a number of materials and diffusion creep, by stress

directed atomic migration, is considered to occur (Herring, 1950; Nabarro,1948; Coble, 1963).

At lower temperatures and relatively low and intermediate stresses, power law creep is generally applicable and numerous mechanisms based on recovery creep have been cited to explain the exponents obtained (Section 2.2). Values of n range from 4.2 to 6.9 in annealed metals and simple alloys in the intermediate stress range, but for two phase alloys the range of values can be much greater and attempts have been made to analyse this behaviour using the concept of an internal or friction stress (Section 2.2.5.)

With high stresses, creep rates are much larger than those predicted by extrapolation of intermediate stress data and the exponent, n, increases rapidly with stress. In these cases, exponential creep laws have been proposed (Garofalo, 1963).

2.1.2. Temperature Dependence

Creep deformation is a thermally activated process, and the temperature dependence of $\dot{\varepsilon}_s$ is normally described by an Arrherius type of equation:

$$\dot{\varepsilon}_s = B \exp (- Q_c / RT) \qquad \text{.....(2)}$$

where B is a function of stress and Qc is the apparent activation energy ('apparent' because the term may contain contributions from a variety of operating mechanisms).

The majority of evidence for single phase materials indicates that Qc is about the same as the activation energy for self diffusion Q_{SD}. For example, Sherby (1962) showed that the creep rate for austenite varied with carbon content in a manner almost identical to the variation of self-diffusivity of Fe in austenite. Similarly

the creep rate of ferrite in many low alloy steels shows almost the same sudden variation at the magnetic transformation temperature as does the self-diffusivity of Fe in ferrite (Sherby and Burke 1967). Especially in simple alloys, Qc is usually found to be independent of stress and strain (Sellars and Quarrell, 1961-62) and insensitive to temperature (Sherby and Burke, 1967).

2.1.3. Effect of Microstructural Parameters

In more complex creep resistant materials, especially where a dispersion hardening phase exists, a number of observations have been reported where Qc exhibits values much higher than Q_{SD}. Indeed, some workers have also found these activation energies to be stress dependent, decreasing with increasing applied stress, but always greater than Q_{SD} (Russell et al, 1968). An approach, to bring the values of Qc and the stress exponent n into line with those observed in pure metals has been made using the concepts of an internal back stress or friction stress (Section 2.2.5). This has led to a general relationship of the form (McLauchlin 1974):

$$\dot{\varepsilon}_s = \kappa \left[\sigma_A - \sigma_i (T)\right]^{n_o} \exp (-\Delta H / RT) \qquad \ldots\ldots\ldots(3)$$

where σ_A is the applied stress, σ_i is the internal back stress (or friction stress) which is temperature dependent, the stress exponent $n_o = 4$, κ is constant and ΔH is a stress independent activation energy which may be equal to that for self diffusion.

Barrett and Sherby (1965) found that $\dot{\varepsilon}_s$ in pure metals was related to the stacking fault energy, γ. This is not surprising as one of the major thermal softening mechanisms occuring during this stage of creep life is the climb of dislocations (Section 2.2.1.). Before such climb can take place, partial dislocations must recombine,

and the separation of partials is inversely proportional to the stacking fault energy. In two phase alloys, segregation of solute to the stacking fault, or precipitation upon the partials comprising the fault, can make reassociation difficult and thus provide a large strengthening effect.

The elastic modulus of a material should also have an effect on secondary creep rate since the stress field around any obstacle to dislocation motion increases with the elastic modulus. Therefore, in high strength materials, dislocations must move correspondingly greater distances over such obstacles before climb may proceed. Attempts have been made to rationalize data where these effects are exhibited due to variations in these material parameters; the following formula has been suggested by Barett and Sherby (1965) :

$$\dot{\varepsilon}_s \alpha D_L \gamma^{3.5} (\sigma/E)^n \quad \text{.....(4)}$$

where D_L is the lattice diffusivity, E is Young's modulus and n is assumed to be a constant for all materials.

This is quite a useful expression as it demonstrates the properties required to confer good creep resistance: low diffusivity and high elastic modulus (associated with high melting point materials) and low stacking fault energy (associated with solid solution and precipitate hardening).

Information concerning grain size effects is often contradictory, early data having been reviewed by Conrad (1961) and Garofalo (1965). Most workers have found a relationship of the form:

$$\dot{\varepsilon}_s \alpha d^{-n} \quad \text{.....(5)}$$

where d is the grain size and the value of the exponent, n, ranges from 1 to 3 - but no general trends emerge. More recently Barrett et al (1967) showed that, for pure metals, the creep rate is

independent of grain size for values of d > 0.1 mm, below which the observed increase in creep rate is attributable to grain boundary sliding (Section 2.4.1.). A major problem in detecting any influence of grain size on creep behaviour in two phase alloys is the variety of structural factors that are affected by heat treatment procedures designed to alter the grain size itself (Mukherjee et al, 1969).

2.1.3.1. Diffusion Creep

For pure metals, the relationship between creep rate and grain size in the diffusion creep regime has been well documented and supported by sound experimental evidence. The flow rate $\dot{\varepsilon}$, due to stress directed atomic diffusion both through the lattice and along grain boundaries, being described by equations of the form (Ashby, 1971)

$$\dot{\varepsilon} \alpha \left(\frac{14\ D\sigma\ \Omega}{kTd^2} \right) \left[1 + \left(\frac{\pi\ \omega\ D_g}{Dd} \right) \right] \qquad \ldots\ldots\ldots(6)$$

where D is the self diffusion coefficient, D_g the grain boundary self diffusion coefficient, Ω is the atomic volume and ω the effective grain boundary width.

However, results on alloys and two phase materials often show widely differing behaviour. Alloying additions, either in solution or as precipitates, do not greatly affect diffusion rates of pure metals but can give rise to enormous differences in creep rates in the range where diffusion creep is expected to predominate (Harris et al, 1969). These results have been interpreted in terms of the capacity of grain boundaries to act as perfect vacancy sources and sinks. Relationships expressing a different grain size sensitivity have been suggested to account for this modified behaviour (Greenwood, 1970) :

$$\dot{\varepsilon} \alpha f(\sigma) / d \qquad \ldots\ldots\ldots(7)$$

A further complication is that, as creep progresses, particles accumulate on those grain boundaries nearly parallel to the applied stress and there is evidence that the creep rate decreases as a result (Burton 1972, Harris 1973).

These aspects of grain boundary behaviour in the diffusion creep regime are of particular importance in creep resistant alloys. Here, the growth mechanisms of cavities, a form of damage that eventually leads to fracture, is considered to depend on the ability of grain boundaries to produce vacancies (Section 3.3.1.).

2.2. Theories of Steady State Creep

Most mechanisms are based on a recovery creep model that predicts a secondary, steady state creep region. Here, a balance is said to be achieved between the rate of recovery, r, and the rate of work hardening, h. When such a balance exists, the strain rate $\dot{\varepsilon}_s$ may be described by the phenomenological relationship:

$$\dot{\varepsilon}_s = (-d\sigma/dt) / (d\sigma/d\varepsilon) = r/h \qquad .....(8)$$

This argument was originally proposed by Bailey (1926) and extended by Orowan (1946-47). However, these early workers ignored any detailed physical mechanism which governed the balance.

It was earlier stated (Section 2.1.2.) that creep deformation is a thermally activated process and that the activation energy Qc corresponded to that for self diffusion Q_{SD}. This intuitively implies that any creep mechanism involves the motion of dislocations and vacancies and their interaction with each other and other structural obstacles.

2.2.1. Dislocation Climb Mechanisms

Climb is mainly a thermally activated process, not critically sensitive to the stresses acting on the dislocations, and it enables the forces resisting dislocation glide to relax continually. Weertman (1957) proposed a model for steady state creep, based on dislocation climb, that yielded a stress exponent of 4.5.

Initially, dislocations are generated from a source and these mutually interact with those produced by sources on parallel slip planes, subsequent dislocation glide is thus arrested by the formation of pile-ups. Further deformation can only take place when the leading dislocations of the pile-ups climb and annihilate one another. Weertman showed that the dislocation climb rate could be related to the vacancy concentration in equilibrium with the stress field at the tip of the pile-up, and derived the following expression:

$$\dot{\varepsilon}_S \alpha \; D_L \sigma^{4.5}/b^{0.5} N^{0.5} G^{3.5}/kT \qquad \ldots\ldots\ldots(9)$$

where N is the number of dislocation sources per unit volume, G is the shear modulus and b is the Burger's vector. This model predicts the empirical stress dependency observed in pure metals (Section 2.1.1) but suffers from the fact that dislocation pile-ups have not been observed during steady state creep (e.g. Evans and Wilshire, 1970).

2.2.2. Dislocation Jog Mechanisms

The intersection of two screw dislocations produces a jog, which because of its edge character can only accompany the dislocation by climb. This non-conservative motion involves the absorption or emission of vacancies (or interstitials) and is considered to be a more likely thermally activated recovery process (Mott, 1956). A

balance is obtained between the applied stress and the chemical dragging force on the jog which is controlled by the vacancy concentration adjacent to the jog, such that (Barrett and Nix 1965) :

$$\dot{\varepsilon}_s \alpha D_L \rho \sinh (\sigma b^2 L / kT) \quad \text{.....(10)}$$

where ρ is the density of mobile dislocations, and L is the inter-jog spacing. Unfortunately this model poorly predicts the expected stress dependency.

2.2.3. Creep Deformation in Solid Solution Alloys

The creep resistance of metals is increased by the addition of elements which will go into solid solution. The strengthening effect has been attributed to lattice distortion and the segregation of solute atoms to dislocations or dissociated partials, both effects reducing cross slip and climb. Weertman (1957a) suggested that solute atom drag on dislocations would make the rate of glide slower than the rate of climb and the secondary creep rate would thus be controlled by the diffusion of solute atoms and the shear modulus :

$$\dot{\varepsilon}_s \alpha D_s \sigma^3 / G^4 \quad \text{.....(11)}$$

where Ds is the self diffusion coefficient of the solute atom and G is the shear modulus.

This σ^3 creep rate dependence was confirmed by Sellars and Quarrell (1961-62), who studied the creep properties of Au-Ni solid solutions over the whole composition range. It has been reported that some solid solution alloys exhibited a stress exponent of 5 this type of behaviour apparently depends on the atom misfit ratio

(Cannon & Sherby, 1970). Mohammed and Langdon (1974, 75) have recently classified solution strengthened alloys into two groups depending on their stress sensitivity.

2.2.4. Creep Deformation in Two Phase Alloys

Dispersions of particles in a matrix offer an effective barrier to dislocation movement, and McClean (1962) concluded that for alloys having a constant volume fraction and particles, a minimum should exist in the creep rate /particle size relationship. Recent work by Threadgill and Wilshire (1974) has shown that this is so.

Earlier, Ansell and Weertman (1959) proposed that at low stresses, dislocations would be unable to cut or bow between particles and would be forced to surmount the obstacles by climb. At higher stresses, greater than the Orowan stress Gb/λ (where λ is the interparticle spacing), dislocations would bow round particles leaving loops. Successive loops would produce a back stress large enough to prevent further dislocation movement, and the rate of climb and annihilation of the innermost loop would control the creep rate.

2.2.5. Friction Stress Theory

Recently, Davies and Wilshire (1971) proposed a recovery model for high temperature creep in which the creep rate is considered to be governed by the growth of a three-dimensional dislocation network developed during creep. Here, the dislocation links between nodes in the network are of sufficient length to act as dislocation sources and glide is the principle mode of deformation. Recovery processes are rate controlled by the growth of these meshes and creep rate is a function of the average mesh size developed.

Particles have been found to retard the rate of network growth by impeding slip and thus reducing the number of dislocations produced at a source and their average distance moved (Parker and Wilshire 1975).

In conjunction with this approach, and using the technique of variable stress tests, Wilshire and his co-workers have proposed the concept of a friction stress, σ_o. This parameter is a function of stress and temperature, and they argue that it reflects the effect of sub-grain size and the presence of a dispersed phase on dislocation glide. The wide variations observed in the stress and temperature dependence of secondary creep rate in two phase alloys may then be rationalized by using the equation (Williams and Wilshire, 1973; Parker and Wilshire, 1975) :

$$\dot{\varepsilon}_s = A^* (\sigma - \sigma_o)^4 \exp(-Qc^* / RT) \quad \text{.....(12)}$$

Where A* is a constant for a given material, σ_o is the friction stress dependent on subgrain size and particle dispersion. The activation energy Qc* derived from this relationship is found to be the same as that for creep of the appropriate single phase material Qc (equation 2), indicating that processes occuring in the matrix are rate-controlling during creep of the two-phase alloy.

2.3. Strengthening Mechanisms in Low Alloy Ferritic Steels

The mechanisms contributing to the creep strength of low alloy ferritic steels have been shown to be complex, but can be generally related to the following factors (Glen & Murray, 1961):

(1) solid solution hardening
(2) matrix transformation structure
(3) precipitation phases
(4) grain size

2.3.1. Solid Solution Hardening

Baird and Jamieson (1972), following accurate creep rate determinations on pure Fe and Fe-Mo alloys, showed that a substantial increase in creep strength was due to the presence of certain combinations of substitutional and interstitial solutes. The strengthening mechanism is regarded as being one of solute drag, whereby creep deformation is limited by the migration of substitutional elements (particularly Mo) to dislocations and their joint movement. The linking effect (due to chemical affinity) of such solute pairs as: Mn-N; Mo-C; Mo-N; and V-C, in preventing this type of segregation produces an interaction solid solution hardening.

It is recognised that under creep conditions, where the solid solutions are highly super-saturated, strengthening by this mechanism decays as precipitation occurs. Indeed, additions of Cr to Mo bearing steels reduce creep strength (Krisch 1971) due to the more rapid precipitation of Cr carbides and nitrides and the consequent removal of interstitials from solid solution.

Attainment of long term creep strength at high temperatures, where coarsening of precipitates and dislocation structures takes place, has been shown to depend significantly on pure substitutional solid solution hardening, particularly at low strain rates (Myers et al, 1968). Mo is found to be the most important strengthening element (Baird et al, 1972) whilst P, Ni and Cu also contribute to a limited extent.

2.3.2. Matrix Structure and Precipitation Phases

The matrix structure, carbide type and morphology resulting from the allotropic transformation and subsequent tempering of low

alloy ferritic steels have been well documented over recent years (e.g. Raynor et al 1968). Small variations in chemical composition have a pronounced effect on the structure produced by the austenite /ferrite phase transformation and it is found that creep properties differ considerably as a result.

Of the several papers published, relating microstructure to high temperature properties, most suggest that of the three common transformation products, a tempered upper bainite confers optimum creep resistance in this range of steels. (Bates and Ridal, 1963; Buchi et al, 1965).

This is thought to be attributable to the finer dispersion of alloy carbides formed by tempering this structure and its higher resistance to particle coarsening. The presence of a fine, stable dispersion of precipitates would act by inhibiting dislocation motion, requiring the climb of line defects and the diffusion of point defects. Barford and Willoughby (1971) contend, however, that there is no substantial evidence to suggest that creep strength is simply related to inter-particle spacing. They further point out that a fine dislocation cell structure, present in a tempered upper bainitic matrix, is mainly responsible for the inhibition of slip; the role of precipitate particles being the stabilization of this partially recovered dislocation structure.

2.3.3. Grain Size Effects

As mentioned earlier (Section 2.1.3.) the effect of grain size on creep resistance is contradictory. In a comprehensive survey of ferritic and austenitic steels, Irvine et al (1961) reached the conclusion that neither in carbon steels nor in steels with low alloying element content has the size of austenitic or ferritic

grains any significant effect on creep resistance.

2.4. Intergranular Deformation

It has been recognized for some time that overall creep resistance in high temperature alloys depends on two main components: that due to matrix deformation and that due to grain boundary deformation. Moreover, a significant part of the overall creep strain at elevated temperatures is attributable to intergranular flow. This involves the relative translation of grains, by shear movement, at their interface (referred to as grain boundary sliding) or in adjacent regions (grain boundary zone shear). These processes also play an important role in promoting intergranular fracture (Section 3.2.1.). Thus, the minimum creep rate measured also includes a contribution due to grain boundary deformation :-

$$\dot{\varepsilon}_{MIN} = \dot{\varepsilon}_{M} + \dot{\varepsilon}_{GB} \qquad \text{.....(13)}$$

Where $\dot{\varepsilon}_M$ and $\dot{\varepsilon}_{GB}$ are respectively the creep rates due to matrix and grain boundary flow. The strain rate due to grain boundary flow $\dot{\varepsilon}_{GB}$ may be described by a similar constitutive law as that for the secondary creep rate $\dot{\varepsilon}_s$ (Equation 3) :

$$\dot{\varepsilon}_{GB} = A_{GB}\, \sigma^{n_{GB}} \exp\left(-Q_{GB}/RT\right) \qquad \text{.....(14)}$$

where n_{GB} and Q_{GB} are respectively the stress exponent and activation energy for creep due to intergranular flow.

2.4.1. Grain Boundary Sliding (GBS)

Although this phenomenon has been well documented over recent years, Bell and Langdon (1969), in their review of the subject, point out that is is often difficult to determine which of several possible

mechanisms is rate controlling. In this context, the most important parameter is the contribution that GBS makes to the overall creep strain. Measurement of GBS, using a variety of techniques (Gifkins, 1973; Gates and Stevens, 1974; Langdon, 1974), has shown that, in the absence of diffusion creep, the total strain observed experimentally may be represented by :

$$\varepsilon_T = \varepsilon_M + \varepsilon_{GBS} \qquad \ldots\ldots\ldots(15)$$

where ε_m is the intergranular strain which occurs independently of the presence of boundaries and ε_{GBS} is that strain due to GBS.

Invariably, the ratio $\varepsilon_{GBS}/\varepsilon_T =$ has been shown to be constant with strain until a late stage of creep life has been reached (Langdon, 1968). This implies a close relationship between matrix deformation and GBS, suggesting that lattice dislocations control sliding, a view favoured by McClean (1974). This mechanism is supported by the fact that the temperature dependence of the two deformation processes have often been found to be similar (Stevens, 1966; Bell and Langdon, 1969). Further, in experiments on bicrystals, it is usually found that solute additions increase the rate of sliding, an effect which may be due to the inhibiting influence of solute atoms on intergranular slip (Bell and Langdon, 1969).

The situation, nevertheless, is still far from clear. Some workers have reported that the stress dependence (Lagneborg and Attermo, 1969; Stevens, 1966), and in some cases the temperature dependence (Lagneborg and Attermo, 1969), of sliding differs from that of dislocation creep. Another feature that is found to govern the rate of sliding is that of boundary angle, the sliding rate generally increasing with increasing misorientation across the boundary. These factors have convinced some workers that grain boundary dislocations are responsible for controlling GBS (Gates, 1973).

2.4.2. Grain Boundary Zone Shear

The study of GBS in more complex alloys, where a second phase is present, has been extremely limited. For the most part, the presence of precipitate particles, particularly on the boundaries themselves, is found to impede GBS (Raj and Ashby, 1972). Further, in conditions where GBS would be expected to contribute significantly to the overall creep strain, the degree of sliding has not been large enough to account for the effect of grain size on creep rate.

These cases are often associated with the important metallographic feature of precipitate free zones adjacent to the grain boundaries. These regions undergo recovery and recrystallization and are consequently softer than the surrounding matrix, enabling high local strains to develop within them atrelatively small elongation values (Nutting, 1961).

This process of grain boundary zone shear has been reported in nickel-based (Venkitsawaran et al, 1973) and aluminium-based alloys (Unwin and Smith, 1969). It has also been suggested that such behaviour is responsible for some of the creep strain in low alloy ferritic steels (Stone and Murray, 1966), where precipitate-free zones are often observed adjacent to prior austenite grain boundaries. More recently Cane (1976) measured such zone shear in a $2\frac{1}{4}$ Cr 1Mo steel and proposed that the creep strain contribution due to zone shear is given by :

$$\varepsilon_{GB} = \frac{\dot{\kappa}\, z\, e}{d} \qquad \ldots\ldots\ldots(16)$$

where e is the precipitate-free zone strain, z is the zone width, κ is a constant and d is the grain size. Clearly, the contribution of deformation adjacent to the grain boundary to the overall strain will be greater in finer grained material.

2.4.3. Effect of Grain Size

The precise effect of grain size on intergranular deformation is somewhat conflicting e.g. in nickel based alloys Brownsword and Hoar (1973) and Wilshire (1970) have respectively reported increasing and decreasing secondary creep rates with increasing grain size. Such differences in behaviour may be explicable in terms of the relative ease of dislocation movement within a grain and at a grain boundary. Thus, a transition in the major deformation process would be expected as the volume-to-boundary area ratio is changed. Certainly, when grain boundary sliding predominates, many workers (Barret et al, 1967) and Gifkins, 1963) have considered grain size dependence to be entirely due to the increasing extent of sliding with decreasing grain size.

Recent work on bainitic low alloy ferritic steels (Cane, 1974) has shown that secondary creep rate increased with decreasing prior austenite grain size, an effect that was attributed to the greater overall volume of grain boundary denuded zone (Equation 16).

CHAPTER 3

CREEP DAMAGE

3.1 Nature of Creep Damage

Creep fracture results from a continuous accumulation of damage the nature of which is sensitive to the test conditions and to the thermal and mechanical history of the material. As at ambient temperatures, failure type can be divided into the two major categories of ductile and brittle behaviour. The most important parameters governing the nature of the creep damage and fracture type being: the applied stress, temperature, atmospheric environment and the relative cohesive strength of the grain boundaries.

At high stresses, thermal and strain induced structural degeneration is such that large plastic strains can be produced by normal dislocation processes. Rupture is associated with the plastic growth of internal holes that nucleate at the interface of coarse precipitate particles or inclusions. Internal necking of materials between the holes leads to coalescence and a fibrous, transgranular fracture surface.

At lower stresses and especially where material is subjected to creep at high temperatures and lower strain rates, ordinary dislocation movement cannot operate to any great extent and deformation is controlled by the other thermally activated processes of grain boundary sliding and vacancy creep (Chapter 2). In this regime a number of metals and alloys, that are normally ductile, fail after very small creep strains; in this sense creep-rupture is referred to as brittle.

Early metallographic studies related this phenomenon to a weakening of the grain boundaries by the formation of hole-like defects whose growth and inter-linkage provided an intergranular fracture path. These defects were classified into two main groups by their morphology and position on the grain boundary: wedge-shaped cavities associated with triple-point junctions are described as "w-type cracks" and spheroidal cavities appearing elsewhere on the boundary are termed "r-type voids." (Garofalo 1965).

The preferential nucleation of voids and cracks on grain boundaries can be attributed to several special properties that they possess at elevated temperatures, summarised by Ashby and Raj (1975) :

(a) The surface energy of a grain boundary that is relinquished, at the nucleation of a void or crack within the boundary, partly compensates for the energy required to form the new surfaces.

(b) Enhanced diffusion along grain boundaries accelerates the growth of cavities.

(c) Their capacity of acting as a sink for matter again accelerates growth.

(d) The ability of certain boundaries to slide (Section 2.4.1.), and especially in cases where the matrix is strong, concentrates stress at triple points, grain boundary ledges and precipitate particles. These stress concentrations favour the nucleation of cracks and voids and the sliding displacements of the boundaries themselves may also contribute to their growth.

Since the first realization, more than twenty years ago, of the full significance that this variety of damage plays in limiting creep life, an enormous amount of data has been recorded and extensively reviewed (e.g. Perry 1974). It is now commonly recognized that failure by these grain boundary defects can be analysed in four separate stages,

summarized by Greenwood (1977): (a) a nucleation stage (b) the growth stage (c) an inter-linkage stage (d) a final stage of relatively rapid fracture.

The initial work in this field also showed that these creep damage features could be identified at an early stage in creep life (Greenwood et al, 1954; Cottrell, 1961), and since then much emphasis has been placed on: (1) directly observing the nature of the damage and in particular its morphology (Section 3.1.1.1.) and grain boundary distribution in relation to the principal stress axes; and (2) indirectly monitoring the accumulation of damage throughout creep life (Section 3.1.1.4.)

At each stage of damage formation (as described above), the nature and severity of defects has been shown to depend on a large number of variables: stress, strain, strain rate, temperature, microstructure, grain boundary segregants, etc; in addition it has been demonstrated that each stage is not independent of another. Not surprisingly, a wide variety of mechanisms have been postulated for the nucleation and growth of cracks and cavities based on either diffusive flux or deformation controlled processes. Large numbers of independent researchers, working with a variety of materials, have produced detailed and seemingly conclusive evidence to support a mechanism that is exclusively controlled by one of the processes. Recent reviews, however, acknowledge the fact that conditions can be established which favour a single controlling process, and that generally no single mechanism of nucleation or growth is applicable (Perry, 1974). It is argued that vacancy - and deformation - controlled processes may occur simultaneously, the relative proportions of which depend upon the material, test conditions and stage of creep life.

When it is established that a process is dominant for the major part of creep life and once the factors that principally govern cavity nucleation and growth have been established, some attempt at prediction of creep failure is possible. This aspect of creep fracture will be discussed in Chapter 4.

3.1.1.1. Methods of Observation

Interpretations of mechanisms of cavity and crack nucleation and growth must rely heavily on metallographic observations of their precise morphology and distribution.

The preparation of specimen sections for optical microscopy provides a simple, convenient means of assessing defect distribution with respect to the principal stress axes. However, for any observations on size and shape to have any true meaning, extreme care must be taken with metallographic preparation. It has been shown that the true profile of cavities can be severely distorted by polishing (which may cause filling in and collapse of cavities) or chemical etching (which may cause rounding-off of cavity edges). To minimize these effects a process of simultaneous polishing and etching has been recommended (Cocks and Taplis, 1967); the process, termed as "skid polishing," usually involves mechanical polishing in a slurry of γ - alumina and mild etching agent. Harris et al (1962), however, warned against the use of any media giving rise to chemical attack and suggest that a better method is to etch by ion bombardment where there is a more uniform atom removal. This technique gives precise definition of cavity profile which can be especially appreciated when specimen sections are viewed by scanning electron microscopy (Needham, 1975). Although optical microscopy can distinguish between r-type

and ω-type cavities when they are present together (Williams 1967), it is increasingly appreciated that it is inadequate when attempting to reveal any fine detail of less than 1μm

At the same time the use of 100kV electron microscopy has proved to be of only limited use in this field (Presland and Hutchinson, 1961-62). Typically, cavity nuclei have a critical size for stability in the range of 0.1 - 1μm. Even at the lower size it is difficult to contain completely within a metal foil which is transparent to 100kV electrons. If voids intersect the specimen surface, they are invariably enlarged and distored during the polishing action. Taplin and Barker (1966) attempted to overcome this difficulty by obtaining shadowgraphs from cracks and cavities in areas of thinned specimens too thick to transmit electrons, a similar technique was used by Johanesson and Thölen (1969) in their studies on Cu and a Cr-Ni-Mo steel. As with optical microscopy, only a cross-section of the voids is observed and true cavity morphology is difficult to interpret.

Recently, the availability of 1000kV electron microscopes has increased the interest of observing grain boundary damage by transmission electron microscopy. The increased penetrating power allows thicker regions of foil to be examined within which undistorted cavities are contained. This has allowed several workers to study the detailed dislocation and microstructural effects on cavity nuclei, and also to make more confident assessments of their nucleation rate (Johannesson and Thölen, 1972; Dyson and Henn, 1973; Fleck et al, 1975).

The ability of certain metals and alloys to fracture intergranualarly at low temperatures has been of considerable use in the assessment of cavity shape, size and distribution. The fracture

surface may be examined directly by scanning electron microscopy or, after taking replicas of the surface, by transmission electron microscopy (Boniszewski and Eaton, 1969). Observations of polyhedral cavities, using this technique, have allowed three dimensional growth laws to be determined (Cane and Greenwood, 1975). Low alloy ferritic steels have been found to be susceptible to intergranular fracture along prior austenite grain boundaries at liquid nitrogen temperatures and several workers have studied the nature of creep damage in these materials using this technique (Boniszewski and Eaton, 1969; Cane, 1976).

3.1.1.2. Damage Morphology

The first detailed study of intergranular damage using optical microscopy (Greenwood et al, 1954) revealed that cavities in copper and α-brass had a rounded morphology, whilst those in magnesium tended to be flatter and more shallow. These observations gave the first indication that there was more than one mechanism of nucleation and growth. With the advent of more advanced techniques, as described above, it was found that the characteristics of voids and cracks deduced from optical microscopy could be quite misleading. For instance, Steigler et al (1967) in their studies on tungsten showed that "ω-type" cracks at triple junctions were in fact smooth, feature-less voids described as "amoeboid" in shape.

The most common observation in the study of specimens after creep at low stress levels is that cavities have regular, polyhedral shapes and a distinct crystallographic nature. This type of damage has been reported in magnesium (Presland and Hutchinson; 1961-62); beryllium (Hyam, 1961); tungsten (Farrell et al, 1967); α-iron

(Taplin and Wingrove, 1967, 1969); and copper (Needham et al, 1975). Such crystallographic cavities have also been observed on the grain boundaries of more complex alloys as austenitic stainless steels (Wadsworth, 1975). In their studies on α-iron, Taplin and Wingrove (1969) showed that the facets of their cavities were bounded by {100}, {110}, {112} and {102} faces.

At higher levels of stress, cavities have been seen to assume more complex "fingered" or "dendritic" shapes (Taplin and Wingrove 1967, 69; Davies and Williams, 1969). A similar phenomenon was observed by Steigler et al (1967) in their work on tungsten. They suggested that the shape of cavities was determined by the balance between the rate of growth and the cavity (by a vacancy or mechanical process) and the rate of surface diffusion. Therefore, as the temperature is increased and the strain rate decreased, there is more opportunity for surface diffusion to predominate and cavities assume regular polyhedral shapes. This view was confirmed by Winzor (1975) who described a terraced appearance of cavities on grain boundaries. It was suggested that the rate of surface diffusion was such that the overall growth process restricted cavities from adopting their equilibrium shape.

3.1.1.3. Distribution of Damage

A useful approach to define mechanistic differences in creep fracture has been the measurement of the angle of formation of grain boundary damage to the stress axis. By definition, if shear is the controlling process, the distribution should peak at 45^{o} (the maximum shear plane) and if vacancy growth is controlling it should peak at 90^{o}.

Gittins and Williams (1967) found that in high purity copper, cavities tended to form on boundaries at 60^{o} - 90^{o} to the applied stress only at low strain rates, shifting to 30^{o} - 60^{o} boundaries which undergo maximum sliding at high strain rates. They inferred that the contribution of GBS to cavity growth is important at higher stresses and that of vacancy processes dominating at lower stresses. Wingrove and Taplin (1969) reached a similar conclusion from their work on α-iron. By comparing the angular distribution of cavities near to and remote from the fracture surface in an Inconel alloy, Venkiteswaran and Taplin (1974) showed that the percentage of damaged boundaries at 45^{o} to the tensile stress increased away from the fracture surface. The authors suggested that this result showed that GBS plays a dominant role in the early stages of cavity growth, whereas in the later stages, vacancy condensation and/or mechanical tearing are the dominant growth processes.

Pre-strain and grain size are also found to have an effect on the angular distribution of damage, however, this will be referred to later (Section 3.1.3.).

3.1.1.4. Damage Assessment

Several workers have used quantitative metallography to measure the number of cavities per unit area at various stages during creep life. The number per unit area N_A is simply converted into the number per unit volume N_V, which is invariably found to obey the relationship:

$$N_V \alpha t^q \qquad \text{.....(17)}$$

the value of the exponent q has been found to be 0.5 in copper (Gittins, 1967) and 1 in magnesium (Ratcliffe and Greenwood, 1965)

and Nimonic 80A (Dyson and McClean, 1972). Greenwood (1973) rationalized these results and those for pure iron to show that in the early stages of creep life the nucleation of cavities proceeds approximately linearlywith strain. Earlier work on silver had shown a sigmoidal variation with strain (Oliver and Girifalco, 1962) whilst in α-iron (Wingrove and Taplin, 1969a) found that the value of q in equation (17) decrease from 4 to 0.5 with decreasing strain rate, but this may be due to lack of detection of small cavities (Evans and Waddington, 1969).

A more convenient technique for assessing nucleation kinetics and growth laws with some accuracy, is afforded by the fact that the formation of cavities and voids produces a decrease in the material density. Cumulative creep damage may thus be monitored by comparative density techniques. The initial work of Boettner and Robertson (1961), on copper, showed that cavity nucleation occurred very early on in creep life; this observation was confirmed in magnesium by Ratcliffe and Greenwood (1965) using high precision density measurements. Since then a number of workers investigating the behaviour of pure metals, using density methods, have found that the density change $\Delta\rho/\rho$ varies with the duration of creep according to the expression (Gittins, 1967; Needham, 1973):

$$-\Delta\rho/\rho \propto t^{u} \qquad \ldots\ldots\ldots(18)$$

The exponent, u, taking a variety of values depending on the material investigated. Similarly, the relationship between the density change and strain is of the form:

$$-\Delta\rho/\rho \propto \varepsilon^{v} \qquad \ldots\ldots\ldots(19)$$

Where the exponent, v, can again assume different values depending on the material.

Greenwood (1969) indicated that the effect of one variable in isolation could be misleading, and that the total void volume is more likely to be proportional to the product of strain and time. Woodford (1969), using a parametric approach, agreed with this proposition and suggested that the total cavity volume could be predicted for any time, stress and temperature by a relationship of the form :

$$-\Delta\rho/\rho \quad \dot{\alpha} \quad \varepsilon \; t\sigma^{p} \quad \exp\left(-Q/RT\right) \qquad \text{.....(20)}$$

It was found that for Cu, P = 2.3 and Ni, P = 7 (Woodford, 1969a). Needham et al (1975) found a similar relationship held true for Mg in the earlier stages of creep life, suggesting that as Cu has an fcc structure and Mg is hcp, the crystallography of the lattice has little bearing on the mechanism of cavitation.

In more complex two phase alloys, precipitation results in an overall density change due to a difference in lattice parameter with varying amounts of solute (Dyson and Holmes, 1970). This makes it rather difficult to separate the density change due to cavitation alone. Some attempt has been made to follow the extent of creep damage in these materials using density methods, however, some of them are open to severe criticism. Gittins (1970a) in his work on an austenitic stainless steel attempted to avoid the problem of precipitation effects by preageing his creep specimens. This approach is not really satisfactory as precipitates have been shown to effect cavitation (Section 3.2.1.) and in effect Gittins was investigating a stable two phase alloy and not a "real" creep resistant material. An alternative method is to compare the density difference between creep tested specimens with those that have been aged at a similar

temperature and time but under no stress (Gittins, 1970; Day, 1965). Again this is not really sound as the kinetics of precipitation are influenced by the applied stress. Wadsworth et al (1976) used a more realistic approach by measuring the lattice parameter of specimens after creep and calculating the density change due to precipitation in Nb stabilized stainless steels. Subtracting this from the overall density change observed produced a value due to creep damage alone.

The possibility of using electrical resistance measurements to obtain information on the extent and progress of cavitation and cracking has been explored with only limited success (Thomas and Tipler, 1974) in more complex alloys. Early work on α-brass using such a technique by Spark and Taplin (1969) produced results that lead them to believe that changes in resistivity reflected variations in the orientation and shape of cavities with respect to time and strain.

3.1.2. Effect of Stress

Early observations indicated that the level of stress influenced the type of grain boundary damage and McClean (1956-57) showed that in a Nimonic 90 the failure mode changed from cavitation to cracking with increasing stress. Stroh (1954) derived an equation for the fracture of a sliding interface due to the stress concentration at the head of a single pile-up of dislocations (Section 3.2.1). McClean (1956-57) invoked this equation in an attempt to analyse the situation that would lead to a changeover in the nature of damage produced during creep. This is often referred to as the Stroh-McClean transition. Later, Waddington (1968) justified this approach when he showed that a critical stress exists for triple point crack nucleation.

However, the transition is not distinct and in many cases cracks and voids have been observed together (e.g. Williams 1967).

3.1.2.1. Stress Reversal

A large number of experiments have been undertaken, especially by Davies and his co-workers, involving a change in the direction of the applied stress during a creep test. Davies and Wilshire (1965) creep tested dilute nickel alloys to the tertiary stage. Stress reversal produced a period of compressive creep and this was followed by a second stress reversal to recommence tensile creep. This latter stage was again found to be tertiary. The authors argued that if the growth of cavities was controlled by vacancy condensation, then compressive creep should have caused void shrinkage due to the reversibility of diffusional growth. As no change in behaviour was observed and the final creep stage was still tertiary, they concluded that void shrinkage had not occurred and hence the growth of grain boundary cavities was a mechanical process.

A more detailed investigation on the effects of stress reversal was carried out on a Cu-Al alloy using constant stress equipment (Davies and Dutton 1966). After deformation in tension to the onset of tertiary creep, specimens were deformed in compression at 180^{o} and 90^{o} to the original stress axis. In the first case void shrinkage was observed and interpreted as showing that sliding was the dominant growth process, a reversal of which should be responsible for reduced cavitation. In contrast, compression at 90^{o} to the original stress axis should maintain the initial sliding direction and cavities would continue to grow. In each case both these effects were respectively observed.

These results appeared to show that growth and shrinkage of

grain boundary damage could be explained in terms of a deformation controlled mechanism. However, this type of stress reversal experiment has been criticised on several fronts. Taplin and Gifkins (1967) pointed out that the degree of cavitation present at the onset of tertiary creep is such that conclusions concerning growth mechanisms at early stages of creep life cannot be made from observations on the effect of stress reversal at later stages. They further suggested that a reversed flow situation does not necessarily cause void closure but could indeed promote continued growth due to the induction of local tensile stresses at the tips of cracks lying parallel to the stress axis. Gittins (1967) showed that sintering can occur on reversal stressing at room temperature and he concluded that cavities were closed by plastic flow and hence GBS is not a prerequisite.

These crticisms of stress reversal observations, taken as a whole, reiterate the view that several modes of growth are possible involving a combination of tearing, vacancy accretion and GBS. Nevertheless, Davies and Williams (1969a) replied by showing, from density measurements on Cu specimens containing isolated creep cavities, that room temperature compression resulted in no change of cavity volume. With similar specimens, high temperature deformation at 180^{o} to the original stress axis resulted in densification and at 90^{o}, continued cavity growth. From these results, they insisted that a vacancy contribution plays an insignificant part in cavity growth.

3.1.2.2. Stress State

When metals are subjected to creep in engineering service, they are not usually under the influence of a simple tensile stress, but rather of a complex, multiaxial stress system. The pioneering work of A. E. Johnson (reviewed in 1962) was designed to examine the effect

of stress systems on creep deformation, damage and fracture life. Using a variety of techniques, involving the combined tension and and torsion of thin walled tubes to produce a homogeneous biaxial stress system which was independent of time, he investigated the behaviour of a variety of metals and alloys. He concluded that they could be classified into two groups whose stress rupture behaviour depended on either the maximum principal stress, σ_1 or some shear component of the stress system usually represented by the octahedral shear stress T_{OCT}. He also recognized that the nature of the creep damage and mode of fracture were different in the two categories.

Of the materials studied, commercial purity Cu and Nimonic 75 were found to have fracture lives that depended on the maximum principle stress and also that failure occurred by the growth of grain boundary cavities that lay perpendicular to the maximum principal stress. An aluminium and magnesium alloy, however, showed that fracture life was markedly affected by the ratio of the maximum principal stress to the octahedral shear stress (σ_1/T_{OCT}). Further, failure in these cases was due to some localized intercrystalline shear mechanism.

More recently Hayhurst (1972), using biaxial tensile loading of cruciform specimens, suggested that the fracture behaviour of Cu and Al could be taken as extreme cases dependent on either the maximum principal stress σ or some stress invariant, respectively. Other metals and alloys would have a stress rupture behaviour lying somewhere between these two extremes. The stress invariant controlling fracture mode in the Al group is conveniently represented by the effective stress $\bar{\sigma}$, where:

$$\bar{\sigma} = 3\tau_{OCT} / \sqrt{2} \qquad \text{.....(21)}$$

Thus, in uniaxial tension $\bar{\sigma} = \sigma_1$

In an attempt to understand the influence of stress state on the nature and severity of creep damage and its separate effect on nucleation and growth mechanisms, Dyson and McClean (1977) have compared the results of tension and torsion tests on Nimonic 80A over a range of effective stresses. Torsion was chosen as the additional test method as it provided a stress system that was accurately known and approximately spatially homogeneous. Also the ratio of maximum principal stress to effective stress could be used as a variable parameter in comparing results for torsion and tension tests :

$$\text{In tension: } \sigma_1 / \bar{\sigma} = 1 \qquad \text{.....(22)}$$

$$\text{In torsion: } \sigma_1 / \bar{\sigma} = 1 / \sqrt{3} \qquad \text{.....(23)}$$

The authors found that for a given effective stress, $\bar{\sigma}$, the creep life in tension was much shorter than that in torsion. This was attributed to the dependence of cavity nucleation on stress state. Using an optical cavity counting method, they were able to show that the number of cavities per unit volume N_V was governed by the relationship :

$$N_V \propto (\sigma_1/\bar{\sigma})^2 \; \bar{\varepsilon}^{\frac{1}{2}} \qquad \text{.....(24)}$$

where $\bar{\varepsilon}$ is the effective strain ($= \varepsilon_{OCT} / \sqrt{2}$).

They argued that since the stability of any nucleus is dependent upon the normal traction across a grain boundary (Section 3.2.) which is effectively equal to σ_1, for a given $\bar{\sigma}$ the critical nucleus size would be much greater in torsion than in tension (Equations (22)

and (23)). Consequently fewer cavity nuclei were stable in torsion and the nucleation rate was correspondingly lower. They were further able to show that cavity growth rate was mainly dependent on the effective stress, $\bar{\sigma}$, with the ratio $\sigma_1/\bar{\sigma}$ having a limited influence, especially at high stress levels. The total cavity volume V being given by :-

$$V \alpha [\bar{\sigma}^{q} t (\sigma_1/\bar{\sigma})^{1.8}]^{4.5} \quad \ldots\ldots\ldots(25)$$

Over the $\bar{\sigma}$ range from 100 to 400 MN m^{-2} the exponent q was found to increase from 1.55 to 7.11. Thus at high strain rates, failure mode in this material could be related to the A1 category i.e. sensitive to $\bar{\sigma}$ and with cavity growth controlled by some shear deformation mechanism. Conversely at low strain rates behaviour could be compared to that exhibited by Cu in Johnson's original classification. This type of study has clearly shown that the nature and severity of creep damage is influenced not only by the level of stress but also by the stress system because it involves the synthesis of their respective effects on the mechanisms of cavity nucleation and growth.

Tensile testing of notched specimens allows the effect of triple tension on creep rupture to be studied. Here, the stress system in spatially inhomogeneous and, because of stress relaxation, time dependent. Consequently the previous value of such tests was merely as a material sorting technique.

Early work by Davis and Manjoine (1952), who tested the rupture strength of a number of different alloys in a notched and unnotched condition, showed that notch sensitivity was a function of notch acuity . The ratio of rupture strengths increasing initially as

the notch sharpness decreased until a maximum was reached and then decreasing as the notch became more blunt. Generally, more ductile materials required sharper notches to induce weakness.

Extending Hayhurst's work on biaxial stress systems to include a hydrostatic stress component, Leckie and Hayhurst (1974) derived damage rate equations that were a function of effective stress combined with either the maximum principle stress or the hydrostatic stress or both. For these constitutive relations they defined two classes of material :-

(a) Those whose creep deformation and rupture characteristics are both controlled by a shear stress component were referred to as Ø/Ø materials.

(b) Materials whose creep deformation mechanisms are defined by shear but whose rupture mode is controlled by the maximum principal stress or other stress relations, were called Ø/Δ materials.

AL and Cu represented ideal cases of each type of behaviour respectively and the authors suggested that other metals and alloys might lie between the two extremes. This analysis was applied to predict the rupture stress of the two classes of material for the multiaxial system existing in the region of circumferentially notched cylinders of the Bridgman type. Although not strictly applicable, the authors argued that, provided the damage fields were fairly uniform, an estimate of the rupture stress could be made. They predicted a distinct notch strengthening effect for Ø/Ø materials, such as AL, and a slight notch weakening effect in Ø/Δ materials, such as Cu. Experimental observations produced results that were in close agreement with these forecasts and furthermore, the nature of the creep damage in the vicinity of the notch in the AL specimen showed clear evidence of a shear mechanism operating.

Efforts to determine the effects of stress system at a notch on the nucleation and growth of cavities and other creep damage, have been brought a step nearer recently by the work of Leckie et al (1976) in analysing the stress redistribution with time at a notch. This has enabled them to predict that for a circular notch, assuming nucleation to be controlled by an effective stress, the maximum nucleation rate would occur towards the outside of the notch. Growth control by the same stress component, $\overline{\sigma}$, would also be a maximum in this region but growth controlled by the maximum principal stress, σ_1, would produce the greatest amount of creep damage at the centre of the specimen. For the case of a sharp notch with peaks in the stress distribution near the notch would exhibit maximum nucleation and growth rates towards the outside of the notch at the stress peak. Hence, for growth controlled by $\overline{\sigma}$ or if a sharp notch is present, fracture would initiate close to the notch and propogate outwards before the decrease in cross-sectional area would allow the crack to proceed inwards across the notch throat.

3:1.2.3. Hydrostatic Pressure

The classic experiment of Hull and Rimmer (1959) has been quoted as a critical test for the definition of the controlling damage growth mechanism under creep conditions. They showed that if a test was carried out where the hydrostatic pressure was equal to the applied stress, further cavitation by the growth of r-type voids was effectively inhibited. This effect was shown conclusively for pure magnesium by Ratcliffe and Greenwood (1967). It is argued that, since pressure should only affect the condensation of vacancies whilst deformation processes such as GBS remain unaffected, the latter make no contri-

bution to cavity growth. McMahon (1968-69), however, has pointed out that hydrostatic pressure may counteract any hydrostatic tension occurring around structural discontinuities, thus preventing a purely mechanical expansion of cavities. Recent investigations on high purity Cu (Needham and Greenwood 1975) have shown that fracture life, t_f, varies according to the following relationship over a wide range of stress and pressure :-

$$t_f \alpha 1 / (\sigma - P)^4 \qquad \ldots\ldots\ldots(26)$$

Similar experiments (Waddington and Williams, 1967) were carried out on an Al 20% Zn, where the variety of damage was principally wedge type cracks. The authors found that the application of a hydrostatic pressure did not prevent the growth of cracks, although the fracture strain and life were both increased. They suggested that this was due to the imposed pressure decreasing the normal stress at the crack tip resulting in a decreasing growth rate, they also observed that the shape of individual cracks after pressure testing was changed, possibly due to increased plasticity associated with the failure process.

3.1.3. Effect of Prestrain

It is well established that room temperature plastic straining can influence the subsequent creep performance of metals and alloys. This influence is manifested in the effect on creep strength, as reflected by the minimum creep rate, and creep life and ductility. Previous studies have shown that prestraining can be beneficial to creep strength and life in some cases (Davies et al 1961-62, Garofalo 1961) or detrimental (Sergeant 1968, Waddington and Evans

1970). However in each case the rupture ductility was impaired.

Two effects of prestraining can be envisaged depending upon whether creep strength is increased or decreased, both however lead to intergranular damage and a loss of creep ductility. Earlier, Bailey (1935), recognized that prestraining would increase the dislocation density within grains thus making them stronger in relation to the boundaries, this would lead to intercrystalline failure (presumably by GBS) at low ductility and an observed increase in creep strength. Recent work has shown that the deleterious effect is often associated with increased grain boundary cavitation and a decrease in creep strength (Waddington and Evans, 1970) suggesting that in these cases prestrain causes damage to the grain boundaries themselves and that rupture ductility is independent of intragranular strength.

In an attempt to quantify the latter effect, Dyson and Rodgers (1974) monitored the influence of cold prestraining on the creep performance and damage of Nimonic 80A. They clearly demonstrated that the material suffered progressive loss of creep strength, life and fracture ductility as prestrain increased. Quantitative metallography revealed a concomitant dramatic increase in the number of grain boundary cavities. The authors suggested that the reduction of creep ductility was simply related to the enhanced cavity density and was not due to any increase in cavity growth rate. They further implied that the decrease in creep resistance was caused by an increase in mobile dislocation density and was independent of cavitation damage.

The idea that prestrain influences the nucleation characteristics of grain boundary damage is in agreement with the earlier work of Davies and Wilshire (1961-62). Pre-deforming in compression produced grain boundary ledges that would act as void nuclei on subsequent

creep testing in tension (Section 3.2.1.). The authors found a remarkable increase in cavities on boundaries in the 30^{o} to 60^{o} bracket where GBS provided the dominant growth mechanism. This indicated that prestrain had substantially increased the number of cavity nuclei, however it should be said that ledge nucleation might not be dominant in the absence of pre-compression.

3.1.4. Effect of Temperature

Many metals and creep resistant alloys exhibit a ductility trough as the temperature is increased through the range 0.4 to 0.7 Tm. This phenomenon is associated with changes in the dominant mode of deformation and damage mechanisms as the temperature is raised. The effect of temperature on creep fracture has been summarized by Gifkins (1969). Earlier, Grant (1959), had shown that there was a limiting temperature, the equicohesive temperature, below which the amount of GBS is very small and therefore grain boundary damage below this temperature (which is dependent on grain size) will be negligible. Above this temperature, that Gifkins equates to approximately 0.4 Tm, the ductility is reduced by a small amount of "ω type" cracks that nucleate at favourable sites such as triple point boundaries. As the temperature increases isolated cavities begin to nucleate and grow by plastic tearing of sharp apices or, as the temperature is further raised, by vacancy capture, which appears to dominate at about 0.55 Tm. At this point the ductility reaches a minimum, the rise with further increase in temperature being ascribed to intergranular recovery processes, such as grain boundary migration, and intergranular weakening, such as particle coarsening.

In α-iron the ductility minimum was found to occur at a temperature that corresponded to that at which GBS provided a maximum contribution to the overall strain (Wingrove and Taplin 1969). A similar result was obtained by Evans (1969) working on Magnox AL80 where the minimum in ductility was attributed to a temperature at which there was maximum void growth and its parallel maximum sliding rate.

3.1.5. Effect of Environment

Several articles have been written containing evidence to suggest that the prevailing atmospheric environment can influence the nature and severity of creep damage. Scaife and James (1968) working on Nb stabilized stainless steels demonstrated that creep properties deteriorated when specimens were tested in air rather than in vacuum. Further, they discovered that both the size and number of cavities increased towards the surface of the specimen. This they attributed to the ease of cavity nucleation in that area due to the grain boundary diffusion of oxygen arguing that the presence of oxygen decreased the activation energy of GBS as originally envisaged by Intrater and Machlin (1959) in their work on Cu.

However, a similar effect was earlier observed by Boettner and Robertson (1961) who were studying cavitation in OFHC Cu. They took the contrary view that the increase in cavity size observed at the surface of specimens was due to the surface acting as a source of vacancies which diffused to nuclei via grain boundaries. Scaife and James point out in their article that, if this were true, then cavity size should be uniform throughout the specimen cross section irrespective of the surrounding environment; this they had found not to be the case.

3.2. Nucleation of Creep Damage

The influence of various macroscopic parameters, and their interaction, on the nature and severity of creep damage have been outlined above; the various observations made of damage mode and fracture behaviour have given some indication of the dominant processes involved in the growth of such structural defects. However, before any mechanistic approach is attempted to explain the nucleation of such damage, account must be taken of the microstructure and chemistry of grain boundaries. The influence of such microscopic parameters on nucleation events is most conveniently defined by the application of classical nucleation theory (Ashby and Raj, 1975):-

The formation of a void, made up of spherical segments of radius r, involves the formation of an area of free surface $F_s\ r^2$, the energy for which is provided by an area of grain boundary surface or inclusion - matrix surface equal to $F_s r^2$ that is removed. In addition, a normal traction σ_n acting across the interface on which the void appears, does work $\sigma_n\ F_v\ r^3$ where $F_v\ r^3$ is the void volume. The total free energy change is therefore given by :-

$$\Delta G^* = -\sigma_n F_v r^3 + r^2 (\gamma_s F_s - \gamma_B F_B) \qquad \ldots\ldots\ldots(27)$$

where γ_S and γ_B are the specific free energies of the surfaces involved and F denotes a shape factor. This energy passes through a maximum and defines a critical void radius r_c where the void has achieved stability :-

$$r_c = \frac{2\gamma_s}{\sigma_n} \qquad \ldots\ldots\ldots(28)$$

when

$$\Delta G = \frac{4\gamma_s^3 F_v}{\sigma_n^2} \qquad \ldots\ldots\ldots(29)$$

The free energy of nucleation ΔG^* governs the rate of nucleation according to the relationship :-

$$\dot{N} \alpha (N_{MAX} - N) \exp (-\Delta G^* / kT) \quad \ldots\ldots\ldots(30)$$

Where N_{MAX} is the total number of potential nucleation sites.

Clearly, the case of nucleation and extent of creep damage will depend upon the relative values of γ_s, F_v and σ_n, which in turn can be influenced by the nature of the grain boundary and the position of nucleation sites (F_v is smaller at grain corners than at edges, and smaller at edges than on the grain boundary surface).

3.2.1. Stress Concentration Mechanisms

On a clean boundary, evaluation of Equation 30 with σ_n equal to the applied creep stress, the nucleation rate can be shown to be equal to zero. At high stresses, in materials with a high yield strength, grain boundary sliding can concentrate stress (increasing σ_n) at grain corners to give a finite nucleation rate (Zener, 1948). Stroh (1957) extended this approach by considering the stress generated by a single pile-up of dislocations, supported by an infinite amount of material. The stress to nucleate a wedge crack being given by:-

$$\sigma_E = \left[\frac{3\pi \gamma_s G}{8(1-\nu)d} \right]^{\frac{1}{2}} \quad \ldots\ldots\ldots(31)$$

Where σ_E is the effective shear stress on the dislocations, γ_s is the fracture surface energy, G is the shear modulus, ν is Poisson's ratio, d is the length of the glide plane containing the dislocation pile-up, n may be expressed by the following relationship to give an alternative criterion for nucleation:-

$$n = 3\pi^2 \gamma_s / 8\sigma_E b \quad \ldots\ldots\ldots(32)$$

where b is the Burgers vector of the dislocations.

An earlier analysis by Stroh (1954) predicted a much higher required stress for nucleation and several authors (e.g. McClean, 1956-57) correlated experimental observations of triple point cracks with this earlier relationship. Later work by Smith and Barnby (1967a) showed that crack nucleation is very much easier when two dislocation pile-ups form an orthogonal complex. They concluded from this, that it is invalid to apply the Stroh relation to experimental results on the appearance of "ω-type" cracks, where the observed stresses are most likely to correspond to those required to make cracks grow to such a length that they are resolved optically.

At lower stresses where cavitation fractures occur several mechanisms have been proposed whereby stress concentrations, sufficiently large enough to rupture atomic bonds, can arise due to grain boundary discontinuities. The magnitude of the concentrated normal stress σ_n is often difficult to calculated.

The most likely nucleation sites are inclusions or second phase particles contained in the boundary plane and several workers have reported observations of the association of voids with particles in a variety of materials (Taplin and Wingrove, 1967; Johannesson and Thölen, 1969; Bonizewski and Eaton, 1969). If particles are poorly wetted by the matrix then nucleation of voids is possible without requiring concentration of the stress by sliding, provided that the particles are greater than the critical size, r_c (Harris 1965). For smaller particles, Harris calculated the rate of sliding required for cavities to grow to a stable size and found that it increased as the particle size decreases. Greenwood and Harris (1965) indicated that the particle/matrix adhesion must be very low to allow vacancy conden-

sation to occur and concluded that the initial breaking of cohesion was most likely to be deformation induced.

Second-phase particles, which are strongly adherent to the matrix, could also act as stress concentrations by obstructing grain boundary sliding; Weaver (1960) showed that cavities do form at such particles and several authors have provided evidence of grain boundary particle fracture during creep (e.g. Irvine et al 1961).

Sliding can concentrate stress at any point in the boundary that deviates from a perfect plane and several mechanisms have been proposed. Chen and Machlin (1956) and later McClean (1963) postulated the existance of long, narrow grain boundary ledges that could be opened up to form a critical nucleus by sliding. Harris (1965) disagreed with this model, showing that an unacceptably high sliding rate was required. Presland and Hutchinson (1961-62; 1963-64) in their work on magnesium found that the majority of voids nucleated on grain boundary kinks, produced by the intersection of sub-boundaries.

Sliding is not always a prerequisite and stress may be concentrated in other ways. Gifkins (1956) suggested that when slip penetrates a boundary, a local stress concentration may form because the Burgers vector of the two grains are non-parallel, resulting in the initiation of cavities. Dyson and Henn (1972) proposed that the impingement of slip lines on grain boundary particles in a Nimonic alloy were responsible for cavity nucleation.

Cottrell (1961) had earlier suggested that the nucleation mechanism, associated with stress concentrations in the grain boundary must be mechanically similar to the triple point process of the Stroh type. Smith and Barnby (1967) considered theoretical models for

cavity nucleation at grain boundary discontinuities where, in the case of a particle, the stresses are supported only by the particle and not by material beyond the dislocation barrier. They considered an infinite sequence of co-planar edge dislocations, each of length 2d, held up by an effective stress, σ_E, against barriers of thickness 2c. Provided c << d, the criterion for nucleation is given by :

$$\sigma_E \left[4\gamma_s G/\pi(1-\nu)d\right]^{-0.5} = (\pi/2)(c/d)^{0.5} \qquad \text{.....(33)}$$

Typical values for equation 32 indicated that cavities could be nucleated at barriers with thickness less than 0.03 μm, the nucleation stress decreasing with barrier width. Thus grain boundary ledges and precipitates could act as suitable nucleation sites, the authors further point out that for barriers of this dimension Stroh's formula (Equation 30) predicts a stress many times greater than that generated by Equation 32. However, as far as precipitate particles are concerned, an optimum size range will exist in which nucleation and growth can occur. For very thick particles nucleation may be impossible, and although thinner particles require smaller stresses for cavity nucleation, grain boundary sliding may be inadequate to enlarge the cavity to the critical size for further growth.

3.2.2. Influence of Impurity Segregation

Referring back to Equation 27, it is clear that any reduction in either the surface energy of the cavity nucleus γ_s or grain boundary energy γ_B will result in a lowering of the energy required for the nucleation event. Measurements of the surface energies of binary systems of solid metals by Hondros and McLean (1968) have shown that surface energy γ_s is lowered by solute in such a way

that

$$\left(\delta\gamma_s / \delta C\right)_{C=0} \sim 10^{0.6} C_s \ \text{Jm}^{-2}\ \text{at.\%}^{-1} \qquad \text{.....(34)}$$

Where C is the actual solute concentration and C_s is the maximum solubility at the temperature required.

Earlier work by Inman et al (1963) had shown that the interfacial energies in Cu were drastically reduced by addition of antimony, suggesting that in these alloys a likely consequence was a worsening of creep fracture resistance. This view was confirmed by Tipler and McClean (1970), who compared the rupture behaviour of OFHC Cu and a Cu - 0.3 at .% Sb alloy. Antimony was found to reduce drastically the rupture ductility and optical metallography revealed that Sb greatly accelerated both r-type and w-type cavitation. The authors suggested that this deliterious effect was entirely due to the way adsorbed impurities (such as Sb) lower the energy required to nucleate cavities, according to the expression :

$$\text{Drop in energy for cavitation} = 10\ C/C_s \ \text{J m}^{-2} \qquad \text{.....(35)}$$

Where C is the actual impurity concentration, and C_s is the maximum impurity solubility at the creep testing temperature.

They further pointed out that wedge shaped cracks at triple points appeared in the alloy at about half the applied stress level necessary to generate them in Cu itself, suggesting that a substantially smaller stress concentration is needed for nucleation in the alloy due to a lower value of surface energy γ_s (c.f. Equation 31). Recent work by Kirby and Beevers (1977), however, revealed that addition of phosphorous to α - iron succeeded in suppressing cavity nucleation and improving rupture ductility. The authors suggest that the lowering

of grain boundary energy by phosphorous additions allowed easier grain boundary migration, thereby preventing a stable grain structure to support the necessary stress concentrations to nucleate cavities.

Recent studies, involving the use of Auger electron spectroscopy, has shown that solutes can adsorb at interfaces in solid metals and that segregation is constrained to a narrow locality close to the boundary surface, generally within a few atom layers of the grain boundary (Seah and Hondros, 1973). The authors explained this behaviour on the basis of a multi-adsorption process, an analogue of the well known BET multilayer surface adsorption. In its extreme this phenomenon could produce a localized brittle phase of roughly intermetallic composition over several atom distances across the grain boundary.

In a later article, Hondros and McClean (1974) extended the analytical solutions for crack nucleation due to Stroh and Smith and Barnby. They showed that at any stress concentration, the requirement for decohesion, in polycrystals subjected to conventional stresses is that the component of the tensile stress σ_Y should exceed the localized atomic cohesion σ_M. They further proposed that relaxation by grain boundary cracking would be preferred to any shear relaxation process when :

$$\frac{\sigma_Y}{\tau_T} > \frac{\sigma_M}{\tau_M} \qquad \text{.....(36)}$$

Where τ_T is the local shear component, and τ_M the shear resistance. The authors suggested that this condition could be more easily satisfied by a reduction in the value of grain boundary cohesion σ_M, as through segregation of impurities and the consequential lowering of the interfacial energies γ_s and γ_B.

3.2.3. Rate of Nucleation

Despite the difficulties of adequate metallographic examination, several studies on the number of cavities observed throughout creep life have provided reliable evidence that in copper (Greenwood, 1969), magnesium (Wheatley, 1971) and a Nimonic alloy (Dyson and McLean, 1972) the number of cavities increases approximately linearly with strain from a very early stage of creep life. This is not surprising as most models for cavity nucleation (as described above) involve deformation induced stress concentrations being set up at irregularities in the boundary. However, recent work by Cane and Greenwood (1975) on α-iron, revealed a non-linear relationship between strain and the number of cavities, suggesting that the rate of nucleation with strain depends on the number of possible sites, and thus decreases as these sites are used up. Other workers (Fleck et al 1975) have reported a progressive departure from linearity due to the possible exhaustion in total cavity nuclei.

A further complicating factor has been proposed by Dyson (1976) in a recent article where he comments on an earlier observation of Tipler et al (1970) in their work on low alloy ferritic steels where not all transverse grain boundaries on the fracture surface contained the same number of cavities. This, Dyson suggests, is due to the fact that different grain boundary facets have different cavity nucleation rates.

The influence of stress on nucleation rate has received relatively little attention. This is partly due to the misleading results obtained by optical metallography, comparing specimens that have undergone constant strain at a variety of stresses (Dyson and McLean, 1972). At high stresses cavities will have had insufficient time to grow to a size resolvable by optical microscopy and at lower stresses cavities

consequently seem more numerous. Results obtained by Cane and Greenwood (1975) by scanning electron microscopy of fracture surfaces in α iron showed that at constant strain and temperature, the number of cavities was proportional to the square of the stress Considerable support for this relationship has been derived from density measurements (Equation 20) on Cu, as reported by Greenwood (1973) who arrived at a relationship for nucleation of the form :

$$N \alpha \sigma^2 \varepsilon \quad \text{.....(37)}$$

Where N is the number of cavities.

3.3 Growth of Creep Cavities

There has been a great deal of discussion over recent years on the possible processes that contribute to cavity growth, and major reviews (Taplin, 1973; Perry, 1974) have attempted, with limited success, to draw some conclusions from the wealth of experimental observations. The major difficulty appears to be deciding to what extent diffusive processes contribute to the growth of intergranular creep damage, compared to growth controlled directly or indirectly by the overall plastic deformation. Previously (Section 3.1) the influence of the variable parameters on the nature and extent of creep damage was outlined and it can be seen that observations on different materials, and indeed the same material, are open to a variety of interpretations that favour either vacancy or deformation controlled growth. Another major problem is encountered when efforts are made to verify the various growth rate laws, as cavity lifetimes cannot be individually determined; although many workers feel that observations on cavities in the largest size group are most likely to be free from criticism, since they would have the highest proba-

bility of being created at the start of creep life.

As mentioned at the beginning of this chapter, conditions are often such as to favour the growth of creep damage by a particular controlling mechanism. An attempt to categorize behaviour in the different regimes of stress and temperature has been made by Ashby (1975) who has constructed "fracture maps" for a number of pure metals. Here, various fields are delineated in which a given mode of fracture is dominant and superimposed on them, contours of constant time-to-rupture.

3.3.1. Diffusional Growth Theories

Greenwood (1952) first proposed that cavity growth could occur by vacancy aggregation and Balluffi and Seigle (1957) calculated the conditions that would enable cavity nuclei of a suitable size (Section 3.2.1.) to grow. The latter showed that the criterion for growth required that vacancy concentration at the grain boundary should exceed that at the cavity surface.

Hull and Rimmer (1959) proposed the first quantitative theory of void growth by diffusive transport by considering an array of spherical voids, where the diffusive flux is driven by a gradient of chemical potential, proportional to the gradient of normal traction acting across the interface at the grain boundary. Since then the analysis has been refined by a number of workers to account for continuous nucleation (Greenwood, 1963) and the effect of the ratio of cavity radius to spacing (r/x) (Speight and Harris, 1967; Weertman, 1973; Speight & Beere, 1975). In all cases the cavity growth rate can be expressed by a relationship of the general form Greenwood, 1977):

$$dv/dt = fD_B \delta_z [\sigma - P - (2\gamma_s/r)] \Omega/kT \quad \text{.....(38)}$$

Where f is a function of r/x, D_B is the grain boundary self diffusion coefficient, δ_z is the grain boundary width, Ω is the atomic volume, σ is the tensile creep stress, P is the superimposed hydrostatic pressure and γ_s is the surface free energy.

Considerable attention is now being focussed on the various constraints that might affect diffusional growth models when applied to more complex creep resistant alloys. In the regime where cavity growth by vacancy accretion is most likely to occur, grain boundary diffusion often predominates over that of lattice diffusion (Raj and Ashby, 1975). Previously (Section 2.1.3.1.) it has been mentioned that the nature of grain boundaries (the presence of precipitate particles, impurities and grain size) and their ability to act as a vacancy source and sink was reflected in the diffusive creep rate, it is thus reasonable to assume that these microstructural parameters will have a similar influence on the diffusional growth of cavities (Greenwood, 1977).

Dyson (1976) has also suggested the possibility that, because in most creep resistant materials cavities are not homogeneously distributed amongst grain boundaries, geometrical constraints would require matrix deformation in adjacent grains to accommodate cavity growth. For unconstrained cavity growth the growth rate is proportional to the maximum principal stress (Equation 38), in the constrained situation; where growth is controlled by deformation rate, Dyson showed that the growth rate would be proportional to some power of the octahedral shear stress. The author further points out that this can lead to an attenuation of cavity growth rate, especially in high strength alloys under low stresses, that would considerably alter predicted creep life and ductility.

During the later stages of creep, and particularly at higher

stresses, cavities with a dendritic morphology have been observed in the boundary plane (Section 3.1.1.2.) Many workers have seen this as a clear indication of deformation controlled growth (Davies and Williams, 1969). However, recent work by Fields (1977) has suggested that this form of instability is due to perturbations in the void periphery. Comparing the situation to the growth of dendrites during solidification, it is shown that less diffusive work is done in advancing a "finger-like" crack front than a straight one.

3.3.2. Models Based on Deformation Mechanisms

Here, deformation is considered to be either directly responsible for the growth of intergranular damage or by generating vacancies for the growth of cavities to continue.

The proposal that a cavity can behave as a shear crack and grow by grain boundary sliding has been suggested by several workers (Gifkins, 1956; Chen and Machlin 1956; Evans, 1969). A quantitative theory has been put forward by Evans (1971) who proposed that sliding cannot occur without concurrent growth, a condition which allows the shear stress acting on a boundary to do work in opening up the cavity. He further showed that an expression for the rate of change of cavity length with sliding displacement would predict a two stage growth process. Throughout most of creep life the rate of growth would be proportional to the sliding rate, when the cavity reached a sufficient size the normal stress would contribute to growth and cavity size increase continuously with sliding displacement. This model is able to predict a number of experimental observations, including the inhibiting effect of hydrostatic pressure.

Williams (1967a) proposed a model for the growth of wedge type cavities at triple points based on the double shear model of Cottrell

(1958), where discrete dislocations are replaced by a continuous distribution of infinitesimal dislocations which simulate grain boundary sliding.

Hancock (1976) has put forward a growth mechanism similar to that operating during low temperature ductile failure. The author demonstrates that viscous flow will dominate any diffusional growth process at large hole sizes and low values of $\sigma/\dot{\varepsilon}$ ratio. Such conditions occur during tertiary creep where sliding boundaries produce regions of high local strain rates, especially when the specimen necks. Formalizing hole growth in this manner reconciles the problems associated with other treatments involving grain boundary sliding, such as that by Evans (1971) quoted earlier, where it is assumed that the initial cavity growth rate is sufficient to overcome the sintering tendency due to diffusion. If the local shear strain rate on the boundary is high enough, Hancock shows that hole growth due to grain boundary sliding can be sufficient to overcome the sintering tendency. Another important aspect of viscous flow cavity growth mentioned in this paper is the behaviour of cavities in regions involving multi-axial stress states as experienced in the region of a notch or specimen neck in tertiary creep. Hancock points out the diffusional hole growth is determined by the magnitude of the maximum principle stress (Section 3.3.1.) whilst viscous hole growth depends on the ratio of the maximum principal stress to the effective stress. This implies, in regions of stress and strain concentration, growth will be dominated by viscous flow with holes tending to grow in the direction of the tensile stress. This could have some important connotations on the mechanism of final fracture which must be considered when attempting to predict remaining creep life (Chapter 4).

One of Greenwood's (1952a) original proposals was that cavities could grow by the aggregation of lattice vacancies which were formed as a result of dislocation interactions with grain boundaries. Several other mechanisms have been proposed since, where cavity growth is controlled by the generation of vacancies formed as a direct result of plastic deformation. Ishida and McLean(1967) considered the slip movements of intergranular dislocations which were presumed to cause grain boundary sliding (Section 2.4.1.). Movement could only occur by a combination of glide and climb, and the vacancies emitted by the latter process migrated to the growing cavity. In addition, the dislocation exerted a force on the growing cavity, tending to open it and prevent sintering. McLean (1971) extended this model to the two dimensional case to show that the degree of sliding depended not only on the orientation of the boundaries to the applied stress but also the orientation of the principal slip planes to the boundary. Consequently, the author predicted a wide variation in the number of cavities on boundaries at a given angle to the applied stress, a phenomenon that is being increasingly observed experimentally (Section 3.2.3.)

CHAPTER 4

CREEP DAMAGE IN LOW ALLOY FERRITIC STEELS

Although there has been surprisingly little documentation of the metallography of creep damage in low alloy ferritic steels, much effort has been placed over many years in attempts to relate embrittlement, exhibited by a loss of rupture ductility with decreasing stress, to the parameters of initial structure, solute additions, impurity content, reactions occurring during deformation and the effect of complex stress systems. Recent studies on the accumulation of creep damage have attempted to relate creep behaviour, essentially controlled by prior heat treatment (Section 2.3), to both time-dependent (diffusion) and deformation-dependent (matrix and grain-boundary slip) processes of cavity nucleation and growth (Chapter 3).

4.1. Metallography of Creep Damage

In low alloy ferritic steels, interpretation of creep damage is complicated by the often poor definition of the grain boundaries, and the tendency for any significant damage resolvable by optical microscopy to be present only adjacent to the fracture, where the hydrostatic stress in the neck contributes to the opening of grain boundary cavities. The fact that damage is difficult to detect and the need for careful metallography was demonstrated by Day (1965) in his work on 1Cr ½ Mo steel, the author was unable to detect any damage by standard metallographic techniques until well into the

tertiary regime, even though density changes were recorded prior to the onset of tertiary creep. Goldhoff and Beattie (1965), investigating the fracture mode of a 1Cr 1¼Mo ¼V steel noticed a change in intergranular damage from rounded cavities to elongated cracks as the stress was raised, suggesting a Stroh-McLean type transition. However, closer examination of the cracks using optical microscopy revealed surface irregularities suggestive of coalescence of several r type cavities. This observation was confirmed by the contemporary work of Stone and Murray (1965) on the same material, who recorded that the major damage mechanism appeared to be cavitation and that no triple point cracking was observed.

Boniszweski and Eaton (1969) employed the technique of electron fractography to observe the creep damage and reheat cracks that occurred in the heat-affected zone of a ½Cr ½Mo ¼V steel weldment. The surfaces of these cracks, that ran along prior austenite grain boundaries, were observed by transmission electron microscopy of carbon extraction replicas. Cavities appeared to be polyhedral with both triangular and hexagonal bases, and were invariably associated with particles of V_4 C_3 of 200 - 600Å in diameter. The growth of cavities was revealed by an increasing coverage of grain surfaces to form a cellular pattern and in some areas linking of adjacent cavities produced a maze-like pattern. In this instance cavities still preserved their original shape and the dendritic morphology was not attributed to the growth of individual cavities (c.f. Section 3.1.1.2). These larger voids also exhibited terraces and striations due to thermal faceting, a phenomenon exclusively associated with creep cavities (Olney and Smith, 1959). The surface of continuous cracks revealed sharp undulations and corrugations in the thermal

faceting which indicated the presence of prior creep cavities. From this the authors suggested that the transition to continuous cracking was the result of the linkage of adjacent cavities aided by considerable surface diffusion. This effect was confirmed by the later studies of Burns et al (1973), on the smoothing of creep fracture surfaces by surface self-diffusion, in a similar material.

Later work by Tipler et al (1970) on a ½Cr ½Mo ¼V steel with a similar bainitic structure, employed scanning electron microscopy of cavitated prior austenite grain boundaries exposed by fracture in liquid nitrogen. This study confirmed much of the earlier work, in that discrete cavities were observed after creep failure and were associated with one or more carbide particles. The technique employed also enabled examination of specimens interrupted during creep and comparison with those taken to rupture. The authors found that in the former fewer grains were cavitated and cavities were more widely spaced, and in the latter boundaries at all stages of cavitation were observed with some faces completely covered by a "honeycomb" network of cavities. The work also showed that very few cavitated grain faces were normal to the principal stress as observations on longitudinal sections had previously shown.

A parallel study on fracture initiation in a 2¼Cr 1Mo steel by Cane (1976) employed complimentary observations by scanning and transmission microscopy of cavitated prior austenite grain boundaries exposed by fracture at - 196^{o}C. Cane pointed out that the incidence of cavities was sensitive to the site location on individual grain facets. Facet edges and corners were found to be particularly prone to enhanced cavity nucleation and growth. Carbon extraction replicas of cavities in these regions showed that not all were associated with

coarse grain boundary particles of $M_{23}C_6$ as had been observed elsewhere on the grain facet.

4.2. Factors Affecting Creep Rupture

Considerable attention has recently been paid to the elevated temperature fracture of low alloy steels of the Cr Mo V and 2¼Cr Mo types. A number of workers have studied the propagation of single cracks using various fracture mechanics parameters to characterize the rate of crack propagation (Neate and Siverns, 1974; Pilkington et al 1974; Gooch, 1977). Others have considered the fracture of smooth bar tensile creep specimens as a function of both stress and microstructure, which in turn is directly attributed to the heat treatment path which the material has undergone (Murphy and Branch, 1969; Tipler et al, 1975; Tipler and Hopkins, 1976; Dunlop and Honeycombe, 1977). The linking factor in all of this work is the fact that fracture is intergranular in nature and is highly dependent upon the microstructural condition of the steel in question.

4.2.1. Effect of Initial Structure

An inherent property of creep resistant low alloy steels is that they are transformable and their detailed microstructures depend strongly upon the manner in which transformation from austenite occurs. Depending on cooling rate the resultant primary transformation product may be ferrite, bainite or martensite, this range of microstructures may be further altered by subsequent tempering.

Early investigations into the effect of transformation product on creep ductility came to the conclusion that ferritic microstructures were more ductile than those of a bainitic or martensitic nature

(Woodford and Goldhoff 1969-70). Nevertheless, Murphy and Branch (1969) have shown in 1Cr Mo V steels, heat-treated to give mixed ferrite/bainite microstructures with bainite contents in the range of 4 - 40%, that ductility does not vary significantly with bainite content. A recent article by Dunlop and Honeycombe (1977) attempts to relate creep strength, as determined by transformation products and subsequent tempering, to ductility in a ½ Cr Mo V steel. A range of homogeneous transformation microstructures were produced by isothermal transformation and in general it was found that creep ductility increased with decreasing creep strength. However, the authors also revealed that reduction in area results showed a considerable variation from this trend and this they related to small differences in the fracture process. For ferritic specimens the reduction in area (R.A.) decreased with decreasing transformation temperature, cavitation damage occurring at ferrite grain boundaries; here, the authors suggest, fracture ductility is strongly dependent on the matrix strength which increases as the transformation temperature is lowered. A sharp increase in R.A. was observed as the transformation moved into the bainitic range and this was clearly seen to be due to the morphology of the intergranular crack path, which ran along an uneven rim of ferrite at the prior austenite grain boundaries. It was proposed that this led to a decrease in the extent of intergranular damage and therefore the amount of plastic deformation prior to fracture increased. This theory is supported by the measurements of the growth rates of macroscopic creep cracks in similar microstructures by Gooch (1977) who showed that there was a general decrease in crack growth rates with increasing ferrite contents in otherwise bainitic microstructures. Bainites produced at lower isothermal transformation temperatures produced damage along straight clean prior austenite grain boundaries

and as a result R.A. decreased again as the transformation temperature was lowered and matrix strength increased.

The connexion between rupture ductility, matrix strength and the propensity to cavitation has been investigated by Tipler et al (1975) in ½Cr Mo V and 1Cr Mo V steels. Longitudinal sections of specimens were assessed for the extent of damage during creep life by optical microscopy. The method of observation was designed to give a reproducable level of detection and since the number of cavitated boundaries were counted and not the total extent of creep damage, results reflected differences in the nucleation characteristics in the variety of transformation microstructures produced by prior heat treatment. In both steels the strain prior to the onset of cavitation increased linearly with rupture ductility which implied that strain contributed more significantly than time-dependent processes to the initiation of cavities. This strain was found to be as low as 0.1% for material that had been austenitized at very high temperatures to produce a fully bainitic structure with a large prior austenite grain size, simulating the heat affected zone of weldments. For structures with a high rupture ductility such as ferrite-pearlite mixtures, cavitation was not observed until the tertiary stage of creep had been reached. The authors further indicated that for all conditions of heat treatment, the higher creep rates were associated with increased accumulation of strain prior to the formation of detectable cavities. They suggested that the above two factors related to the capacity of material to deform without imposing high local stresses at the grain boundaries which gave resistance to cavitation. The austenitizing temperature was also found to have a significant effect in that the onset of observed cavitation was delayed at lower austenitizing temperatures i.e. as the creep strength decreased.

4.2.2. Effect of Impurities and Solute Additions

Creep tests on low alloy ferritic steels frequently show ductility minima associated with corresponding strength maxima which are dependent on the presence of specific alloying elements. There is considerable justification for believing that strain-aging type reactions or strain induced precipitation are responsible for these effects as described in Section 2.3. The effect of composition on ductility in Cr Mo V steels was reviewed by Stone and Murray (1965), in the same article they reported some interesting results produced by additions of Ce, Ti and B, and Zr and B. Ce had a beneficial effect on ductility and reduced rupture strength and this was related to the development of precipitate free zones adjacent to the prior austenite grain boundaries (Section 4.2.3). Additions of Ti and B and Zr and B improved ductility without improving creep strength and there was little denudation adjacent to the grain boundaries. The authors postulated that in this case Ti, Zr and B would affect the cavitation process by inhibiting the migration of vacancies to voids and thus retarding growth.

The effect of composition on rupture ductility in steels with similar creep strengths can be quite marked. Tipler et al (1975) reported the increased strain required for the appearance of cavitation in a ½ Cr Mo V steel compared with that recorded for a 1Cr Mo V steel, irrespective of their ductility. A similar observation was made by Viswanathan (1975) who showed that despite a higher tensile and creep strength, a Cr Mo V steel had superior rupture ductility relative to a Cr Mo steel. There is general agreement that these effects are due to differences in the nucleation and growth characteristics of cavities in these alloys most likely determined by the influence of precipitates, this will be discussed later (Section 4.2.4).

Information relating to the effect of impurities on creep and rupture strength is meagre and conflicting. The results of Hopkins et al (1971) show that in Cr Mo V steels, the presence of impurities markedly impairs both creep life and rupture ductility. A similar effect of Al was reported for Cr Mo steels by Trumpler (1967) and by the work of Ratliff and Brown (1967) on Cr Mo V steels. Bentley (1966-68) demonstrated that in Cr Mo V steels, Cu and Sn increased the susceptibility to creep rupture at prior austenite grain boundaries, without measurable intragranular hardening.. Bruscato's results (1970) on a 2¼ Cr Mo steel indicated no effect on ductility at lower temperatures and a drastic reduction in ductility due to impurities at higher temperatures. In a recent paper by Viswanathan (1975) the effect of large additions of Sb, P and Sn on the creep properties of Cr Mo steels were reported. Results showed that the addition of these impurity elements did not modify the creep strength or ductility of the steels. Previous studies by the same author (Viswanathan, 1974) had revealed that large changes in toughness were brought about by an embrittling treatment of similar steels doped with the same impurities, which suggested that the role of impurity elements may be different in creep and temper embrittlement. However, Wolstenholme (1976) has provided strong evidence to show that P segregates to prior austenite grain boundaries in a 2¼ Cr Mo steel and leads to both temper embrittlement revealed by impact tests and also promotes cavitation and accelerated strain to failure in creep tests. It was reasoned that this was due to the increased number of voids nucleated per unit strain by the lowering of the interfacial energy in the presence of a high P concentration (Section 3.2.2.)

The effect of impurity levels on the cavitation characteristics

in a variety of Cr Mo V steels with a simulated weld heat-affected zone structure, has been investigated by Tipler and Hopkins (1976). It was shown that a reduction in the amount of trace elements had a significant effect in reducing the propensity to cavitation. In the high-purity steels the time and strain for the onset of cavitation were found to be greater than in the commercial purity steels, and the rate of formation of cavities was less by one to two orders of magnitude for similar creep strengths. The authors again explained the results in terms of segregation of impurities to grain boundaries, reducing interfacial energies, and allowing a smaller stable cavity size in the "impure steel" (Equation 28). Cavities would thus be expected to nucleate at a lower threshold time or strain and also nucleate at a higher rate than in steel with a lower level of segregating impurities. These results have been subsequently confirmed by the recent work of Myers and Price (1977) on the stress relief cracking of weld heat-affected zones in 2Cr Mo and ½ Cr Mo V steels, they also confirmed that 2Cr-Mo steels were more tolerant to the presence of impurities.

4.2.3. Effect of Prestrain and Complex Stresses

Information concerning the effect of these two parameters on the rupture ductility of low alloy ferritic steels is extremely limited and their influence on damage characteristics is non-existant.

Yeldham and Brook (1974) have published a short technical note referring to the effect of prestrain on the stress-rupture properties of a 2¼Cr Mo steel. It was found that the high rupture ductility of the steel was not significantly affected by the prestrain, the principal effect of the latter was to increase the rupture life.

Hardness measurements indicated that stress-accelerated recovery occurred in the prestrained material which enabled it to withstand considerable deformation without detriment to its performance at a high service temperature. This was confirmed by the transgranular fracture mode with no evidence of cavitation or triple-point crack formation.

The notch sensitivity of low alloy ferritic steels has been investigated by Goldhoff and Brothers (1968) who related crack initiation and propagation in a Cr Mo V steel to smooth bar ductility with bar section size and notch geometry as variables. The work suggested that the mode of initiation and rate of damage growth in material heat treated to give a high ductility depended on shear processes, under these circumstances notch strengthening was observed (c.f. Section 3.1.2.2.). For material heat treated to give a brittle matrix, however, the maximum principal stress was found to control the failure with intergranular damage growth limiting creep life and the ratio of notched strength to smooth bar strength generally being less than unity. An interesting observation was made by Tipler et al (1975) in their study of Cr Mo V steel mentioned earlier. Steels heat-treated to a brittle condition were found to be prone to the stress concentration of fiducial pop marks on the specimen shanks where more cavitated boundaries were observed than elsewhere in the guage length, implying that stress state has some influence on cavity nucleation characteristics in these materials (c.f. Section 3.1.2.2.).

4.3. Cavity Nucleation Mechanisms

Several workers have observed the presence of grain boundaries depleted of fine precipitate after creep testing (Stone and Murray

1965; Tipler et al 1975), this is especially true for material austenitized at high temperatures followed by tempering. In his work on 2¼Cr Mo steel, Cane (1976) reported the preferred growth of $M_{23}C_6$ on prior austenite grain boundaries, at the expense of Mo_2C during tempering and subsequent creep to rupture, resulting in local denudation of Mo_2C within the matrix and precipitate-free zones (PFZ's) forming at prior austenite grain boundaries. The author produced results to show that cavity density (number per unit area) was inversely related to PFZ width, implying that wide PFZ's conferred the ability of accommodating local stress concentrations (Section 2.4.2.) and inhibiting cavity nucleation (Section 3.2.1.)

Cane invoked Ashby's model (1966) for cavity nucleation at a hard particle/ductile matrix interface, similar to this situation. Here, the stress concentration existing at the interface is produced by the impedence of glide of prismatic vacancy loops, generated by recovery of primary slip tensile stresses set up at the interface, by precipitates at the edge of the PFZ. Cane demonstrated that stress concentrations could be generated by boundaries under tension as well as under shear and that decohesion occurs when the stress concentration, σ_c, equals the cohesive strength of the particle/matrix interface. The magnitude of σ_c is given by :

$$\sigma_c \alpha urx/bz^2 \qquad \text{.....(39)}$$

Where u is the plastic displacement at the particle / matrix interface, r is a geometrical factor, x is the particle diameter, b is the Burger's vector of the loops' glide plane, z is the PFZ width.

The author showed that this approach was consistent with a number of observations. It explained the inverse relationship between

PFZ and cavity density and demonstrated clearly that large particles act as more favourable cavity nuclei than do small. The selective nature of cavity formation on individual grain facets (Section 4.1.) could be explained in terms of the inhomogeneous strains within PFZ's due to variations in width and the non-uniform stresses during the relative translation of adjacent grains. Further, since stress concentrations may be induced on boundaries under tension as well as those under shear by this mechanism, this accounted for the observations that cavitated grain facets, exposed by low temperature fracture, were rarely normal to the applied tensile stress (Section 4.1.)

Beckitt et al (1968) investigating the rupture ductility of ½ Mo steels, associated Mo_2C grain boundary precipitates with low ductility and the onset of void type cavitation. In their work, they revealed that the misfit between Mo_2C and ferrite was much greater than that for the other grain boundary carbides (Fe_3C and $M_{23}C_6$). They proposed a model, involving interface dislocations, which could accommodate the misfit, and in so doing, nucleate voids. It was postulated that stress concentrations at the interface, produced by sliding, would cause the coherency dislocations to move along their slip plane producing a displacement in the matrix at the end of the precipitate. The continuous generation of interface dislocations by sliding, was thought to be sufficient to form a stable cavity nucleus. A similar conclusion was drawn by Swift and Rodgers (1973) in their studies on embrittlement in 2¼Cr Mo steels by post weld heat treatment.

Boniszewski and Eaton (1969), in their work on Cr Mo V steels, found that at low stresses heterogeneous nucleation of cavities at V_4C_3 particles, of approximately 300Å in diameter, predominated; as predicted by the theory of Smith and Barnby (Section 3.2.1.). However,

they also suggested the importance of the "physiochemical factor" associated with nucleation at particles. They pointed out that at low temperatures the degree of solid solution was likely to be low because of precipitation. With increasing temperature, precipitates would begin to dissolve and solute to concentrate at the grain boundaries. As discussed previously (Section 3.2.2.) such segregation is conducive to cavity nucleation and might explain the differences in behaviour exhibited by low alloy ferritic steels with different compositions (Section 4.2.2.)

CHAPTER 5

CREEP LIFE AND FRACTURE

Early work on creep life prediction involved extrapolation techniques applied to data obtained from short term creep tests. Here, only macroscopic behaviour was considered and parametric plots were produced by determining the stress and temperature dependences of rupture life. However, it was soon realized that this technique, based on arbitary relationships, had serious shortcomings in that it did not account for any of the mechanistic changes occurring in the mode of deformation and damage accumulation.

Attention was then turned to the later stages of creep life and observations on the state of damage in this regime convinced many workers that the final fracture mechanism was of considerable importance in determining creep life. Several models for predicting life have been developed, involving the interelationship between the macroscopic parameters of the onset of tertiary creep, secondary creep rates and creep ductility and the various types of failure mechanism.

In cases where the processes of nucleation and growth of damage, to the stage of link-up, have been observed to occupy a major part of creep life, another avenue of approach is afforded. It has been demonstrated that by integrating the nucleation and growth rates, a phenomenonological damage parameter may be invoked to predict rupture life. This technique has been conveniently extended to include the effect of complex stress systems and variable conditions of stress and

temperature on rupture life.

5.1. Fracture Mechanisms

The mode of final failure is strongly dependent on testing conditions and material parameters and the mechanism by which inter-granular cavities are linked to produce decohesion that is often the rate controlling process in establishing models for creep life prediction.

5.1.1. General Observations

The mechanism by which cavities link up to produce grain boundary decohesion is often revealed by observing the nature and extent of creep damage in specimens taken to rupture. Early work by Rogers (1959) on Cu, indicated that the area between voids necked and fractured locally in a ductile manner, provided that the metal did not work harden too much. This is termed the void sheet mechanism and has been observed in Cr Mo V steels by Tipler et al (1970), who found crack linkage with very little coalescence; the resulting fracture surface had a honeycomb structure produced by the necking of inter-cavity ligaments.

However, Needham and his co-workers (1975) demonstrated that in Cu and Mg, cavity shape was retained almost up to the point when fracture occurred; implying that, in these materials at least, cracking of the grain boundary area between cavities was a difficult process and that separation at grain boundaries must depend on cavities growing sufficiently large that they coalesce.

Other workers have considered that cavities interlink across a grain boundary to produce a crack that propogates through the

material, once a suitable fracture criterion has been achieved. This is usually the ease of propagation of a single fatal crack of the Griffith-Orowan type (Taplin, 1965). In their work on Brass and Cu, Taplin and Barker (1966) concluded that mechanical tearing due to stress concentrations at cavity apices and concomitant grain boundary sliding was responsible for inter-linkage.

It is not always appropriate to assume that, when cavities on any one grain boundary link completely together, fracture automatically and immediately results. There is much evidence to suggest that even heavily cavitated material may possess a large measure of ductility; superplastic behaviour in ultrafine grain material has been observed despite the existance of intergranular damage throughout most of the deformation process (Taplin, 1973). This effect might be attributed to the viscous growth of cavities in the direction of the tensile stress (Section 3.3.2.) preventing the formation of cracks in a perpendicular plane.

5.1.2. Effect of Grain Size

Grain size has been found to have a significant influence on the mechanism of fracture and the mode in which damage is aggregated on grain boundaries. It is also a useful parameter with which apparent differences in observed fracture behaviour in the same materials can be reconciled.

The aspect has been studied in some detail by Taplin and his co-workers, who recognized the interaction, between cavity groups on different boundaries, that was necessary for the production of a crack capable of propagation. Working with Cu, Fleck et al (1970) showed that in coarse grained material, failure was a question of critical crack length; whilst in fine grained material, such a

critical crack could not be formed on the given grain edges because they were too short. In the latter case failure occurred by the ductile sheet mechanism. In a later article, Taplin (1970) remarked that the interlinkage of multiple-facet cracks would be impeded by triple junctions; a view confirmed in later work on an Inconel superalloy by Venkiteswaran and Taplin (1974). Here, an increase in rupture ductility and failure time was observed as the grain size decreased, attributable to the larger number of triple junctions that limited crack propagation.

This effect has been observed in low alloy ferritic steels. Dunlop and Honeycombe (1977) disclosed that close to the fracture surface, cavities were seen to have interlinked to form cracks which often occupied whole prior-austenite grain boundaries. These cracks appeared to be barred from further propagation at triple junctions. Tait and Knott (1976) reported an increase rupture ductility with decreasing grain size in a ½Cr Mo V steel, the authors attributed this to the inability of cracks on certain grain facets to satisfy the Griffith criterion and therefore "run" at low stresses.

5.1.3. Tertiary Creep

The onset of tertiary creep and the strain/time relationship in this regime have been the subject of a number of studies in attempts to relate fracture mechanisms to this stage of accelerating creep.

Kramer and Machlin (1958) first suggested that when voids had achieved a critical size, tertiary creep began and fracture processes became significant. Davies and Dennison (1959-60) experimenting with sintered nickel alloy powders found that pre-existing voids drained off excess vacancies causing an increase in creep rate, implying that the onset of tertiary creep was the direct result of the existence of voids on the grain boundary. Later work by Davies and Dutton (1967)

and Davies and Evans (1965) confirmed this and further showed that tertiary creep was associated with an increased rate of recovery (caused by the presence of cavities) and not a change in work hardening. Dyson and McLean (1977) have also commented upon the autocalalytic nature of tertiary creep, in that strain generates cavities which in turn would promote recovery (by coarsening dislocation networks) and lead to further strain. Ratcliffe and Greenwood (1965) found that the rate of change of density in magnesium increased just before fracture reflecting that grain boundary cavities coalesced to produce decohesion rather than linked together by cracking.

Davies and Williams (1969b), investigating the behaviour of Cu, showed that the beginning of true tertiary creep occupied a transitional period during which the time dependence was of the form $t^{4/3}$, true tertiary was achieved when an exponential type of behaviour was observed. The authors attributed this transition to the presence of an array of cavity sizes at the beginning of tertiary creep, and that those below a critical size would not contribute to the increase in strain rate. The implications this would have on the fracture mechanism remained unclear. The strain/time curve generated by the diffusive growth of voids and their coalescence at fracture has been evaluated theoretically by Harris et al (1974). They demonstrate that the tertiary creep rate is strongly dependent on the initial void spacing and the increase in stress across a normal grain boundary, due to the decrease in load bearing area during the fracture process. The authors point out that this could have important consequences when employing extrapolation techniques on lightly stressed components.

The effect of grain size on the onset of tertiary creep has been studied by Wilshire (1970), who found that the onset of tertiary and the secondary creep rate both varied in the same manner with grain size. He concluded that the same mechanism, of grain boundary sliding controlled both cavity growth and their interlinkage to produce fracture. Venkiteswaran and Taplin (1974) observed an extended tertiary creep stage in an Inconel alloy as the grain size was decreased, attributed to the presence of a larger number of triple junctions that limited crack propagation.

5.2. Creep Life Prediction

For some time the expected lifetimes of components, operating within the creep range, were predicted using empirical or parametric relationships based on data from uniaxial stress rupture tests. With some understanding of the mechanisms of the nucleation, growth and interlinkage of damage to produce fracture, theoretical models have been derived to predict fracture in given regimes of stress and temperature. These models are based on the kinetics of the rate controlling process leading to fracture, considered to be either the growth of grain boundary damage or its interlinkage. In many cases, good agreement is obtained between the observed variables of stress, creep rate and time to fracture.

5.2.1. Parametric Plots

After realising that both tempering and creep obeyed the same rate-process theories of diffusion (Equation 2), Larson and Miller (1952) extended the original theory of Holloman and Jaffe (1945) for the time and temperature dependence of hardness. Thus, the

temperature dependence of rupture life could be described by the inverse of the creep rate temperature dependence, such that for constant stress :

$$t_f = A \exp (Qc/RT) \quad \ldots\ldots\ldots(40)$$

Where A is a constant and Qc is the activation energy for creep deformation. For a given stress, Equation 40 can be reduced to :

$$T(C + \log t_f) = Qc/2.3R = \text{constant} \quad \ldots\ldots\ldots(41)$$

Where C = log A, T is the temperature in degrees absolute, and tf is the rupture life in hours. Similarly :

$$T(C - \log r) = Qc/2.3R = \text{constant} \quad \ldots\ldots\ldots(42)$$

Where r is the secondary or minimum creep rate in % hr^{-1}. The value of C was found to be 20 for a wide range of materials and to be independent of stress. The authors attributed this number theoretically to the creep rate at infinite temperature (1/T = 0) where adjacent atoms separate at the speed of light. Using equations 41 and 42 it was demonstrated that master stress/rupture curves could be constructed from short term data and long time properties interpolated from these.

Since then, it has been recognized that such extrapolation techniques are limited to small ranges of stress and temperature. This is not surprising, since equations 41 and 42 take no account of the mechanistic changes in creep deformation in the various regimes of stress and temperature, reflected in different values of Qc (Chapter 2). Further, it is debatable as to whether the value of Qc in equation 41 reflects the mode of creep deformation or that of

rupture processes, this will be discussed in Chapter 8.

Another means of data presentation often used is the Manson-Haferd approach (1953), in which extrapolation of test data relies on linearity of iso-stress, temperature vs. log-time plots. Whilst still subject to the same restrictions as the Larson-Miller parameter, this method has been considered preferable, since creep rupture processes are less sensitive to temperature excursions than to stress excursions utilised on the Larson-Miller plots.

5.2.2. Empirical Relationships

In the power law creep regime the rupture time is often found to be proportional to the reciprocal of the stress raised to a large power:

$$t_f \alpha 1/\sigma^m \qquad \ldots\ldots\ldots(43)$$

The power law exponents for rupture, m, is often very close to that for creep (Equation 1), suggesting to many workers that the creep and fracture process are closely linked. In a series of torsion and tension tests on a Nimonic alloy, Dyson and McLean (1977) showed that both sets of data could be represented at low stresses by:

$$t_f \alpha 1/\sigma_i^2 \qquad \ldots\ldots\ldots(44)$$

Where σ_1 is the maximum principal stress. At higher stresses, the empirical relationship was :

$$t_f \alpha 1/[(\bar{\sigma})^{2\cdot5}\sigma_1]^2 \qquad \ldots\ldots\ldots(45)$$

Thus, at fast creep rates, fracture life is governed by the magnitude of the effective stress $\bar{\sigma}$. The authors argued that this empirical

relationship could be understood in terms of the influence of the stress system on the mode of deformation and the resultant mechanisms of damage nucleation and growth (Section 3.1.2.2.) At low stresses, diffusive cavity growth and coalescence occurs, governed by σ_1. At high stresses deformation processes are important for both cavity growth and interlinkage (Section 5.1.1.). Consequently fracture life is governed by some measure of the shear effort represented by $\bar{\sigma}$.

The observation that creep and fracture processes were closely linked, was first made by Monkman and Grant (1956). They showed that the creep rupture properties of a wide variety of metals and alloys could be described by :

$$\dot{\varepsilon}_s \, t_f = C_{M-G} \qquad \ldots\ldots\ldots(46)$$

Where C_{M-G} is the Monkman-Grant constant for a given alloy. This relationship has since been verified by a large body of data (Davies and Wilshire, 1962; Dobes and Milicka, 1976) and is now a widely accepted empirical rule. Viswanathan (1974) reviewing the creep properties of a wide range of 2¼Cr Mo steels, found that for a given steel $\dot{\varepsilon}_s \times t_f$ had a constant value of 4.4 independent of strength and testing temperature. If this relation were strictly correct, the steady state creep stage would dominate the creep process (primary and tertiary stages would be negligible) and the Monkman-Grant constant would correspond to the creep ductility. A number of models have been suggested (Section 5.2.3.), where intercrystalline failure is controlled by either diffusive or mechanical mechanisms, that are consistent with this relation.

In fact, deviations from Equation 46 are observed, especially in alloys where tertiary creep constitutes a large proportion of

the total creep life. This was found to be the case in an Inconel alloy, investigated by Venkiteswaran and Taplin (1974) where an extensive teritary creep stage was observed. The authors suggested that in this case fracture life was a function of the ease of linkage and propagation of grain boundary cracks and hence not related to the creep deformation process and concomitant damage accumulation.

A relation to predict the time to fracture under variable conditions of stress and temperature was first developed by Robinson (1962) who stated that the creep damage under each set of conditions is proportional to the fraction of the total rupture life spent under those conditions, expressed thus:

$$\sum_{i=1}^{\nu} \Delta t_i / t_{f_i} = 1 \qquad \text{.....(47)}$$

Where Δt_i is the time spent at stress, σ, or temperature, T, t_{f_i} is the rupture time at σ or T and ν is the number of stress or temperature changes. This relationship has no fundamental basis since it assumes that the damage accumulated in a given period is independent of the previous periods under a different temperature or stress. Certain workers (Woodford, 1973; Hart, 1976) have shown that it may be used with reasonable reliability for temperature changes, but cannot be used for stress changes. This is an understandable result since the nucleation and growth of damage is far more sensitive to stress than temperature (Chapter 3).

5.2.3. Theoretical Models

Theoretical models attempt to relate the supposed mechanisms of cavity nucleation, growth and interlinkage with the observed empirical observations described in Section 5.2.2. The major dilemma involved

has been deciding the fracture criterion i.e. predicting the condition for the onset of rapid failure due to final crack propagation. Two schools of thought have emerged: those who believe that creep life is governed by the growth (either diffusional or mechanical) of grain boundary damage until coalescence results in the decohesion of a single grain boundary; those who support a fracture criterion based on linear fracture mechanics. Interpretations of the latter have varied from a "net section stress" approach where stress relaxation produces a constant stress across the boundaries, to the other extreme of a crtical stress intensity being achieved before crack extension can take place.

5.2.3.1. Models Based on Damage Coalescence

Greenwood (1973) has proposed a simple geometrical criterion for fracture involving the coalescence, by diffusional growth, of widely spaced individual cavities along a grain boundary, such that at fracture :

$$N_f^3 \, v_f^2 = F \qquad \text{.....(48)}$$

Where N_f and v_f are respectively the average number of cavities per unit area of grain boundary and the average cavity volume at fracture. F, is a dimensionless constant which must be exceeded before failure occurs. Using this criterion and the relationships for cavity nucleation and growth (equations 37 and 38), simple substitution reveals that for a power law stress exponent of 5, the time to fracture is given by :

$$t_f \propto 1/\sigma^{4.6} \qquad \text{.....(49)}$$

This relationship has been confirmed experimentally in a number of pure metals and alloys, where cavity nucleation and growth is observed to form the greater part of creep life: Woodford (1969) in Ni; Needham et al (1975) in Cu and Mg; Winzor (1975) in a Cu/Sb alloy. In a later paper (1977) by the same author, the theory has been extended to include the effects of both stress and temperature changes. This approach has been criticized by Taplin and his co-workers on a number of occasions (e.g. Venkiteswaran and Taplin, 1974) who argue that cavities do not grow by entirely diffusional processes and that fracture does not occur when cavities interlink on a single grain boundary facet.

Williams (1967) extended Cottrell's theory of cleavage crack nucleation (1958) to calculate the rate of growth of grain boundary wedge cracks. From this he derived an equation for creep life, using as his criterion that fracture occurred when the crack had grown to one grain diameter in length. Nix et al (1977) have recently produced an approximate treatment of cavity growth by plastic flow, which provided a basis for a model of intercrystalline creep fracture in the power law creep range. Extending the earlier work of Williams they have assumed that propagation of the crack, across a single grain facet, was controlled by the plastic growth of cavities and, as in diffusional growth, by the creep process itself. Using their theoretical model, the authors showed that the predicted dependence of rupture time on applied stress and grain size corresponded closely with experimental measurements for an austenitic stainless steel.

5.2.3.2. Models Based on Linear Fracture Mechanics

The observations, that the length of the longest crack is always

much smaller than the diameter of the sample in ruptured specimens, and the loud noise accompanying the fracture, have suggested to many that the final fracture is quite rapid and spontaneous. Consequently, there has been considerable interest in the behaviour of pre-cracked specimens in the creep regime and subsequent analysis using similar approaches to those for evaluating toughness at low temperatures.

Siverns and Price (1973) determined the rate of crack growth in single-edge notched specimens of 2¼Cr Mo steel at elevated temperatures, and showed that the growth rate and time to failure could be described in terms of the initial stress intensity factor due to a sharp crack. However, it has been argued that stress relaxation at the tip of a crack during creep would be difficult to calculate, thus rendering this approach less useful (Greenwood, 1977).

Venkiteswaran and Taplin (1974), investigating the creep fracture behaviour of an Inconel alloy, produced a quantitative criterion of failure, reflecting the ease of crack interlinkage and subsequent propagation, in terms of a creep fracture toughness parameter K_f. where:

$$K_f = \sigma_f (C_{AV})^{1/2} \qquad \ldots\ldots\ldots(50)$$

σ_f is the initial applied stress, C_{AV} is the average crack length and K_f is the fracture toughness parameter that is constant for a given material and microstructural condition. This criterion is a development of a theory due to Kachanov (discussed in Section 5.2.4.) whereby the net stress increases as the cross-sectional area is reduced by accumulation of damage and that neither cracks nor cavities give rise to any stress concentrations. The authors argue that since the average crack length also decreases with increasing creep stress

(Section 5.1.1.), a constant value of K_f is generated which could be related to rupture life (Fleck et al, 1976).

5.2.4. Phenomenological Constitutive Equations

Recently, considerable interest has been centred on developing the creep fracture theory of Kachanov (1961) who proposed a criterion based on the reduction in grain boundary area, due to damage accumulation, and consequent increase in the true applied stress and strain rate. The time to rupture could thus be described in terms of a single variable referred to as the damage parameter ω :

$$t_f = f\,(1/\dot{\omega}) \qquad \text{.....(51)}$$

ω has no true physical meaning, but is equal to unity at rupture. The theory also proposes that the rate of accumulation and the strain rate are interdependent and that the damage rate depends both on the stress state and the damage :

$$\dot{\varepsilon} = g(\sigma,\omega) \qquad \text{.....(52)}$$

and

$$\dot{\omega} = \eta(\sigma,\omega) \qquad \text{.....(53)}$$

In a recent paper, Leckie and Hayhurst (1977) have indicated how physical laws for creep fracture, based on damage nucleation and growth, may be converted into constitutive phenomenological equations by employing such a single state variable as the damage parameter ω. Utilizing the constitutive equations generated by Greenwood (1973) for rupture under variable stress and temperature, and those due to Dyson and McLean (1977) for stress state, the authors constructed an isochronous rupture surface. It was proposed that the form of such a surface would enable estimation of rupture life under conditions of both multiaxial stress and transient conditions of stress and temperature.

CHAPTER 6

EXPERIMENTAL PROCEDURE

6.1. Materials and Specimen Preparation

Two groups of low alloy ferritic steels were prepared for investigation: 2¼Cr 1 Mo and ½Cr ½ Mo ¼V. Depending on the degree of purity required, the materials were initially prepared by either vacuum or air melting. The composition of each alloy series is recorded in Table 1, and identified by code letters. Carbon analysis was undertaken using a conductimetric technique; Cr, Mo, V, Sn and N contents were assessed by chemical methods, and the wt% of the remaining elements quoted were determined on a spectographic quantometer.

6.1.1. Melting Practice and Extrusion

The majority of material used was prepared by vacuum melting, which allowed close control of alloy content and limited the take up of tramp elements. The base material of high purity Japanese Fe, together with the other major alloying elements of Cr, Mo, and V, were initially melted in an alumina crucible by induction heating in an argon atmosphere of 20cm. Once molten, the pressure was reduced to 3μm and the liquid alloy allowed to boil for 20 minutes; after which, argon was readmitted to give a pressure of 10cm, and the more volatile elements of Si, Mn and Sn added, if required. Three minutes

were then allowed for mixing before teeming into a steel mold.

As heavy shrinkage occurred on solidification, the piped material was removed (and sent for analysis) and the surface skimmed to give a 73mm diameter billet, suitable for extrusion. The billets were pre-heated for 2 hrs at 1170°C before extrusion in a 1000 tonne vertical extrusion press using a Fuminite/molybdenum sulphide-containing grease as a lubricant. Samples were cut from both ends and the middle of the 16 mm diameter extruded bar, to ensure that there was no segregation of alloying elements, especially carbon.

6.1.2. Heat Treatment

After extrusion, the bar produced was cut up into 8 cm lengths, a size suitable for specimen machining after heat treatment. Austenitization treatment was conveniently carried out in a gas curtained furnace, which produced a tolerable depth of decarburization. Temperatures were carefully monitored, throughout the heat treatment, by attaching thermocouples to the extruded bar sections.

6.1.2.1. 2¼Cr 1Mo Alloys

Both the high purity (CRM series) and the tin-doped alloys (CRMS series) underwent the same heat treatment process. The materials were initially austenitized for one hour at 1100°C and then furnace cooled to 950°C where they were held for a further hour, after which the materials were air cooled to room temperature. Subsequent tempering took place at 710°C for 16 hours, again followed by air cooling to room temperature.

This procedure produced a fully bainitic matrix as indicated in Figure 4. The prior austenite grain boundaries were revealed after careful etching in a 2% Nital solution, Figure 6, and the austenite

grain size of about 100μm was determined by a mean linear intercept method.

6.1.2.2. ½Cr ½Mo ¼V Alloy

This alloy (Series CRMV) underwent a careful heat treatment process designed to reproduce the microstructure, and particularly the prior austenite grain size, of an as-welded heat affected zone of a multipass manual metal arc weld bead. The heat input of this process, 1600 J mm^{-1} could be simulated by a single thermal cycle of rapid heating to a peak austenitizing temperature, followed by water cooling (Alberry, 1977). Specimens were introduced into a furnace held at 1306°C and heated for exactly 5 mins. 10 secs. to achieve a peak temperature of 1270°C (± 10°C) before cooling. Accurate temperature control was achieved by means of a calibrated Pt/Pt-13Rh thermocouple which was attached to the centre of each extruded bar section, with the joining effected by a capacitance discharge technique. Each specimen was individually heat-treated, the final part of a typical heating curve is reproduced in Figure 5.

To test the reproducability of the microstructure, several specimens were seletected for prior austenite grain size determination. A decoration technique (Alberry, 1977) was used to delineate those boundaries that were difficult to resolve in the entirely bainitic matrix (Figure 7). Small samples were removed from post heat-treated specimens and quickly heated to ∿ 805°C followed by water quenching. Austenite nucleated heterogeneously on the prior austenite grain boundaries and transformed to a darker etching fine grained bainite, (Figure 8). The grain size was found to be 170μm (± 15μm) in all specimens examined and also to be uniform throughout the bar sections that were heat treated.

6.1.3. Specimen Preparation

Standard creep rupture specimens of guage length 25.4 mm and 6.35 mm diameter with 9.53 mm ($\frac{3}{8}$") BSF threaded ends were machined from the extruded bar sections, after heat treatment (Figure 1(a)). The guage length was machined uniformly to within $\pm$ 0.025 mm and with as smooth a finish as possible. Notched specimens had a circumferential Bridgeman groove, of radius 1 mm, cut in the centre of the guage length (Figure 1(b)).

Prior to creep testing, four diamond indentations were made along the guage length, using a Vickers hardness machine (Figures 2(a) and 2(b)). Their initial spacing was measured to $\pm$ 20μm using a travelling microscope, thus measurement of creep strain could be made to an accuracy of $\pm$ 0.08%. In addition the guage width was determined with a micrometer and the minimum diameter across the notch throat again measured using the travelling microscope. These measurements provided post test reduction in area data as well as enabling the load to be calculated for the required stress. Finally, all specimens were degreased prior to insertion into the creep apparatus.

6.2. Creep Testing

Creep testing was carried out using a constant load, Dension type T47E creep machine (Figure 3(a)). Heating was provided by a 25cm, three zone nichrome wound furnace, controlled by a platinum resistance thermometer and saturable reactor. The temperature was monitored by tying two Pt/Pt-13%Rh. thermocouples to each end of the specimen guage length (Figure 3(c)). The temperature variation along the guage length was never greater than $1^{o}C$ and fluctuations around the required testing temperature were also of the order of $1^{o}C$.

All tests were carried out in an Ar/5% H_2 gas atmosphere, the specimen being wholly contained in a vacuum jacket, as shown in Figure 3(b). The jacket was evacuated and flushed with the gas mixture three times at room temperature, before the furnace was switched on. Throughout the test and subsequent cooling, the Ar/5% H_2 mixture was passed through continuously, at a pressure slightly greater than atmospheric, regulated by means of a needle valve arrangement shown in Figure 3(b). This procedure resulted in negligible tarnishing of the specimen during the test.

Before the application of the load, applied across a lever system giving a magnification of ten, the specimen was held for three hours at the required test temperature. This also allowed final adjustments to be made to the furnace controls. During the test, the strain rate was monitored by means of a calibrated dial guage, accurate to 2.5 x 10^{-3}mm., operated by the motion of the lever arm of the loading mechanism. When failure occurred the same lever arm activated a microswitch which stopped a digital clock in the control panel, providing a means of measuring the fracture life to an accuracy of 6 mins. After failure the furnace was switched off and the specimen allowed to cool, usually taking about 15 mins to reach 200^{o}C from a test temperature of 690^{o}C. Interrupted tests were also undertaken on specimens at some stage prior to failure, in which case, more rapid cooling under load was desirable to prevent the sintering of existing creep damage. If grain boundary sliding measurements were to be taken (Section 6.4.) the specimen was returned to the creep machine and heated to temperature under a reduced load, to compensate for the decrease in cross-sectional area which had occurred during the first period of creep deformation. This procedure was followed until failure occurred.

6.3. Tensile Testing

All tensile testing both at room and elevated temperatures was carried out on an Instron Universal Testing Machine at a constant cross-head speed of 0.05 mm/min. A load/elongation curve was automatically plotted during each test. Elevated temperatures were achieved using a similar furnace to that employed for creep testing (Section 6.2), however, no vacuum jacket was used and the tests were done in air. Temperature fluctuations did not exceed $\pm$ 1^{o}C.

6.4 Grain Boundary Sliding Measurements

Specimens were prepared for mean step height measurement by filing a flat approximately 2 mm wide down the guage length. This was first polished with "600" grade emery paper and then with 1µm and ¼µm. paste on a selvet cloth. The creep test was interrupted at various stages during the life and the mean step height, of sliding boundaries, measured using a Zeiss Interference microscope.

A perfectly polished surface before creep showed no offsets of interference fringes. However, grain boundary sliding during creep resulted in step formation where a pair of boundaries that have slid meet the surface, which, in turn, caused offsets of the fringes. The magnitude of the offset is proportional to the height of the step.

The specimen was viewed at a magnification of 480 x, first in white light. A typical area of a CRM series steel deformed in creep is shown in Figure 9(a) and with the fringes in Figure 9(b). From these, the magnitude of the offset could be determined to the nearest whole number of fringes, that is, fringes could be matched across the boundary. The precise magnitude of the offset was then measured in green light from a thallium source, Figure 9(c). Since the magnitude of the offsets was found to be extremely small (even at tertiary creep, Section 7.1.3)

the most convenient method of measurements was found to be that of photographic enlargements. The offsets of approximately 150 boundaries per specimen were measured on enlargements of 750 x magnification, using an optical graticule. Fractional fringe displacement values were obtained and simply converted to μm., since one fringe displacement was caused by a step height of $\lambda/2$, where λ is the wavelength of the thallium light, equal to 0.54μm. It was therefore possible to measure each offset to an accuracy of 0.01μm.

6.5. Metallography

6.5.1. Optical Microscopy

Examination of ruptured and partially crept specimens by optical microscopy, after preparation by conventional polishing and etching techniques, was undertaken to give a rough indication of the nature and extent of creep damage. It was soon realised that the resolution of grain boundary cavities, even in the later stages of creep life, could not be achieved by using optical techniques and, moreover, their morphology was easily disguised by polishing and etching.

Longitudinal sections were cut from the guage lengths of specimens and mounted in Bakelite, the initial polishing being done on successively finer emery papers down to "600" grade. Intermediate polishing was by 6, 1 and ¼μm. diamond paste on a nylon napping cloth; a minimal amount of pressure was used, as it was found that alloy carbides were easily removed and thus confused the interpretation of grain boundary damage. The final polish was carried out, using a slurry of γ alumina and a solution of 2% Nital in distilled water, on a selvet cloth. This sequence of preparation produced a lightly etched matrix with the

minimal distortion of creep cavities and cracks. Before examination, the specimens were thoroughly washed and ultrasonically vibrated in methanol for 10 minutes. Any photography required was done on a Zeiss Ultaphot II microscope, using 35 mm film.

6.5.2. Scanning Electron Microscopy

Scanning electron microscopy was employed to examine a variety of surfaces that revealed creep damage in both ruptured and partially crept specimens:-

(a) Longitudinal sections prepared by ion beam etching

(b) Fracture surfaces, including those of specimens ruptured by tensile testing at room and elevated temperatures.

(c) Fracture surfaces of deformed specimens, exposed by impact at low temperatures.

Two instruments were used: the Cambridge Stereoscan Mk IIA and the Philips PSEM 500. The latter was used particularly for quantitative work, having the additional features of eucentric goniometer stage and micron marker strips.

Longitudinal sections of thickness 1mm were spark machined from specimens, these were mounted and polished down to ¼µm diamond paste in the usual fashion. The specimens were then carefully removed from the Bakelite and remounted in a specimen holder that consisted of two titanium plates with apertures of 3mm diameter, the specimen was sandwiched between these. This in turn was inserted into an Edwards IBT200 ion beam thinning accessory at an angle of 30^{o} to the incident beam of ionised argon gas, the specimen was rotated continuously. An accelerating gun voltage of 4kv was used which produced gun and specimen currents of 0.75 mA and 40µA respectively. Etching took

about 16 hours and produced a uniformly etched circular area, of 3 mm diameter, on the specimen suitable for examination. The definition of grain boundary damage was best revealed by tilting the specimen at 45^{o} to the incident electron beam.

Elements, of approximately 5 mm in length, with the fracture surface at one end, were carefully sectioned off creep and tensile rupture specimens and examined in the usual manner. To expose the damage on grain boundary facets situated away from the fracture surface and to examine creep cavities in situ on grain facets of partially crept and deformed specimens, it was necessary to promote intergranular fracture. With these materials, it was found that this could best be achieved by impact fracture at -196^{o}C of a notched ligament of between 1 and 2 mm in diameter.

A position on the guage length was chosen for examination (usually 5 to 10 mm from the fracture surface or, in the case of interrupted test specimens, from the test piece shoulder) and a circumferential trench was cut using a heavy-duty hacksaw. This was followed by the creation of a fine circumferential notch using a jeweller's saw, to such a depth as to leave a ligament of material of the required dimensions. The specimen was then placed on a small jig, which supported either end, and immersed in a stainless steel container of liquid nitrogen, and left to soak for 15 minutes. Fracture was simply effected by impact with a sharp instrument opposite the notch.

6.5.3. Transmission Electron Microscopy

Carbon extraction replicas were taken from polished and etched longitudinal sections of crept specimens. To promote efficient removal of the carbon film it was found necessary to etch away the supporting matrix in a 2% Nital solution under a current of 1 amp. The film,

containing a high level of alloy precipitates, could then be floated off in distilled water before mounting on copper grids.

Thin foils were prepared from the guage lengths of fractured and partially crept specimens. The guage length was carefully turned down to 3 mm. diameter and thin discs of 0.35 mm thickness sliced off the resulting rod using a Polaron M400 unit. To avoid magnetic effects in the microscope the discs were polished down on "600" grade emery paper to a thickness of 180μm or 120μm for 1000kV and 100kV microscopy respectively. Perforation was carried out on a Struers polishing unit using an electrolyte of 95% Acetic and 5% Perchloric acid at room temperature. The cell voltage was 40 volts giving a current of 0.16 amps and a flow rate of 4 was used. The resulting foils were stored in sealed containers of ethanol, where they could be kept for about a week before deteriorating.

Transmission electron microscopy at 1000kV was carried out on an AEl EM7 electron microscope and at 100kV on a Philips EM301 instrument.

6.6. Quantitative Metallography

A quantitative assessment of cavity size at various stages of creep life was obtained by scanning electron microscopy of grain boundary facets exposed by intergranular fracture at-196^{o}C. For this purpose, grain facets most nearly perpendicular to the stress axis were chosen for cavity size measurement. To ensure that true cavity diameters on individual grain facets were measured, the specimen was tilted until a maximum dimension was recorded. Depending on the average cavity size, a number of fields on each facet were photographed together with a superimposed micron marker strip, that had previously

been calibrated. The negatives were then enlarged on to transparent "air mail" photographic paper, so that the final magnification was between 1,000 x and 10,000 X, depending on the average size of the cavity population. At the highest magnification, the limiting detectable cavity size was $\sim$ 0.1μm.

A typical example of a grain boundary facet population suitable for analysis is shown in Figure 10. Quantitative measurements were made using a Zeiss TGZ 3 Particle Size Analyser in which 48 size channels were available. The range of sizes measurable was from 1.21 to 27.11 mm. and the width of successive channels increased in an exponential manner from 0.08 mm. at the lower end to 1.75 mm. at the upper end. Approximately 500 cavities were measured for each specimen, cavity size distributions were subsequently obtained for a variety of stress levels and strain increments.

6.7. Auger Electron Spectroscopy

To detect any segregation of elements at prior austenite grain boundaries during creep, intergranular surfaces, exposed by fracture at -196^{o}C, were examined using Vacuum Generators Auger electron spectroscopy equipment. Specimens were machined from ruptured or partially crept test pieces to the dimensions shown in Figure 1(c) The circumferential notch was cut in such a position as to be 10 mm from the original fracture surface or test piece shoulder. Before insertion into the instrument, specimens were thoroughly degreased and ultrasonically cleaned to remove all traces of machining oils. After insertion into the equipment, they were subsequently baked at 200^{o}C, overnight, under high vacuum.

Immediately prior to examination, the specimens were impact

fractured at -196^{o}C and manoeuvered into position so that the intergranular surface was in the impinging electron beam. A differential intensity trace for auger electron kinetic energy values, from zero to 1000eV, was obtained from a pen recorder. After analysis, the fracture surface was examined under a scanning electron microscope to ensure that it was completely intergranular.

The spectrometer analyser used in this equipment was of the hemispherical retarding field type, fitted with a pass grid held at a constant potential of 200eV. Consequently, the analyser sensitivity falls off rapidly at high values of kinetic energy, and spectrum intensities are not directly proportional to the inverse of kinetic energy of Auger electrons. To derive a value of element concentration, from such intensity spectra, values obtained were normalised to take account of the detector sensitivity:

$$\text{Atomic } \% = \frac{I}{K.E.} \times P.E. \times \frac{G_I}{G200} \qquad \ldots\ldots\ldots(54)$$

Where I is the relative intensity value obtained from the pen recording K.E. is the kinetic energy of auger electrons peculiar to the element under investigation, P.E. is the pass energy equal to 200eV, G_I is the gain in intensity at zero P.E. and G200 that due to a P.E. of 200eV.

CHAPTER 7

RESULTS

7.1. 2¼Cr 1Mo Alloy Steels

7.1.1. Room Temperature Tensile Testing

Specimens of the CRM series alloy, in both the tempered and untempered condition, and a tempered sample of the CRMS series alloy were strained to failure at room temperature, as described in Section 6.3. The results are shown in Table 2 and the load/elongation curves have been reproduced in Figure 11. The uniform strain to the maximum load ε_u was interpolated from the load/elongation curve and is recorded in Table 2.

The CRM and CRMS series alloys, in the tempered condition, exhibited markedly similar characteristics of ultimate tensile strength (UTS) and ductility (described by the fracture strain ε_f and reduction in area R.A.). The Sn doped CRMS series alloy, however, showed evidence of a yield point and a small Lüders extension; it also appeared to work harden with strain at a rate greater than that of the CRM series specimens in both the tempered and untempered condition. The latter revealed a 40% increase in UTS whilst still possessing comparable ductility and, as in all specimens, an extensive local necking strain to fracture.

7.1.1.1. Metallography of Fracture

All specimens exhibited a typical ductile "cup and cone" type fracture with clear evidence of necking. Scanning electron microscopy

of a central area of the fracture surface, Figure 16, revealed that fracture followed a transgranular path. The intimate mixture of cleavage facets (denoted by the area marked A in Figure 16) and characteristic ductile cusps (denoted by area B) suggested that failure was due to a combination of microvoid coalescence and transgranular cleavage. The cusps were noticeably fine, ranging in size from a maximum of 2μm to a minimum of 0.2μm.

Polished and etched longitudinal sections of ruptured specimens exposed the nature and extent of damage in those areas removed from the fracture surface. The optical micrograph in Figure 17 shows that damage was confined to the necked region of the specimens, being most pronounced immediately behind the fracture surface. More detailed optical microscopy showed that larger holes, formed by void coalescence, tended to retain a near spherical morphology and were not noticeably distorted in the direction of the applied tensile stress, Figure 18. There was also evidence of transgranular cracking, Figure 19, supporting scanning electron microscope observations of cleavage facets, as mentioned earlier.

7.1.2. Creep Testing

The CRM and CRMS series alloys were creep tested, as described in Section 6.2, at 838K; notched specimens of the CRMS series were also subjected to creep at similar levels of stress. The relevant data gained from these creep tests is reported in Tables 3 to 5.

7.1.2.1. Shape of the Creep Curve

The readings obtained by monitoring the deformation/time characteristics of the two series of alloys were converted to strain/time curves. Typical curves, for two stress levels, 180 and 200MNm^{-2},

have been reproduced in Figure 12.

A significant feature of the creep test results was the similarity in behaviour of the CRM and CRMS series alloys. At both high and low levels of stress the shape of the creep curves for both alloys were identical, and the variation in the measured parameters of minimum creep rate, time to fracture and ductility could be regarded as being insignificant. Further, from Figure 12, it is apparent that the shape of the creep curve was independent of the level of stress. At each stress, the following sequence was observed: after a very short period of primary creep the secondary stage extended for approximately one third of the total creep life before giving way to a prolonged period of tertiary creep. The final stage of this latter period was characterised by a rapidly increasing strain rate prior to fracture, such that the creep curve was almost parallel to the ordinate of fracture time.

7.1.2.2. Effect of Stress on Ductility

For both alloys the level of stress appeared to have little effect on the fracture strain at stresses greater than about 210MNm^{-2}. However, at applied stresses below this level, a steep rise in ductility from the minimum plateau of 14% was observed, reaching a maximum of about 50% at 175MNm^{-2} as illustrated in Figure 13. Measurements on the reduction in area of the ruptured specimens are also plotted in Figure 13, the same general trend was observed but the change in value of this parameter was less than 10% between the two stress regimes. Post test measurements on the diameter of the uniformly strained sections of the guage length yielded the parameter ε_u, the uniform strain to the onset of necking - comparable to that quoted in Table 2 for the room temperature tensile tests. For both alloys, the ratio of $\varepsilon_u/\varepsilon_f$ was

found to be $\sim$ 0.5.

7.1.2.3. Effect of Stress on Creep Rate and Time to Fracture

The minimum creep rate $\dot{\varepsilon}_s$ is plotted against stress for both sets of alloys in Figure 14. The values closely follow a straight line in this double-log plot and hence the stress dependence may be expressed in the form of Equation (1). The data reported in Tables 3 and 4 was analysed using a computer programme which employed a method of least squares to fit the best straight line. In this way the value of the stress exponent was found to be 4.9 ± 0.3, where the variation is at the 95% confidence limit.

The time to fracture for both series of alloys was found to decrease sharply with increasing applied stress and a double-log plot, Figure 15, showed that data could again be fitted to a single straight line of slope -10.1 ± 0.6, satisfying the relationship expressed in Equation (43).

7.1.2.4. Effect of Notches

Notched specimens of the CRMS series alloy were creep tested under the same nominal stresses of 180, 200 and 250MN $^{-2}$, as those used for plain specimens; the required load having been determined for the cross-sectional area across the notch throat. The minimum creep rates, recorded in Table 5, were calculated by making post test measurements on the fiducial marks at the notch shoulders (Section 6.1.3.). In all tests, it was found that the parallel-sided regions of the guage length had undergone zero strain, deformation being restricted to material in the notch itself.

A dramatic reduction in minimum creep rate was observed due to the presence of a notch, such that, for each stress investigated,

the ratio of minimum creep rates for notched and plain specimens respectively was found to be ~ 0.06. However, the stress component n was determined as 4.5 ± 1.0, similar to the value obtained for tests on plain specimens in both alloy series (Section 7.1.2.3.). Due to the extremely low deformation rate creep tests on notched specimens were interrupted before failure.

7.1.3. Observations on Grain Boundary Sliding

Interrupted tests, at a stress of $200 MNm^{-2}$, were carried out on the CRMS series alloy and the nature and extent of grain boundary sliding, after various increments of strain, was monitored using the interference technique described in Section 6.4. Detailed quantitative work, involving step height measurements, was however, severely hampered by the complexity of the sliding interfaces. Nevertheless, a number of interesting observations were made using information contained in the interference patterns produced on the specimen surface after creep deformation.

Although the major sliding interface was clearly recognised as being that of the prior austenite grain boundaries, a significant contribution to the overall deformation was provided by sliding of adjacent bainite plate boundaries within the austenite grains themselves. This phenomenon was particularly marked when the bainite plate boundaries made some acute angle to the applied stress, Figure 20. Consequently, the broad range of step heights, provided by the variety of sliding boundaries, made it difficult to arrive at any meaningful average value.

The offset of interference fringes, at the steps created by sliding at prior austenite grain boundaries, was not sharp, as

described by workers investigating such behaviour in single phase materials using a similar technique (Langdon, 1974; Winzor, 1975). Rather, a more gradual change in the displacement of a particular fringe was observed at the approach to a boundary and again on leaving, Figure 21(a). This was indicative of material deformation in a zone adjacent to the boundary and could lead to an assessment of apparent step height, Figure 21(b), again making detailed measurements difficult. The converse was true of sliding bainite plate boundaries where the offset of fringes was clearly more abrupt, Figure 21(a).

During the later stages of creep life, after the onset of tertiary, quite significant steps of up to 3μm in height were produced at prior austenite grain boundaries, Figures 22(a) and (b). As can be seen, the complexity and non-uniformity of boundary steps is much more pronounced.

7.1.4. Metallography of Creep Damage

Typical polished and etched longitudinal sections of creep fractures observed in these alloys are shown in the optical micrographs of Figures 23(a) and (b). Creep damage was confined to the necked region of specimens where the structure was heavily deformed in the direction of the applied tensile stress. Due to such heavy deformation in these areas, with attendant grain boundary rotation, the type of cavitation could not be unambiguously identified. However, individual holes were seen to be notably elongated in the stress direction, Figure 24, and no intergranular crack interlinkage was observed. In the uniformly extended region of these specimens the prior austenite grains retained their equiaxed shape and despite repeated etch/polish treatments, no grain boundary creep cavitation was observed.

Scanning electron microscopy of the creep fracture surfaces confirmed

that at all stress levels in both alloys, the mode of failure was completely transgranular. Figure 25 shows that typical dimpled characteristics of ductile fracture by micro-void coalescence; a large variation in cusp size was noted, from a maximum of 15μm to a minimum of ∿ 0.2μm. Attempts to expose prior austenite grain boundaries by intergranular fracture in liquid nitrogen (Section 6.5.2.) were not successful, merely producing a completely transgranular cleavage fracture, Figure 26. A number of interrupted tests were completed in which specimens were taken well into the tertiary range. Fracture in liquid nitrogen was then effected in the necked region of the test piece. Voids developed in the specimen during creep could be clearly distinguished in the cleavage facets, Figure 27 shows a colony in the early stages of growth. The size range of voids exposed in this fashion yielded a mean value of ∿ 1μm. It was difficult to determine the location of such voids with respect to the prior austenite grain boundaries.

The notched specimens of CRMS series material interrupted before failure, were also subjected to rigorous examination by optical microscopy and scanning electron microscopy (after ion beam etching), especially in the region of the notch. Without exception, no creep damage was observed.

7.1.5. Transmission Electron Microscopy

Transmission electron microscopy of carbon extraction replicas was carried out on test piece heads and the guage lengths of ruptured specimens. Material in the initial heat treated condition was also examined. Due to the severe tempering treatment given to both alloys, no difference in carbide type and distribution was observed between pre and post - test specimens.

The predominant carbides present were identified as $M_{23}C_6$ and M_2C, Figures 30 and 31. The latter existed as fine needles in Widmanstätten arrays, while $M_{23}C_6$ was present as massive spheroidal and rod shaped particles within the bainite and on the prior austenite grain boundaries, Figure 28(a) and (b).

The $M_{23}C_6$ particles were surrounded by areas denuded of M_2C, indicating that $M_{23}C_6$ grew at the expense of M_2C. This was in agreement with the finding of Baker and Nutting (1959), who summarized the carbide reactions occurring during the tempering of 2¼Cr 1Mo steel as follows:

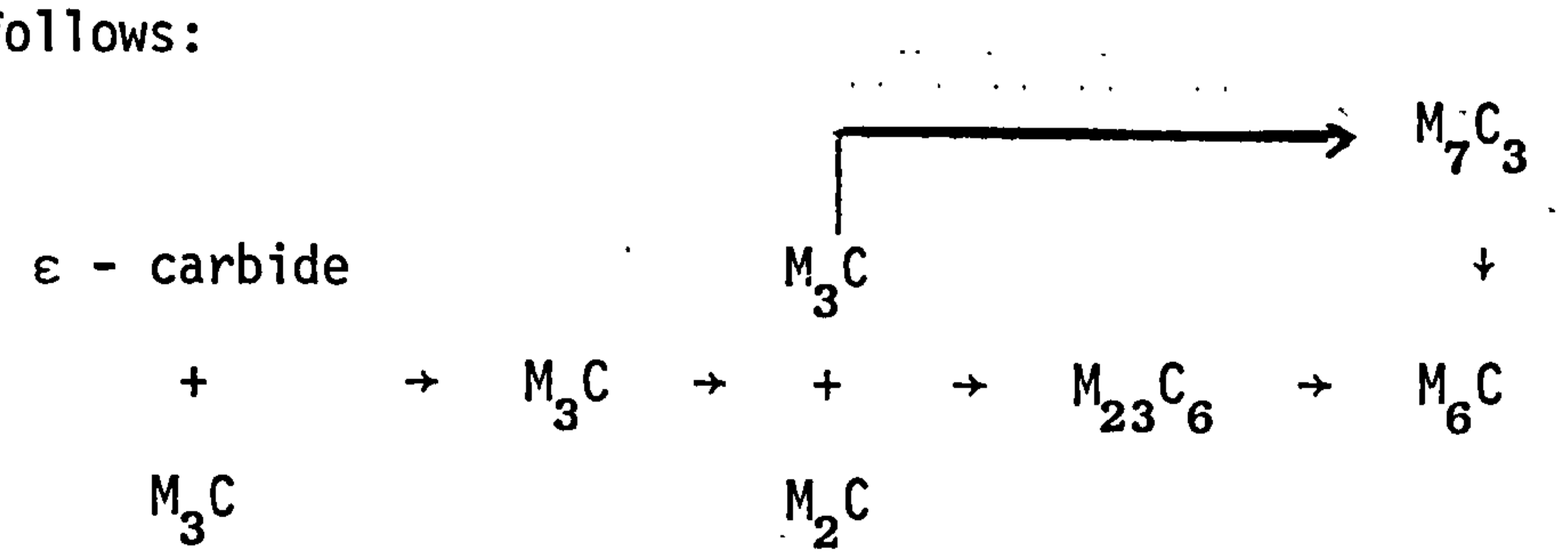

The carbide M_6C does not form until complete dissolution of M_2C, and this was again confirmed as no M_6C was identified.

It was also evident that the prior austenite grain boundaries played an important role in governing the stability of the M_2C, as areas adjacent to such boundaries were extensively denuded of this precipitate, Figures 29 (a) and (b). This indicated that M_2C needles first dissolved in these zones, causing them to expand, and consequently contributed to the existence of massive $M_{23}C_6$ particles within the boundaries. The dimensions of these precipitate-free zones were markedly uniform in all the materials examined and were determined as being between 2 and 3 microns in width.

A quantitative assessment of precipitate size yielded mean values for the diameters of coarse $M_{23}C_6$ and the M_2C particles lying between 0.2 to 0.6μm and 200 to 800Å respectively.

7.2. ½Cr ½Mo ¼V Alloy Steel

7.2.1. Tensile Testing

Specimens of the CRMV series alloy were strained to failure, at a constant strain rate, at both room temperature (290K) and at various temperatures above this. The procedure employed for tensile testing at elevated temperatures has been described in Section 6.3. The results of such tests have been recorded in Table 6; in addition it was noted that the duration of each test was approximately 2 to 3 hours.

Typical load/elongation curves, for the two extremes of temperature investigated (290 and 773K) have been reproduced in Figure 34. Similar behaviour was observed at the three test temperatures up to 673K, and the curves produced resembled that of specimen CRMV/U1. As expected, the rise in temperature produced a decrease in the UTS, however the ductility remained constant at approximately 15%. The decrease in load before failure indicated substantial necking of the specimens.

In contrast, specimen CRMV/U4, tested at 773K, failed in a more abrupt manner with the load still increasing (Figure 34). Although the general trend of a decrease in tensile strength and strain hardening with rise in temperature was followed, the sudden intervention of fracture decreased the ductility to half that observed at the lower temperatures investigated.

7.2.1.1. Metallography of Fracture

The fracture surfaces of the tensile specimens were examined by scanning electron microscopy. Those specimens tested at the three lower temperatures all displayed a typical ductile "cup and cone" failure, with substantial necking behind the fracture surface, as represented by specimen CRMV/U2 in Figure 35(a). Higher magnification

Figure, 35(b), showed that the surface was completely covered by a fine scale of ductile cusps. No transgranular cleavage facets were observed as in the CRM series alloys (Section 7.1.1.1.) which exhibited a similar ductile failure mode. A proportion of the cusps were seen to be associated with coarse spherical particles, Figure 35(c), of approximately 1 to 3μm in diameter.

Reflecting the lower ductility recorded in the tensile test at 773K, specimen CRMV/U4 exhibited a different failure mode and fracture surface topology. Figure 36(a) clearly shows that the initial fracture occurred along an intergranular path, producing the faceted region, denoted by the area marked "A". The remainder of the fracture surface, comprising about 60% of the total area, consisted of transgranular, ductile cusps as observed in those specimens ruptured at lower temperatures. The sharply defined grain facets of the intergranular region are shown in Figure 36(b). In Figure 36(c) the finer detail of the grain surfaces is revealed. Of particular note was their remarkably smooth and featureless appearance. In the area marked "A", the clean separation of adjacent grain surfaces is quite pronounced, suggesting that grain boundary cracking was involved in the fracture process.

7.2.1.2. Microstructure

After rupture, thin foils were prepared from the guage length of the tensile specimens and examined by transmission electron microscopy. The detailed analysis of the microstructure of this alloy, after high temperature deformation, will be discussed later (Section 7.2.4.). However, some significant features related to the tensile deformation will be highlighted here.

The microstructure of specimen CRMV/U1 closely resembled that observed in the original heat treated material (Section 7.2.4.), displaying broad plates of Fe_3C bounding the bainite grain boundaries. The two specimens tested at 573 and 673K respectively both showed significant spheroidisation of the Fe_3C plates to form coarse particles on the bainite grain boundaries as revealed in the dark field view of Figure 38. The bright field image of the same area, Figure 37, indicates that there was little intergranular precipitation. This was not the case with specimen CRMV/U4, ruptured at 773K, where small platelets of V_4C_3 were associated with dislocations within the bainite grains, Figure 39.

7.2.2. Creep Testing

Specimens of the CRMV series alloy were creep tested at three different temperatures: 963, 863 and 803K. The relevant data obtained has been recorded in Table 7. The behaviour of notched specimens at 963K was investigated at several stress levels and the results are contained in Table 8. Further, the effect of variable stress at this temperature was determined and the parameters of time at stress and minimum creep rate at each stress level can be found in Table 9.

7.2.2.1. Shape of the Creep Curve

The deformation/time characterisitics of this alloy, at the three temperatures investigated, were converted to strain/time curves, and several have been reproduced in Figure 40. For the results obtained at 963K, two curves are shown, representing high and low levels of stress.

The most significant feature, at all temperatures studied, was the very limited region of tertiary creep observed. Indeed, at high stress levels in the high temperature regime (e.g. specimen CRMV12) and in tests

at lower temperatures (e.g. specimen CRMV9) it was difficult to detect any accelerated creep stage. Also of note was the prolonged period of primary creep, forming a significant proportion of the total creep life at high stresses and for deformation at lower temperatures. Tests resulting in longer creep life displayed extended periods of secondary or constant creep, in the case of specimen CRMV2, accounting for approximately half the creep life. Tests over shorter periods tended to exhibit a point of inflexion from which the minimum creep rate could be determined by the drawing of a tangent to the curve.

7.2.2.2. Rupture Ductility

At each temperature investigated, the rupture ductility decreased with an increase in the applied stress. At 963K a sharp fall in the value of strain at failure (ε_f) was observed when the stress was raised from 45 to 50MNm^{-2}. As the temperature of creep deformation was lowered, specimens exhibited almost zero ductility. The combined effect of stress and temperature on creep ductility were best represented in terms of the Larson-Miller rupture parameter P_F (Section 5.2.1.).

Figure 41 shows creep ductility plotted against the rupture parameter P_F. At high values of the latter (i.e. low stress and high temperature) a sharp rise in ductility is observed. Moving to lower parameter values (i.e. high stress and low temperature) the ductility is seen to fall off less rapidly to a plateau at an extremely low strain level.

The low ductility with limited necking exhibited by this material is revealed in Figure 45, showing a typical test piece after rupture.

7.2.2.3. Effect of Stress on Creep Rate and Time to Fracture

Values obtained for the minimum creep rate $\dot{\varepsilon}_s$, at the three tempera-

tures investigated, have been plotted against stress to produce the double-log plot in Figure 42. The data obtained lay on three straight lines, representing the respective test temperatures, and thus the relationship:

$$\dot{\varepsilon}_s \quad \alpha \quad \sigma^n \qquad \text{.....(1)}$$

was obeyed at each temperature.

However, the stress sensitivity was found to increase as the test temperature was dropped and curve fitting analysis produced the following values for the exponent n :-

$$2.65 \pm 0.11 \quad \text{at} \quad 963 \text{ K}$$

$$6.22 \pm 0.21 \quad \text{at} \quad 863 \text{ K}$$

$$12.04 \pm 0.28 \quad \text{at} \quad 803 \text{ K}$$

Values obtained for the time to fracture t_f were found to be directly proportional to the applied stress in a double-log plot, obeying the relationship:

$$t_f \quad \alpha \quad 1/\sigma^m \qquad \text{.....(43)}$$

Again, the data for a particular temperature could be confined to a single straight line, Figure 43. A particular feature here was the limited deviation of experimental points at the two lower temperatures. In contrast to the variation of stress sensitivity with temperature displayed by the minimum creep rate, the value of the exponent m remained constant:

$$-3.33 \pm 0.35 \quad \text{at} \quad 963 \text{ K}$$

$$-3.36 \pm 0.09 \quad \text{at} \quad 863 \text{ K}$$

$$-3.65 \pm 0.22 \quad \text{at} \quad 803 \text{ K}$$

7.2.2.4. Effect of Notches

Notched test pieces were subjected to three similar levels of applied stress to those employed to investigate the behaviour of plain specimens. Comparison of fracture life in each case reveals little variation between notched and plain specimens. Specimen CRMV/N2 exhibited a slight notch weakening effect, with a reduction in creep life to 0.94 of that shown by a plain specimen at the same stress. The other tests produced a marginal notch strengthening result.

7.2.2.5. Variable Stress Tests

Two separate experiments were completed involving a stress variation from a low level to a higher one (specimen CRMV/R1) and vice versa (specimen CRMV/R2). In each test, the two stresses used had a ratio of approximately 2. The specimen underwent creep deformation at the initial stress for a period t_1, equal to approximately half the creep life expected at that stress. The time from the application of the final stress σ_2 to fracture of the test piece was recorded as t_2.

The creep curves for the stress increase and decrease tests, reflecting deformation under the unfluence of the final stress, have been reproduced in Figures 44(a) and 44(b) respectively. These curves have been compared, on the same graph, with those generated by a constant stress equal in value to σ_2. In each case, a marked difference in behaviour was observed when the creep characteristics of variable and constant stress tests were compared.

Referring initially to the variable stress test involving a transition from low to a high stress, a substantial increase in creep life, to almost double that at a constant stress, was observed. Also of interest was the reappearance of a primary creep stage under the final

stress. The prolonged period of tertiary creep provided another significant feature, involving over half the period t_2, and accounted for the relatively high ductility recorded on the test piece after fracture. This was in marked constrast to the curve produced by the constant stress of $90MNm^{-2}$, where no accelerated creep was recorded before fracture.

The test involving a stress reduction, displayed converse effects to those described previously, the most notable being a creep life reduced by 30% under the changing stress sequence. Again, in comparison with results obtained under a single stress, the minimum creep rate was reduced and the previous history of deformation at a higher stress did not induce any significant tertiary creep. However, a distinct primary creep stage was noted after the final stress had been applied and the strain rate fell sharply in a short space of time (Figure 44(b)). These deformation characteristics conspired to produce a lower strain to failure under the variable stress system than that measured under constant stress.

7.2.3. Metallography of Creep Damage

7.2.3.1. Creep Fracture Surface

After failure, the fracture surface of test pieces was examined by scanning electron microscopy. Tests at 963 and 863K produced a completely intergranular fracture with clearly defined grain facets, Figure 46(a). A significant amount of grain boundary decohesion could be observed in the plane of the fracture path, with individual grains held to the surface by slender ligaments of material, Figure 46(b).

Closer inspection of grain facets revealed that they were completely

covered by a maze of shallow cusps or cavities, Figure 47. Each facet exhibited dense populations of these cavities which were bounded by thin, tapering walls. Although these lacked definition, producing a rather diffuse morphology, it was possible to detect a distribution in the size of cavities on a particular facet. A consistent feature was the type of distribution in relation to particular sites on an individual facet, Figure 48 clearly demonstrates that populations of larger cavities were prevalent in regions bounded by grain corners and edges. It was more difficult to determine, with any degree of confidence, any trends in the dimensions of those surface features with changes in applied stress or test temperature. Figures 49(a) and(b) show two specimens tested at widely different temperatures and applied stress, yet the fracture surface topology remains similar.

Detailed examination of grain edges in the advanced stages of decohesion showed that surface undulations could be matched across the boundary, Figure 50(a). This micrograph also exposed a single cavity wall ligament bridging across two adjacent grain edges, with extensive regions of wall breakdown on both sides. In some instances it was possible to view down a parted boundary to see similar cavitated facets to those exposed by the creep fracture path itself, Figure 50(b).

As can be seen from the micrographs presented, such damage associated with the creep fracture surface was not restricted to grain facets at a unique angle to the applied stress. Again,due to the diffuse nature of cavity morphology, the degree of damage in relation to angular displacement from the stress axis could not be determined precisely. However, it could be said that the depth of cavities found on facets nearly perpendicular to the stress axis was greater than those formed on facets that formed more acute angles.

Specimens crept at 803K exhibited a different mode of failure and Figure 51(a) displays a mixed trans- and intergranular fracture path with a proportion of the surface composed of a ductile shear lip. A similar fracture surface was observed on the tensile specimen ruptured at 773K (Figure 36(a)). Smooth, clean facets were associated with the intergranular region in the latter specimen but closer examination of the grain facets of specimens failed during creep deformation revealed the same form of damage as observed in tests at higher temperatures, Figure 51(c). There was also a small amount of cleavage fracture on some grain surfaces, indicated by the area marked A in Figure 51(b).

Comparing the creep damage, exhibited on grain facets, of specimens crept at 803K to those deformed at higher temperatures, it was quite apparent that the cusps appearing in the former case were on a much smaller scale than those previously observed. Moreover, the cavities were much shallower and consequently more difficult to make out. Another marked feature of the cavitation at this temperature was the apparent linearity of the surface defects, cavities seemed to be arranged in neat rows running in various directions across the grain facet. This phenomenon can be seen in Figure 51(c), where lines of cavities are running in the direction marked by the arrows on the micrograph.

7.2.3.2. Longitudinal Sections

Longitudinal sections, taken from the guage length of ruptured specimens, were examined by optical microscopy after prior polishing and etching. Confirming observations described previously, extensive grain boundary decohesion could be seen in the region behind the

fracture surface. Some of the cracks shown in Figure 52(a) extend across two grains.

In those areas removed from the fracture surface, cavitated grain boundaries were exposed by heavy etching. Figure 52(b) shows a boundary in which the cavities are in an advanced state of coalescence with cavity wall breakdown evident; however, in such cases it was uncertain to what extent this was due to the action of the etchent. With less heavily cavitated boundaries, Figure 52(c), it was difficult to resolve the morphology of cavities, even at high magnifications.

This technique, although not revealing the precise detail of cavities, clearly confirmed that the phenomenon was uniquely associated with prior austenite grain boundaries. Even after extreme etching procedures, no void-like defects were found on bainite plate boundaries Similarly, no creep cavities were revealed in the threaded regions of test pieces when examined after fracture.

As suggested in Section 3.1.1.1., etching by a focussed ion beam had proved successful in exposing the morphology of creep damage in single phase materials. The technique was applied to longitudinal sections of CRMV series alloy after creep rupture; after treatment (Section 6.5.2.) specimens were examined by scanning electron microscopy. Figure 53(a) shows a region of specimen CRMV, 5mm behind the fracture surface, after ion beam etching for approximately 20 hours. In the micrograph a series of parallel prior austenite grain boundaries, almost normal to the stress axis, are heavily decorated with creep cavities; in this case the etching treatment has been quite severe and regions rich in precipitate particles formed raised projections on the surface. At a higher magnification, individual cavities could be identified, Figure 53(b). Nevertheless, it was still difficult to decide whether a particular defect was the result of a single nucleation event or due

to the coalescence of adjacent cavities. The result of reducing the etching time to 10 hours is shown in Figure 54(a). The lighter etch enabled individual defects to be more easily distinguished, but set against this was some loss in the clarity of cavity outline.

Consequently, due to the extremely small scale of the grain boundary damage (certainly, below a micron could be expected) and the probable errors likely to occur in measurement of size and population, it was decided that quantitative work on longitudinal sections should not be attempted. Notwithstanding these limitations, this technique revealed the process by which the decohesion of prior austenite grain; boundaries took place. The micrograph in Figure 53(a) shows a group of cavities on a prior austenite grain boundary in various stages of development. It can be seen that they assume an elliptical shape by growth in the boundary plane and ultimately coalesce to produce the "binocular" morphology indicated by the arrow. Figure 54(b) shows a boundary nearer the fracture surface in the same specimen, complete decohesion has been achieved and it is still possible to discern the matching halves of coalesced cavities directly opposite each other across the boundary.

7.2.3.3. Fractographic Observations

The grain boundary creep damage, produced in the CRMV series alloy, could be conveniently exposed by impact fracture at liquid nitrogen temperatures, as described in Section 6.5.2. The technique allowed detailed observations to be made on the nucleation and growth of creep cavities throughout creep life. The quantitative aspects will be reported in Section 7.4.

7.2.3.3.1. General Characteristics

It has previously been mentioned that failure along an intergranular path could only be achieved if the cross-section of the guage length was reduced to below $1mm^2$. Another factor that determined the proportion of grain boundary area exposed, using this technique, was the degree of creep deformation specimens had undergone. Those interrupted for examination after limited creep, exhibited a high proportion of transgranular cleavage with only isolated regions of grain boundary exposed, Figure 55(a). Conversely, specimens investigated by impact fracture at the end of creep life produced larger areas of grain facets, Figure 55(b). Dimensional measurements made on the intergranular surface exposed, and comparison with previous grain size determinations (Section 6.1.2.3.), showed that the boundaries exposed by low temperature impact fracture were those of the prior austenite grains. A completely intergranular fracture surface was never obtained by impact of pre-crept specimens at low temperatures. The threaded areas of a number of specimens were also fractured in a similar manner after creep failure of the test piece, a surface of 100% transgranular cleavage was found in every case, typical of that shown in Figure 56.

In tests where the creep damage was to be reviewed after creep fracture, it was important to ensure that the specimen was cooled as soon as possible after the failure event. The impact fracture surface of a specimen held at the test temperature for 24 hours after failure is shown in Figure 57(a). The intergranular nature is clear with resolvable grain facets. The detail of an individual grain face is displayed in Figure 57(b), gross sintering has completely broken down the features of creep damage to produce an amorphous topology, rendering quantitative work impossible. However, in some instances

it was observed that the degree of cavity sintering varied from one facet to another. The region shown in Figure 57(c) illustrates this phenomenon; the faces marked A show severe degradation of the surface damage, whilst facets at a different spatial orientation exhibit cavity networks that have retained their original morpholgy.

7.2.3.3.2. Distribution of Cavities in the Early Stages of Creep Life

Specimens examined after short periods of creep deformation, typically at the onset of secondary creep, revealed grain facets characterized by several colonies of cavities covering a small fraction of the surface area, Figure 58(a). A feature of such colonies was a central region containing a high density of damage such that adjacent cavities impinged upon each other to produce tapering cavity walls, Figure 58(b). Such areas also displayed a range of cavity sizes. Away from the colony centre, the number of cavities per unit area decreased until discrete entities could be identified. These had adopted a sharp, spherical profile and again a size distribution was noticeable (Figure 58(c)).

The paucity of damage prevalent on grain faces during the early stages of creep life, highlighted preferred sites of cavity nucleation; facet edges and corners were especially prone to cavitation. Such sites were characterised by a high density of cavities and enhanced cavity coalescence. An extreme example of this is illustrated by Figure 59(a) where a grain edge, running normal to the stress axis, contains a number of cavities - the grain facets on either side, however, are smooth and almost devoid of damage. In Figure 59(b) a grain corner, whose apex points along the tensile axis, displays a cone-shaped region

of cavitation. The population density clearly decreases in those zones removed from the triple-point junction, discrete voids appear at some distance down the grain face, Figure 59(c). Further, cavities in sparsely populated areas can be associated with the minimum size, whilst those situated near the grain corner and along the edges are considerably larger due to coalescence by wall breakdown.

Grain facets orientated normal to the stress axis also tended to provide favourable sites for cavity nucleation. Again this was manifested by dense populations and enhanced coalescence. The facet in the plane of the micrograph in Figure 59(d) is normal to the stress axis and is almost completely cavitated; adjacent facets with acute spatial displacements from the axis reveal scant areas of cavitation. Similarly, the facet marked A in Figure 59(f) is approximately perpendicular to the stress axis, it will be noted that there has been a greater degree of cavity coalescence than has occurred on facet B.

A further interesting phenomenon, commonly observed, is illustrated by reference again to Figure 59(d). The heavily cavitated facet contains a broad band of material, distinctly bounded by areas of dense cavitation, in which the formation of creep damage has been completely supressed. The converse of this situation is shown in Figure 59(e) where a band of intense cavity nucleation has occurred to produce a network of extremely small cavities, growth being prevented by impingement. In both cases, the boundary separating areas of extreme population characteristics was sharp and somewhat linear. It was also noted, especially in areas of the grain surface containing discrete cavities, that there was often a detectable linearity in the arrangement of adjacent cavities. This echoed similar observations made on the morphology of damage on the creep fracture surface itself, Section 7.3.1.

7.2.3.3.3. Damage Morphology in the Later Stages of Creep Life

Specimens examined by fractography in the teriary creep regime and after creep failure showed a considerable increase of creep damage, in the form of grain boundary cavitation, such that a greater proportion of the total grain surface area was involved. A general coarsening of the cavity network structure was also observed.

Those grain facets that had occupied a plane normal to the tensile axis displayed the highest degree of creep damage. Indeed, after creep failure, those grain faces occupying this unique spatial orientation were almost entirely covered by a network of cavities. A typical example is illustrated by Figure 60, where a large facet normal to the stress axis has been completely cavitated. This micrograph exhibits a number of important features characteristic of the damage morphology at these later stages of creep life. In particular, there is clearly a wide variation in cavity size with isolated colonies of small cavities "trapped" by encroaching fronts of larger bodies. The lack of shadowing produced by the scanning electron beam at the centre of each cusp.suggests that the cavities themselves were rather shallow, elliptical voids. The boundary walls give the surface network a tapered relief and in some instances, wall breakdown and the presence of previous partitions can be discerned between adjacent cavities.

The above observations imply that during the later stages of creep life, cavities no longer retained their individual identity, but coalesced to form larger entities by the degradation of boundary walls. The progressive coarsening of creep damage in such a manner during tertiary creep is illustrated by Figure 61(a) showing a completely cavitated facet. At a higher magnifaction, Figure 61(b), the surface network presents a maze-like pattern due to the breakdown of several

partitions. In specimens examined after creep failure, and especially in tests with extensive creep lives, there was evidence to suggest that, once smaller cavities had been consumed by the coarse expanding species, a stable network structure was established, Figure 62(a). Here, the boundary walls appear to have adapted a configuration to reduce the surface tension forces acting on the three dimensional network. In Figure 62(b) the cavity shown in the centre of the micrograph has adopted a straight-sided equiaxed shape by the preferential dissolution of selected boundary walls. This behaviour is somewhat analogous to that of a decaying soap bubble froth which coarsens to produce a network of large bubbles. The behaviour of cavities at the interface of adjacent grains is shown in Figure 63. The specimen has been taken to the start of the tertiary creep regime and already the breakdown of cavity walls, connecting the two faces, to produce stunted ligaments can be observed. It is important to note, however, that there has been no distortion of cavity profiles at the interface and the cusps can be 'matched' on each facet.

As suggested previously, Section 7.2.3.1., the damage morphology of the creep fracture surface of specimens tested at 803K revealed slight variations from that observed after creep failure at higher temperatures. This modified behaviour was reflected in fractographic studies on CRMV series alloy pre-crept at 803K. Cavitation was again heterogeneously distributed on the prior austenite grain surfaces, Figure 64(a), but on a much finer scale (Section 7.2.3.1.). A feature of the cavitation damage at this temperature was the appearance of dense populations, over a large proportion of the total grain boundary area, during the early stages of creep life. Consequently it was more difficult to define preferred nucleation sites. Another marked

characteristic of the cavity populations at this temperature was the limited size range exhibited and the minimal amount of coalescence with a tendency for adjacent cavities to retain their individual profiles, Figure 64(b).

The coarsening of the cavity wall network, that accompanied the later stages of creep deformation in specimens tested at 963 and 863K, exposed the sub-surface layers of grain facets. These areas were, of course, previously occupied by cavities in their early stages of development. The coarse, open structure produced is typified by Figures 62(a) and 62(b) which reveal that the grain surface is covered by a debris of minute particles that appear as fluorescent dots under the electron beam. Within each area bounded by cavity walls it will be noted that there are several particles, a similar observation was made on cavities in the earlier stages of development, although their resolution was more difficult e.g. Figure 58(b). The dimensions of these particles were measured in a number of specimens and they were found to lie in the size range of 500 to 1,000 Å.

7.2.3.4. 1MV Transmission Electron Microscopy

A limited amount of high voltage electron microscope work was completed in a series of specimens tested at 963K, under a stress of $45MNm^{-2}$. The samples of pre-crept specimens examined were representative of the various stages of the creep curve (Figure 74) at this stress, viz: the primary creep stage ($t = 9 \times 10^4 s$), the beginning of both secondary ($t = 32.4 \times 10^4 s$) and tertiary creep ($t = 50.4 \times 10^4 s$) and finally after creep failure ($t = 77.5 \times 10^4 s$).

Creep cavities were observed in thin foils taken from specimens pre-crept to the various degrees , indicated above. This included

material examined after very limited strain in the primary regime and also that taken from a specimen after creep failure. In all cases, the cavities were exclusively located at prior austenite grain boundaries, easily identified in the electron microstructure. Sizes ranged up to approximately 0.7μm and the minimum dimension detected was 0.1μm. Ultra-high magnifications revealed an internal structure of those creep cavities being studied and thus confirmed that the voids were contained within the foil thickness. In some of the electron micrographs, discussed below, it will be noted that: due to the limited transparency, even to 1MV electrons, of the thick foils used it was extremely difficult to expose the internal structure of cavities and the surrounding matrix at the same time. Also revealed at high magnifications was the invariable association of particles on the cavity surfaces. These had a narrow size range of 500 to 1,000 Å, similar to that recorded for particles on cavity floors exposed by fractography.

As emphasized earlier, creep cavities were observed after limited creep strain and Figure 65(a) shows a prior austenite grain boundary in material interrupted during primary creep. A large cavity appears at the grain corner and another further along the grain edge, between the two is a very small void with a diameter of 0.1μm. A striking characteristic of the voids studied in their earlier stages of developments, using this technique, was the well defined crystallographic nature characterised by a geometric, three-dimensional morphology. The feature is well illustrated by the void marked A in Figure 65(a) which exhibits a straight-sided, hexagonal shape. The internal structure of this void is revealed in Figure 65(b) where several particles can be located on the cavity facets.

Occasionally it was possible to detect a dislocation network associ-

ated with a dispersion of fine particles. Observations on the dislocation structure in the matrix in the immediate vicinity of grain boundary voids proved rather disppointing; again, probably due to the foil thickness. However, the cavity shown in Figure 67 is related to some interesting behaviour displayed by the matrix. The grain boundary region to the right of the cavity is heavily decorated with precipitate particles and is noticeably bowed in the plane of the micrograph. Further, there are some interesting interference fringe contours emanating from the cavity interface and extending into the adjacent matrix. The foil thickness dictates that it is rather unlikely that these fringes are band contours but rather due to stress fields set up by the growing cavity advancing into the matrix.

Heavily cavitated prior austenite grain boundaries were observed in material during tertiary creep and after failure. Figure 68(a) shows a heavily cavitated triple point boundary in a thin foil taken from Specimen CRMV1, the cavity at the triple point junction exhibits the largest dimension, reflecting similar observations made during fractographic studies. It was surprising to note that even after accelerated creep had occurred, grain boundary voids were displayed at the very early stages of developments, Figure 68(b).

A phenomenon commonly observed using this technique and illustrated in Figures 65(a) and 68(a) was the apparent suppression of creep damage at certain prior austenite grain boundaries. These were characterised by interfacial bainite plates having the same orientation across the boundary, creep cavities were only observed at boundaries where the ferrite grains had developed in different crystallographic directions. The diagram in Figure 80 represents the situation observed in Figure 68(a) and it will be noted that the grain boundary, denoted by the

letter D, has a parallel alignment of bainite plates across the boundary and consequently no cavities have been nucleated.

7.2.3.5. The Distribution of Creep Damage in Notched Specimens

Examination of notched specimens ofter creep failure showed that damage had been confined to the region of the notch. The micrograph shown in Figure 69(a), obtained by scanning electron microscopy, reveals extensive cracking at the notch throat behind the creep fracture surface. Closer examination of the latter, Figure 69(b), confirmed that failure had occurred by grain boundary decohesion and the surface topology of grain facets closely resembled that observed on the fracture surface of plain test pieces, with intricate cavity wall networks, Figure 69(c). Ion beam etching of longitudinal sections taken from the parallel-sided region of the guage length revealed no grain boundary cavitation.

7.2.4. Microstructure Produced During Creep

The CRMV series alloy in the heat treated condition exhibited a microstructure characterised by a coarse prior austenite grain size (170μm) and a matrix of lower bainite. The latter was composed of ferrite plates bounded by massive sheets of Fe_3C, Figure 70(a). Within the ferrite plates, complex dislocation tangles could be observed Figure 70(b), typical of a structure produced by shear transformation. No precipitation, either at prior austenite gtain boundaries or intragranularly, was observed in the heat treated condition. The diffraction pattern produced by a sheet of Fe_3C is shown in Figure 70(c) and its corresponding analysis in Figure 70(d).

Early in creep life, during the primary stage, the appearance of a fine precipitate dispersion was observed within ferrite plates; this

was true of all temperatures investigated. The particles had a platelet morphology and were often associated with dislocation networks, Figure 71(a). They were small in dimensions, ranging from 500 to 1,000Å and could only be resolved within a particular ferrite plate when the latter was tilted to the required Bragg angle. Consequently, in some of the micrographs shown, some ferrite plates appear to be devoid of precipitate. Analysis of precipitates in this alloy, by selected area diffraction, was often impeded by the presence of a thin oxide film on the surface of the thin foil. Fortunately those spots produced by the oxide could be easily eliminated (Keown and Dyson, 1966) and those due to the precipitate identified, Figure 71(b).

The dispersed phase was found to be VC and at the higher temperatures investigated showed some coarsening during tertiary creep. This is illustrated by the dark field image in Figure 71(d) where the white spots are due to VC precipitates. The bright field image of the same area showed the dislocation structure produced during tertiary creep, no significant sub-cell formation within the ferrite plates was observed at any temperature studied.

Throughout creep life, there was a progressive breakdown of Fe_3C to produce a spherodized precipitate along the ferrite plate boundaries, Figures 72(a) and 72(b); again, this was most pronounced during deformation at higher temperatures. Despite the dissolution of Fe_3C, within the bainitic matrix, there was no development of precipitate-free zones observed at the prior austenite grain boundaries; a similar result has been reported by Cane (1978). In all material studied after high temperature creep deformation, no Mo_2C precipitates were identified. This is in agreement with a number of other workers: Prnka and Sobotka (1973), Smith and Williams (1975), Cane (1977),

who suggest that the breakdown of stable VC to Mo_2C only occurs after prolonged service exposure at high temperatures.

7.2.5. Quantitative Fractography

Quantitative analysis of cavitated areas, on those grain surfaces approximately normal to the tensile stress axis, was undertaken after impact fracture of crept specimens in liquid nitrogen. The cavity measurement technique adopted has been described previously in Section 6.6.

7.2.5.1. Cavity Size

The data generated by cavity size measurements was converted to relative frequency values of cavity width occurring in a given size range. The mean cavity width $\bar{d}$ of the population, produced after a given creep time and strain, was determined using the relationship:

$$\bar{d} = \sum_{i=1}^{n} f_i d_i / \sum_{i=1}^{n} f_i \qquad \text{.....(55)}$$

Where the cavity widths d_1, d_2, ...dn occur with frequencies f_1, f_2 .....fn. The mean cavity width and maximum cavity width, d_m, were determined at a number of stresses after various increments of creep strain, the results have been recorded in Table 10. The values of strain quoted, refer to the elongation measured at the region of guage length where fractographic observations were made. It will be noted that the cavity size distributions produced after successive deformations was studied in depth at $45MNm^{-2}$ (963K) and $130MNm^{-2}$ (863K).

Cavity size distribution curves were also constructed in the form of frequency histograms, where relative frequency of cavity width was plotted for successive dimensional increments. Typical curves for those

cavity populations investigated at $45MNm^{-2}$ (963K) have been reproduced in Figures 73(a) and 73(b). The frequency histograms, representing cavity populations observed up to the termination of steady state creep ($t = 50.4 \times 10^4 s$), are characterized by positively skewed distributions. As creep deformation progressed, during this period, the modal value shifted to a larger cavity width and a broadening of the distribution curves has taken place to include a larger proportion of cavities exhibiting a maximum dimension, Figure 73(a). The frequency histogram representing the cavity population at fracture is shown in Figure 73(b), the distribution has assumed a more symmetric shape, with the mean and modal values converging.

At higher stresses within the same temperature regime (963K), the values for $\bar{d}$ and d_m quoted in Table 10 reflect a similar trend in the distribution of cavity sizes throughout creep life. Narrow, skewed curves were observed up to the end of secondary creep and broader, symmetrical curves (extending over a greater range of cavity sizes) characterising the tertiary creep stage and the cavity distribution at failure. Quantitative assessment of those cavity populations produced during tests at lower temperatures, however, displayed normal distributions, confined to a narrow range of cavity widths, throughout creep life. In the extreme case, the mean and maximum value of cavity width converged to approximately the same dimension in populations produced by creep deformation at $300MNm^{-2}$(803K), indicating that there was little variation in the size of cavities at the various stages of creep.

The increase of maximum cavity width with creep strain and time at $45MNm^{-2}$ (963K) is illustrated in Figure 74, where the cavity growth curve has been superimposed on the creep curve. The very early stage

of creep life was characterised by a rapid growth rate which quickly decayed into a stage of decelerating growth that extended to the end of steady state creep, at which point a minimum in the rate of cavity width increase was reached. The broad inflexion, representing the cavity growth curve, was then completed by a final stage in which the rate of cavity growth increased sharply from the beginning of tertiary creep to failure. Similar behaviour was exhibited by the maximum cavity width, recorded after various increments of strain, during creep deformation at $130MNm^{-2}$ (863K). In those tests completed at lower temperatures, and involving a larger applied stress, the rate of cavity growth in the plane of the grain boundary was almost negligible throughout creep life.

7.2.5.2. Cavitated Area

The average cavitated area, as a percentage of the total grain surface area of those boundaries normal to the stress axis, has been recorded in Table 10 for a number of cavity populations investigated at various combinations of stress and strain. This parameter has been plotted as a function of normalised strain $\varepsilon/\varepsilon_f$ for two different stress levels, Figure 75. The curves generated may be regarded as representing the mean rate of cavitation in terms of progressive creep deformation.

The curve reflecting behaviour at the lower stress level reveals an initial period of increasing cavitation rate until a maximum reached and the rate gradually decreases to fracture, where the grain facets were almost entirely cavitated. The point of inflexion is coincident with the onset of tertiary creep. At the higher stress level, the proportion of damaged grain boundary surface area increased more rapidly with strain during the early stages of creep life. After

a comparatively small fraction of the total creep strain had been incurred at this stress level, the grain facets were saturated with cavities and the rate of cavitation decreased to a negligible level well before accelerated creep was observed. At still higher stresses this trend was exaggerated until it appeared that grain facets were almost entirely cavitated, soon after the application of the load.

7.2.6. Auger Electron Spectroscopy

A number of specimens were prepared from material that had been crept to failure at 963K under two different stresses of 60 and 90MNm^{-2}. After intergranular fracture had been effected under high vacuum conditions, the prior austenite grain boundaries thus exposed were subjected to chemical analysis by Auger electron spectroscopy. Typical spectra generated, by material ruptured at the two different stress levels, have been reproduced in Figures 76(a) and 76(b). The ordinate of the trace is formed by a differential value of the amplified signal strength and reflects the concentration, in atomic %, of elements present in the vicinity of the prior austenite grain boundaries. The abcissa forms a linear measure of the Auger electron kinetic energy and the characteristic intensity peaks due to several elements have been identified on the two spectra.

A surprising feature, observed on all the traces produced, was the apparent absence of intensity peaks due to the elements Mo and V. However, at the lower end of each spectrum, where the back-scattered electrons are characterised by low values of kinetic energy, intensity peaks due to the presence of S (K.E. = 150eV) and P (K.E. = 118eV) could be identified. Due to their low energy, the escape depth of auger electrons associated with these elements is correspondingly small and thus the intensity trace generated is more representative of a monolayer situation at the grain

boundary. Using one of the large intensity peaks due to Fe as a standard and correcting for the detector sensitivity (Equation 54), the following grain boundary concentrations of S and P were determined for the material tested at the two stress levels; assuming monolayer segregation :

STRESS MNm^{-2}	P At. %	S At. %
60	5.0	2.7
90	2.5	3.0

In both cases, the grain boundary concentration for both elements is considerably greater than the bulk value determined for the heat treated material (Table 1). It is also interesting to note that the specimen that underwent creep deformation at the lower stress revealed a higher level of segregation at the grain boundary. Some caution must be taken, however, when considering the validity of these absolute figures, especially with those quoted for S as this element is extremely mobile under the influence of the electron beam.

Despite the high concentration of Cu present in the bulk alloy (0.15 at %), segregation of the element at the prior austenite grain boundaries was not detected, the major Cu intensity peak should appear at 920eV. This region of both spectra has been amplified tenfold, since the technique is least sensitive here, and,as shown,there is no detectable change in the background level.

CHAPTER 8

DISCUSSION

8.1. 2¼Cr 1Mo Alloy Steels

A significant feature of the creep rupture mode of these alloy steels, in the heavily tempered condition, was the similarity in behaviour with that observed in specimens strained to failure at room temperature. Also of note, was the negligible effect on minimum creep rate, ductility (at high and low temperatures) and damage accumulation, of large additions of Sn. In complete contrast, the introduction of a Bridgman-type notch produced a substantial strengthening effect by apparently suppressing the nucleation of creep damage. These observations, together with the microstructural evidence on precipitate distribution and damage morphology, have provided a basis for possible mechanisms of cavity nucleation, growth and coalescence to final fracture.

8.1.1. Creep Deformation

The value of the stress exponent of minimum creep rate, 4.9, exhibited by both series of alloys falls close to that of 4.5 derived by Weertman (1957) in his model for dislocation climb (Section 2.2.1.). According to the findings of Cannon and Sherby (1970) a stress exponent of 5 is to be associated with single phase solid solution alloys with a large elastic modulus, the dominant mode of deformation again being attributed to dislocation climb. Further, if precipitation hardening had provided a significant strengthening effect in these steels, a

much larger value for the stress exponent would have been expected (Section 2.2.4.). The fact that this material could be regarded as a simple single phase solid solution was confirmed by the absence of a fine dispersed phase of M_2C and the consequent large $M_{23}C_6$ particles that could provide little strengthening. Moreover, untempered material showed a much higher tensile strength presumably due to the presence of M_2C on a fine scale and the consequent increase in matrix strength.

A contribution to the overall creep strain was provided by grain boundary sliding at prior austenite grain boundaries and also by the relative translation of adjacent bainite plates. The nature of interference fringes on the surface of crept specimens also indicated that GBS was accompanied by shear accommodation within narrow zones adjacent to the prior austenite grain boundaries. The denudation of M_2C precipitates in these areas, to produce precipitate free zones, corresponded to these shear concentrations, where the flow stress was lower than that of the matrix. Similar conclusions have been reported in other materials (Venkiteswaran et al, 1973; Unwin and Smith, 1969; Stone and Murray, 1965) and Cane (1976) working on 2¼Cr 1Mo alloy steel found that shear strain concentrations of 50% were not unusual at strains of 2% in a PFZ of width 2.5μm, similar to that observed in this investigation.

8.1.2. Nucleation of Damage

The ductile cusp size observed on the fracture surface of creep rupture specimens, and more especially those measured on the fracture surface of specimens strained to failure at room temperature, corresponded to the proportions of alloy carbides present within the matrix. Fractographic studies of specimens interrupted during tertiary creep, revealed that voids did not form preferentially on grain boundaries and

provided a more exact correspondence in size to that of the alloy carbides. A similar relationship between carbide size and ductile cusp dimensions has been reported by Gladman et al (1970) who invoked the model proposed by Gurland and Plateau (1963) for nucleation by strain induced decohesion at the interface between particle and matrix.

The similarity between high and low temperature behaviour was further evidenced by the lack of damage observed in the uniformly strained regions in both temperature regimes of deformation. Further, it appeared that a high degree of creep strain was required before interfacial separation occurred, Figure 27 shows cavities in the early states of development after 10% strain, again reflecting mechanisms operative during low temperature ductile fracture.

Cane (1976), investigating creep damage characteristics in 2¼Cr 1Mo steel, after a variety of heat treatments, showed that the incidence of grain boundary cavitation was severely restricted by wide precipitate free zones at prior austenite grain boundaries. The author implied that stress concentrations required for nucleation at coarse grain boundary particles would be dissipated by shear accommodation in the adjacent zones. Figure 32 reveals that cavity density falls off dramatically as the width of precipitate free zones increases. The material investigated in this study exhibited PFZ's of widths up to 3μm and consequently it might be expected that grain boundary cavity nucleation would be suppressed completely, as was in fact observed.

8.1.3. Growth of Creep Damage

Damage in all creep specimens, at both high and low levels of applied stress, was seen to take the form of coarse holes elongated in the direction of the applied stress. The variety of ductile cusp

sizes observed on the creep fracture surfaces, indicated that growth of individual voids had occurred in the later stages of creep life. As mentioned previously voids were not associated with prior austenite grain boundaries. These observations suggested that hole growth occurred mainly by a continuum process not by one involving vacancy diffusion, in which case cavities would have been expected to retain their spherical morphology and growth principally confined to those situated on grain boundaries.

Hancock (1976), investigating the creep damage of a heavily tempered 1 Cr ½Mo alloy steel, reported that the prevailing form of creep damage, at low values of stress/strain rate ratio $\sigma/\dot{\varepsilon}$, consisted of large elongated holes of mean radii $\leqslant 40\mu m$. Conversely, at high values of this parameter, hole radii varied from 0.2 to 3μm and remained approximately spherical in the deformation regime described by a high $\sigma/\dot{\varepsilon}$ ratio. The author proposed that at low values of $\sigma/\dot{\varepsilon}$, cavities grew by viscous flow. Dislocation motion producing strains at the surface of the cavity, such that the growth rate is given by :

$$dR/dt = R\dot{\varepsilon} - \gamma/2\mu \qquad \text{.....(56)}$$

Where R is the cavity radius, γ the surface energy and μ the shear modulus. High values of the $\sigma/\dot{\varepsilon}$ ratio would favour growth by a vacancy flux mechanism described by Equation (38). The author further indicated that the dominance of either process was dependent on the initial hole radius. Using an arbitrary cavity spacing of 1μm, Figure 33 illustrates that for a $\sigma/\dot{\varepsilon}$ of $9MNsmm^{-2}$, the diffusion hole growth becomes the slower mechanism for hole radii > 0.7μm. At a ratio of $45MNsmm^{-2}$ viscous growth dominates for hole radii > 1.7μm.

This analysis might usefully be applied to the results obtained in

the present study. As mentioned earlier, void growth did not commence until an advanced stage of tertiary creep had been achieved. For all stress levels, tangents drawn to the creep curve at this stage (Figure 12) yielded a strain rate value of $\sim 1.5 \times 10^{-5} s^{-1}$, thus the ratio of $\sigma/\dot{\varepsilon}$ for all specimens tested fall in the range 12 to 17 MNsmm^{-2}. Further, typical void nuclei were of the order of 1μm. Reference to Figure 33 clearly shows that these boundary parameters put hole growth for the alloys investigated into the viscous growth regime. Later stages of creep life, characterised by mean hole radii of up to 15μm, is dominated by viscous growth and accounts for their markedly elongated nature.

Since the rate of hole growth by a viscous process depends on the relative value of strain rate, Equation 56, those values exhibited by the creep of notched specimens were low enough to preclude growth of any damage by this mechanism. Further, the low strains experienced by material in the region of the notch would have been insufficient to cause interfacial separation within the matrix or at grain boundary particles. The considerable notch strengthening observed in these alloys, in their particular heat treated condition, might be explained in terms of Ø/Ø material behaviour described in Section 3.1.2.2. Here, the deformation and failure mechanisms are controlled by the effective stress $\bar{\sigma}$, a measure of the shear component of stress. The stress dependency of deformation, n, was found to be comparable with that for plain specimens; thus dislocation climb can be considered to be the major deformation mechanism of material within the notch. The mechanism of shear failure is provided by grain boundary sliding, already shown to contribute significantly to creep damage in this material.

Recent work by Bryant (1977) has shown, that for a Bridgman notch of similar dimensions to that used in this study, the effective stress is considerably lower than the nominal applied stress across the notch.

Therefore, it might be expected that the rate of deformation and damage accumulation, both controlled by $\bar{\sigma}$, would be lower in a notched specimen under a similar stress to that applied to plain specimens, resulting in considerable notch strengthening.

8.1.4. Effect of Sn Additions

The addition of quantities of Sn was seen to have negligible effect on both the rate of creep deformation and damage accumulation. This is not surprising, since the nucleation and growth of creep damage did not appear to be associated with grain boundaries, where segregation of impurities could enhance cavitation by a lowering of the interfacial energy (Section 3.2.).

8.1.5. Creep Fracture

The macroscopic behaviour of this material during creep provided certain clues as to the ultimate fracture process. The prolonged period of tertiary creep, terminating in a stage of rapid strain rate producing a considerably proportion of the overall fracture strain, indicates that fracture was a time dependent process in contrast to rapid crack propogation. Further, the ratio of the uniform strain ε_u to the fracture strain ε_f was found to be a constant, 0.5, at all levels of stress, suggesting that the material failed when a constant volume fraction of damage had been produced. Metallographic examination showed that damage was elongated in the direction of the applied stress, thus preventing coalescence of cavities or fracture of the material between voids, in contrast to transgranular cracking at room temperature where cleavage facets were observed.

Thus, the elongation of creep damage accounts for the prolonged

period of tertiary creep. The drop in ductility with increasing applied stress can be explained in terms of the failure of material in the ligaments between the voids, at high stresses this would occur at lower overall creep strains.

8.2. ½Cr ½Mo ¼V Alloy Steel

8.2.1. Rupture Processes

The CRMV series alloy had been given a careful beat treatment to simulate typical structures experienced in the HAZ region of steam pipe weldments. In this condition, the material exhibited an extra-ordinary range of mechanical behaviour charcterised by dramatic changes in rupture ductility and failure mode within different regimes of temperature. This behaviour is illustrated by the fracture map shown in Figure 77, where the rupture ductility has been plotted as a function of deformation stress (it would have been equally appropriate to have used temperature as the variable on the abssisca). Tensile data, obtained by deformation at a constant strain rate, has been combined with that generated by creep tests to produce a deep ductility trough with an almost negligible strain to failure at 300MNm^{-2}. With a further reduction in the deformation stress, the rupture ductility passed through this minimum value to show a significant rise to almost 2% at 45MNm^{-2}. This ductility trough could be related to a progressive change in the mode of failure. High stresses and low temperatures, involving extensive rupture ductility, were associated with a trans-granular fracture path; in contrast, the low ductilities that accom-panied a decrease in the deformation stress (or rise in temperature) exhibited a failure mode that became predominantly intergranular.

The detailed metallography of the damage produced by both tensile and creep deformation suggested that three major mechanisms of damage accumulation were operating within the broad regimes delineated by failure mode. The fields in which a given mechanism is dominant have been superimposed on the ductility curve in Figure 77. Each process was sensitive to the applied stress, temperature and also to the test conditions: no boundary cavitation was observed on the grain facets exposed by fracture during tensile deformation (Section 7.2.1.1.).

Such a broad range of behaviour exhibited by the CRMV series alloy was in complete contrast to that described for the CRM series alloys, where low and high temperature fracture modes showed many similarities. It is hoped, in the following discourse, to relate a particular process of damage accumulation and fracture mode to the following parameters: precipitation and its effect on matrix strength; the chemistry of those regions adjacent to the grain boundary; possible mechanisms of grain boundary cavity nucleation and growth.

8.2.2. Creep Resistance

A different value of the stress exponent (n) of secondary creep rate characterised each temperature at which the creep properties of this material were investigated. A very low stress sensitivity ($n \tilde{-} 2.5$) was associated with deformation at high temperatures whilst tests at 803 K yielded an exponent of approximately 12. Attempts to rationalize the steady state creep data using Equation 12, and thus invoking the concept of a friction stress σ_o, did not prove fruitful. Further, the absence of any signficant sub-cell formation, during creep at all temperatures, dictated against this approach.

As suggested previously, Section 2.2.4., large values of the stress

exponent can be related to creep deformation in complex alloys where dispersion hardening is the dominant strengthening mechanism. Conversely, low values are indicative of behaviour similar to dislocation movement in single phase solid solution alloys, These arguments reflect the precipitation effects, due to a large extent to the prior austenitising heat treatment, observed during creep at the various temperatures studied. The heterogeneous precipitation of very fine VC platelets on dislocations within the ferrite plates occurred at an early stage in creep life and provided the dispersion remained stable, as observed at lower temperatures, would account for the large stress exponent. Some coarsening of VC precipitates was observed in material crept for long periods at 973 K, but it is difficult to attribute the low stress sensitivity at this temperature to a complete loss of matrix strength.

Figure 78 shows a double log plot of stress against the temperature-compensated strain rate parameter P'_R (Equation 42). The change of gradient exhibited at the juction of various stress and temperature regimes, implies that there is a change in activation energy for steady-state creep (Equation 2) as the temperature is changed. Simple calculations show that these changes are quite substantial, of the order of 100 kJ mol^{-1}, and mirror the dramatic change in the value of the stress exponent.

These observations strongly suggest that a contribution to the overall strain was made by a process other than intragranular deformation, to an extent sensitive to the prevailing test temperature. The enhancement of the minimum creep rate by grain boundary deformation has been referred to in Equation 13. The term $\dot{\varepsilon}_{GB}$ comprises a combination of grain boundary shearing and the strain produced by the growth of grain boundary cavities. However, there was a complete absence of any evidence

to indicate that there had been any shear translation of adjacent grains during creep deformation. Indeed, the matching of common features across decohered boundaries after creep failure (Section 7.2.3.3.3.) provided proof that grain boundary sliding had been completely suppressed in this material. Further, at all temperatures investigated, precipitate-free zones adjacent to the prior austenite grain boundaries were conspicuous by their absence and thus the accommodation of strain in this region would have been severely limited. Therefore, it must be assumed, by the process of elimination, that a significant proportion of the total creep strain at any temperature was due to that cavity growth occurring in a plane parallel to the stress axis. A rider to this argument is that geometric constraints on the cavity growth rate will be applied by the grain structure's inability to accommodate this strain by boundary sliding, this will be referred to again later (Section 8.2.3.2.).

8.2.3. Creep Damage

8.2.3.1. Cavity Nucleation

During the earlier stages of creep life, discrete colonies of cavities were observed at those preferred sites on particular grain facets (i.e. those approximately normal to the tensile axis). Since gross coalescence and cavity wall breakdown did not occur until the tertiary stage of creep had been attained, the reciprocal of the mean area occupied by each cavity in the plane of the boundary would be directly proportional to the number of cavities nucleated per unit area of grain boundary, N. The mean cavity width $\bar{d}$, derived from the size distribution curves for cavity populations in these earlier stages of development, is thus related to N by :

$$1 / \bar{d}^2 \alpha N \qquad \text{.....(57)}$$

Figure 79 shows a double-log plot of the parameter $1/\bar{d}^2$ as a function of the applied stress σ. A good linear fit for the quantitative fractographic data is obtained and yields a relationship of the form:

$$N \alpha \sigma^{5/4} \qquad \text{.....(58)}$$

The magnitude of the stress exponent, obtained using a similar technique, for α - iron was shown to be 2 (Cane, 1974). Other investigators, utilizing a parametric approach with density change measurements (Equation 20), reported larger exponents for a variety of pure metals, as quoted in Section 3.1.1.4.

This variation, in the stress-dependence of cavity nucleation, between pure iron and the CRMV series alloy can be related to the possible nucleation mechanisms prevailing in the two materials and the influence of various parameters on the nucleation events (Section 3.2.) The Auger electron spectroscopy results indicated the possible segregation of P to the prior austenite grain boundaries, in sufficient quantities to lower the surface energy of nuclei (Equation 34). The reduction in γ_s would permit smaller nucleii to remain stable (Equation 28) and further, reduce the magnitude of the stress concentration required for the nucleation event (Equation 33). Thus, the presence of tramp elements in a commercially cast material might be expected to reduce the stress-dependence of nucleation in a commercially cast material. There is now much evidence to suggest that the principal culprit might be P, Tipler and Hopkins (1976) investigated cavitation in similar low alloy ferritic steels and showed that a very small reduction in the bulk concentration of P (from 0.008 to 0.003 wt%) decreased the rate of nucleation by two orders of magnitude. Similarly, Wolstenholme (1976)

indicated an enhancement of creep cavitation by increasing the P content of a 2¼Cr Mo steel from 0.010 to 0.026 wt%. Although the degree of confidence that can be placed on the results is not high, the segregation of such elements appears to be time dependent, as indicated by the higher concentration of P detected after longer periods of creep.

A significant clue to the mechanism of nucleation was provided by the position of preferred sites in relation to the stress axis, grain configuration and orientation of the matrix structure. The incidence of heavily cavitated grain edges and corners, occupying a plane normal to the tensile axis, can be explained in terms of dislocation slip planes impinging on the grain boundary delineating these areas: dislocations with their Burger's vector aligned parallel to the stress axis will be subjected to a larger stress than those capable of motion in slip planes normal to the axis. Consequently, a greater number of dislocations will arrive at grain boundary features perpendicular to their motion and the stress axis. Further, the length of a matrix slip plane is greatest from triple junctions, at opposite positions of the grain configuration, and decreases in zones removed from such points, as illustrated in Figure 80. The presence of discontinuities at the boundary interface, such as particles of ledges, provide a barrier to the further movement of mobile dislocations. Therefore, a situation can be envisaged whereby larger pile-ups of dislocations can accumulate in the vicinity of a tripe point, where longer slip planes impinge; the simple Stroh analysis (Equation 32) predicts a reduction in the stress required to induce a nucleation event as the number of dislocations is increased. A further indication of the probable role played by matrix dislocations and their interaction with the boundary

interface, in this material, was provided by the apparent suppression of cavitation at certain prior austenite grain boundaries characterised by a parallel alignment of ferrite plates in adjacent grains. This phenomenon was also reflected in fractographic studies. Presumably, at such a boundary, there would be a close relationship between the slip planes in the ferrite plates on either side of the interface, such that the behaviour of dislocations impinging on the facet surface is modified, dissipating the influence of barriers and the stress field required for nucleation. Conversely, those regions of the prior austenite grain boundaries with a large mismatch of slip planes (due to the orientation of the ferrite plates) would correspond to those areas observed with dense cavity populations, Figure 80. A similar argument was put forward by Gifkins (1956), Section 3.2.1. The linearity observed in the arrangements of cavities on the creep fracture surface (Section 7.2.3.1.) gave further support to the stress dependency of nucleation, involving the pile-up of dislocations along their respective slip planes.

The association of a number of fine carbide particles with creep cavities suggests that their presence was an essential component in the nucleation event. This statement is by no means implying a conclusive argument, since there were far more particles present than cavities nucleated! However, the analysis by Smith and Barnby (1967) of the criterion for cavity nucleation at boundary discontinuities (Equation 33) invokes an optimum size range for easy nucleation, unaided by intra-granular deformation. Large particles require grain boundary sliding to enlarge the cavity nucleii above the critical size for growth, a feature illustrated by Cane (1974) in his work on 2¼Cr 1Mo steels. Here, the degree of cavitation could be directly related to strain accommo-dation in precipitate-free zones, adjacent to the prior austenite grain

boundaries, and the presence of gross boundary precipitates of $M_{23}C_6$, 0.3μm in diameter (Section 4.3.). The other extreme of the Smith-Barnby barrier size range might be associated with the situation prevailing at grain boundaries in pure, single phase metals. Since there are no particles present, it is thought that minute perturbations or ledges (on an atomic scale) are responsible for nucleation; the large stress concentration required and scarcity of such defects may account for the high stress dependence and the necessary accompaniment of grain boundary sliding for cavity nucleation. It would appear then that in the CRMV series alloy investigated here, the presence of fine VC carbides (500 to 1000Å in size) provided the ideal barrier size for cavity nucleation and thus accounts for the low stress dependency of nucleation without the aid of interfacial deformation.

Grain boundary voids were detected in their earliest stage of development in material after creep fracture, suggesting that nucleation was continuous with strain. The small cavity shown in Figure 68(b) has a diameter of approximately 0.1μm, substituting suitable values for surface energy ($2Jm^{-2}$ in pure iron) and applied stress ($45MNm^{-2}$) into Equation 28 yields a critical radius of 0.08μm. The curves representing the variation of cavitated area with strain showed that as deformation proceeds the nucleation rate $dN/d\varepsilon$ increased to a maximum value before saturation occurred and the rate decreased to fracture, the point of inflexion moving to lower values of the total strain at higher stresses. This implies a sequence of events whereby at the onset of deformation cavities nucleate at the most favourable sites and as the strain increases the pile-ups of dislocations at grain boundary barriers causes a sudden burst of activity elsewhere on the grain facets. The stress sensitivity is again reflected by the fact that at higher stresses (and lower temperatures) more sites become available earlier in creep

life and saturation is achieved at lower overall strains. This behaviour is in contrast to that observed in pure metals, where the density of suitable nucleation sites is very much lower than in complex alloys, consequently a state of saturation of nucleii is never reached. This leads to an acceleration in the nucleation rate towards the end of creep life, probably due to the ability of growing cavities to act as stress concentrations for further nucleation on the sparsely populated grain facets (Cane and Greenwood, 1975).

8.2.3.2. Cavity Growth

The striking spherical morphology retained by cavities throughout a large proportion of creep life and the absence of intragranular deformation strongly suggests that growth was diffusion controlled. The measurement of maximum cavity width, at the various stages of creep life, provided a reliable guide to the study of growth kinetics up to the start of tertiary creep where cavity coalescence occurred. Assuming a perfectly spherical shape, the maximum cavity volume V_m is simply related to d_m and this parameter has been plotted on a logarthmic scale against time for two different stress levels in Figure 81. Linear relationships were obtained for both sets of data with time dependence for cavity growth decreasing at the higher stress level:

$$V_m \alpha t^{1/2} \quad \text{at} \quad 45 MNm^{-2} \qquad \ldots\ldots\ldots(59)$$

$$V_m \alpha t^{1/4} \quad \text{at} \quad 130 MNm^{-2} \qquad \ldots\ldots\ldots(60)$$

The modified diffusional growth rate equations proposed by Speight and Harris (1967) accounting for continuous nucleation predicts the observed time dependence for growth at the lower stress only. At the higher stress level, the time dependence is modified by the stress

dependence of cavity nucleation, although a stress-induced diffusional growth process still applies. In the latter stress regime, the dense populations of cavities on a particular facet have restraints on growth imposed by the proximity of their neighbours, thereby reducing the rate of growth. In α-iron, where the population density produced can be compared to that prevailing at lower stresses in the CRMV alloy, a similar relationship holds for cavity growth during the early stages of creep life, with the maximum cavity length, width and height proportional to $t^{\frac{1}{2}}$ (Cane and Greenwood, 1975). Alternatively, the geometric constraints on cavity growth proposed by Dyson (1976) (Section 3.3.1.) might apply at the higher stress level. This author demonstrated that these constraints were most likely to occur in high strength alloys with high cavity population densities which are inhomogeneously distributed, resulting in the rate of cavity growth predicted by vacancy diffusion under a constant grain boundary load being an upper bound.

The cavity wall configuration adopted during the later stages of creep life (especially after prolonged exposure to high temperatures) by cavity coalescence and wall breakdown, indicated a change in the controlling mechanism for material removed from the grain boundary. This effect has been investigated previously by Burns et al (1973) who studied the smoothing of cavity wall networks in a Cr Mo V valve steel. They attributed the attenuated kinetics of wall breakdown to capillarity-motivated mass transport by surface diffusion. Using a simple model, first proposed by Kuczynski (1949) the authors showed that the decrease in cavity wall height x in time t could be represented by :

$$x = \frac{D_s \gamma_s \Omega^{4/3}}{kT} t\rho^3 \qquad \text{.....(61)}$$

where D_s is the surface self diffusion coefficient, γ_s is the grain boundary surface energy, Ω is the atomic valume and ρ the cavity wall radius. Equation (61) predicted that the quantities transported by surface diffusion would be 200 times that carried by stress directed vacancy diffusion through the lattice when cavity impingement had occurred. Detailed measurements on the smoothing out of the cavity wall network during annealing at 838 K, yielded a value of D_s substantially less than that for pure α-iron. The authors proposed that this finding was linked to the segregation of tramp elements, namely Pand Sn, to the prior austenite grain boundaries - thus inhibiting surface diffusion. The retention of the cavity network morphology on certain grain facets, observed in the CRMV series alloy after annealing (Section 7.2.3.3.1.) might be explained in terms of larger concentrations of P at those boundaries, thus delaying the sintering of damage by surface diffusion. This effect could be quite important when considering the mechanism of creep fracture, as outlined below.

8.2.4. Creep Fracture

The relation between creep life and stress for CRMV series alloy was of the form:

$$t_f \alpha 1/\sigma^{3.5} \qquad \ldots\ldots\ldots(62)$$

and was closely obeyed at all three temperatures investigated. This suggests that fracture took place after a given fraction of the grain boundary area was occupied by cavities and final crack propagation was a function of the degree of damage corresponding to the nucleation rate (Equation 58) and the growth rate (Equation 59 and 60) prevailing at a particular stress and temperature. This suggestion was supported by

the metallography of damage observed using a variety of techniques. The presence of grain boundary cracks of facet length immediately behind the creep fracture surface; the absence of deformation incurred by material separating adjacent cavities; the tendency to preserve the networks of intercavity necks, all imply a fracture criterion based on diffusive coalescence rather than crack propagation.

The theoretical value of the stress exponent of fracture life, derived from such a criterion and employing the empirical laws for cavity nucleation and diffusive growth, was given as 4.6 (Section 5.2.3.1). This relationship is obeyed by a number of pure metals and alloys, an exception being α-Fe which exhibits a stress exponent of $m = 7$ (Cane and Greenwood, 1975). The higher stress dependency implies that fracture is more sensitive to individual cavity size and spacing probably due to the unique cavity morphology and distribution existing in α-Fe. The converse is true for the CRMV material, where the high density of cavity populations and dominance of surface over lattice diffusion in the later stages of creep life (Section 8.2.3.) is responsible for the low stress sensitivity.

The fracture criterion, invoked above, for the CRMV series alloy can also be used to explain (in a qualitative fashion) the rupture ductility and tertiary creep behaviour exhibited at the various levels of stress and regimes of temperature. At low stresses and high temperatures the nucleation rate produces a relatively low density of cavity nuclei on the grain facet surface. Consequently, a larger proportion of material, in regions between adjacent cavities, must be removed by processes involving lattice and, in the later stages, surface diffusion. However, before a situation is reached whereby a sufficient amount of decoherence has been achieved to allow the propagation of a final crack, the ligaments of material between cavities may deform plastically to

produce a larger tertiary creep strain and the concomitant higher ductility. At high stresses this effect is minimized by the high density of creep damage created.

8.2.5. Effect of Notches

In contrast to the significant notch strengthening observed in the CRM series of alloys, where fracture was controlled by shear deformation processes, no strengthening effect was observed in the case of the CRMV alloy. Indeed, one specimen displayed slight notch weakening. As in the case of the former (Section 8.1.3.) this behaviour can be related to that displayed by Ø/Δ materials (Section 3.1.2.2.) whose rupture mode is governed by the maximum principal stress. A slight notch weakening effect was predicted for ideal materials such as Cu, where stress directed lattice diffusion controls fracture life. Thus the behaviour of notched CRMV material gives further vindication to the proposal that the production of creep damage, at least in the early stages of creep life, can be closely related to that in more simple materials.

8.2.6. Effect of Stress Changes

The results obtained from variable stress tests and subsequent comparison with behaviour expected at a constant stress, showed that a life fraction rule (Equation 47), employed to predict remaining creep life, was completely invalid for this material: the low to high stress change produced a life fraction excess of 1.9 and the reverse situation an excess of 0.23 above the creep life expectancy using this relationship.

The inadequacy of such an approach is due to the fact that no account is taken of the previous history of the material in terms of

damage production. This argument was reflected in the creep curves generated by deformation at the final stress level and comparison with those produced at a constant stress. The differences observed are associated with the nucleation and growth charactertistics prevailing at a particular stress and the laws governing the stability of cavity nuclei. Previous deformation at a high stress produced a decrease in creep life at the lower stress level; this effect is simply related to increasesin damage rate at higher stresses (Equation 58). A sufficient proportion of mature cavities would be large enough to resist sintering at the lower stress level, the cavitation produced during this initial period of deformation resulting in a reduction of expected creep life at the lower stress. In contrast, the reverse situation revealed an increase in creep life after prior strain at a lower stress level. Here, a low density of relatively large cavities exist on the boundaries when the final stress is applied and presumably further nucleation is inhibited since the high stress is transferred to material between adjacent cavities produced at the lower stress, promoting plastic deformation of the network walls. Material crept at a similar high value of stress, without prior deformation, has a much higher population density resulting in a shorter creep life (as explained above) than material pre-crept at the lower stress.

8.2.7. Behaviour Under Conditions of Constant Strain Rate

The tensile test completed at 773 K showed a marked drop in ductility which was associated with a partially intergranular fracture mode. The change in failure characteristics coincided with the appearance of a fine matrix dispersion of VC precipitates. A similar result for this alloy in the same heat-treated condition has been reported by Alberry

and Jones (1977) in a recent paper on the mechanical properties of low alloy ferritic steels and simulated HAZ's. Reiterating a previous view held by Myers (1972), the authors proposed that the considerable strengthening of the matrix at this temperature concentrated strain at the prior austenite grain boundaries. They further suggested that deformation in this region was promoted by the segregation of impurity elements to the boundary, these lowered the surface energy and inhibited boundary migration. This seems a reasonable explanation in view of the Auger results on crept specimens that indicated the presence of P at the grain boundaries.

The fracture surface of the above specimen exhibited clean undamaged grain facets; yet, a specimen crept at a similar temperature and deformed for a similar length of time as the tensile test, revealed heavily cavitated grain boundaries. There is a surprisingly simply explanation involving the constraints applied to cavity growth by deformation at a constant strain rate: In any system generating plastic strain in a specimen, the product of the stress and remaining area must always be equated. Under a constant rate of strain (i.e. a tensile test), if any cavities form they would immediately produce a component of strain and would tend to relax the stress imposed by the constant strain rate. Consequently, if the load is to remain constant the material adjacent to a cavity nucleus would deform in order to create a decrease in the remaining area, this necking action would suppress cavity growth. Under creep conditions, however, the load is constant and the previous constraints no longer apply.

CONCLUSIONS

(A) 2¼Cr 1Mo Alloy Steels

(I) In a heavily tempered condition, the creep fracture of these alloys was characterised by a substantial strain to failure whilst retaining adequate strength. The rupture mode at both high and low temperatures exhibited many similar features and the addition of Sn as a tramp element had no effect on the deformation and fracture properties in either regime.

(II) Grain boundary sliding contributed significantly to the overall creep strain at 838K. This phenomenon was not uniquely associated with prior austenite grain boundaries, the interfacial translation of adjacent bainite plate boundaries within the grains was also observed.

(III) The presence of wide precipitate free zones along the prior austenite grain boundaries, formed by the preferential growth of $M_{23}C_6$ and dissolution of M_2C, prevented the nucleation of intergranular damage by the accommodation of strain within these regions. The dominant mechanism of damage accumulation involved decohesion; after large plastic strains, at the interface of coarse $M_{23}C_6$ particles and the matrix.

(IV) The growth of damage did not occur until an advanced stage of tertiary creep had been achieved. The high strain rates associated

with this stage of creep life induced hole growth by a viscous process, producing a transgranular fracture and promoting high ductilities. The presence of a Bridgman-type notch introduced a hydrostatic component of stress and in suppressing the nucleation of damage produced a marked increase in creep life. This effect was in line with current theory and confirmed that, in this material, fracture was controlled by shear processes.

(B) ½Cr ½Mo ¼V Alloy Steel

(V) The simulated heat affected zone structure of this series of alloy steel displayed marked differences in fracture behaviour over a range of temperature extending from the ambient to those experienced under typical power plant operating conditions. This change in the mode of failure was reflected in the rupture ductility that dropped dramatically almost to zero as the temperature was increased, producing a deep ductility trough.

(VI) Using a variety of techniques, it was shown that the nucleation growth and interlinkage of creep cavities at the prior austenite grain boundaries was the predominant form of damage accumulation over a range of temperature and applied stress. Electron fractography enabled a detailed examination and quantitative assessment of such damage.

(VII) Evidence suggested that cavity nucleation was effected by stress concentrations induced at grain boundary carbide particles by dislocation motion. Nucleation was not homogeneous and preferred sites depended on the orientation of grain boundaries to the stress axis and the relative alignment of bainite plates across the boundary. The stress exponent of nucleation rate was found to be lower than that

found for pure iron; it is argued that the presence of carbide particles and the segregation of tramp elements to the boundary lowered the magnitude of the stress concentration required for the nucleation event and consequently reduced the stress dependence.

(VIII) The deformation behaviour under a variety of stress systems and cycles together with detailed observations on cavity morphology support a stress induced diffusional growth process whereby the growth rate of a nucleated cavity depended upon the maximum principal stress. The growth process was not aided by the interfacial translation of adjacent grains. At low stresses, the growth rate obeyed the same empirical relationship for growth by vacancy accretion as observed in pure α-iron; at higher stresses, however, the population density was such as to impose constraints on growth and resulted in a decreased rate of growth.

(IX) In the later stages of creep life the coalescence of adjacent cavities occurred by the removal of material in boundary walls by grain boundary diffusion. Final fracture resulted when a critical proportion of grain boundary area had been decohered.

(X) Creep life was shown to be a function of the degree of damage corresponding to the nucleation rate and growth rate, of grain boundary cavities, prevailing at a particular stress and temperature. The previous stress history of material had a large influence on the remaining creep life. Consequently, remaining life estimates and creep life prediction must involve a precise knowledge of the cavitational characteristics in the various stress and temperature regimes experienced in a service environment.

(XI) At intermediate temperatures, commonly associated with temper embrittlement problems, the presence of P as a segregant at the grain boundaries and the considerable matrix strengthening due to precipitation of VC combined to produce a brittle, intergranular fracture mode.

REFERENCES

Alberry, P.J. and Jones, W.K.C., 1977, Met Tech., 4 , 45.

Alberry, P.J., 1977, Priv. Comm.

Ansell, G.S. and Weertman, J., 1959, Trans. A.I.M.E., 215 , 838.

Ashby, M.F., 1966, Phil. Mag., 14 , 1157.

Ashby, M.F. and Raj, R., 1975, Conf. "The mechanics and physics of fracture", Inst. of Phys./Met. Soc., Paper 1 6.

Bailey, R.W., 1926, J. Inst. Met., 35 ,27.

Bailey, R.W., 1935, J. Jun. Inst. Eng., 46 , 1.

Baird, J.D. and Jamieson, A., 1972, J.I.S.I., 210 , 847.

Baird, J.D., Jamieson, A., Preston, R.R. and Cochrane, R.C., 1972, Conf. "Creep strength in steel and high temperature alloys", Sheffield, Pg. 207.

Balluffi, R.W. and Seigle, L.L., 1957, Acta Met., 5 , 449.

Barford, J. and Willoughby, G., 1971, Met. Sci. J., 5 , 32.

Barrett, C.R. and Sherby, O.D., 1965, Trans, A.I.M.E., 233 , 1116.

Barrett, C.R. and Nix, W.D., 1965, Acta Met., 13 , 1247.

Barrett, C.R., Lytton, J.L. and Sherby, O.D., 1967, Trans. A.I.M.E., 239 , 170.

Bates, H.G.A. and Ridal, K.A., 1963, "Joint International Conf. on Creep", London, Inst. Mech. Eng. 1 , 99.

Beckitt, F.R., Keown, S.R. and Pickering, F.B., 1968, United Steel Co. Ltd., Report No. PM 5281/3/68/A.

Bell, R.L. and Langdon, T.G., 1969, Conf. "Interfaces", Melbourne, Butterworths, Pg. 115.

Bentley, K.P., 1966-68, Welding Inst. Paper C347.

Boettner, R.C. and Robertson, W.D., 1961, Trans. A.I.M.E., 221 , 613.

Boniszewski, T. and Eaton, N.F., 1969, Met. Sci. J., 3 , 103.

Brownsword, R. and Hoar, M.R., 1973, Scripta Met., 7 , 643.

Bruscato, R., 1970, Weld. J. Res. Supp., 35 , 1485.

Buchi, G.J.P., Page, J.H.R. and Sidey, M.P., 1965, J.I.S.I., 203 , 291.

Burns, D., James, D.W. and Jones, H., 1973, Met. Sci. J., 7 , 204.

Burton, B., 1972, Met. Sci. and Eng., 10 , 9.

Cane, B.J., 1974, C.E.R.L., Report No. RD/L/R 1892.

Cane, B.J. and Greenwood, G.W., 1975, Met. Sci. J., 9 , 55.

Cane, B.J., 1976, Met. Sci. J., 10 , 29.

Cane, B.J., 1977, C.E.R.L. Report No. RD/L/R 1965.

Cane, B.J., 1978, Priv. Comm.

Cannon, W.R. and Sherby, O.D., 1970, Met. Trans., 1 , 1030.
Chen, C.W. and Machlin, E.S., 1956, Acta Met., 4 , 655.
Coble, R.L., 1963, J. App. Phys., 34 , 1679.
Cocks, G.J. and Taplin, D.M.R., 1967, Metallurgia, 75 , 229.
Conrad, H., 1961, "Mechanical behaviour of materials at elevated temps.", Ed., J.E. Dorn, McGraw-Hill, Pg. 149.
Cottrell, A.H., 1958, Trans. A.I.M.E., 212 , 838.
Cottrell, A.H., 1961, "Structural processes in creep", I.S.I. Special Report No. 70, Pg. 1.

Davies, P.W. and Dennison, J.P., 1959-60., J. Inst. Met., 88 , 471.
Davies, P.W. and Wilshire, B., 1961-62, J. Inst. Met., 90 , 470.
Davies, P.W., Richards, J.D. and Wishire, B., 1961-62, J. Inst. Met., 90 , 431.
Davies, P.W. and Evans, R.W., 1965, Acta Met., 13 , 353.
Davies, P.W. and Wilshire, B., 1965, Phil. Mag., 11 , 189.
Davies, P.W. and Dutton, R., 1966, Acta Met., 14 , 1138.
Davies, P.W. and Williams, K.R., 1969, Met. Sci. J., 3 , 48.
Davies, P.W. and Williams, K.R., 1969(a), Met. Sci. J., 3 , 220.
Davies, P.W. and Williams, K.R., 1969(b), J. Inst. Met., 97 , 337.
Davies, P.W. and Wilshire, B., 1971, Scripta Met., 5 , 475.
Davies, P.W. and Dutton, R., 1967, Acta Met., 15 , 1365.
Davis, E.A. and Manjoine, M.J., 1952, "Strength and ductility of metals", A.S.T.M. Special Publ. No. 128, New York, Pg. 67.
Day, R.V., 1965, J.I.S.I., 203 , 279.
Dobes, F. and Milicka, K., 1976, Met. Sci. J., 10 , 382.
Dunlop, G.L. and Honeycombe, R.W.K., 1977, Met. Sci. J., 8 , 261.
Dyson, B.F. and McLean, D., 1972, Met. Sci. J. 6 , 220.
Dyson, B.F. and Henn, D.E., 1973, J. Microscopy, 97 , 165.
Dyson, B.F. and Rodgers, M.J., 1974, Met. Sci. J., 8 , 261.
Dyson, B.F., 1976, Met. Sci. J., 10 , 349.
Dyson, B.F. and McLean, D., 1977, Met. Sci. J., 11 , 37.
Dyson, D.J. and Holmes, B., 1970, J.I.S.I., 208 , 469.

Evans, H.E. and Waddington, J.S., 1969, Phil. Mag. 20 , 1075.
Evans, H.E., 1969, Met. Sci. J., 3 ,33.
Evans, H.E., 1971, Phil. Mag., 23 , 1101.
Evans, W.J. and Wilshire, B., 1970, Met. Sci. J., 4 , 89.

Farrell, K., Loh, B.T.M. and Steigler, J.O., 1967, Trans. A.S.M., 60 , 485.
Fields, J., 1977, To be published.
Fleck, R.G., Cocks, G.J. and Taplin, D.M.R., 1970, Met. Trans., 1., 3415.
Fleck, R.G., cocks, G.J. and Taplin, D.M.R., 1975, Acta Met., 23 , 415.
Fleck, R.G., taplin, D.M.R. and Beevers, C.J., 1976, Met. Sci. J., 10 , 413.

Garofalo, F., von Gemmingen, F. and Domis, W.F., 1961, Trans. A.S.M., 54 ,430
Garofalo, F., 1963, Trans. A.I.M.E., 227 , 351.
Garofalo, F., 1965, "Fundamentals of creep and creep rupture in metals", New York, Maçmillan.
Gates, R.S. and Stevens, R.N , 1974, Met. Trans., 5 , 505.
Gates, R.S., 1973, Acta Met., 21 , 855.
Gifkins, R.C., 1956, Acta Met., 4 , 98.
Gifkins, R.C., 1963, J. Aust. Inst. Met., 8 , 130.
Gifkins, R.C., 1969, "Fracture", Proc. 2nd. Tewksbury Symp., Univ. of Melbourne, Pg. 579.
Gifkins, R.C., 1973, Met. Sci. J., 7 , 15.
Gittins, A., 1967, Met. Sci.J., 1 , 214.
Gittins, A. and Williams, H.D., 1967, Phil. Mag., 16 , 849.
Gittins, A., 1970, J. Mat. Sci., 5., 223.
Gittins, A., 1970(a), J. Mat. Sci., 5 , 233.
Gladman, T., Holmes, B. and McIvor, I.D., 1970, I.S.I. Special Report No. 45 Pg. 68.
Glen, J. and Murray, J.D., 1961, I.S.I. Special Report No. 69, Pg. 40.
Glen, J., Leesells, J., Barr, R.R. and Lightbody, G.G., "Structural processes in creep", I.S.I., London, Pg. 222.
Goldhoff, R.M. and Beattie, H.J., 1965, Trans. A.I.M.E., 233 , 1743.
Goldhoff. R.M. and Brothers, A.J., 1968, J. Basic Eng., 67 , 10.
Gooch, D.J., 1977, Mat Sci. and Eng., 27 , 57.
Grant, N.J., 1959, Proc. Conf. "Atomic mechanisms of fracture", M.I.T., Pg. 563.
Greenwood, G.W., 1963, Phil. Mag., 8 , 707.
Greenwood, G.W. and Harris, J.E., 1965, Acta Met., 13 , 936.
Greenwood, G.W., 1969, Phil. Mag., 19 , 423.
Greenwood, G.W., 1970, Scripta Met., 4 , 171.
Greenwood, G.W., 1973, "Physical metallurgy of reactor fuel elements", Met. Soc., London, Pg. 53.
Greenwood, G.W., 1973, International Conf. on "Strength of metals and alloys", Inst. Met. / I.S., Cambridge.
Greenwood, G.W., 1977, 4th. International Conf. on Fracture, Waterloo, Canada, 1 , 293.

Greenwood, J.N., 1952, Bull. Inst. Met., 1 , 104.
Greenwood, J.N., 1952(a), Bull. Inst. Met., 1 , 120..
Greenwood, J.N., Miller, D.R. and Suiter, J.W., 1954, Acta Met., 2 , 250.
Gurland, J. and Plateau, J., 1963, Trans. A.S.M., 56 , 442.

Hancock, J., 1976, Met. Sci. J., 10 , 319.
Harris, J.E., Haddrell, V.J. and Rickards, G.A., 1962, J. Nuc. Mat., 6 , 144.
Harris, J.E., 1965, Trans. A.I.M.E., 233, 1509.
Harris, J.E., Jones, R.B., Greenwood, G.W. and Ward, M.J., 1969, J. Aust. Inst. Met., 14 , 154.
Harris, J.E., 1973, Met. Sci. J., 7 , 1..
Harris, J.E., Tucker, M.O. and Greenwood, G.W., 1974, Met. Sci. J., 8 , 311.
Hart, R.V., 1976, Met. Tech., 3 ,. 1.
Hayhurst, D.R., 1972, J. Mech. and Phys. of Solids, 20 , 381.
Herring, C., 1950, J. App. Phys., 21., 437.
Holloman, J.H. and Jaffe, L.C., 1945, Trans. A.I.M.E., 162., 223.
Hondros, E.D. and McLean, D., 1968, "Surface energy of solid metals", H.M.S.O., Monograph No. 28., London, Pg. 39.
Hondros, E.D. and McLean, D., 1974, Phil. Mag., 29., 771.
Hopkins, B.E., Tipler, H.R. and Branch, G.D., 1971, J.I.S.I., 209 , 745.
Hull, D. and Rimmer, D.E., 1959, Phil. Mag., 4 , 673.
Hyam, E.D., 1961, "Structural processes in creep", I.S.I. Special Report No. 70. Pg. 76.

Inman, M.C., McLean, D. and Tipler, H.R., 1963, Proc. Roy. Soc., A221 , 613.
Intrater, J. and Machlin, E.S., 1959-60, J. Inst. Met., 88 , 305.
Irvine, K.J., Murray, J.D. and Pickering, F.B., 1961, "Structural processes in creep", I.S.I. Special Report No. 70 Pg. 246.
Ishida, Y. and McLean, D., 1967, Met. Sci. J., 1 , 171.

Johannesson, T. and Tholen, A., 1969, J. Inst. Met., 97 , 243.
Johannesson, T. and Tholen, A., 1972, Met. Sci. J., 6 , 189.
Johnson, A.E., Henderson, J. and Khan, B., 1962, "Complex stress creep, relaxation and fracture of metallic alloys", Edinburgh, H.M.S.O.

Kachanov, L.M., 1961, "Rupture time under creep conditions" in "Problems of continuum mechanics", Philadelphia.

Keown, S.R. and Dyson, D,J., 1966, J.I.S.I., 204 , 832.
Kirby, B.R. and Beevers, C.J., 1977, Scripta Met., 11 , 659.
Kramer, D. and Machlin, E.S., 1958, Acta Met., 6 ,454.
Krisch, A., 1971, Jernkont. Ann., 155 , 323.
Kuczynski, G.C., 1949, Trans. A.I.M.E., 185 , 169.

Langdon, T.G., 1968, Scripta Met., 2 , 17.
Langdon, T.G., 1974, Can. Met. Quart., 13 , 223.
Lagneborg, R. and Attermo, R., 1969, J. Mat. Sci., 4 , 195.
Larson, F.R. and Miller, J., 1952, Trans A.S.M.E., 74 , 765.
Leckie, F.A. and Hayhurst, D.R., 1974, Proc. Roy. Soc. A340 , 323.
Leckie, F.A., Hayhurst, D.R. and Henderson, J.T., 1976, Univ. of Leicester Engineering Dept. Report No. 76/3.
Leckie, F.A. and Hayhurst, D.R., 1977, Acta Met., 25 , 1059.

Manson, S.S. and Haferd, A.M., 1953, N.A.C.A. Tech. Note No. 2890.
McLean, D., 1956-57, J. Inst. Met., 85 , 468.
McLean, D., 1962, Met. Reviews, 7 , 481.
McLean, D., 1963, J. Aust. Inst. Met., 8 , 45.
McLean, D., 1971, Phil. Mag., 23 , 467.
McLean, D., 1974, Can. Met. Quart., 13 , 145.
McLauchlin, I.R., 1974, Proc. Conf. "Creep strength in steel and high temperature alloys", Met. Soc., London, Pg. 86.
Mohammed, F.A. and Langdon, T.G., 1974, Acta Met., 22 , 779.
Mohammed, F.A. and Langdon, T.G., 1975, Met. Trans., 6A , 927.
Monkman, F.C. and Grant, N.J., 1956, Proc. A.S.T.M., 56 , 593.
Mott, N.F., 1956, "Creep and fracture of metals at high temperatures", H.M.S.O., London, Pg. 21.
Mukherjee, A.K., Bird, J.E. and Dorn, J.E., 1969, Trans. A.S.M., 62 , 155.
Murphy, M.C. and Branch, G.D., 1969, J.I.S.I., 207 , 1347.
Myers, J., Willoughby, G., Ham, R.K. and Barford, J., 1968, Met. Sci. J., 2 , 209.
Myers, J., 1972, C.E.G.B., Conf. "Welding research related to power plant", Marchwood, Southampton, Paper 20.
Myers, J. and Price, A.T., 1977, Met. Tech., 3 , 406.

Nabarro, F.R.N., 1948, Proc. Conf. "Strength of solids", London, Pg. 15.
Neate, G.J. and Siverns, M.J., 1974, International Conf., "Creep and fatigue in elevated temperature applications", Sheffield.

Needham, N.G., 1973, Phd. Thesis, Univ. of Sheffield.
Needham, N.G., Wheatley, J.E. and Greenwood, G.W., 1975, Acta Met., 23 ,23.
Needham, N.G., Priv. Comm.
Nix, W.D., Matlock, D.K. and DiMelfi, R.J., 1977, Acta Met., 25 ,495.
Nutting, J., 1961, "Structural processes in creep" I.S.I. Special Report No. 70, Pg. 147.

Oliver, P.R. and Girifalco, L.A., 1962, Acta Met., 10 , 765.
Olney, M.J. and Smith, G.C., 1959, J.I.S.I., 193 , 107.
Orowan, E., 1946-47, J. West Scotland I.S.I., 54 , 45.

Parker, T.D. and Wilshire, B., 1975, Met. Sci. J., 9 , 248.
Perry, A.J., 1974, J. Mat. Sci., 9 , 1016.
Pilkington, R., Hutchinson, D. and Jones, C.L., 1974, Met. Sci. J., 8 , 237.
Presland, A.E.B. and Hutchinson, R.I., 1961-62, J. Inst. Met., 90 , 239.
Presland, A.E.B. and Hutchinson, R.I., 1963-64, J. Inst. Met., 92 , 264.
Prnka, T. and S obotka, A., 1973, Neue Hütte, 18 , 548.

Raj, R. and Ashby, M.F., 1972, Met. Trans., 3 , 1937.
Raj, R. and Ashby, M.F., 1975, Acta Met., 23 , 653.
Ratcliffe, R.T. and Greenwood, G.W., 1965, Phil. Mag., 12 , 59.
Ratliff, J.L. and Brown, R.M., 1967, Trans. A.S.M., 60 , 176.
Raynor, D., Whiteman, J.A. and Honeycombe, R.W.K., 1968, J.I.S.I., 204 , 349.
Robinson, E.L., 1962, Trans. A.S.M.E., 74 , 777.
Russel, B., Ham, R.K., Silcock, J.M. and Willoughby, G., 1968, Met. Sci. J., 2 , 201.

Seah, M.P. and Hondros, E.D., 1973, Proc. Roy. Soc., A335 , 191.
Scaife, E.C. and James, P.L., 1968, Met. Sci. J., 2 , 217.
Sellars, C.M. and Quarrell, A.G., 1961-62, J. Inst. Met., 90 , 329.
Sergeant, R.M., 1968, J. Inst. Met., 96 , 197.
Sherby, O.D., 1962, Acta Met., 10 , 135.
Sherby, O.D. and Burke, P.M., 1967, Progress in Mat. Sci., 13 , 325.
Siverns, M.J. and Price, A.T., 1973, International J. on Fracture, 9 , 199.
Smith, E. and Barnby, J.T., 1967, Met. Sci. J., 1 , 1.
Smith, E. and Barnby, J.T., 1967(a), Met. Sci. J., 1 , 56.
Smith, P. and Williams, K.R., 1975, C.E.G.B. Report No. SSD/MID/R75/75.
Spark , I.J. and Taplin, D.M.R., 1969, J. Aust. Inst. Met., 14 , 298.

Speight, M.V. and Harris, J.E., 1967, Met. Sci. J., 1 , 83.
Speight, M.V. and Beere, W., 1975, Met. Sci. J., 9 , 190.
Steigler, J.O., Farrell, K., Loh, B.T.M. and McCoy, H.E., 1967, Trans. A.S.M., 60 , 494.
Stevens, R.N., 1966, Met. Revs., 11 , 129.
Stone, P.G. and Murray, J.D., 1965, J.I.S.I., 203 , 1094.
Stroh, A.N., 1954, Proc. Roy. Soc., A223 , 404.
Stroh, A.N., 1957, Advances in Phys., 6 , 418.
Swift, R.A. and Rogers, H.C., 1973, Weld. J. Res. Suppl., 52 , 145.

Tait, R.A. and Knott, J.F., 1976, Conf. "Grain Boundaries", Inst. Met., Jersey, Paper C1.
Taplin, D,M.R., 1965, J.Aust. Inst. Met., 10 , 336.
Taplin, D.M.R. and Barker, L.J., 1966, Acta Met., 14 , 1527.
Taplin, D.M.R. and Wingrove, A.L., 1967, Acta Met., 15 , 1231.
Taplin, D.M.R. and Gifkins, R.C., 1967, Acta Met., 15 , 650.
Taplin, D.M.R., 1969, Phil. Mag., 20 , 1079.
Taplin, D.M.R., 1970, Met. Eng. Quart., 10 , 31.
Taplin, D.M.R., 1973, "The hot fracture story", Jubilee Conf. Proc., Banaras Hindu Univ., India.
Thomas, G.B. and Tipler, H.R., 1974, N.P.L. Report No. DMA74.
Threadgill, P.L. and Wilshire, B., 1974, Met. Sci. J., 8 , 117.
Tipler, H.R. and McLean, D., 1970, Met. Sci. J., 4 , 103.
Tipler, H.R., Taylor, L.H. and Hopkins, B.E., 1970, Met. Sci. J., 4 , 167.
Tipler, H.R., Taylor, L.H., Thomas, G.B., Williamson, J., Branch, G.D. and Hopkins, B.E., 1975, Met. Tech., 2 , 206.
Tipler, H.R. and Hopkins, B.E., 1976, Met. Sci. J., 10 , 47.
Trumpler, W.E., 1967, A.S.M.E., Paper 67, Met-12.

Unwin, P.N.T. and Smith, G.C., 1969, J. Inst. Met., 97 , 299.
Venkiteswaran, P.K., Bright, M.W.A. and Taplin, D.M.R., 1973, Mat. Sci. Eng., 11 , 255.
Venkiteswaran, P.k. and Taplin, D.M.R., 1974, Met. Sci. J., 8 , 97.
Viswanathan, R., 1974, Met. Tech., 1 , 284.
Viswanathan, R., 1974, Scripta Met., 8 , 1225.
Viswanathan, R., 1975, Met. Tech., 2 , 245.

Waddington, J.S., 1968, Phil. Mag., 17 , 51.

Waddington, J.S. and Evans, H.E., 1970, J. Nuc. Mat., 37 ,118.
Wadsworth, J., Keown, S.R. and Woodhead, J.H., 1976, Met. Sci. J., 10 , 105.
Wadsworth, J., 1975, PhD. Thesis, Univ. of Sheffield.
Weaver, C.W., 1960, Acta Met., 8 , 343.
Weertman, J., 1957, J. Appl. Phys. 28 , 362.
Weertman, J., 1957(a), J. Appl. Phys., 28 , 1185.
Weertman, J., 1973, Scripta Met., 7 , 1129.
Wheatley, J.E., 1971, PhD. Thesis, Univ. of Sheffield.
Williams, J.A., 1967, Acta Met., 15., 1119.
Williams, J.A., 1967(a), Phil. Mag., 15 , 1298.
Williams, K.R. and Wilshire, B., 1973, Met. Sci. J., 7 , 176.
Wilshire, B., 1970, Scripta Met., 4 , 361.
Wingrove, A.L. and Taplin, D.M.R., 1969, J. Mat. Sci., 4 , 789.
Wingrove, A.L. and Taplin, D.M.R., 1969(a), Scripta Met., 3 , 649.
Winzor, F.A., 1975, PhD. Thesis, Univ. of Sheffield.
Wolstenholme, D.A., 1976, Conf. "Grain Boundaries", Inst. Met., Jersey, Paper C7.
Woodford, D.A., 1969, Met. Sci. J., 3 , 50.
Woodford, D.A., 1969(a), Met. Sci. J., 3 , 234.
Woodford, D.A. and Goldhoff, R.M., 1969-70, Mat. Sci. and Eng., 5 , 303.
Woodford, D.A., 1973, International Conf. "Creep and fatigue in elevated temperature applications", Sheffield.

Yeldham, D.E. and Brook, R., 1974, Met. Tech., 1 , 199.

Zener, C., 1948, "Fracturing of metals", A.S.M., Cleveland, Pg. 1.

ACKNOWLEDGEMENTS

This work is dedicated to my parents, without their understanding and kindness during three difficult years, I could not have continued. I would also take this opportunity to express my sincere thanks to Professor G. W. Greenwood, Mr. John Beynon and the staff of Weston Park Hospital for all they did on my behalf during a grim period of illness.

Thanks are again due to Professor Greenwood for his enthusiastic guidance and supervision of this project and, further, for the provision of research facilities. The award of a maintenance grant from the Science Research Council is gratefully acknowledged.

The technical staff of the Department of Metallurgy assisted on many occasions and I would especially thank Mr. Alan Sheldon for his support. I am also indebted to Drs. N. G. Needham, T. English (B.S.C. Swinden Laboratories) and P. J. Alberry (C.E.G.B. Marchwood Engineering Laboratories) whose advice and expertise were greatly appreciated. Finally, I would like to thank Mrs. Eva Paisley for her patience and forebearance in typing this thesis.

TABLE 1

CHEMICAL ANALYSIS OF ALLOY STEELS IN WEIGHT PERCENT

Code	Melting Practice	C	Cr	Mo	V	Mn	Si	Sn	Cu	P	Al	S	N*
CRM	Vacuum	0.13	2.32	1.05	<0.02	<0.02	0.02	N.A.	<0.02	N.A.	0.006	N.A.	N.A.
CRMS	Vacuum	0.12	2.23	0.99	<0.02	<0.02	<0.02	0.04	<0.02	N.A.	0.014	N.A.	N.A.
CRMV	Air	0.13	0.70	0.69	0.37	0.55	0.29	0.02	0.15	0.01	<0.01	0.01	N.A.

* Refers to Soluble Nitrogen Content

N.A. = Not Analysed

TABLE 2

Results of room temperature tensile tests on 2¼Cr 1Mo alloys

Series	Condition	UTS MNm^{-2}	ε_f %	ε_u %	R.A. %
CRM	Untempered	863	22	7.5	68
CRM	Tempered	521	24	10.3	83
CRMS	Tempered	512	24	11.1	80

TABLE 3

Results of creep tests at 838 K on CRM series alloy

Specimen	Stress MNm^{-2}	$\dot{\varepsilon}_s$ s^{-1}	t_f $s \times 10^{-4}$	ε_f %	ε_u %	R.A. %
CRM1	175	6.03×10^{-8}	166.0	49.0	N.R.	90.0
CRM2	180	7.50×10^{-8}	102.2	43.0	N.R.	88.5
CRM3	190	8.91×10^{-8}	56.2	27.5	13.0	89.5
CRM4	200	1.14×10^{-7}	28.8	18.5	10.5	88.5
CRM5	220	2.09×10^{-7}	15.9	15.0	8.0	85.0
CRM6	250	3.89×10^{-7}	3.6	17.0	8.5	88.0

TABLE 4

Results of creep tests at 838 K on CRMS series alloy

Specimen	Stress MNm^{-2}	$\dot{\varepsilon}_s$ s^{-1}	t_f $s \times 10^{-4}$	ε_f %	ε_u %	R.A. %
CRMS1	180	7.00×10^{-8}	93.3	35.0	N.R.	91.0
CRMS2	200	1.52×10^{-7}	20.7	18.0	10.0	87.5
CRMS3	250	3.16×10^{-7}	3.5	12.5	7.5	81.0

TABLE 5

Results of creep tests at 838K on CRMS Series alloy, using notched specimens.

Specimen	Stress MNm^{-2}	$\dot{\varepsilon}_s$ s^{-1}	t_f $s \times 10^{-4}$
CRMS4N	180	4.12×10^{-9}	Interrupted
CRMS5N	200	9.30×10^{-9}	Interrupted
CRMS6N	250	2.00×10^{-8}	Interrupted

TABLE 6

Results of tensile tests on CRMV series alloy .

Specimen	Temperature K	UTS MNm^{-2}	ε_f %
CRMV/U1	290	1100	15.3
CRMV/U2	573	1000	14.9
CRMV/U3	673	875	15.0
CRMV/U4	773	680	8.1

TABLE 7

Results of creep tests on CRMV series alloy.

SPECIMEN	TEMPERATURE K	STRESS MNm^{-2}	$\dot{\varepsilon}_s$ s^{-1}	t_f $s \times 10^{-4}$	ε_f %
CRMV 1	963	45	1.12×10^{-8}	77.5	1.67
CRMV 2	963	50	1.30×10^{-8}	62.8	0.81
CRMV 3	963	60	2.46×10^{-8}	44.7	0.92
CRMV 4	963	70	3.41×10^{-8}	20.5	0.44
CRMV 6	963	80	4.51×10^{-8}	18.4	0.43
CRMV11	963	85	5.14×10^{-8}	14.4	0.51
CRMV12	963	90	6.46×10^{-8}	5.6	0.37
CRMV 5	963	110	1.27×10^{-7}	4.5	0.30
CRMV 7	863	130	6.00×10^{-10}	64.4	0.25
CRMV13	863	170	3.10×10^{-9}	23.9	0.20
CRMV14	863	220	1.32×10^{-8}	10.8	0.14
CRMV 8	863	280	7.48×10^{-8}	4.8	0.17
CRMV 9	803	200	2.00×10^{-10}	31.1	0.10
CRMV15	803	220	7.00×10^{-10}	20.9	0.05
CRMV16	803	250	3.40×10^{-9}	12.3	0.05
CRMV10	803	300	2.68×10^{-8}	7.1	0.03

TABLE 8

Results of creep tests at 963K on CRMV series alloy, using notched specimens.

Specimen	Stress MNm^{-2}	t_f $s \times 10^{-4}$
CRMV/N1	45	81.6
CRMV/N2	70	19.2
CRMV/N3	90	5.7

TABLE 9

Results of creep tests, under variable stress at 963K on CRMV series alloy.

Specimen	σ_1 MNm^{-2}	σ_2 MNm^{-2}	t_i $s \times 10^{-4}$	t_2 $s \times 10^{-4}$	$\dot{\varepsilon}_s^1$ s^{-1}	$\dot{\varepsilon}_s^2$ s^{-1}	ε_f %
CRMV/R1	45	90	38.9	10.6	1.15×10^{-8}	5.50×10^{-8}	1.69
CRMV/R2	110	50	2.25	45.8	1.30×10^{-7}	9.41×10^{-9}	0.50

TABLE 10

Results of quantitative analysis of cavity size distribution after creep of CRMV series alloy.

SPECIMEN	TEST TEMPERATURE K	STRESS MNm^{-2}	TIME s x 10^{-4}	STRAIN %	$\bar{d}$ µm	d_m µm	COVERAGE %
CRMV17	963	45	9.0	0.12	0.91	2.60	7
CRMV18	963	45	21.6	0.30	1.00	3.02	20
CRMV22	963	45	32.4	0.51	1.25	3.20	40
CRMV23	963	45	41.4	0.62	1.35	3.40	53
CRMV24	963	45	50.4	0.74	1.50	3.50	69
CRMV29	963	45	63.0	0.95	3.84	7.80	82
CRMV 1	963	45	77.5	1.58	7.20	13.10	96
CRMV19	963	60	4.3	0.15	0.79	2.30	NR
CRMV20	963	60	22.3	0.45	0.95	3.00	NR
CRMV 3	963	60	44.7	0.92	4.11	7.50	NR
CRMV29	963	90	3.0	0.20	0.64	2.10	NR
CRMV12	963	90	5.6	0.35	2.51	4.70	NR
CRMV25	863	130	6.5	0.04	0.51	1.86	26
CRMV26	863	130	12.0	0.08	0.51	1.95	84
CRMV27	863	130	25.2	0.12	0.52	2.04	95
CRMV28	863	130	40.0	0.14	0.53	2.10	95
CRMV 7	863	130	64.4	0.20	1.55	3.00	97
CRMV 8	863	280	4.8	0.17	0.32	0.41	95
CRMV21	803	300	3.5	NR	0.29	0.3	90
CRMV10	803	300	7.1	0.03	0.29	0.3	95

Figs. 1(a). (b) and (c) show the critical dimensions of the various test pieces used in this investigation.

Fig. 1(a) Parallel-sided creep specimen. Similar pieces were used for tensile tests.

Fig. 1(b) Notched creep specimen.

Fig. 1(c) Dimensions of specimens used for analysis by Auger electron spectrosopy.

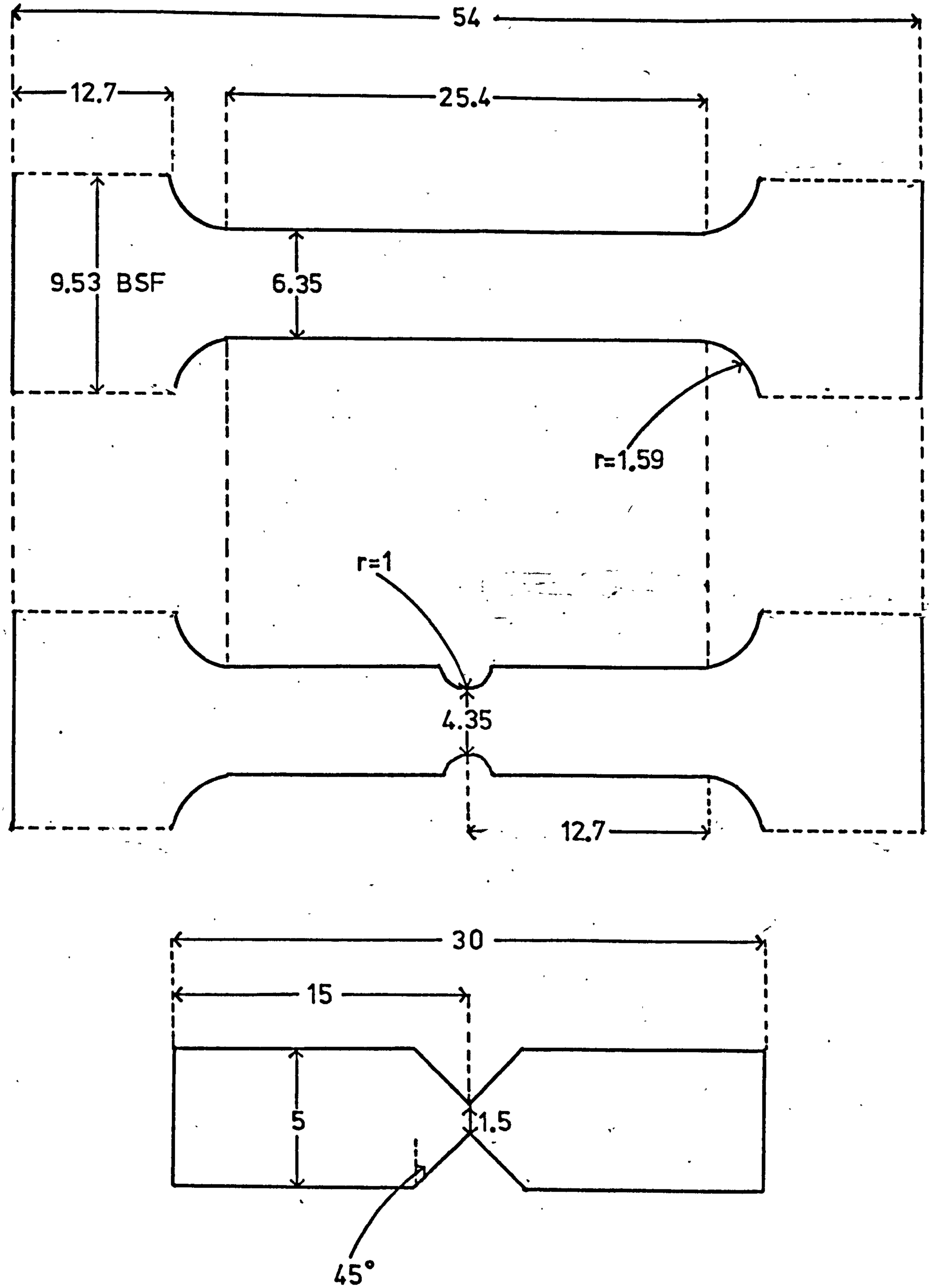
54
12.7
25.4
9.53 BSF
6.35
r=1.59
r=1
4.35
12.7
30
15
5
1.5
45°

Fig. 2(a) Parallel- sided creep specimen.

Fig. 2(b) Notched creep specimen.

Note the fiducial diamond indentations on the guage lengths.

Fig. 3(a) Dennison T47E creep machine set up for a test, prior to the application of the load.

Fig. 3(b) Vacuum sheath encasing the creep specimen is in position. Also shown is the arrangement for regulating the gas pressure during a test.

Fig. 3(c) Creep specimen in position between the pull rods, prior to loading into the vacuum sheath. Also shown is the arrangement of thermocouples on the specimen guage length.

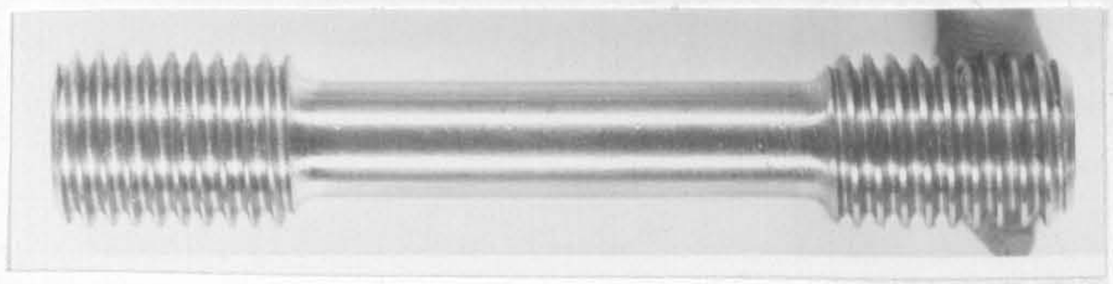

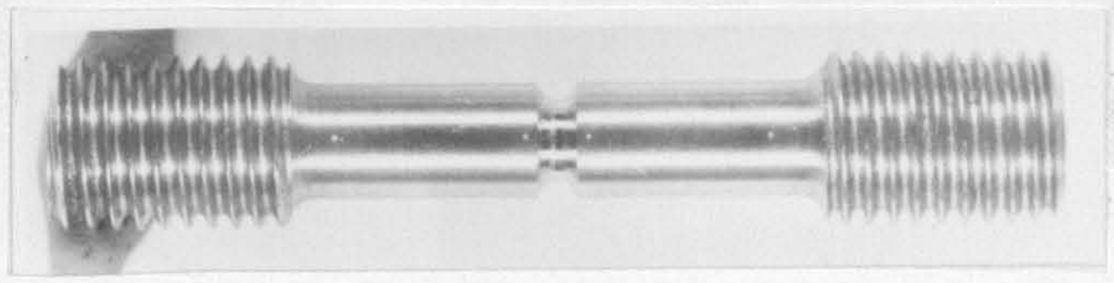

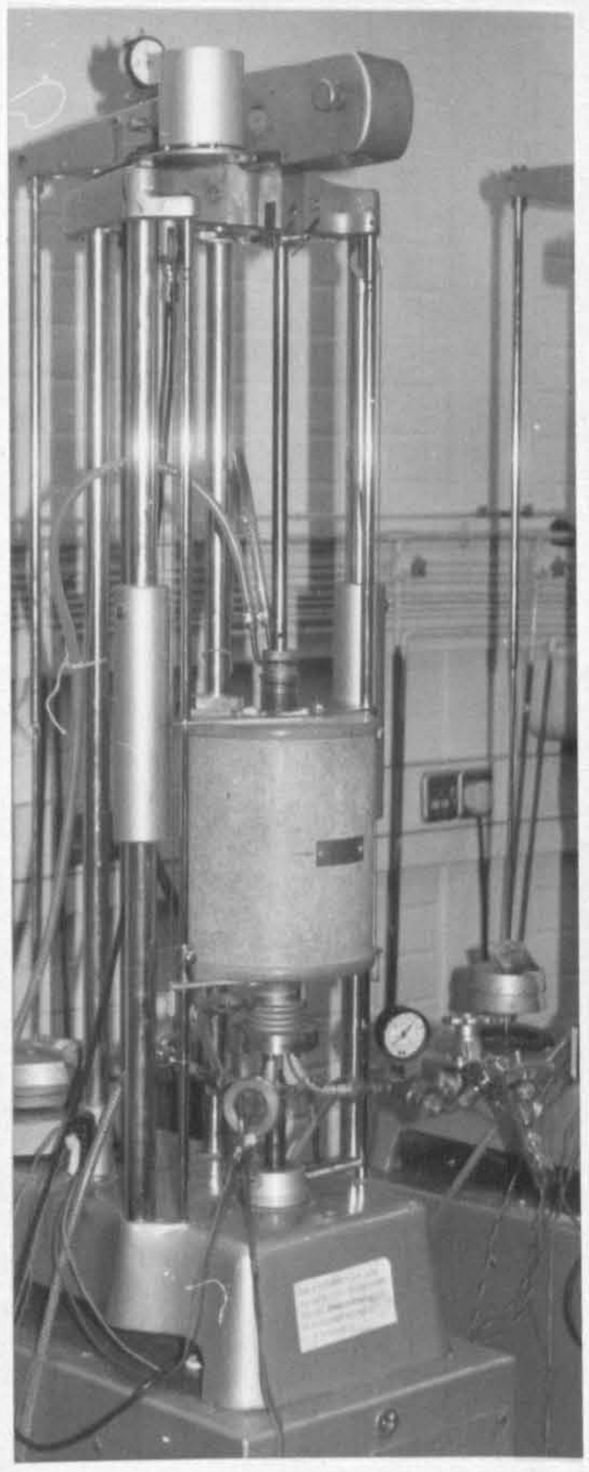

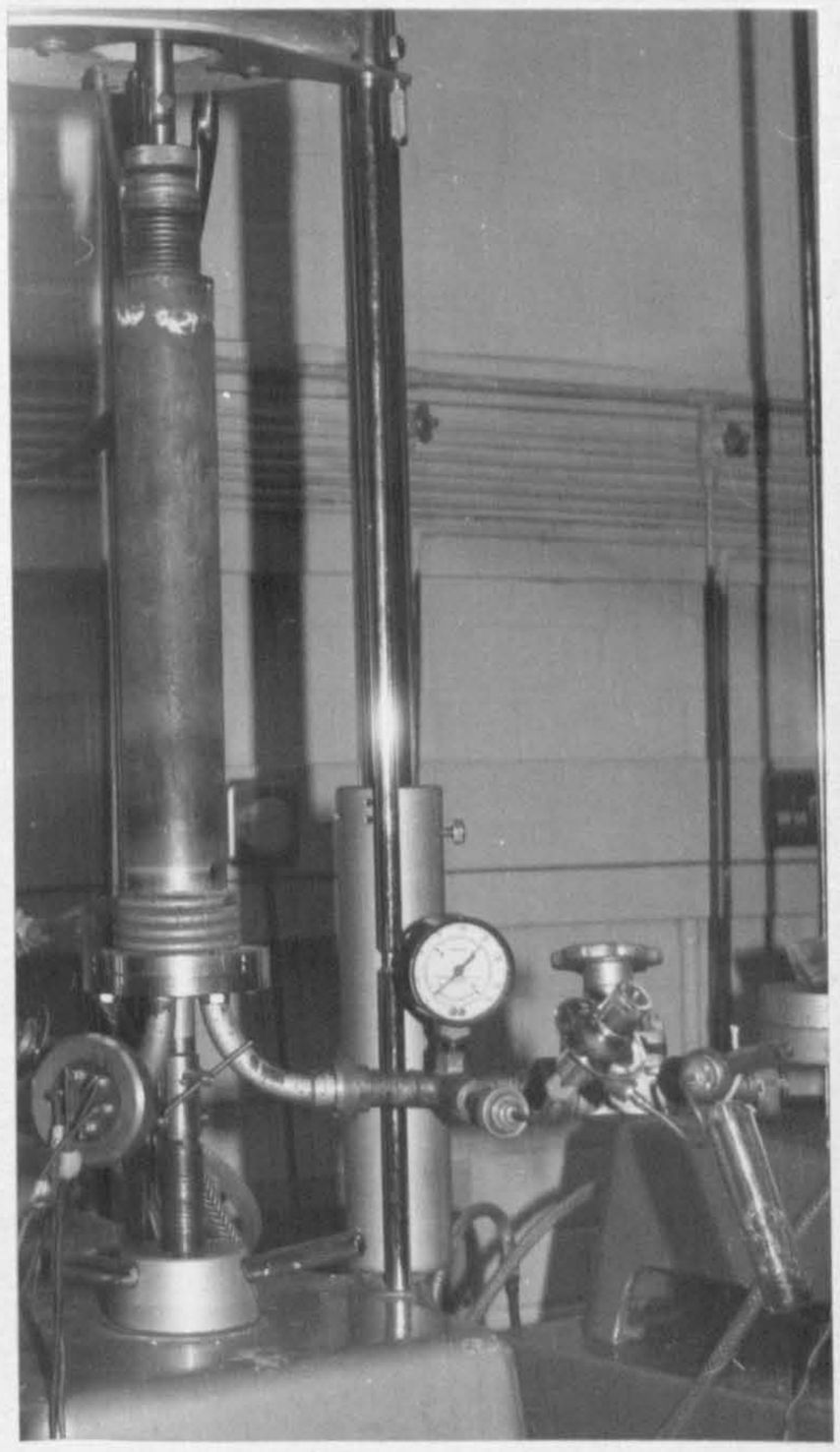

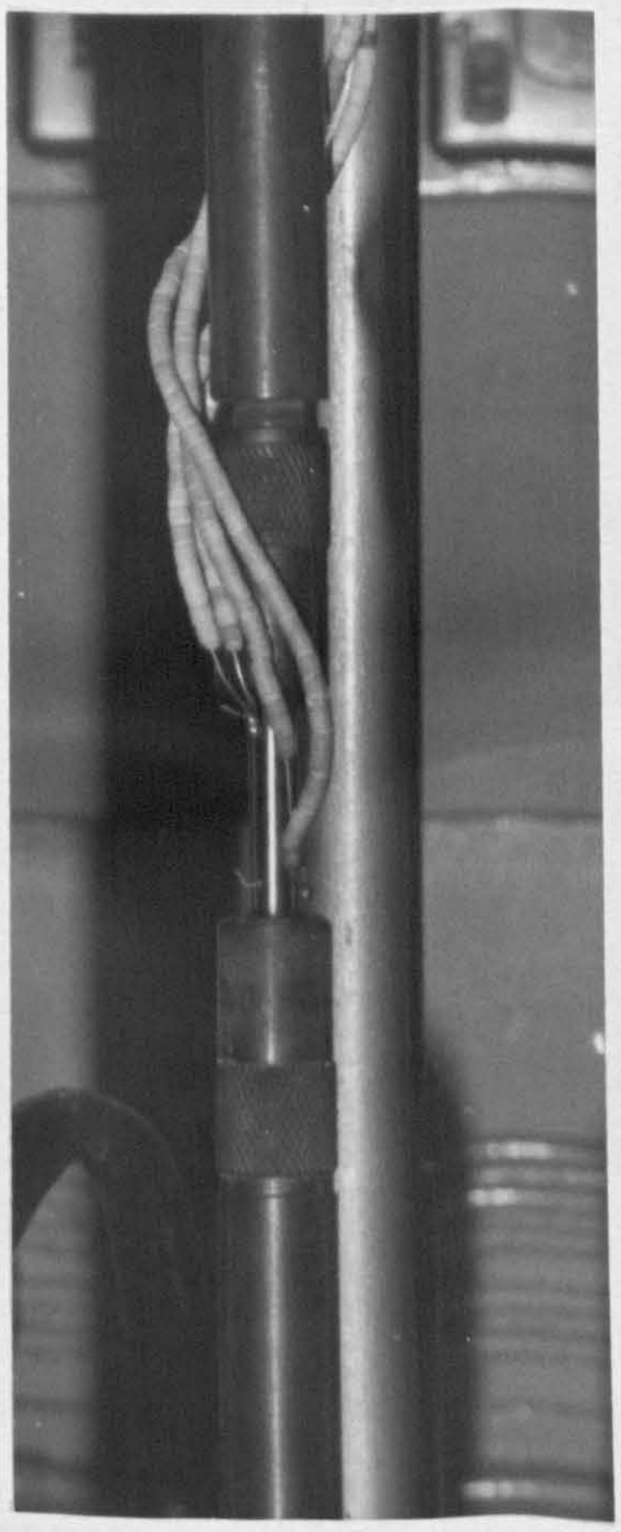

Fig. 4 Continuous cooling transformation chart for $2\frac{1}{4}$ CrMo steels. The red line indicates the cooling rate expected during air cooling of a specimen after heat treatment.

CONTINUOUS COOLING TRANSFORMATION CHART

$2\frac{1}{4}$ Cr. Mo.

ANALYSIS Wt %

C	Si	Mn	P	S	Cr	Mo	Ni	Al	Nb	V
0·14	0·23	0·46	0·010	0·010	2·28	1·05	0·21	—	—	—

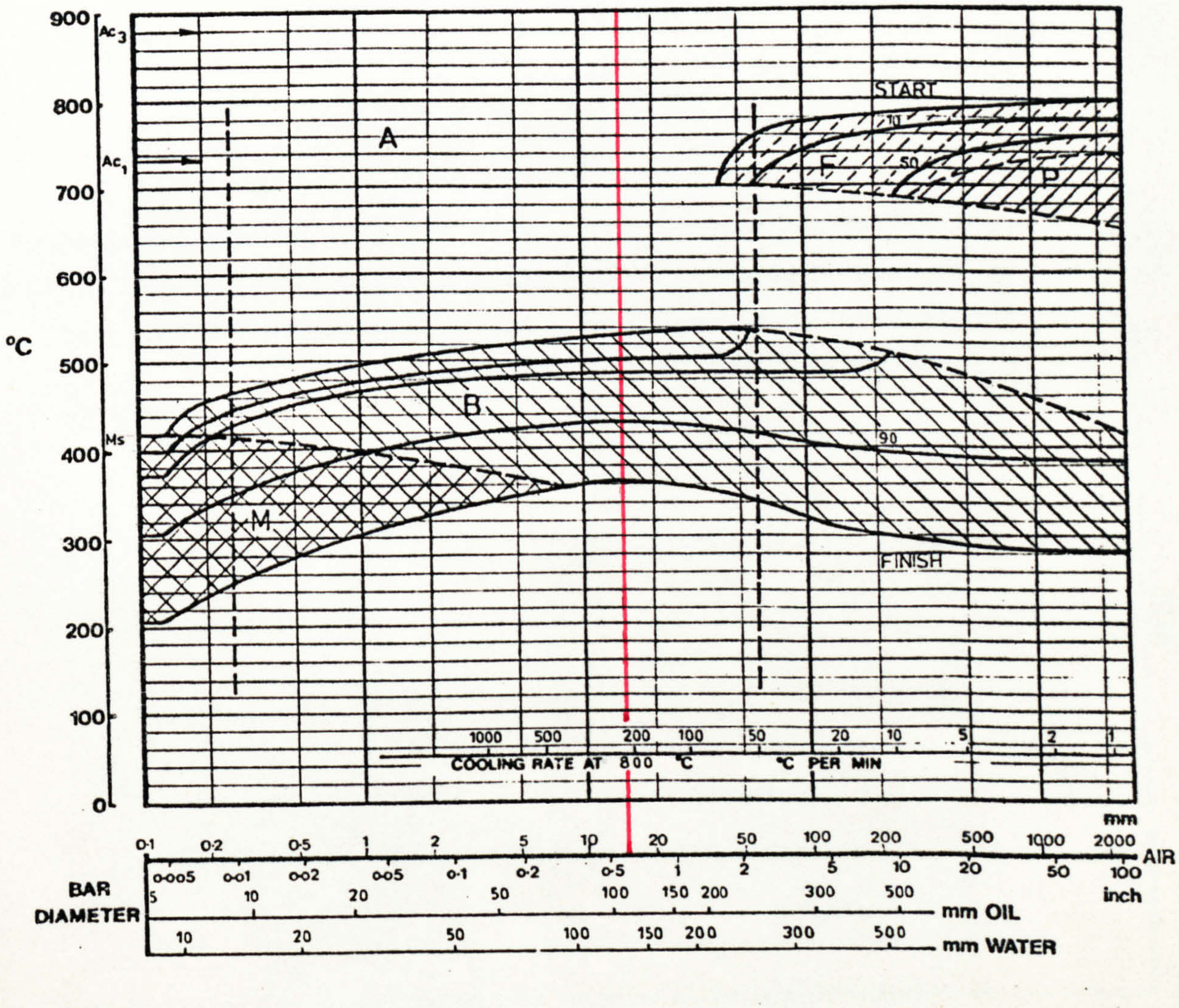

Fig. 5 Typical heating cycle produced in the CRMV series alloy steel to the austenitising temperature. Careful reproduction of this temperature rise generated a consistent microstructure with a constant prior austenite grain size.

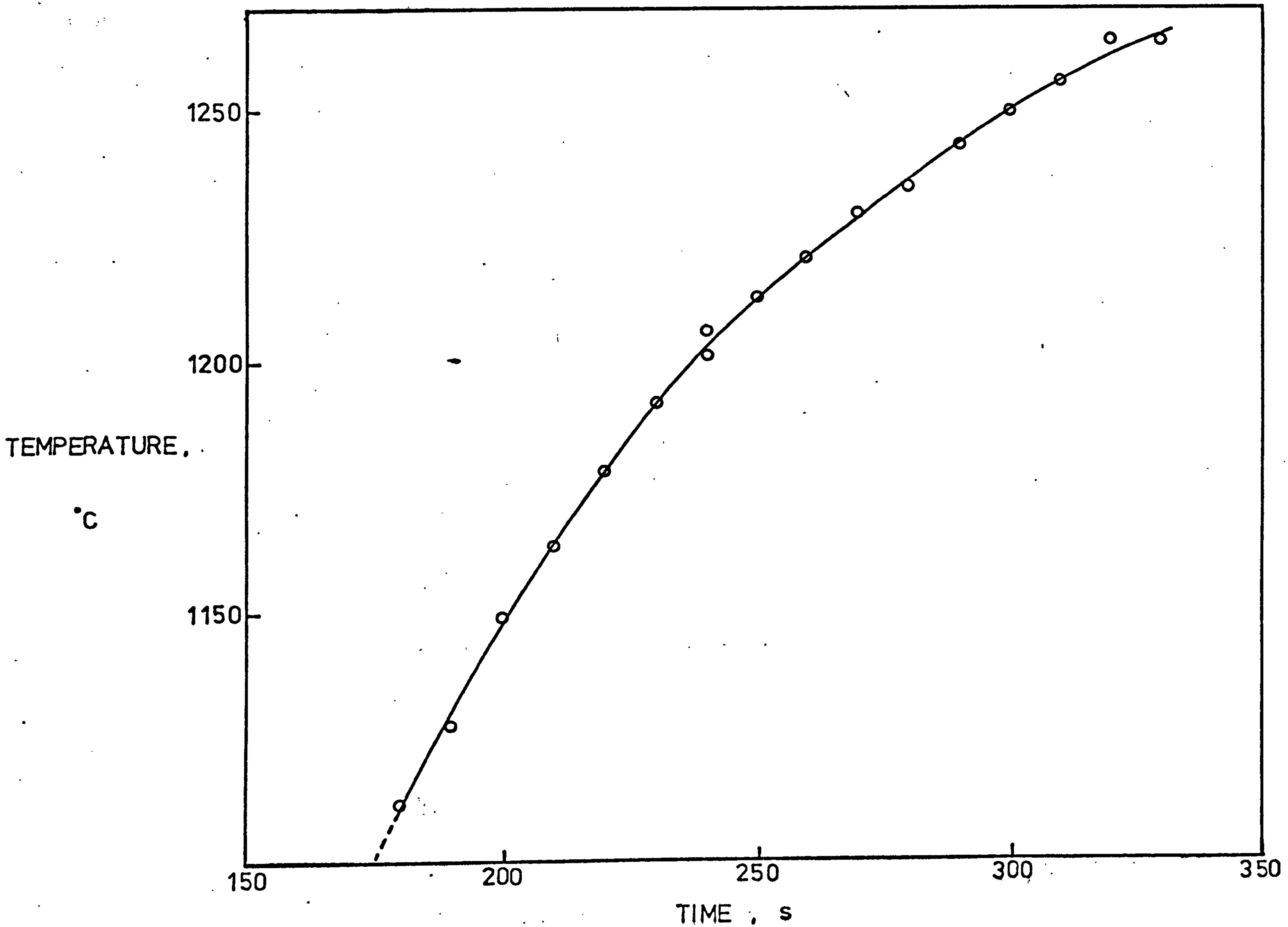
1250
1200
1150
TEMPERATURE,
°C
150
200
250
300
350
TIME , s

Fig. 6 CRM series alloy steel in the heat-treated condition. The specimen has been etched in 2% Nital to reveal the prior austenite grain boundaries and the bainitic matrix.
X1750

Fig. 7 CRMV series alloy in the heat-treated condition. After etching in 2% Nital the bainitic matrix is revealed but the prior austenite grain boundaries remain indistinct.
X150

Fig. 8 CRMV series alloy in the heat-treated condition. Here the specimen has been rapidly heated to 1076K and subsequently quenched. The prior austenite grain boundaries can now be delineated, allowing grain size determinations to be made.
X150

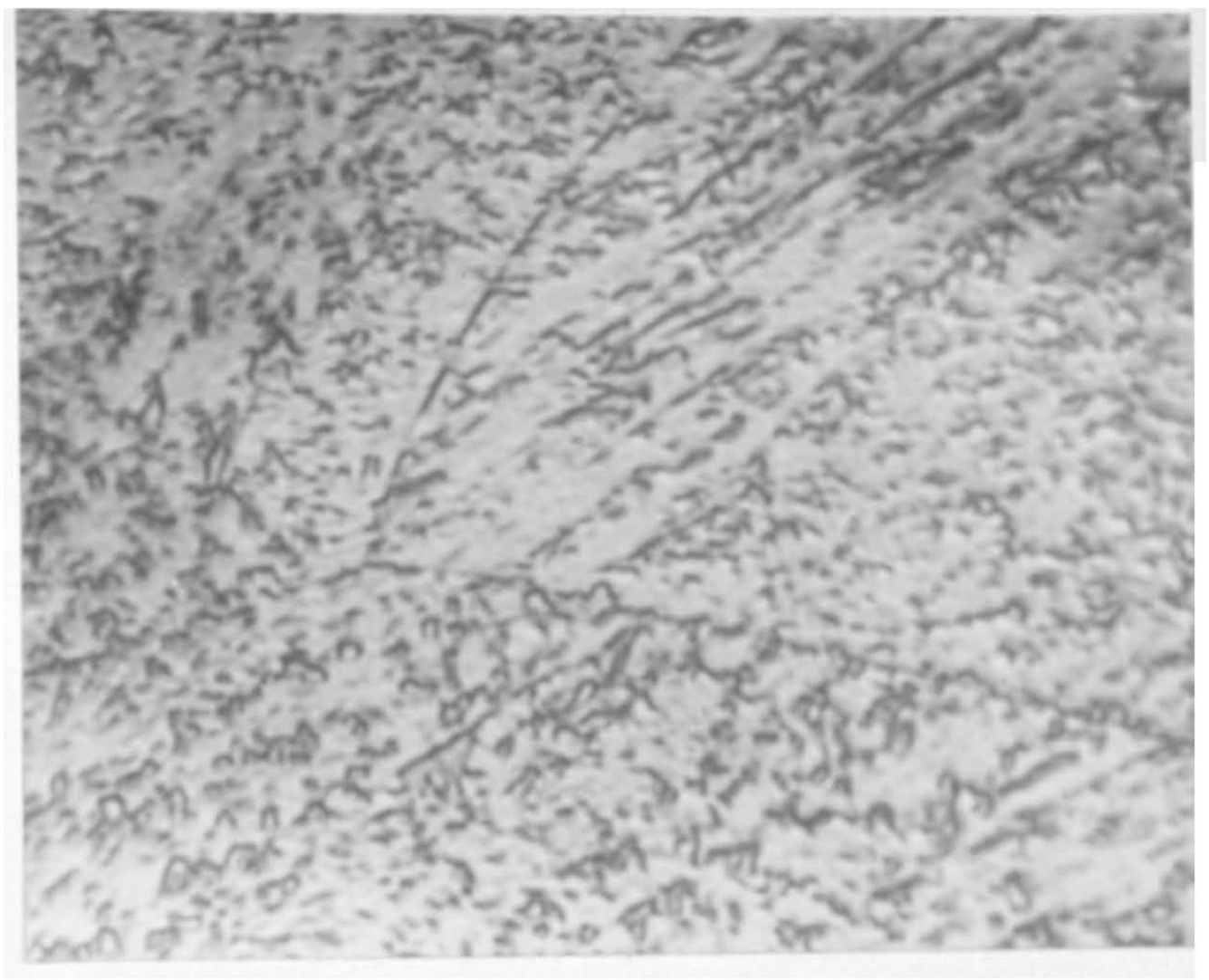

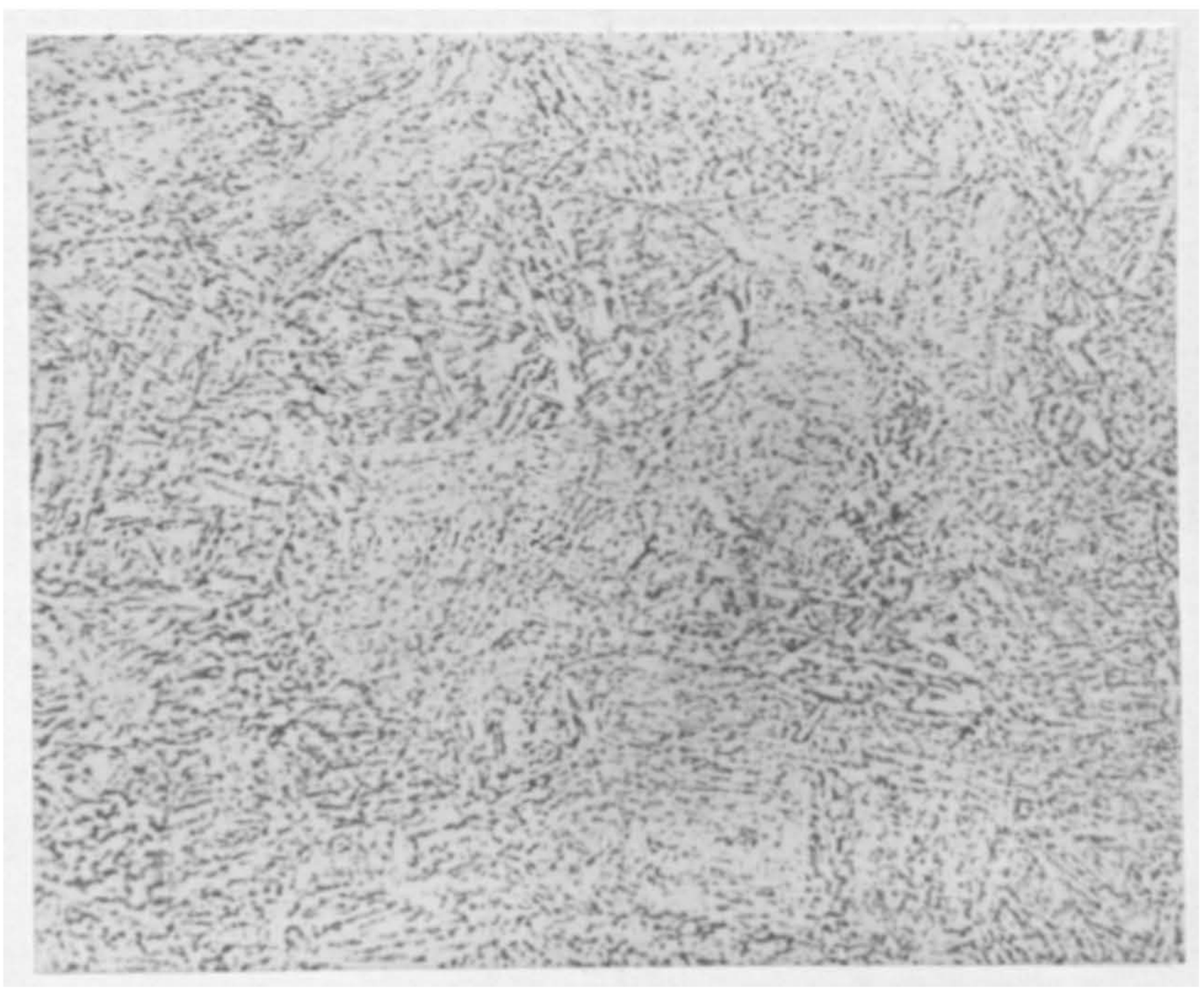

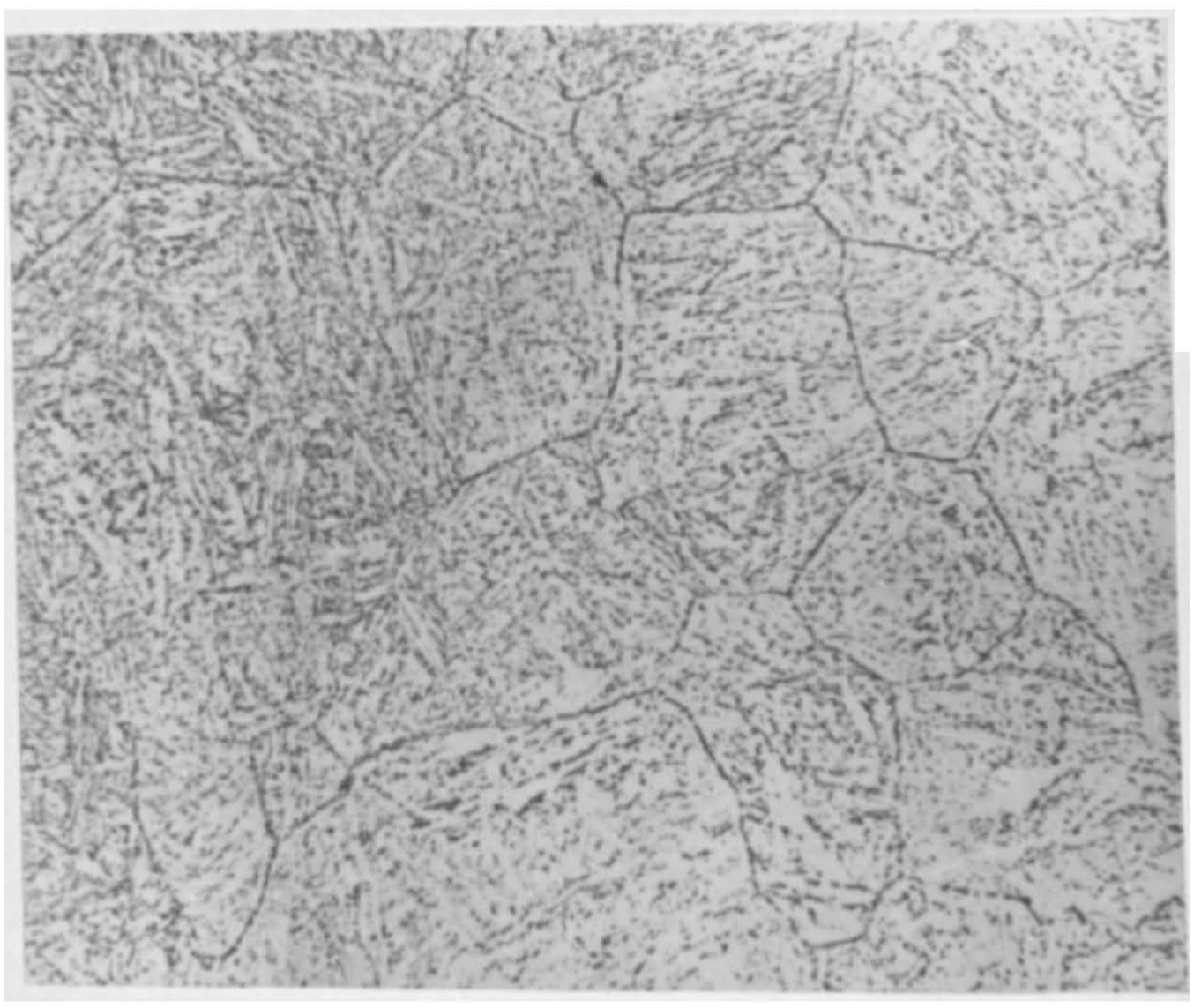

Fig. 9 Series of three photographs illustrating the interference technique for revealing grain boundary sliding in CRM & CRMS series alloy steels. In each case the stress axis is vertical.

Fig. 9(a) Typical area viewed in white light.
X500

Fig. 9(b) Same area, viewed in white light, with offset interference fringes due to the interfacial translation of bainite plate and prior austenite boundaries.
X500

Fig. 9(c) Same area viewed in light from a thallium source.
X500

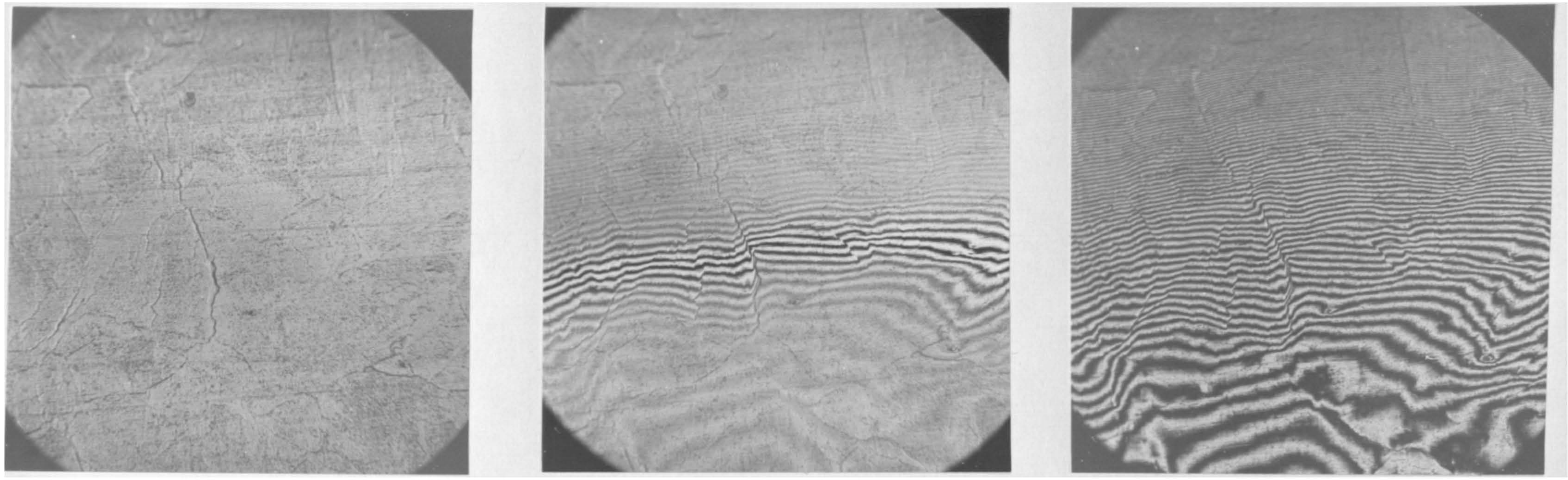

Fig. 10 Enlarged scanning electron micrograph, as used for quantitative analysis of cavity populations produced during creep in CRMV series alloy steels. The micron marker band allowed accurate assessment of the magnification. The cavitated prior austenite boundary facet is perpendicular to the stress axis.
X10,500

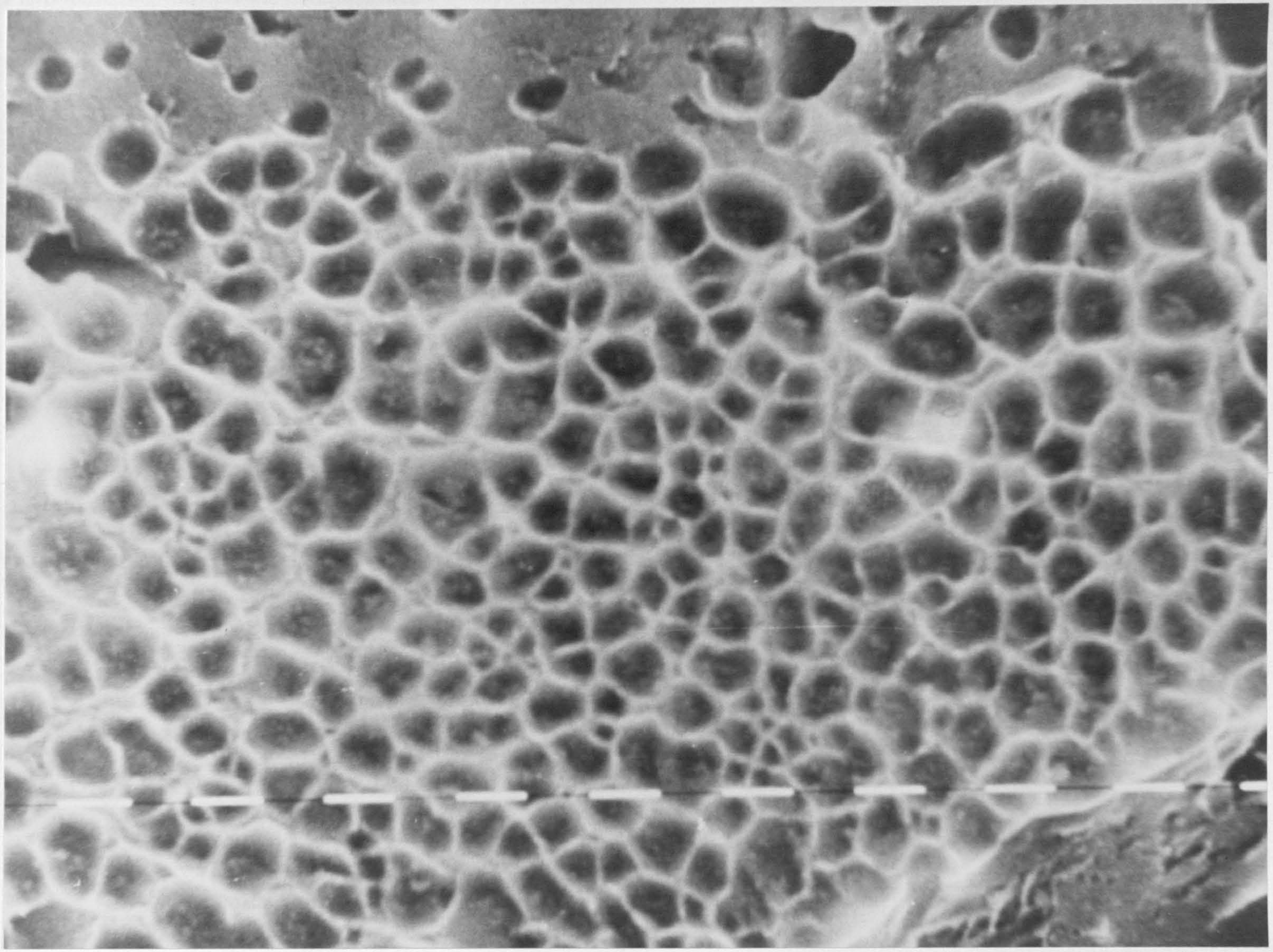

Fig. 11 Load/elongation curves for CRM and CRMS series alloy steels, in the tempered (T) and untempered (U) condition. The specimens had been strained to failure at room temperature.

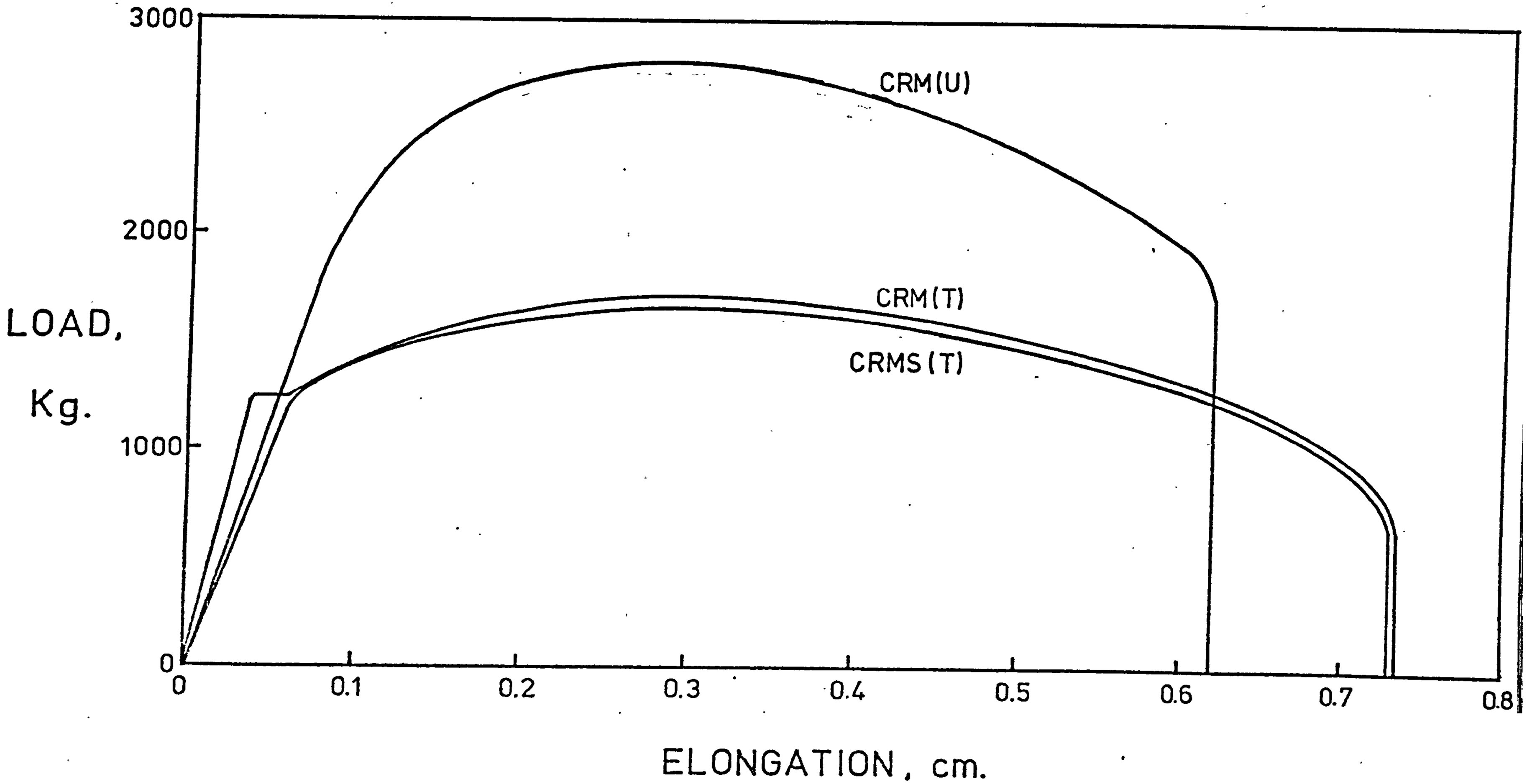
3000
2000
1000
0
LOAD,
Kg.
CRM(U)
CRM(T)
CRMS(T)
0
0.1
0.2
0.3
0.4
0.5
0.6
0.7
0.8
ELONGATION, cm.

Fig. 12 Typical creep curves for tests at 180 and 200 MN m^{-2}, 838K on CRM and CRMS series alloy steels.

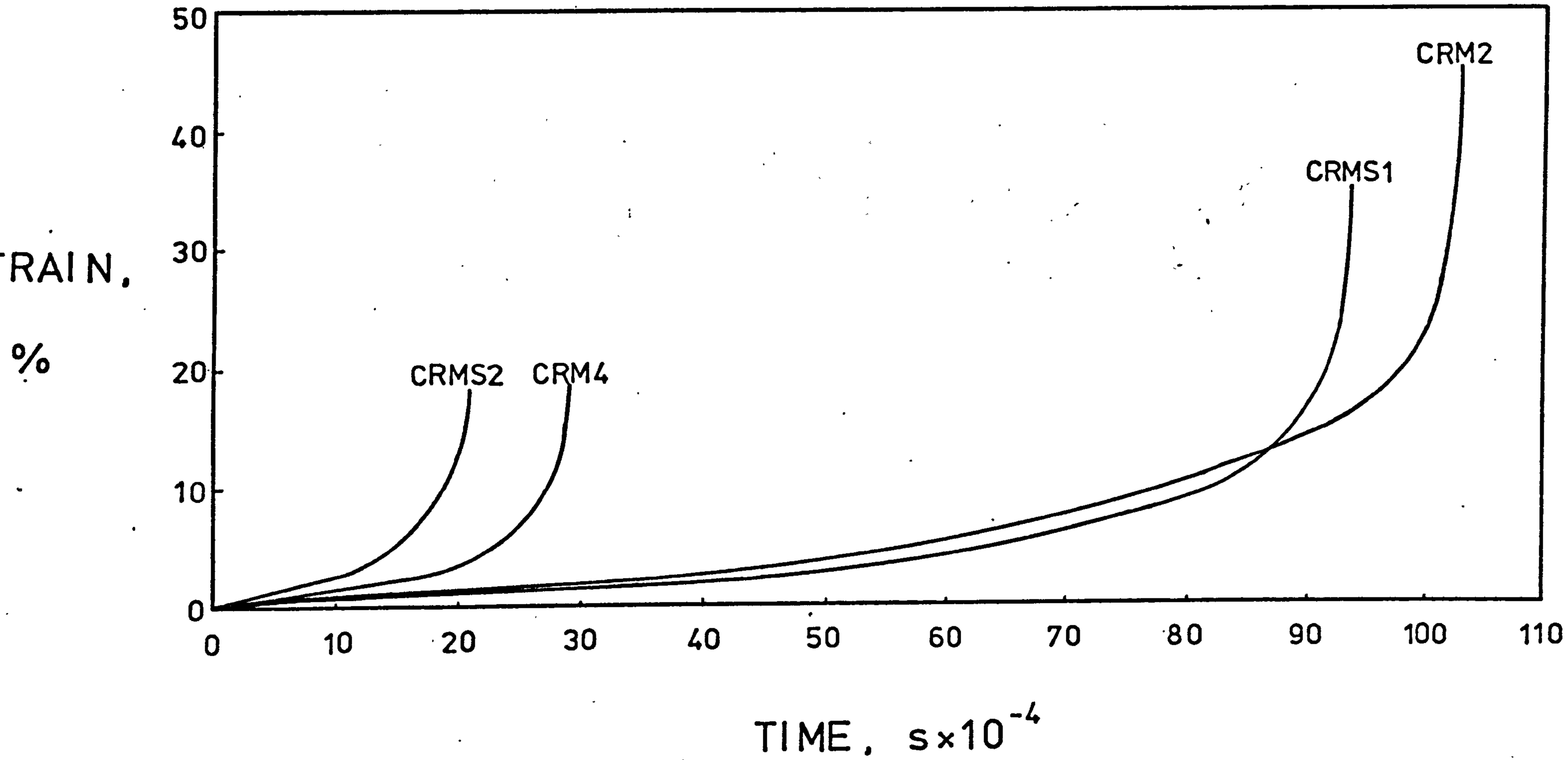
STRAIN, %
50
40
30
20
10
0
0
10
20
30
40
50
60
70
80
90
100
110
CRM2
CRMS1
CRMS2
CRM4
TIME, s×10⁻⁴

Fig. 13 Reduction in area and fracture strain vs. stress for $2\frac{1}{4}$Cr1Mo alloy steels, creep tested at 838K.

O CRM series.

□ CRMS series.

REDUCTION IN AREA, %

FRACTURE STRAIN, %

90
80
50
40
30
20
10

160 170 180 190 200 210 220 230 240 250 260

STRESS, MN m^{-2}

Fig. 14 Minimum creep rate plotted as a function of stress for $2\frac{1}{4}$Cr1Mo alloy steels creep tested at 838K.

- O CRM series.
- □ CRMS series.

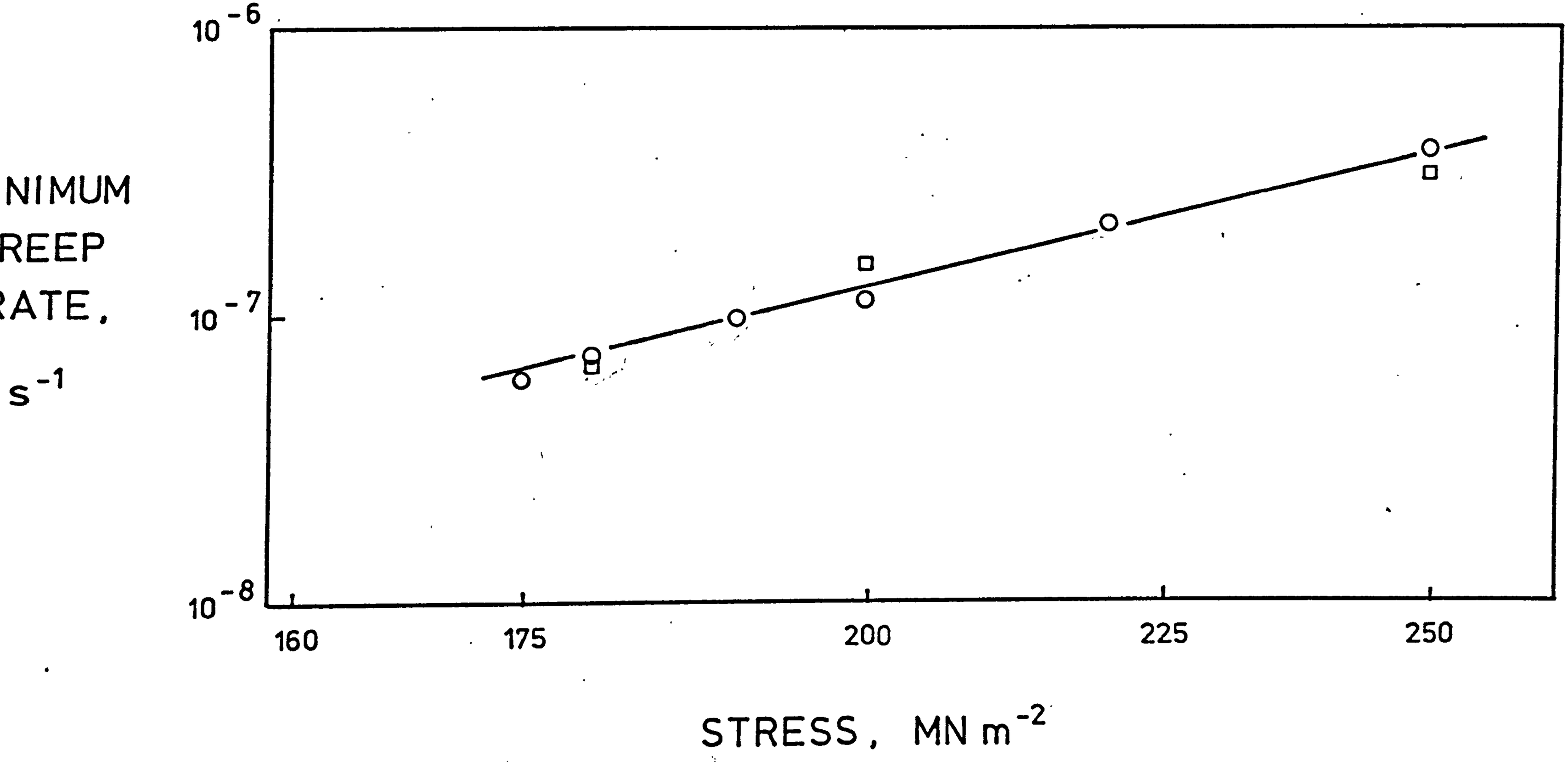
MINIMUM CREEP RATE, s⁻¹
10⁻⁶
10⁻⁷
10⁻⁸
160
175
200
225
250
STRESS, MN m⁻²

Fig. 15 Time to fracture plotted as a function of stress for $2^1/4$Cr1Mo alloy steels creep tested at 838K.

O CRM series.

□ CRMS series.

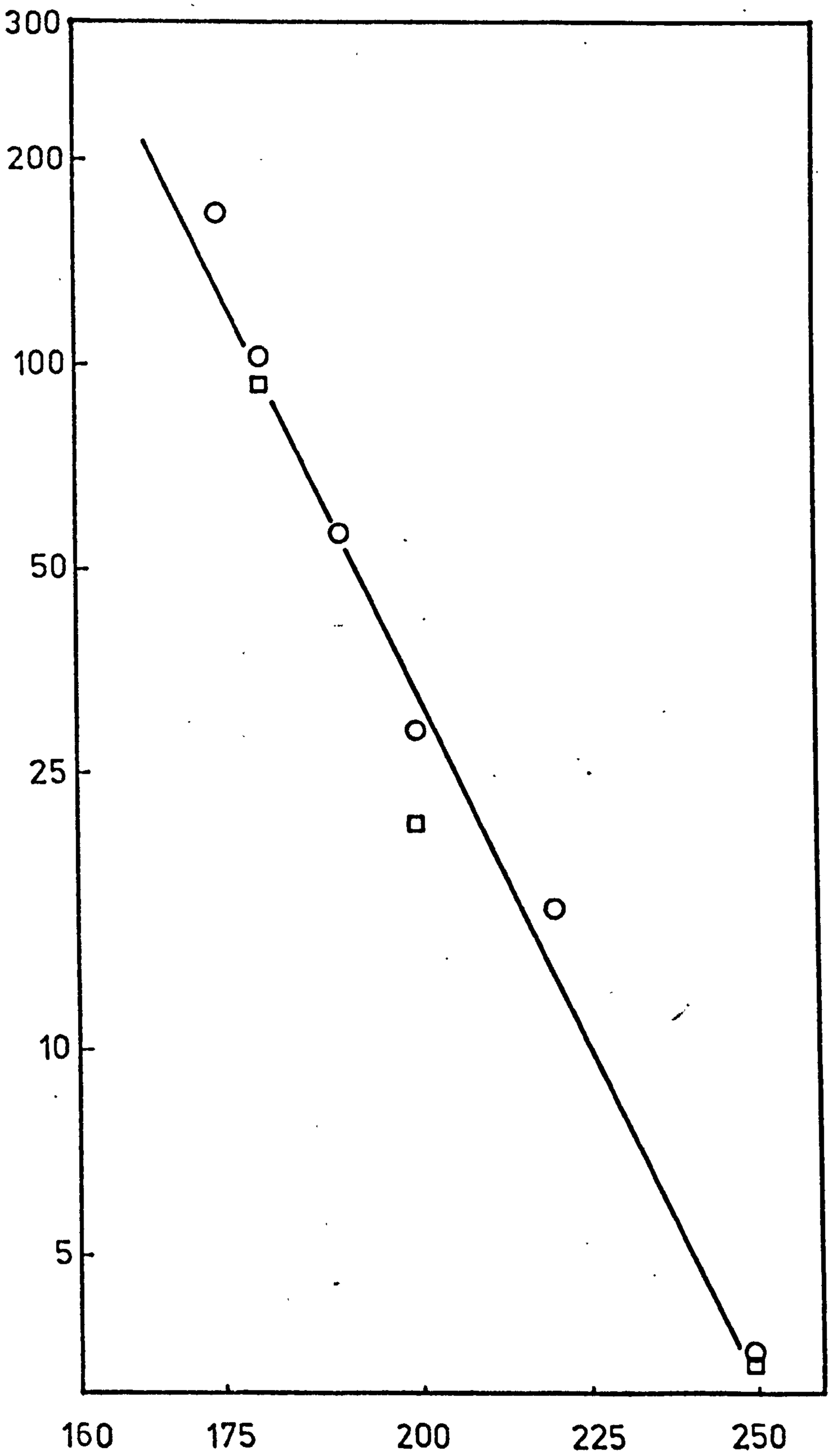
300
200
100
50
25
10
5
160
175
200
225
250
TIME TO FRACTURE, s×10^-4
STRESS, MN m^-2

Fig. 16 Central area of the fracture surface of tempered CRMS material, strained to failure at room teperature.
X3000

Fig. 17 Necked region of CRMS sreies alloy strained to failure at room temperature. The specimen has undergone a repetitive polish/etch treatment. Stress axis vertical.
X30

Figs. 18 & 19 High magnification optical micrographs of the specimen shown in Fig. 17, in the polished and etched condition respectively.

Fig. 18 X350

Fig. 19 X850

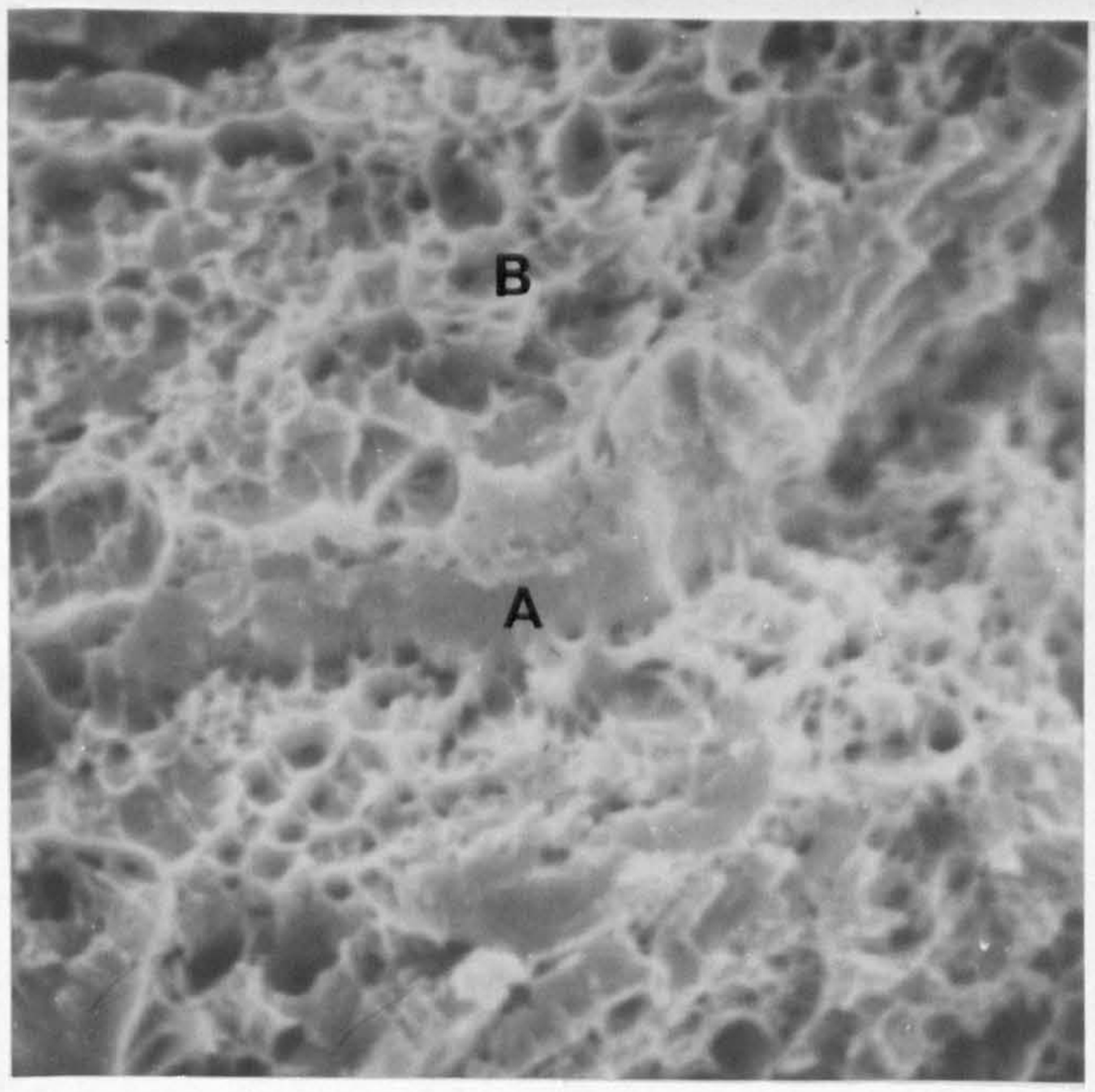
B
A

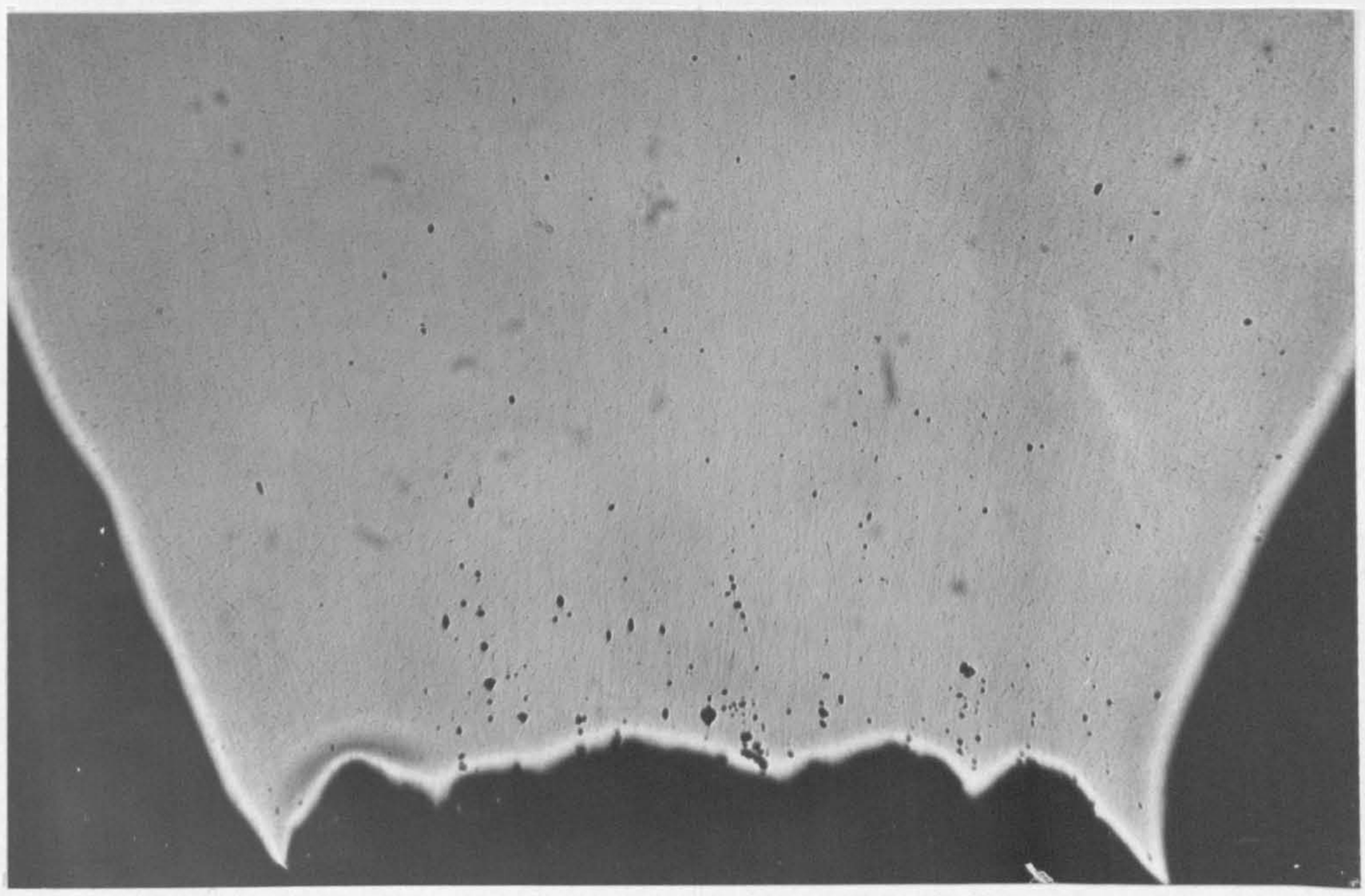

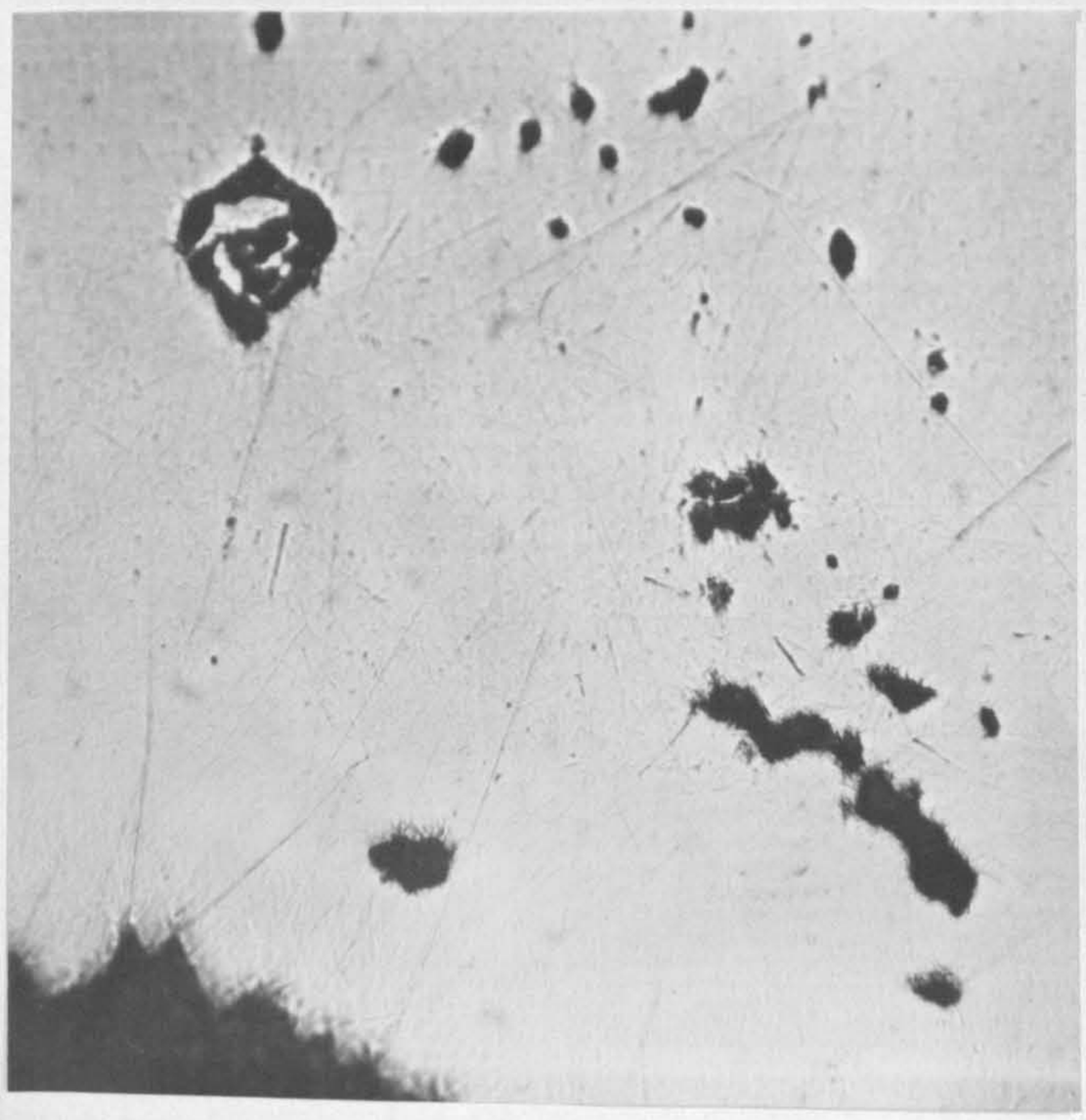

Fig. 20(a) CRM series alloy, creep tested at 838K and 180 MNm^2 to 2% strain. The area is viewed in white light, stress axis vertical.
X500

Fig. 20(b) Same area, viewed in white light, with offset interference fringes due to sliding bainite plate boundaries.
X500

Fig. 21(a) Another area viewed on the same specimen as shown in Fig. 20. The offset interference fringes at the prior austenite grain boundary indicates deformation in adjacent precipitate free zones.
X750

Fig. 21(b) Analysis of a typical interference fringe at the prior austenite grain boundary, as shown in Fig. 21(a).

Fig. 22(a) CRM series alloy, creep tested at 838K and 180 MNm^2 to 6% strain (tertiary regime). Extensive step formation can be seen on the surface. Stress axis vertical.
X750

Fig. 22(b) Same area viewed in whit light showing offset interference fringes.
X750

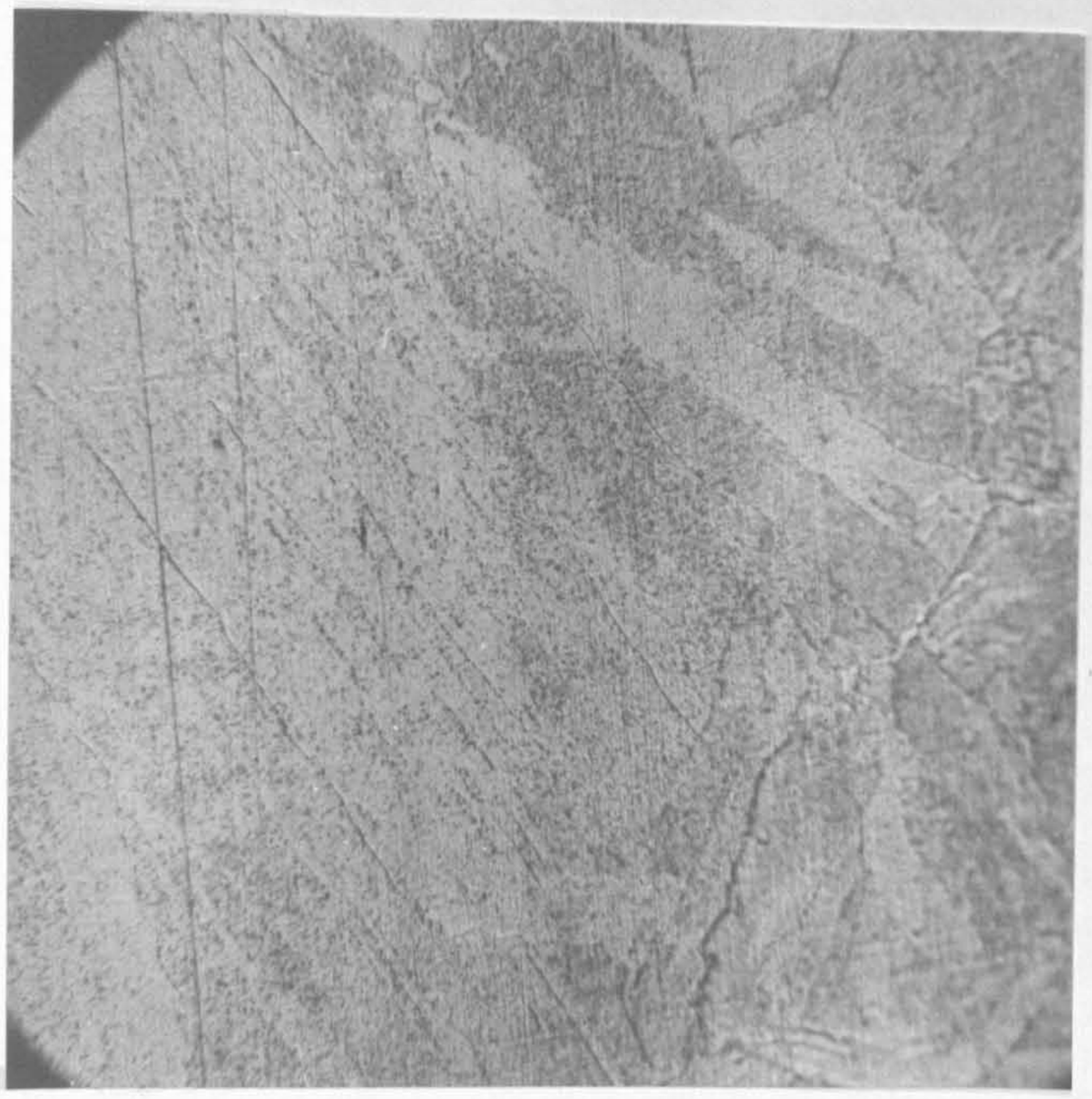

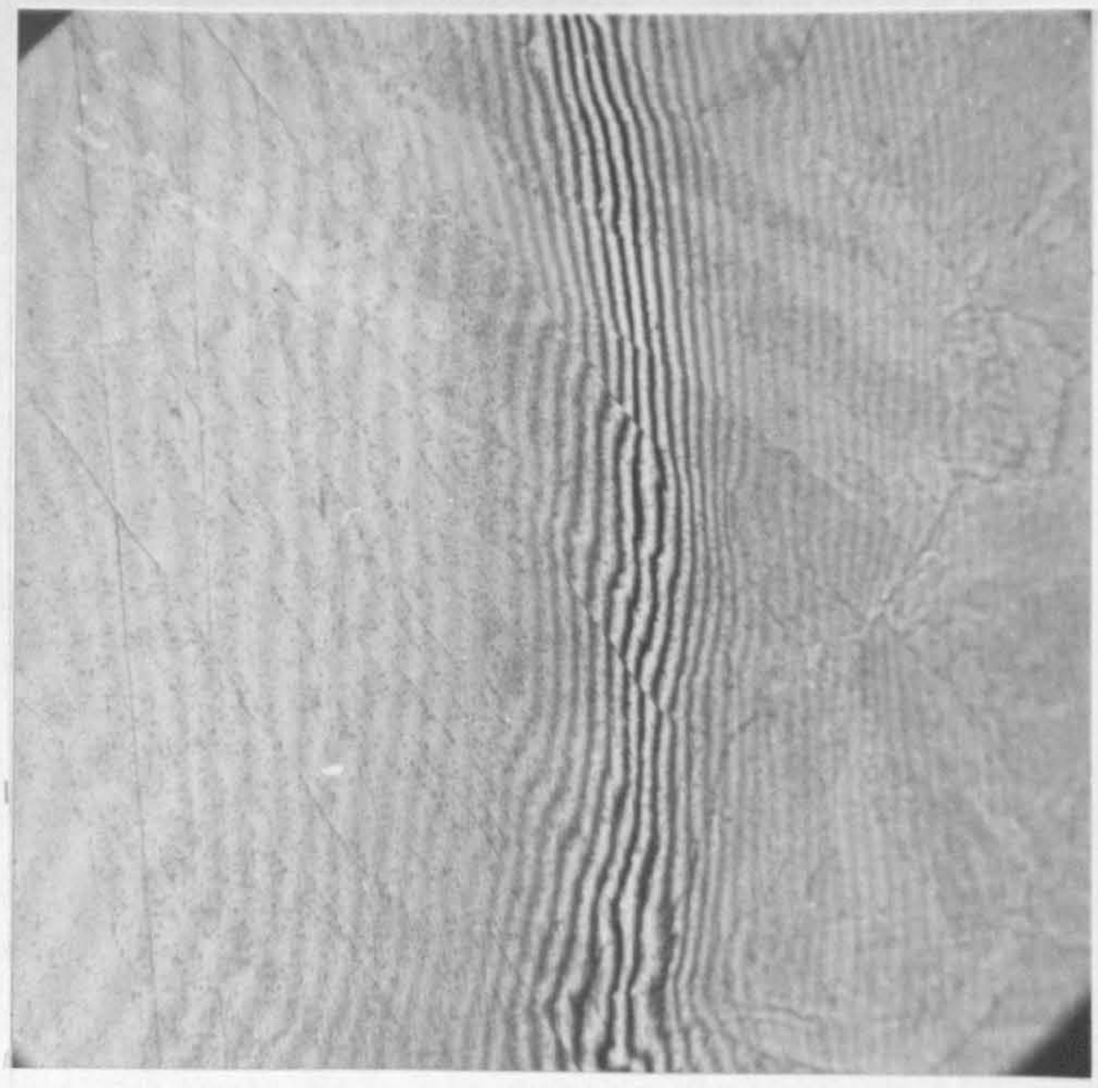

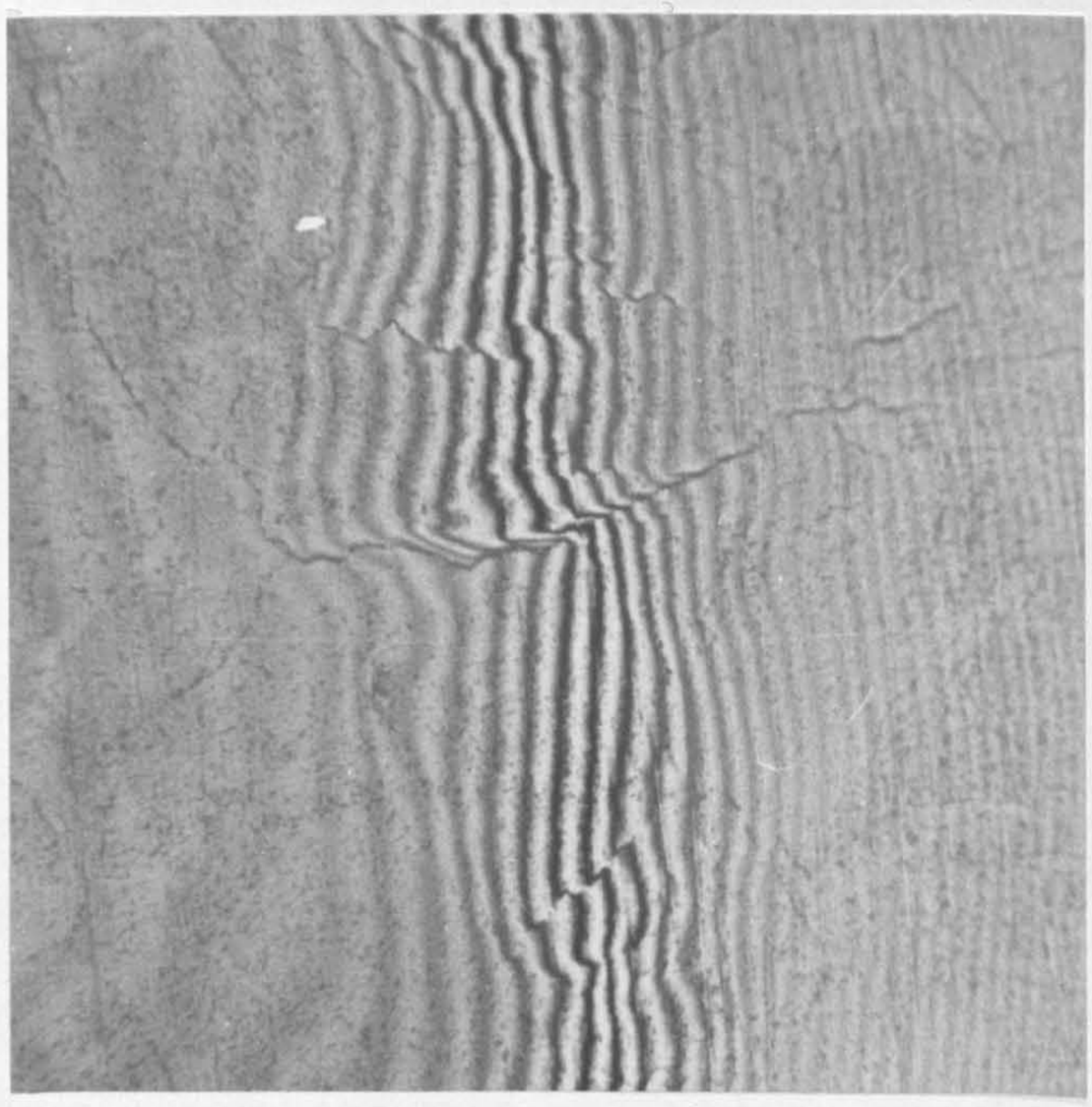

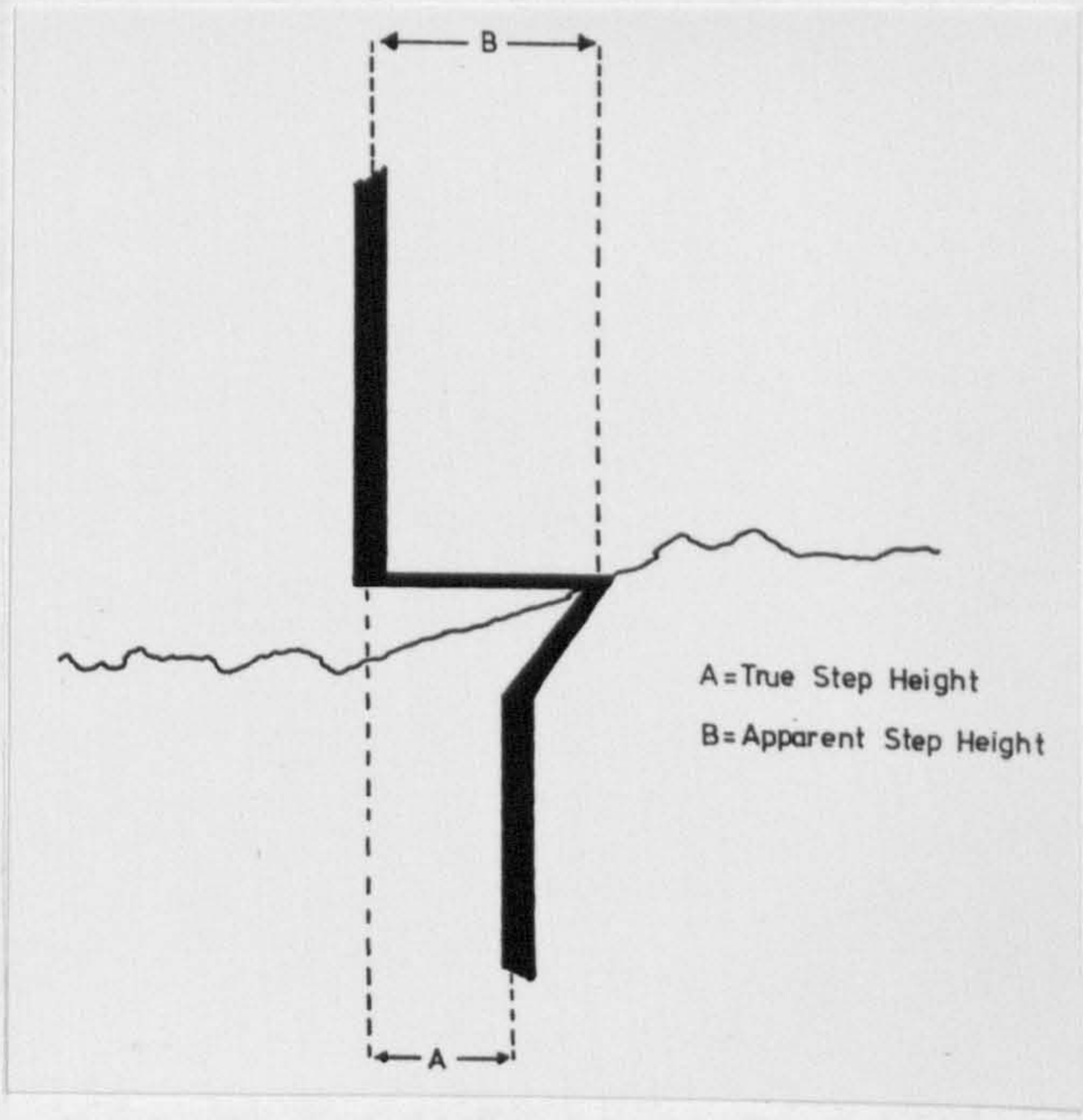
B
A
A=True Step Height
B=Apparent Step Height

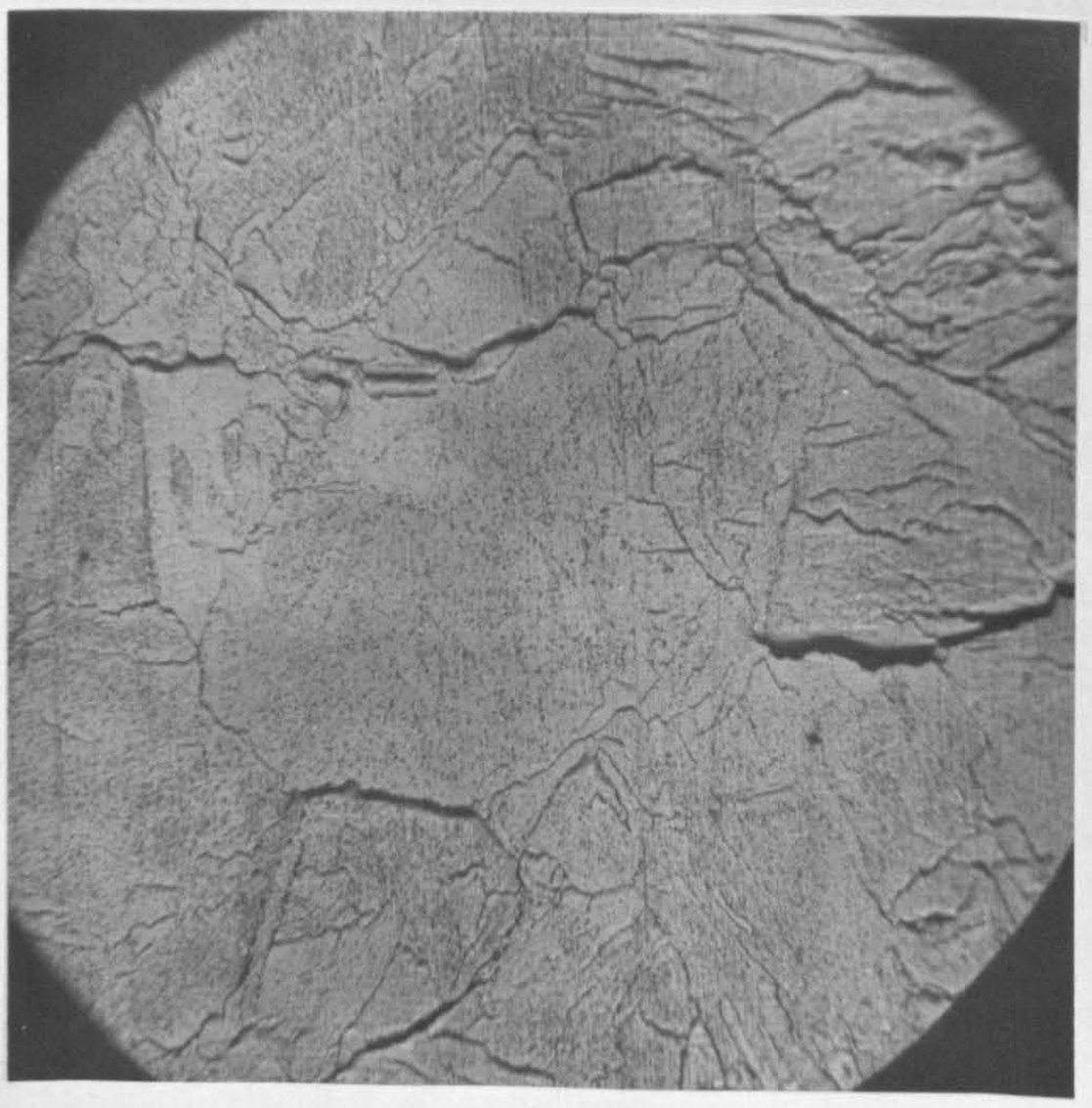

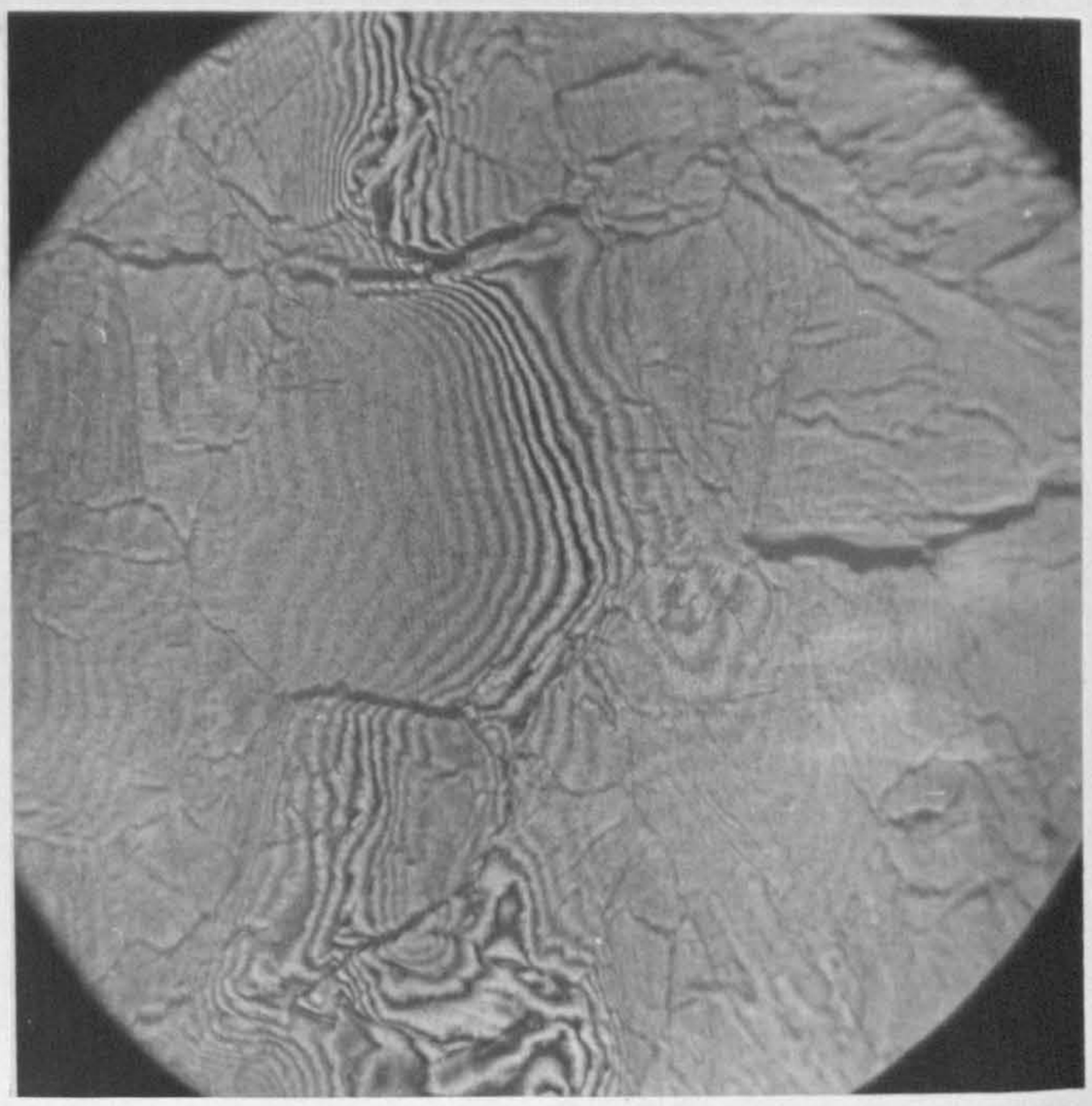

Fig. 23(a) Necked region of specimen CRM 4 after creep rupture, showing the nature of damage behind the fracture surface. The specimen is in the polished condition and the stress axis is vertical.
X30

Fig. 23(b) Same area as shown in the previous micrograph, the specimen has been etched in 2% Nital. Note the gross distortion of the prior austenite grains.
X30

Fig. 24 Elongated holes found behind the fracture surface in specimen CRM 4. Stress axis vertical.
X4000

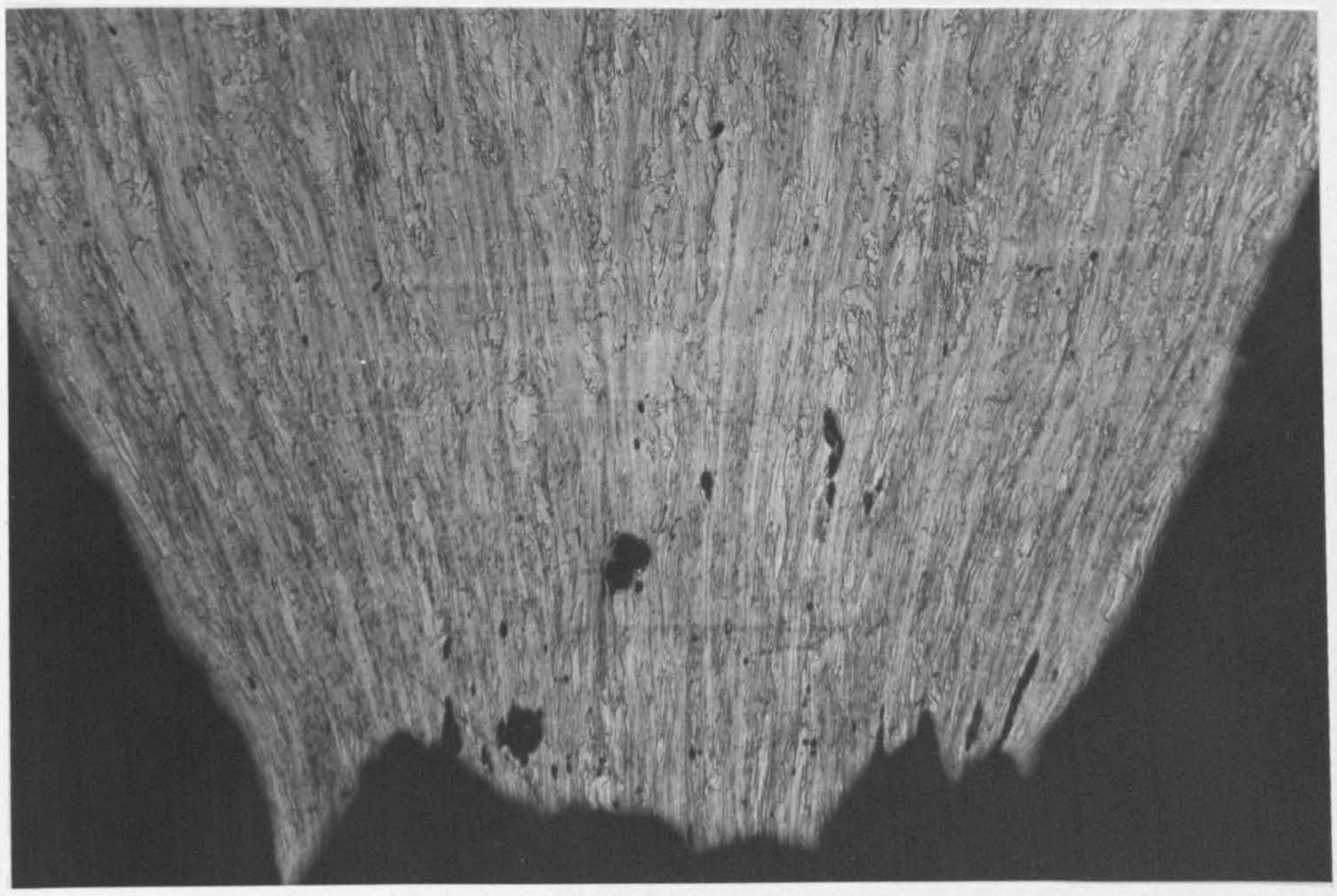

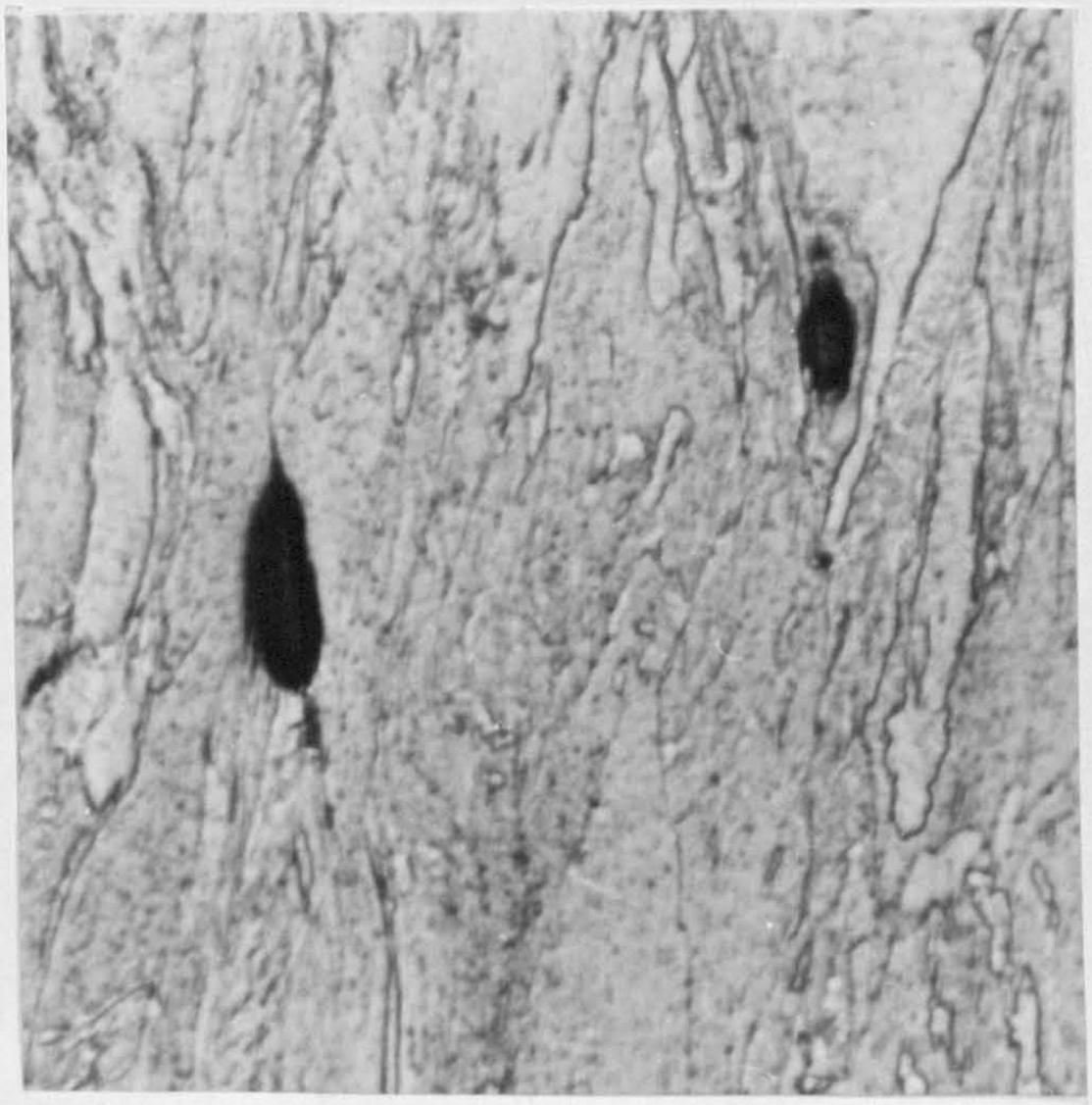

Fig. 25 Fracture surface of specimen CRM 2 after creep rupture, showing a range of ductile cusp sizes.
X1060

Fig. 26 CRM series alloy fractured in liquid N_2 after creep failure. The surface exhibits a completely transgranular cleavage fracture.
X210

Fig. 27 CRM series alloy crept at 838K and 180 MNm^2 for 50 x 10^4 s. The specimen has been fractured at -196C to reveal voids within the cleavage facets.
X1500

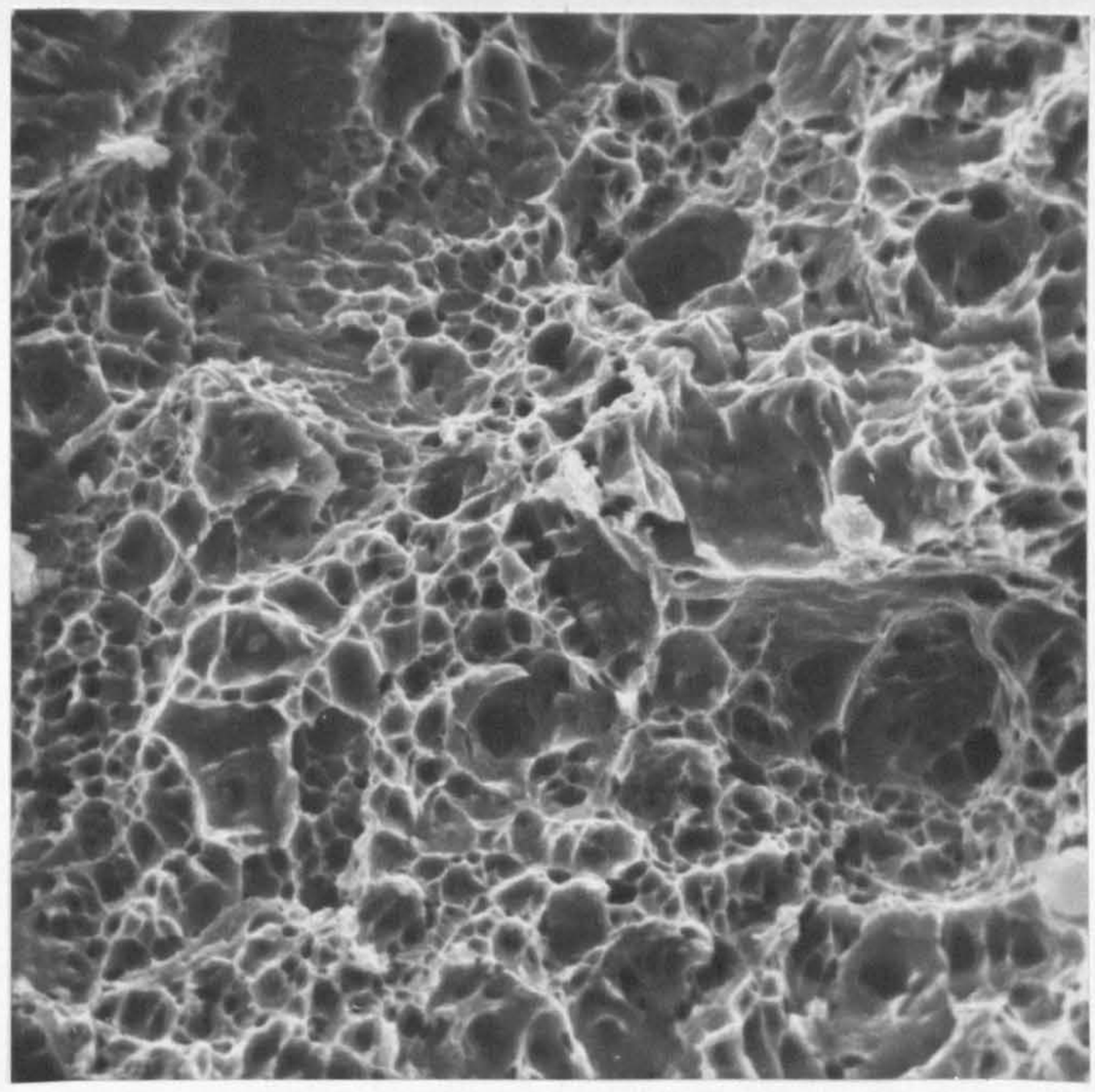

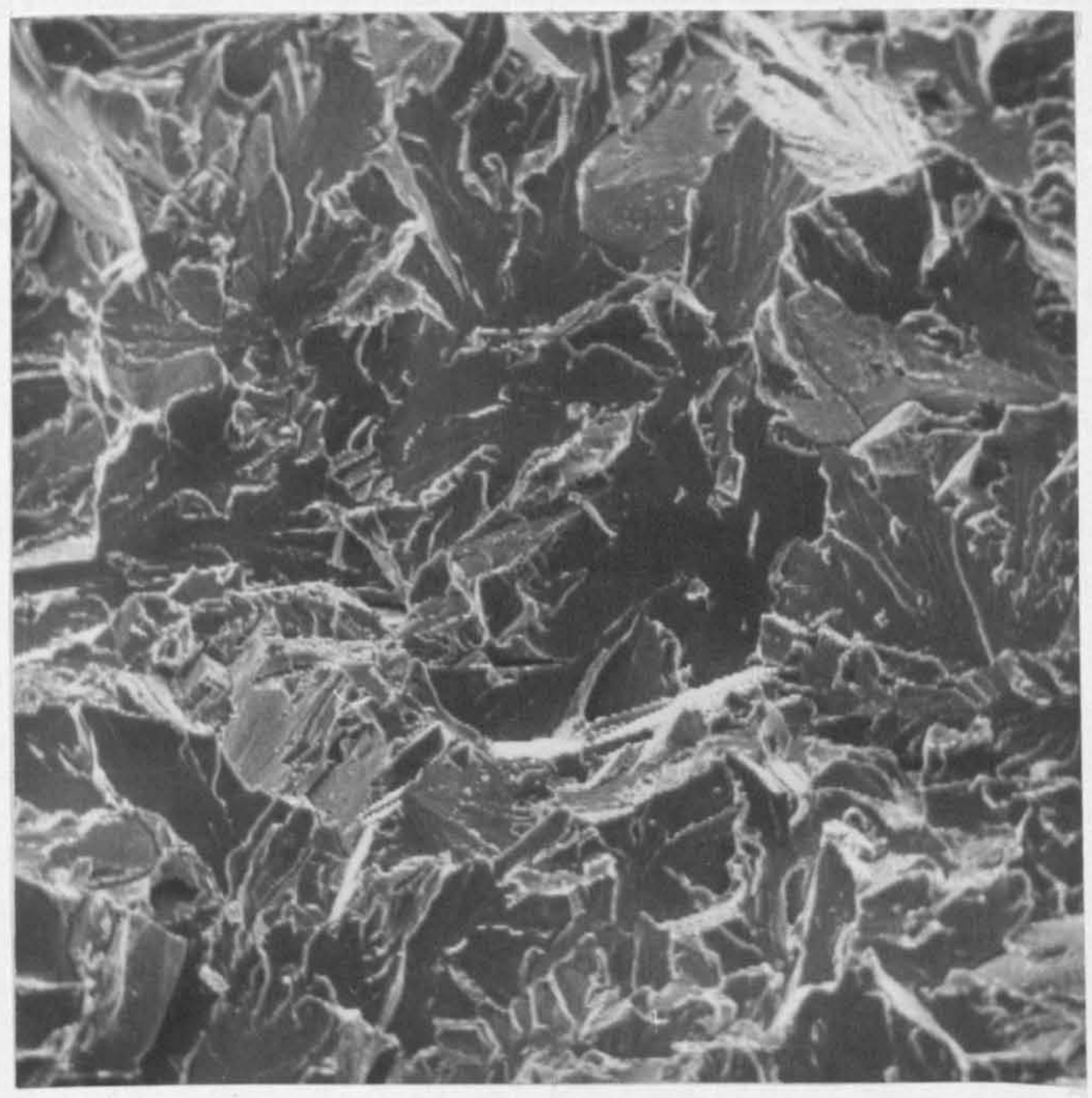

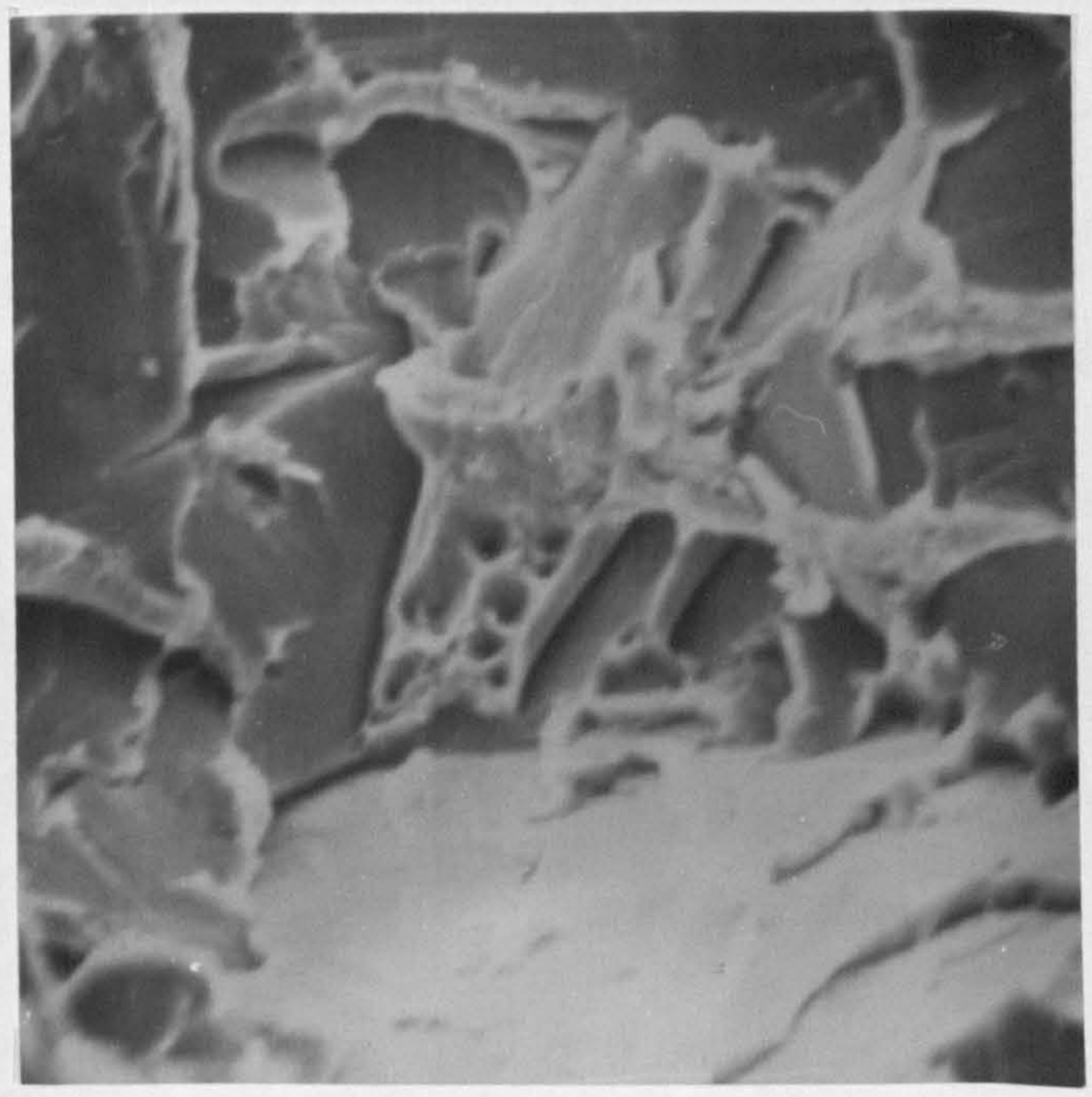

Fig. 28(a) Precipitation of $M_{23}C_6$ and M_2C at a prior austenite grain boundary, typical of that observed in CRM and CRMS series alloys. The extraction replica was taken from material after creep rupture. The large particles (A) are $M_{23}C_6$ and the small, lenticular precipitates (B) are M_2C.
X58300

Fig. 28(b) Similar precipitate morphology found within the bainitic matrix.
X58300

Figs. 29(a) and (b)

Low magnification electron micrographs of extraction replicas taken from similar specimens. Denuded, precipitate free zones can be seen adjacent to the prior austenite grain boundaries. Coarse particles of $M_{23}C_6$ have grown at the expense of M_2C
X5500

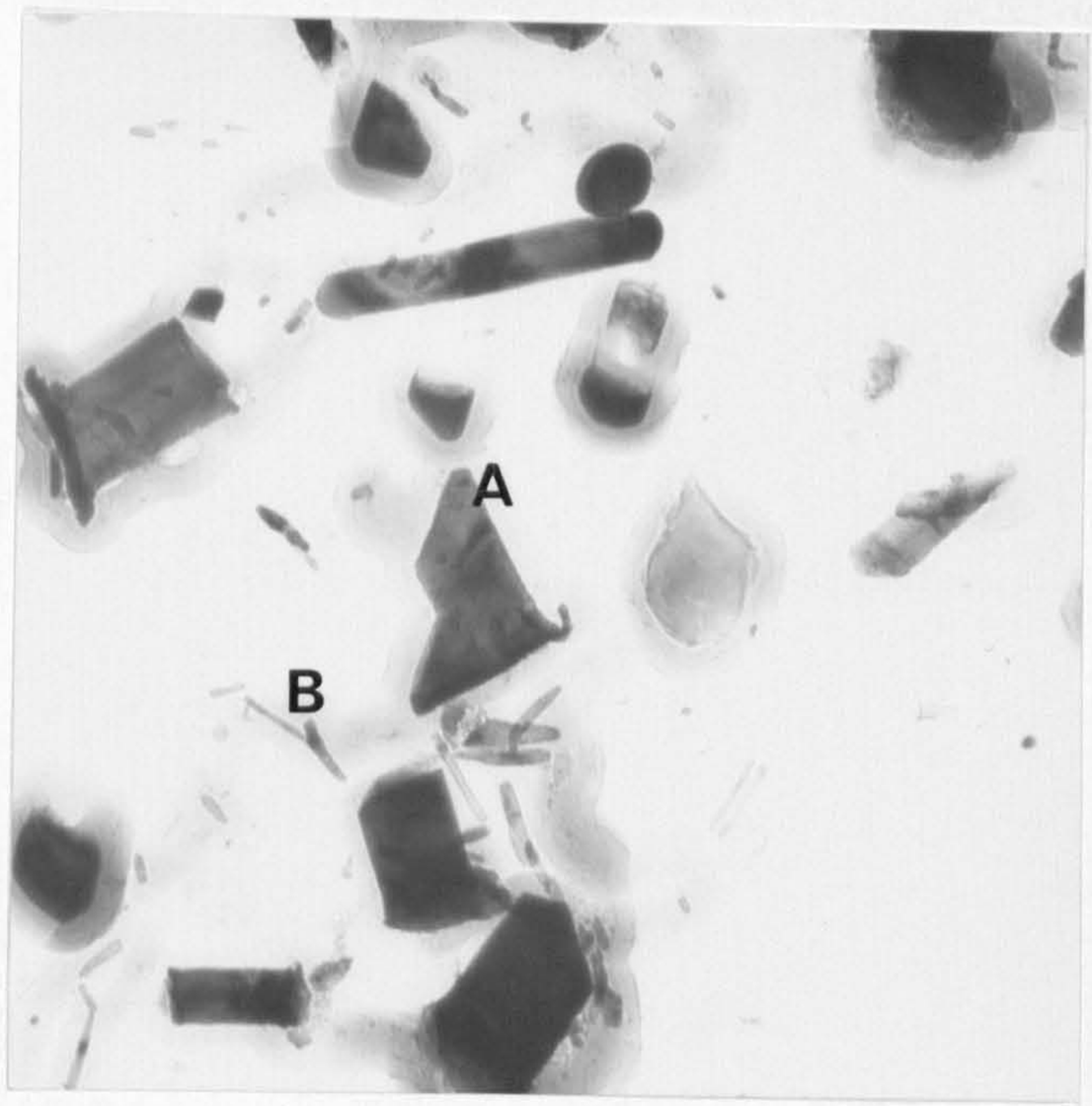
A
B

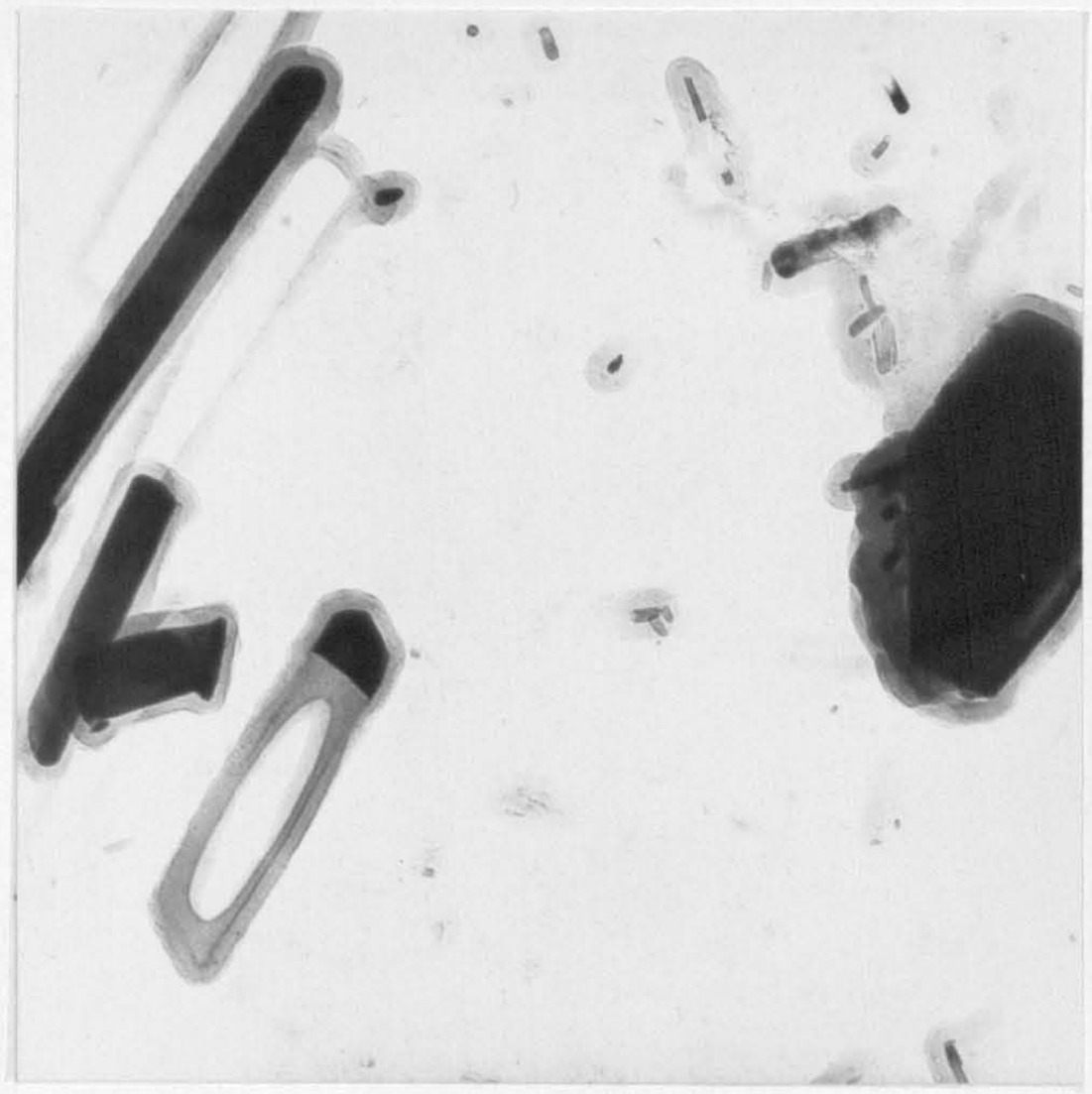

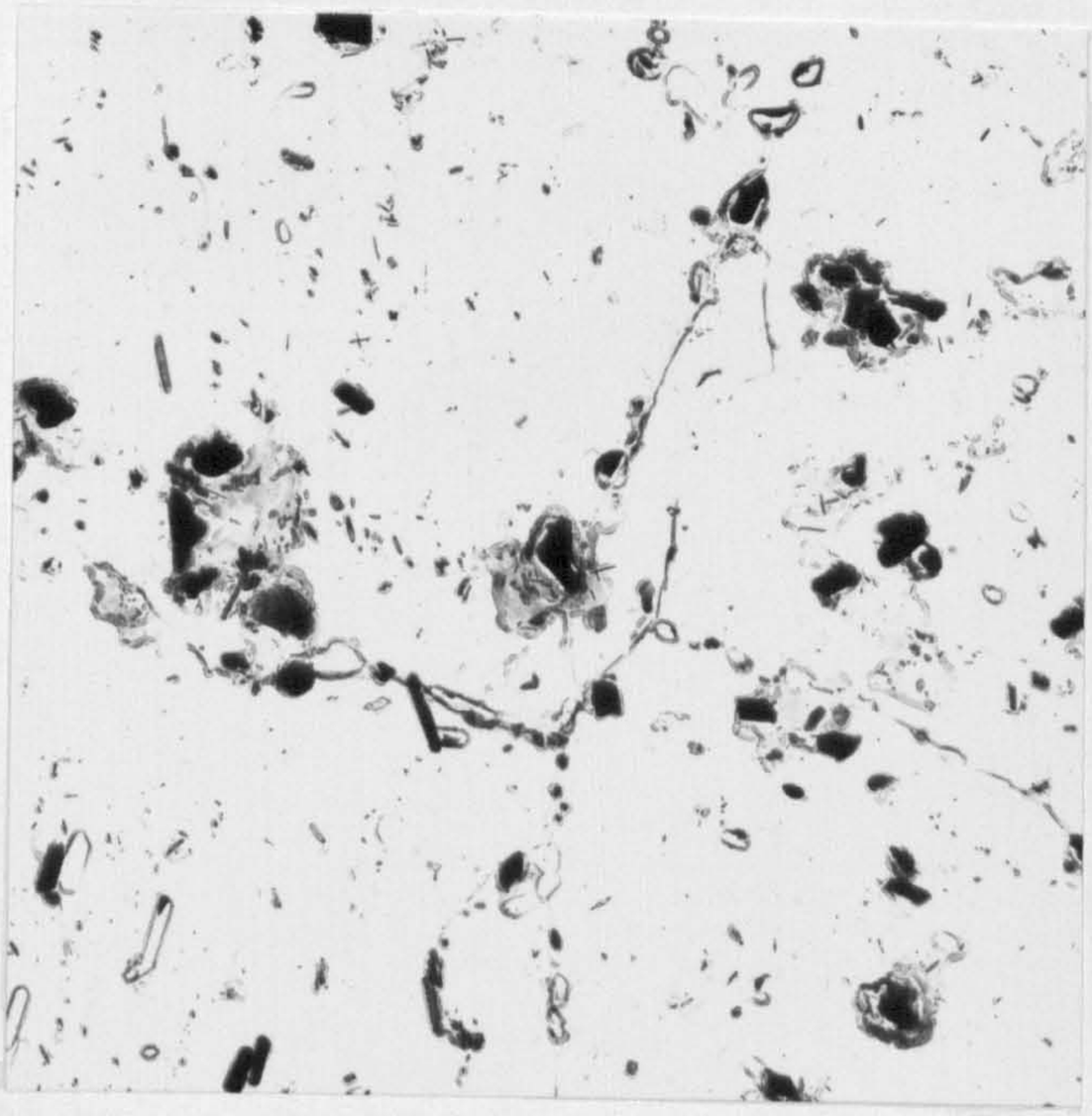

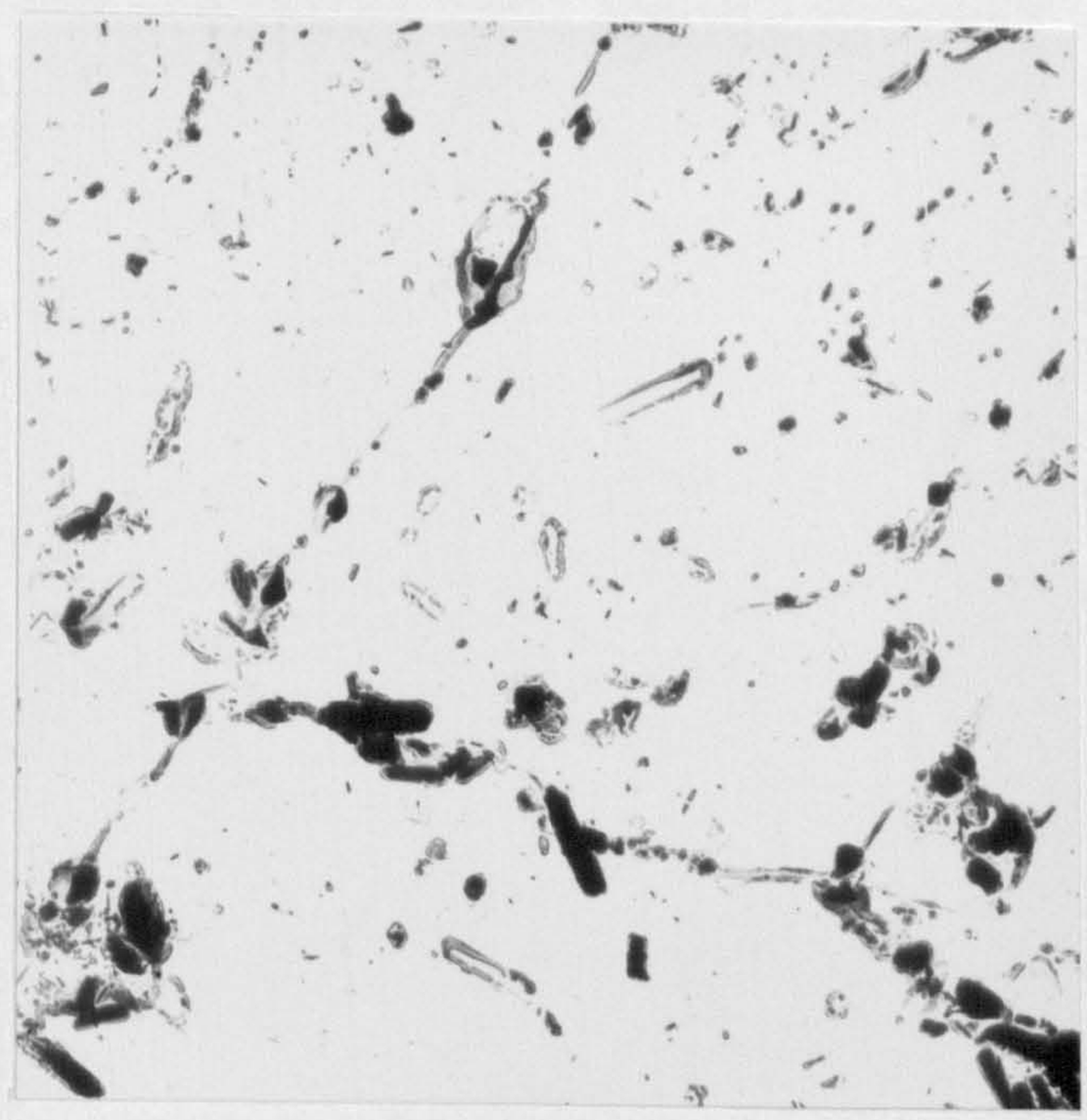

Fig. 30 Diffraction pattern and its analysis, produced by a single $M_{23}C_6$ precipitate particle, as shown in previous micrographs.

Fig. 31 Diffraction pattern and its analysis, produced by M_2C precipitates in Fig. 28.

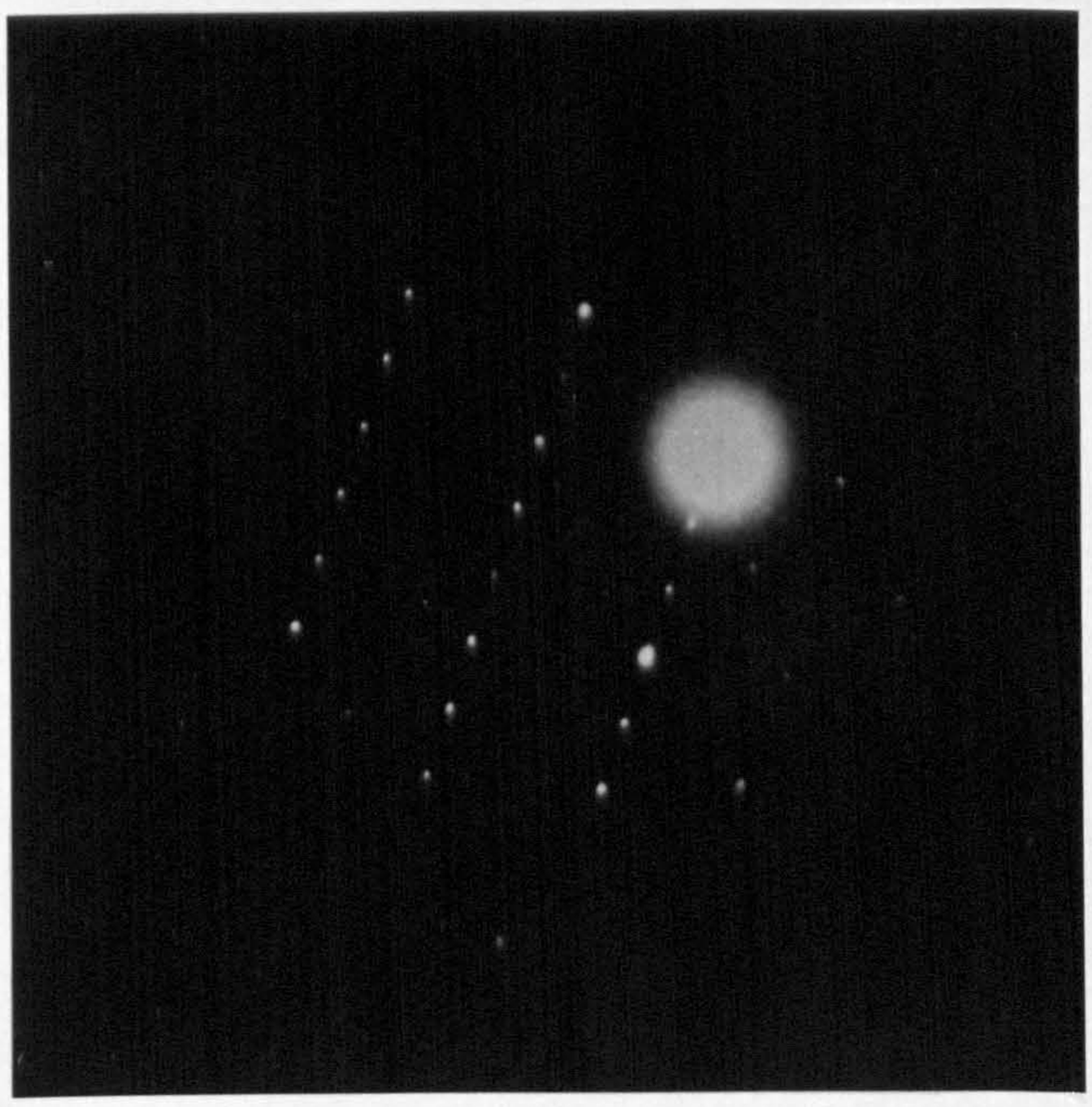

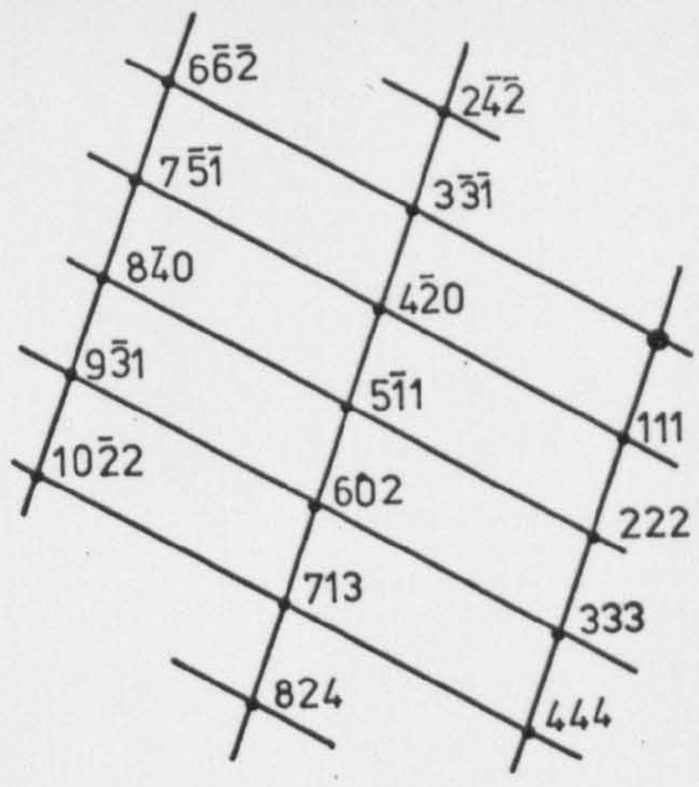

(123) ZONE, $M_{23}C_6$

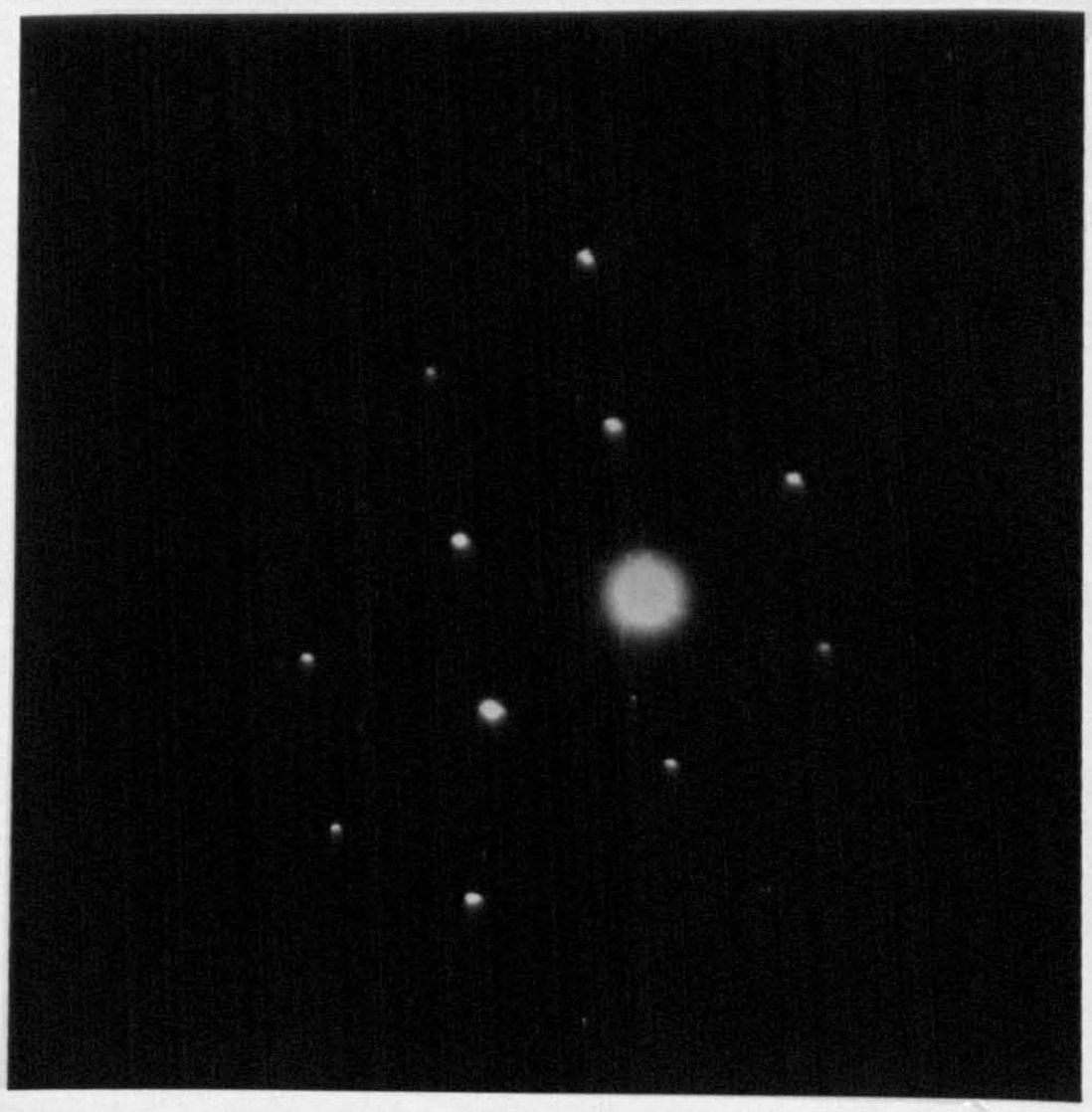

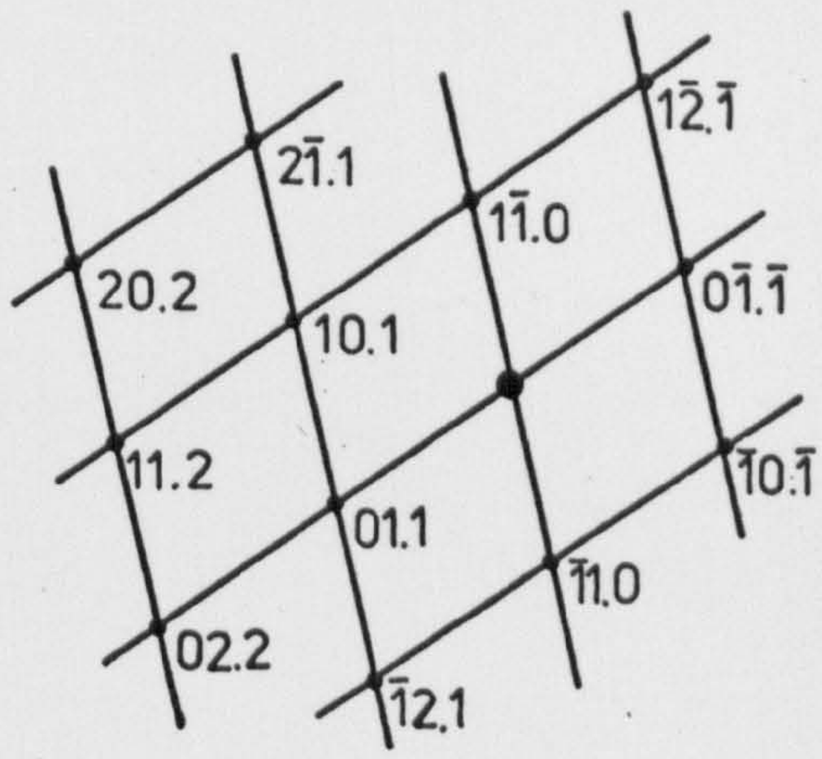

(11.1) ZONE, Mo_2C

Fig. 32 Cavity density as a function of precipitate free zone width for two series of $2^1/4$Cr1Mo alloy steels given different austenitising heat treatments to induce a variety of grain sizes. The results are represented by a single curve showing that cavity formation is inversely dependent on the depletion of matrix precipitate (M_2C) adjacent to the grain boundaries.
Cane, (1976).

Fig. 33 Hole growth rates for diffusive and viscous flow as a function of hole radius for $1Cr^1/2Mo$ steel during creep at 923K. The regime of behaviour expected from typical cavity nuclei observed in the CRM and CRMS series alloys is indicated by the red line.
Hancock, (1976).

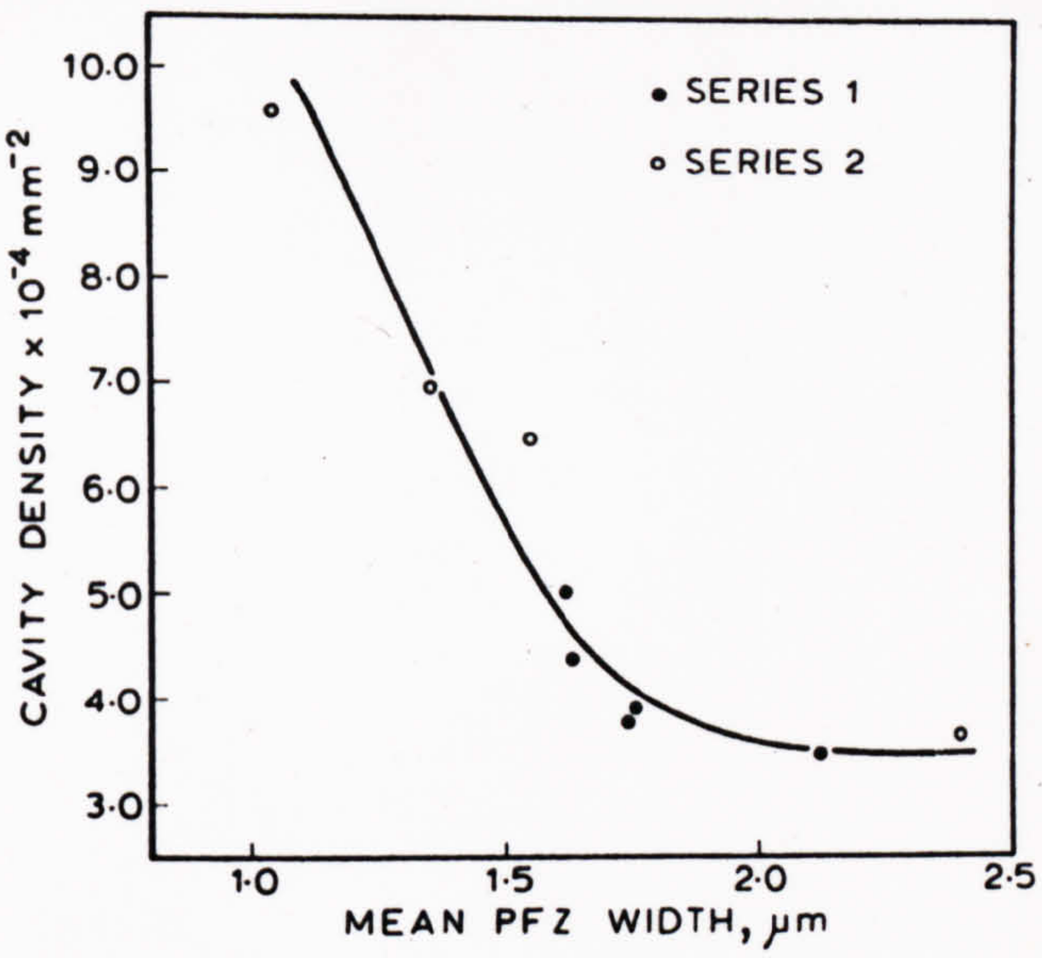
10·0
9·0
8·0
7·0
6·0
5·0
4·0
3·0
CAVITY DENSITY x 10^{-4} mm^{-2}
1·0
1·5
2·0
2·5
MEAN PFZ WIDTH, μm
• SERIES 1
∘ SERIES 2

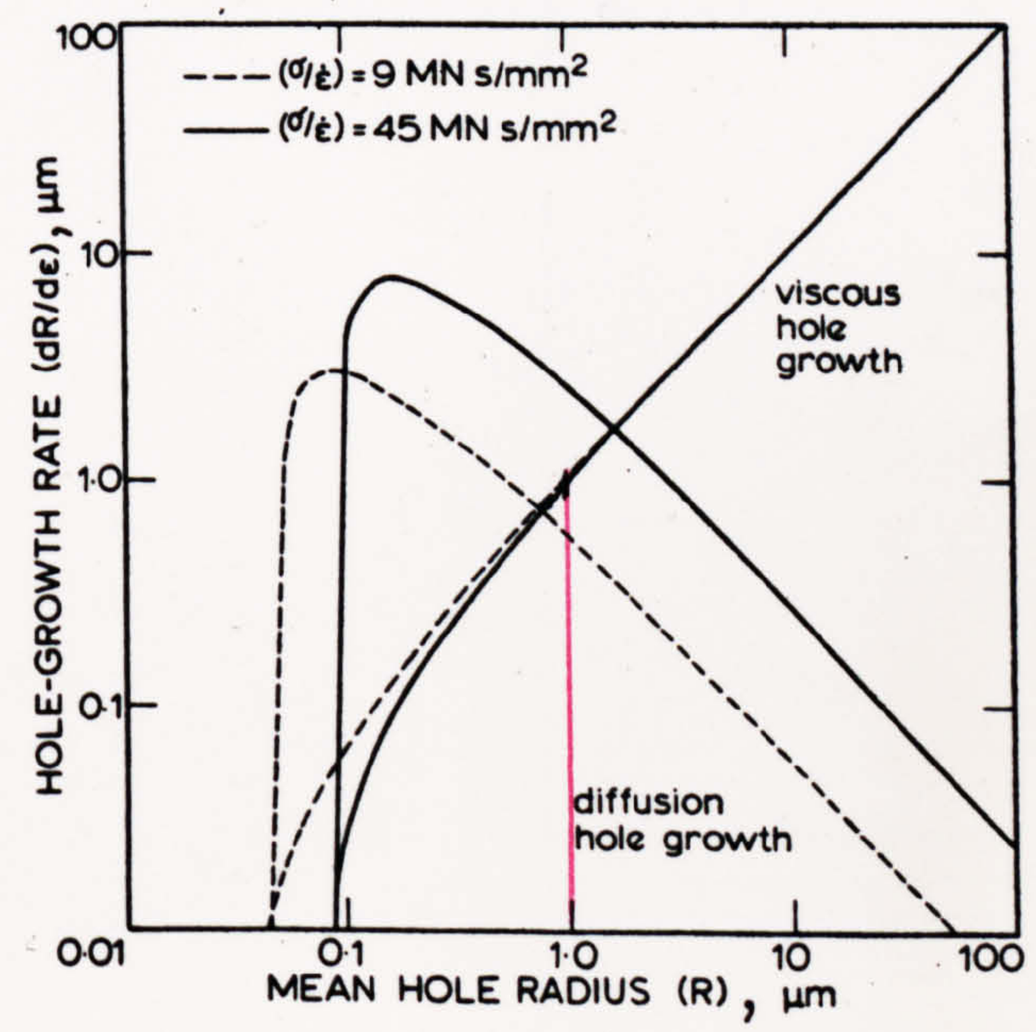
100
10
1·0
0·1
0·01
HOLE-GROWTH RATE (dR/dε), μm
(σ/ε̇) = 9 MN s/mm²
(σ/ε̇) = 45 MN s/mm²
viscous hole growth
diffusion hole growth
0·1
1·0
10
100
MEAN HOLE RADIUS (R), μm

Fig. 34 Load/elongation curves for CRMV series alloy taken to failure, at constant strain rate, at 290K (CRMV/U1) and 773K (CRMV/U4).

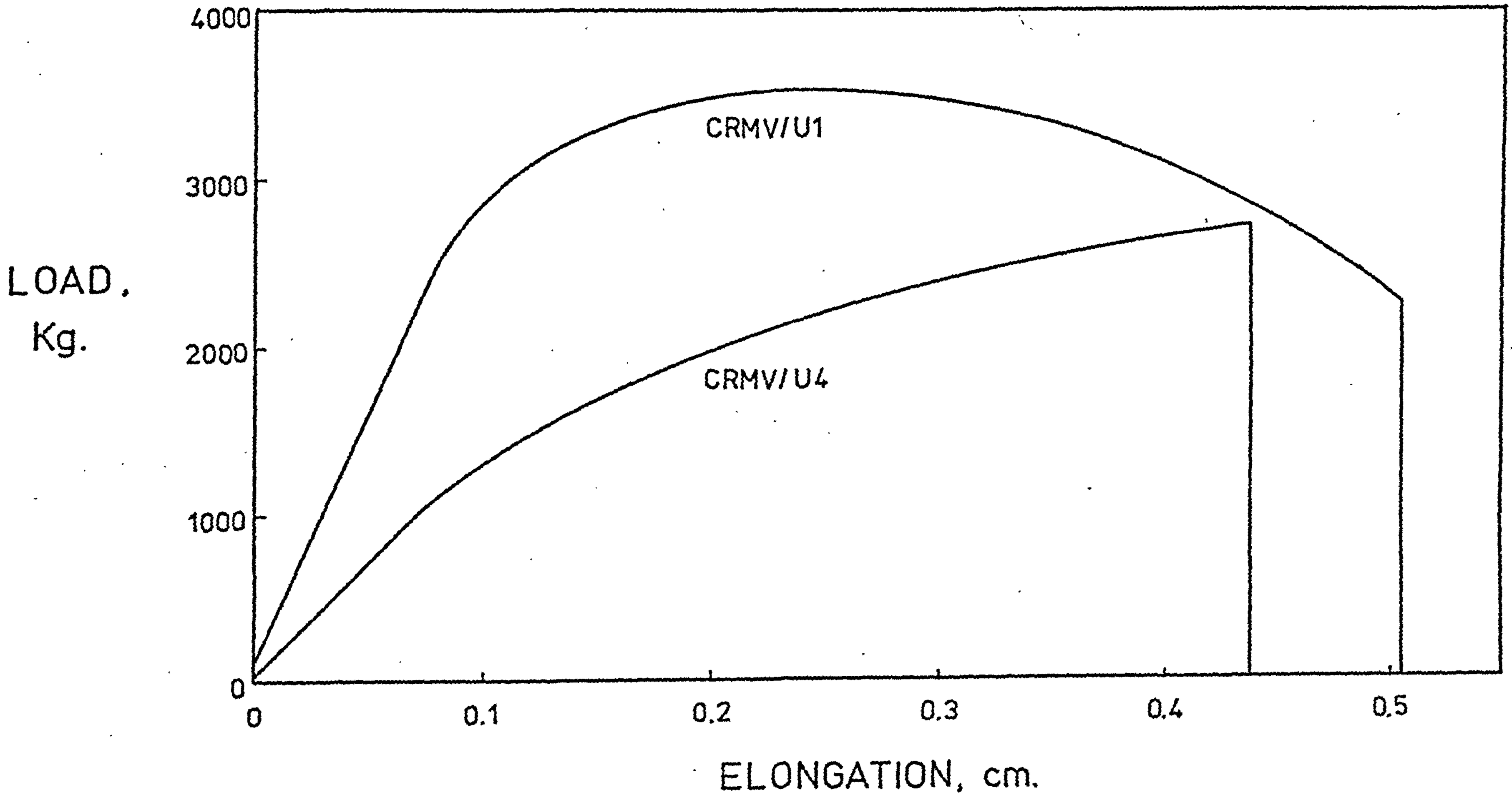
LOAD,
Kg.
4000
3000
2000
1000
0
CRMV/U1
CRMV/U4
0
0.1
0.2
0.3
0.4
0.5
ELONGATION, cm.

Fig. 35(a) Fracture surface of specimen CRMV/U2, strained to failure at room temperature, showing ductile "cup-and-cone" type failure.
X25

Fig. 35(b) Central area of Fig. 35(a), revealing the transgranular nature of the fracture path.
X120

Fig. 35(c) Same area, showing the formation of microvoid cusps and the association of particles.
X1200

Fig. 36(a) Fracture surface of specimen CRMV/U4, strained to failure (at constant strain rate) at 773K. The failure exhibits a mixed trans- and intergranular nature.
X20

Fig. 36(b) High magnification view of the intergranular region of the same specimen, showing the exposed grain facets.
X320

Fig. 36(c) Individual grain boundary facets from the same area. Note their smooth, featureless appearance.
X1275

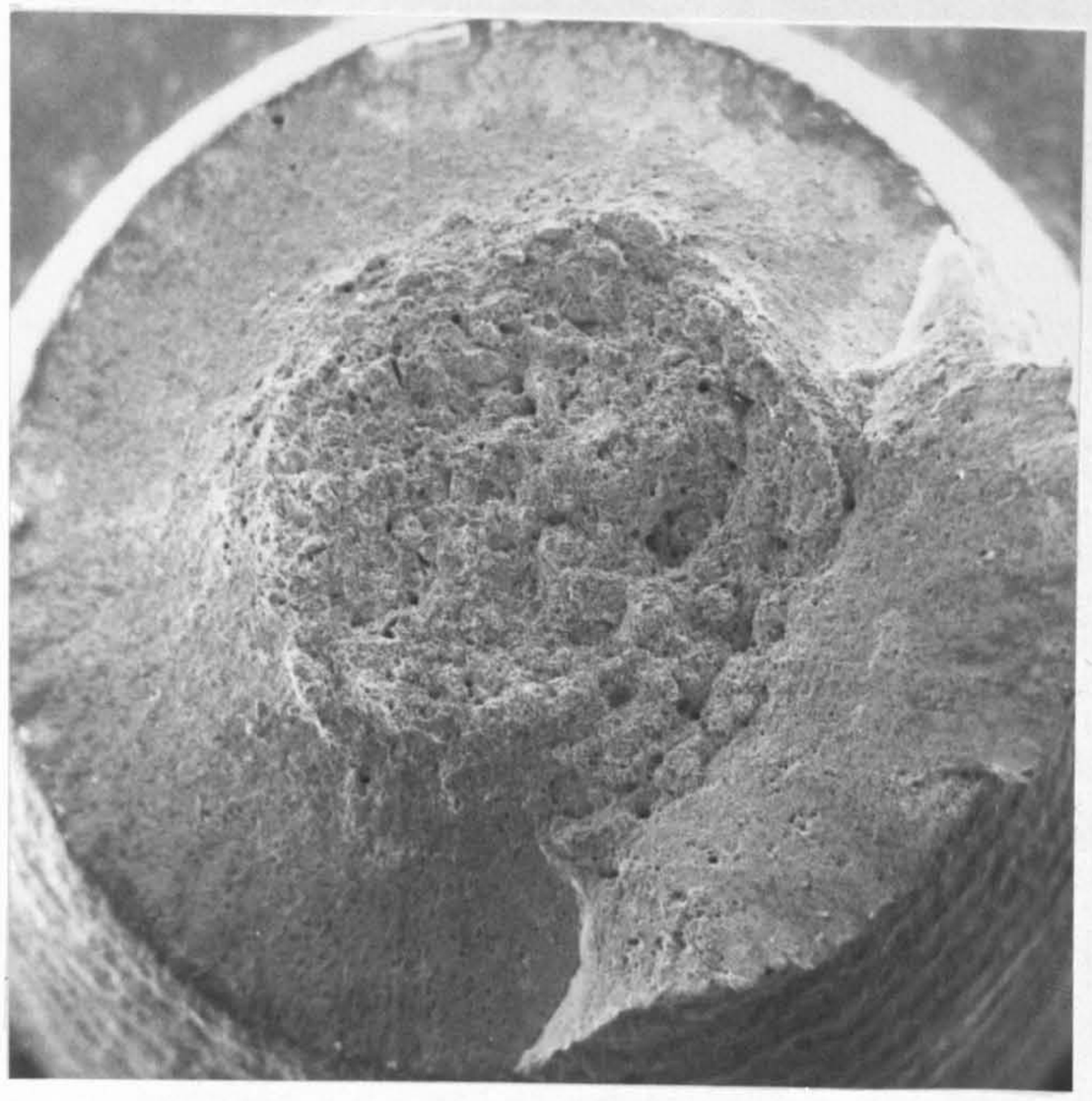

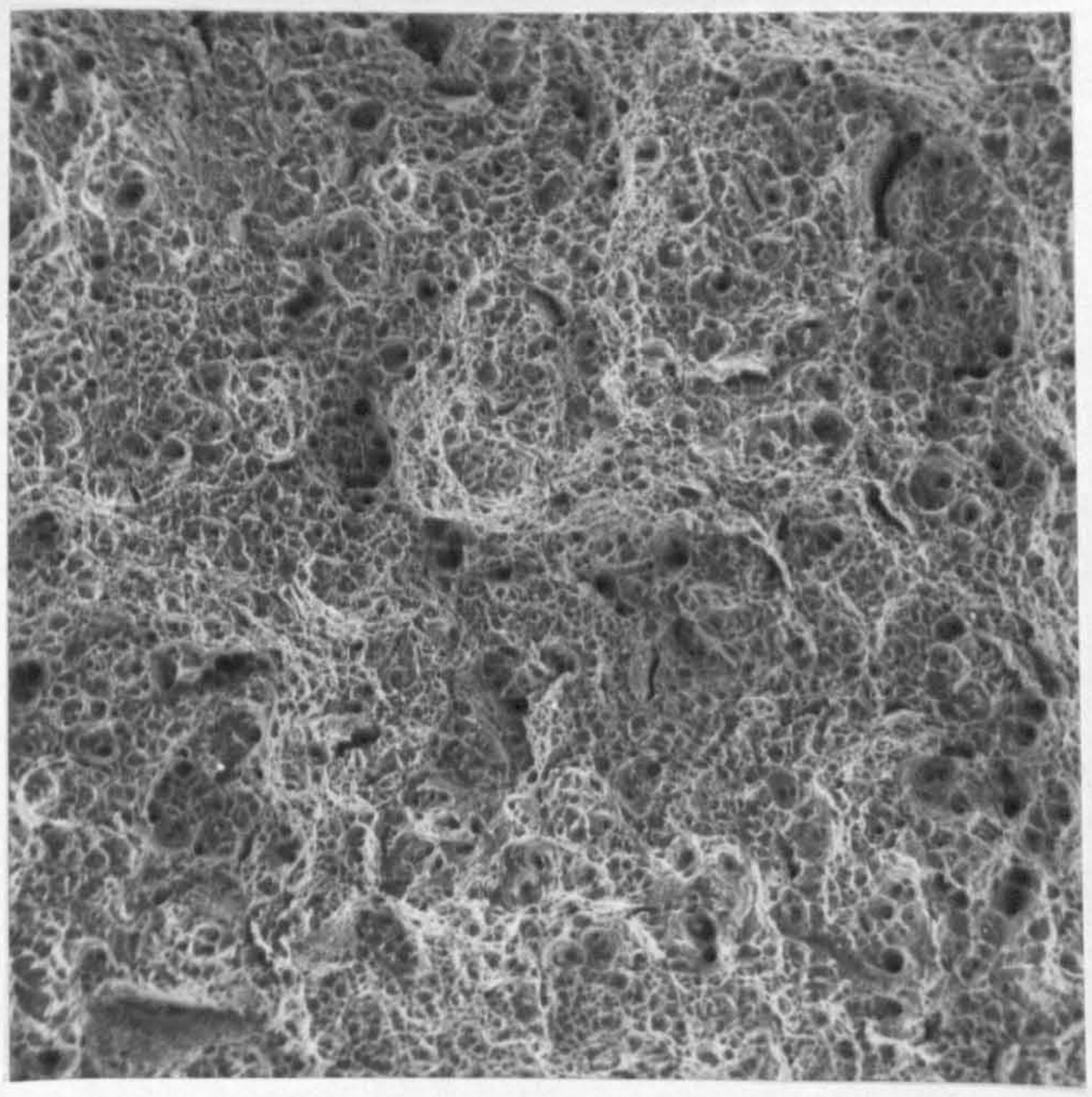

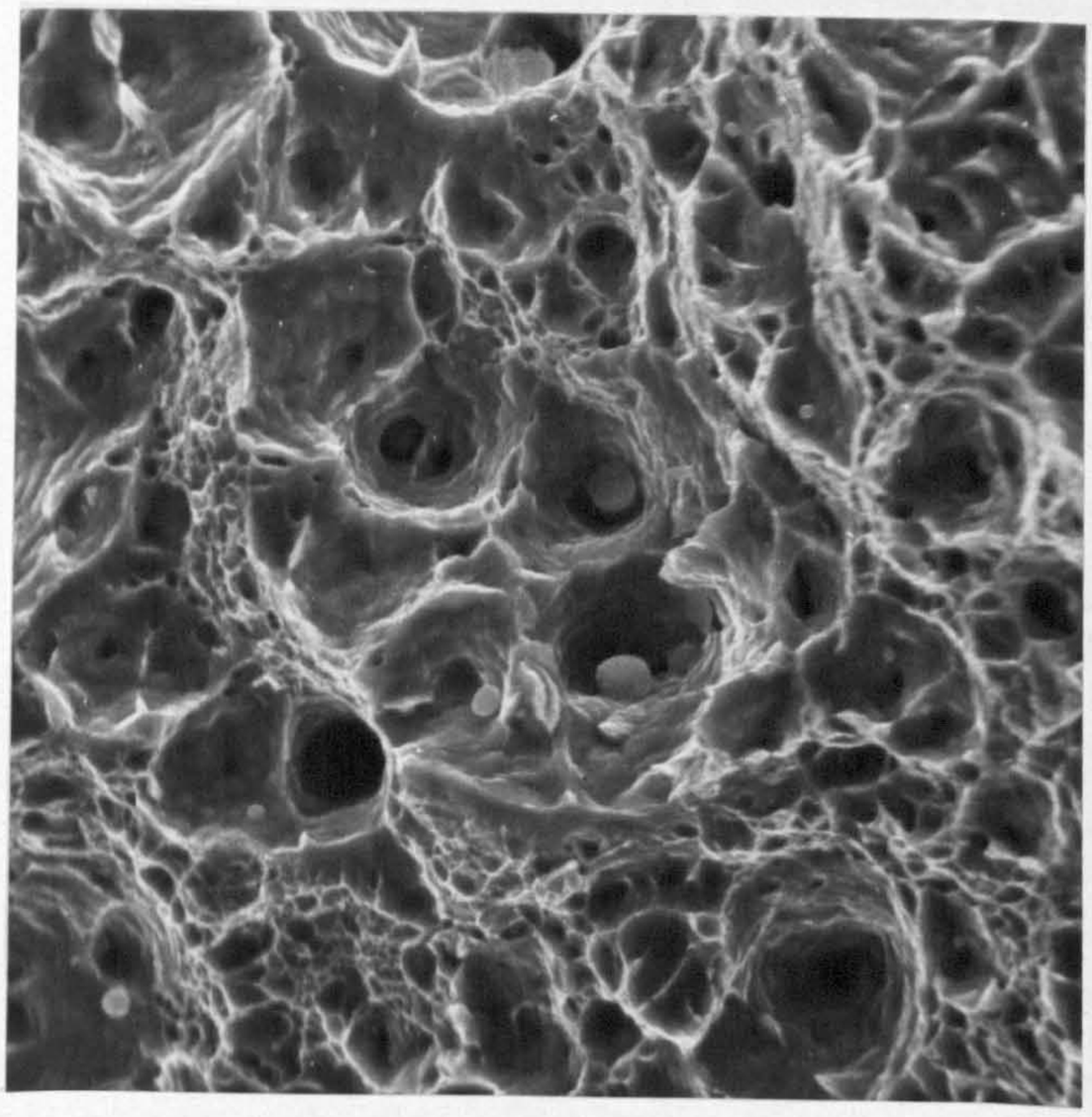

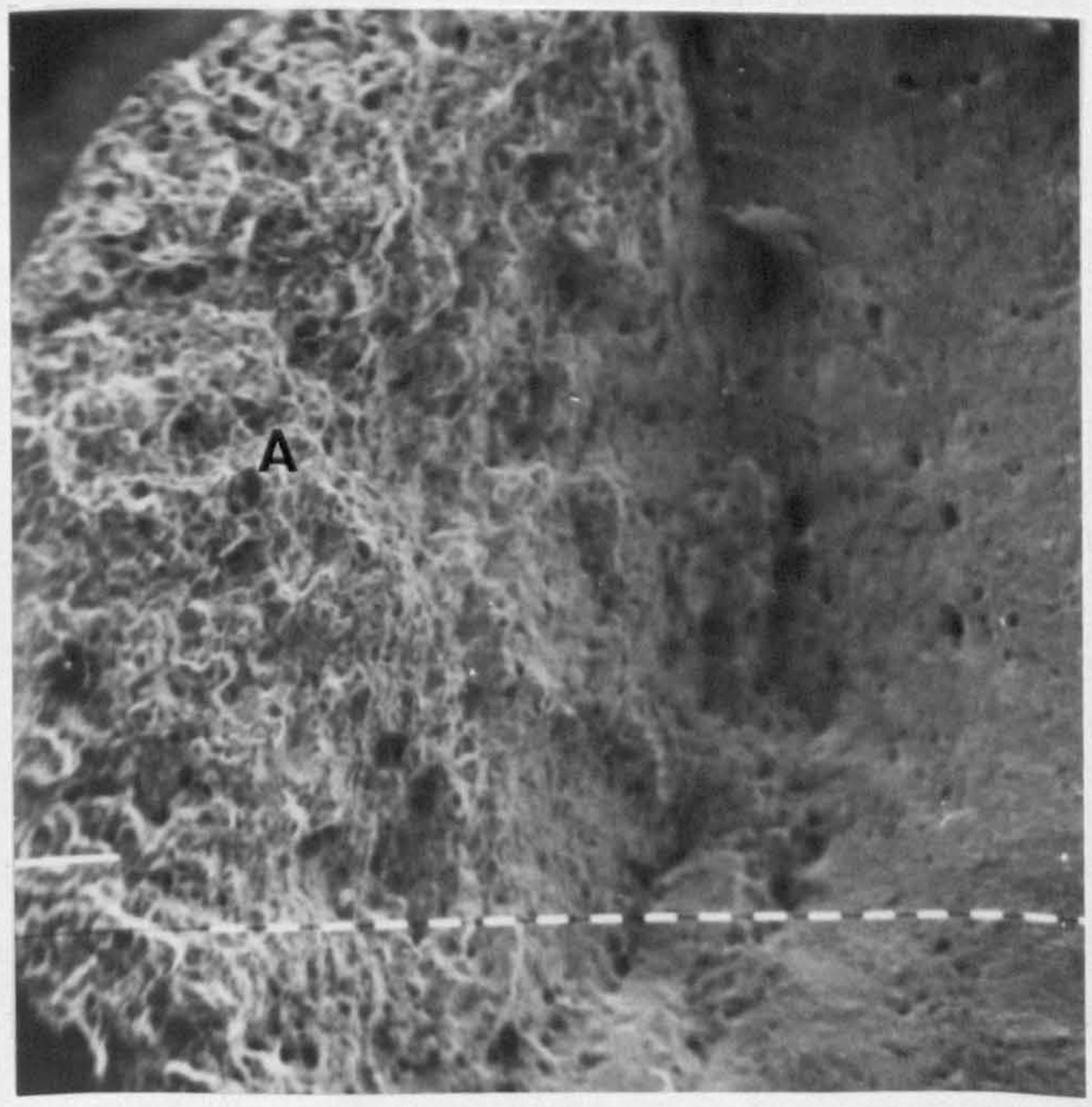
A

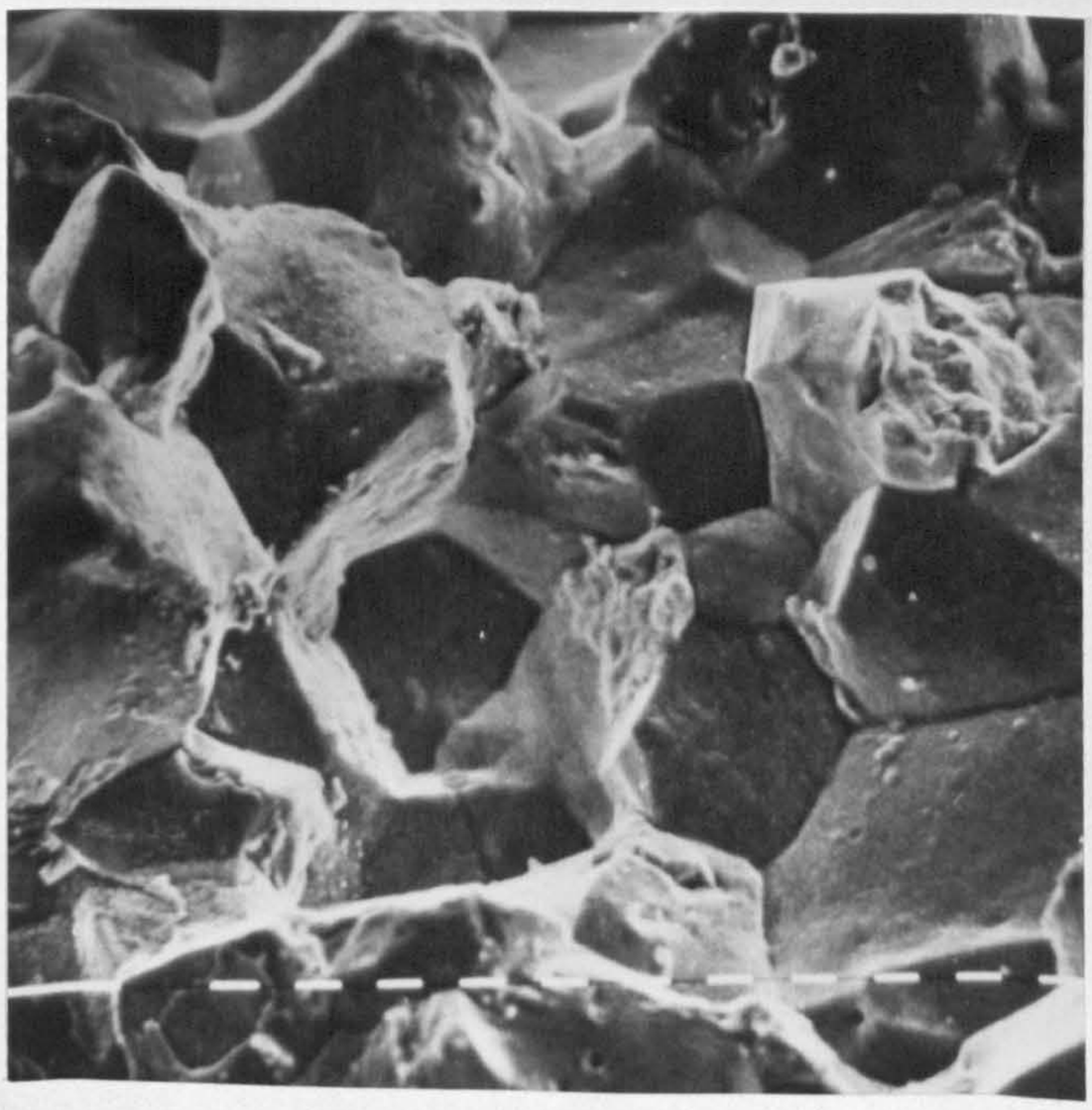

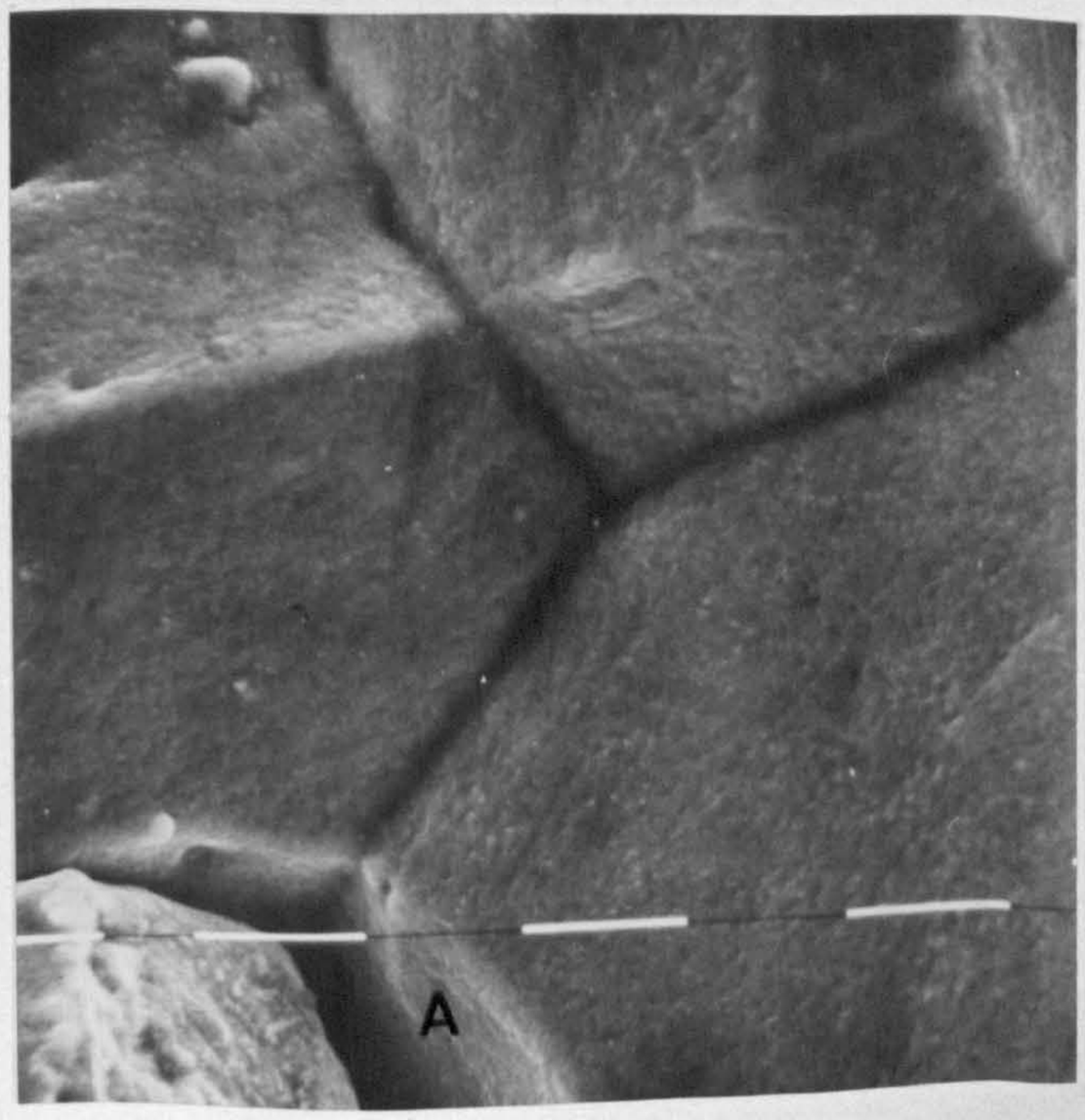
A

Fig. 37 100kV electron micrograph of a thin foil taken from specimen CRMV/U2 after failure. The bainite plates are bounded by coarse Fe_3C particles and there is no intergranular precipitation.
X11600

Fig. 38 Dark field image of the same area using an Fe_3C reflection. Coarse, spherodised carbides line the bainite plate boundaries.
X11600

Fig. 39 100kV electron micrograph of a thin foil taken from specimen CRMV/U4 after failure. Within the bainite plates there has been intense precipitation of VC on matrix dislocations.
X15800

Fig. 45 Typical test piece after creep failure. Note the absence of necking in the specimen guage length.

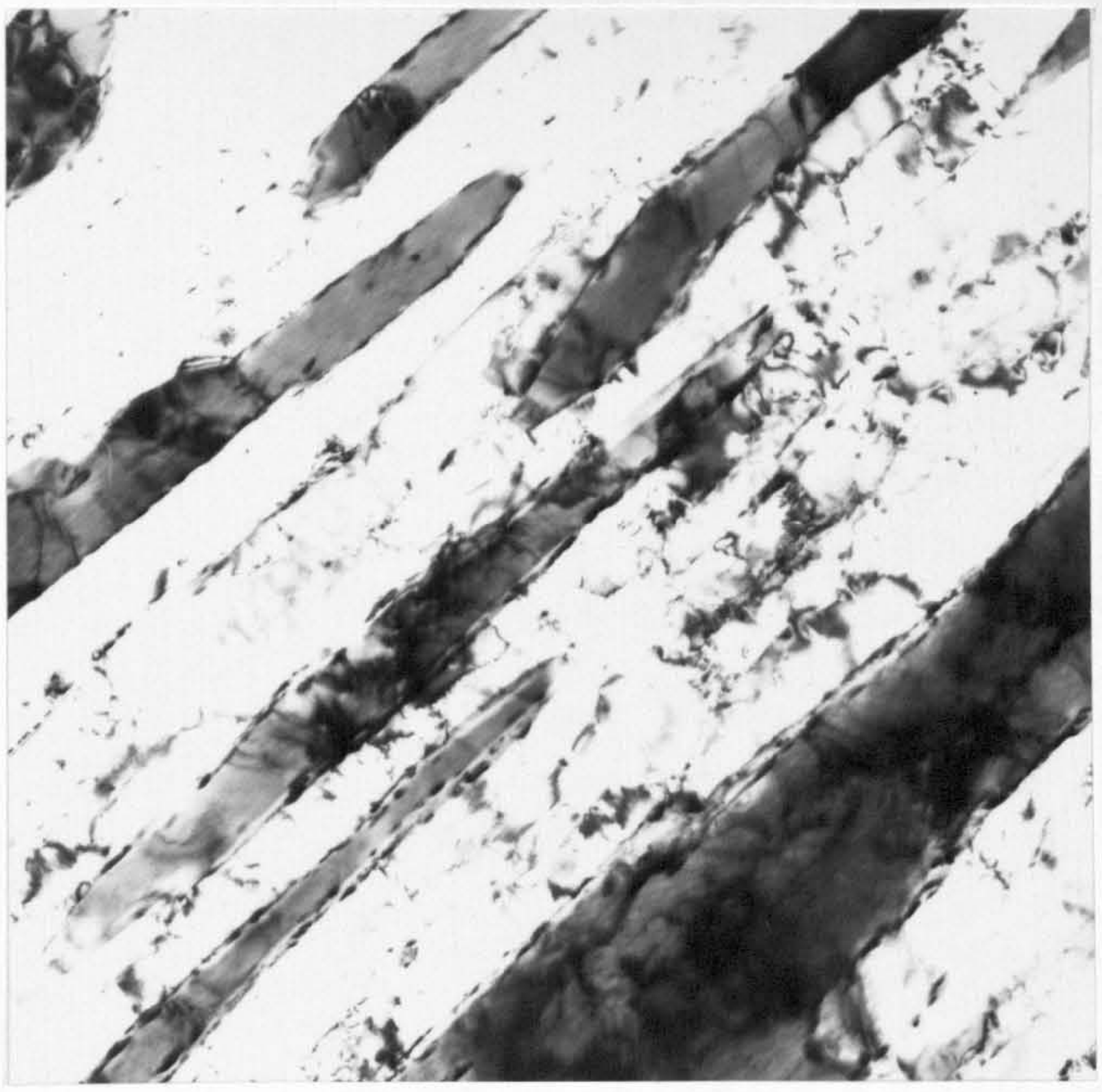

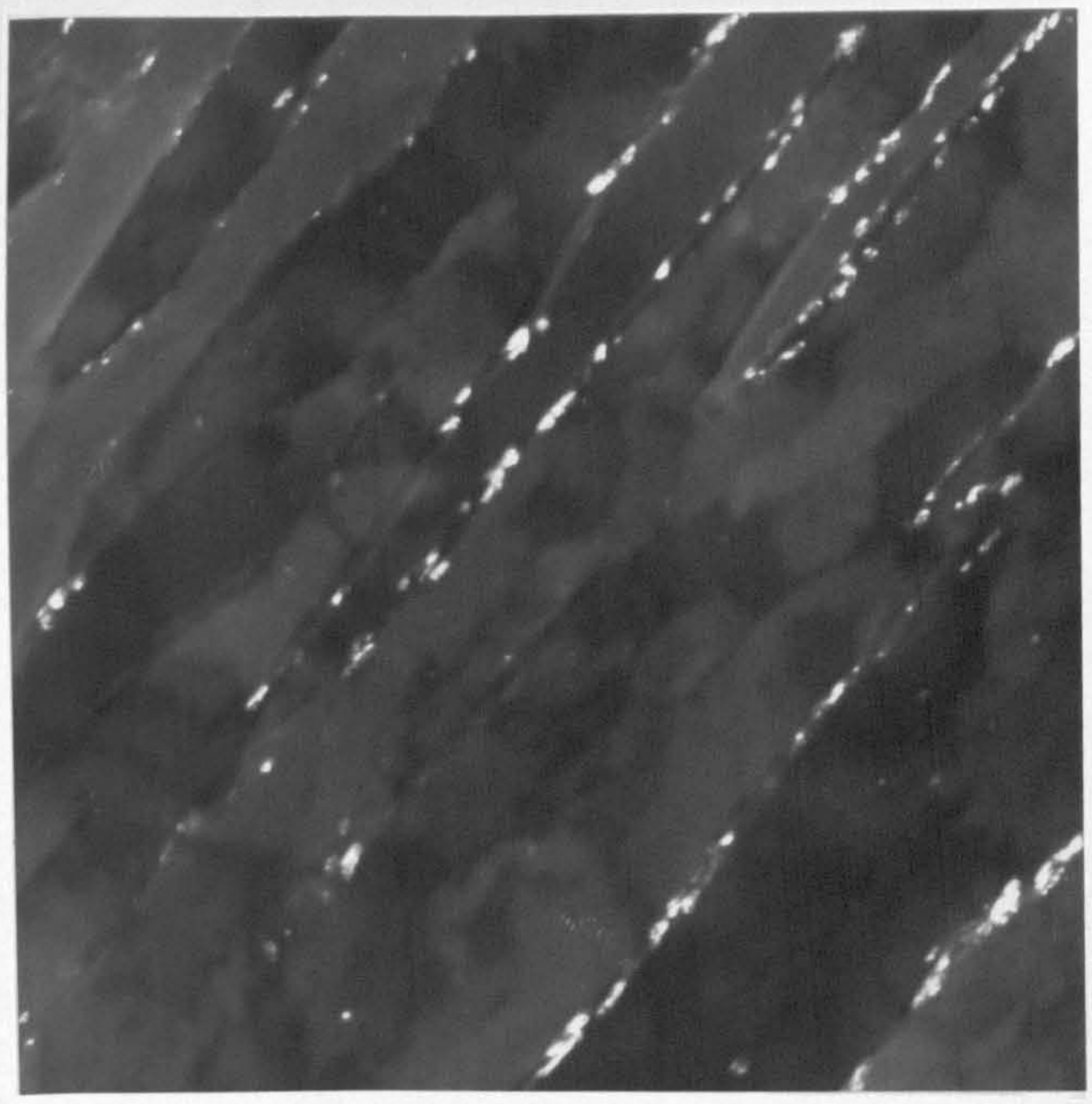

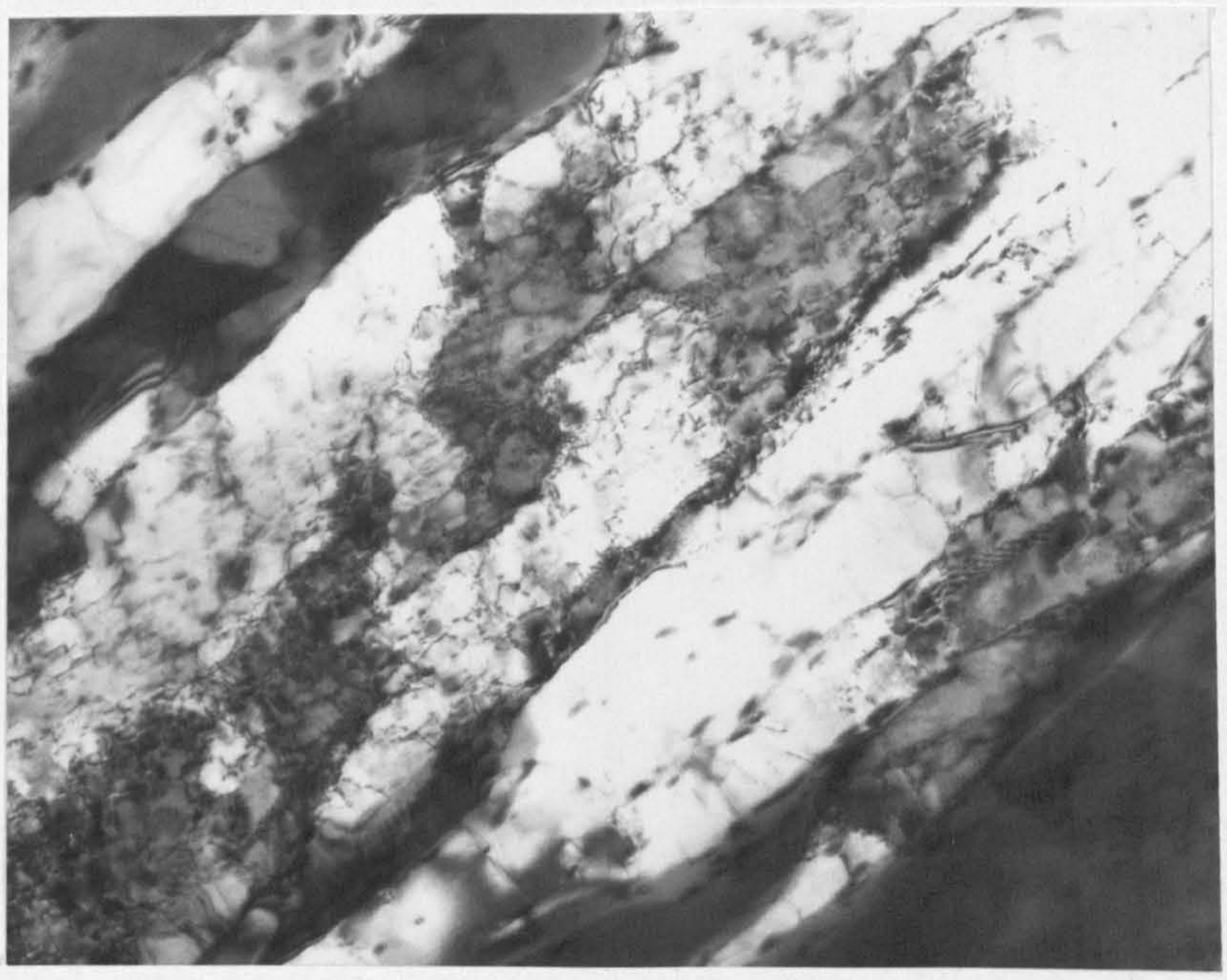

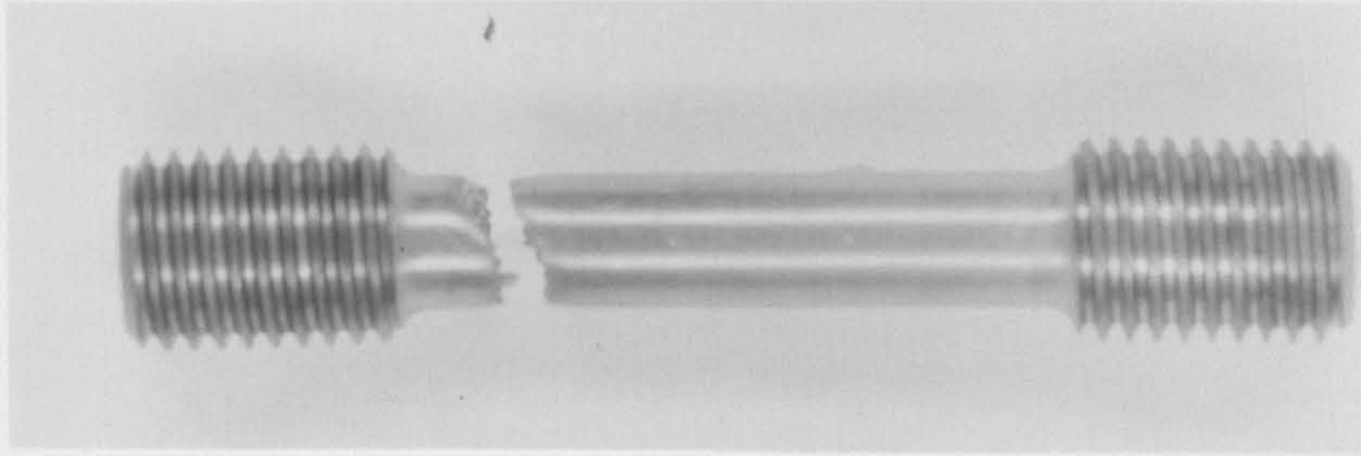

Fig. 40 Typical creep curves generated by deformation of CRMV series alloy at 963, 863 and 803K.

CRMV 2	50 MNm^{-2}	963K
CRMV12	90 MNm^{-2}	963K
CRMV13	170 MNm^{-2}	863K
CRMV 9	200 MNm^{-2}	803K

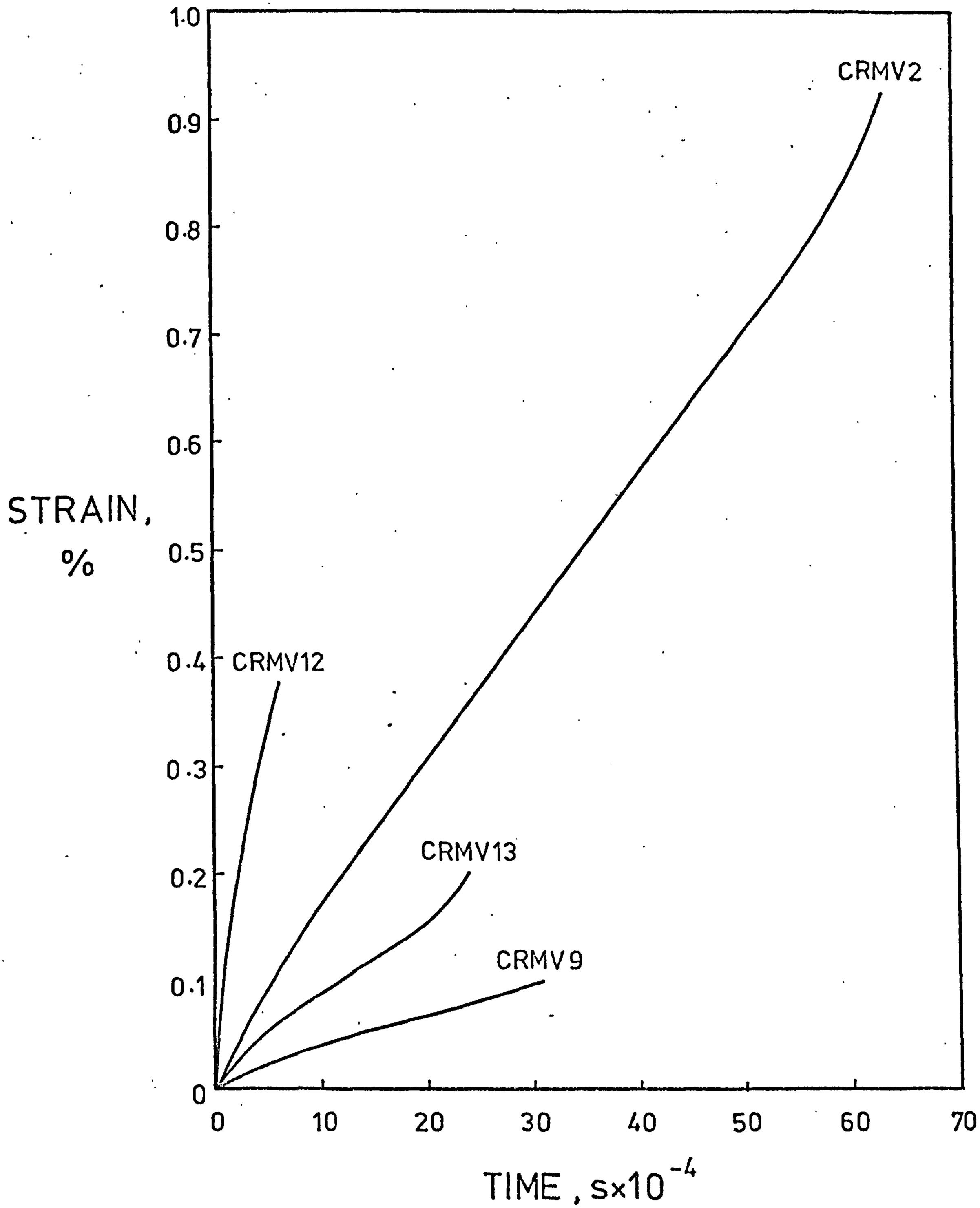
1.0
0.9
0.8
0.7
0.6
0.5
0.4
0.3
0.2
0.1
0
STRAIN, %
CRMV2
CRMV12
CRMV13
CRMV9
0
10
20
30
40
50
60
70
TIME , s×10 -4

Fig. 41 Rupture ductility data for CRMV series alloy, plotted as a function of the Larson-Miller parameter P_F.

○ 963K

□ 863K

Δ 803K

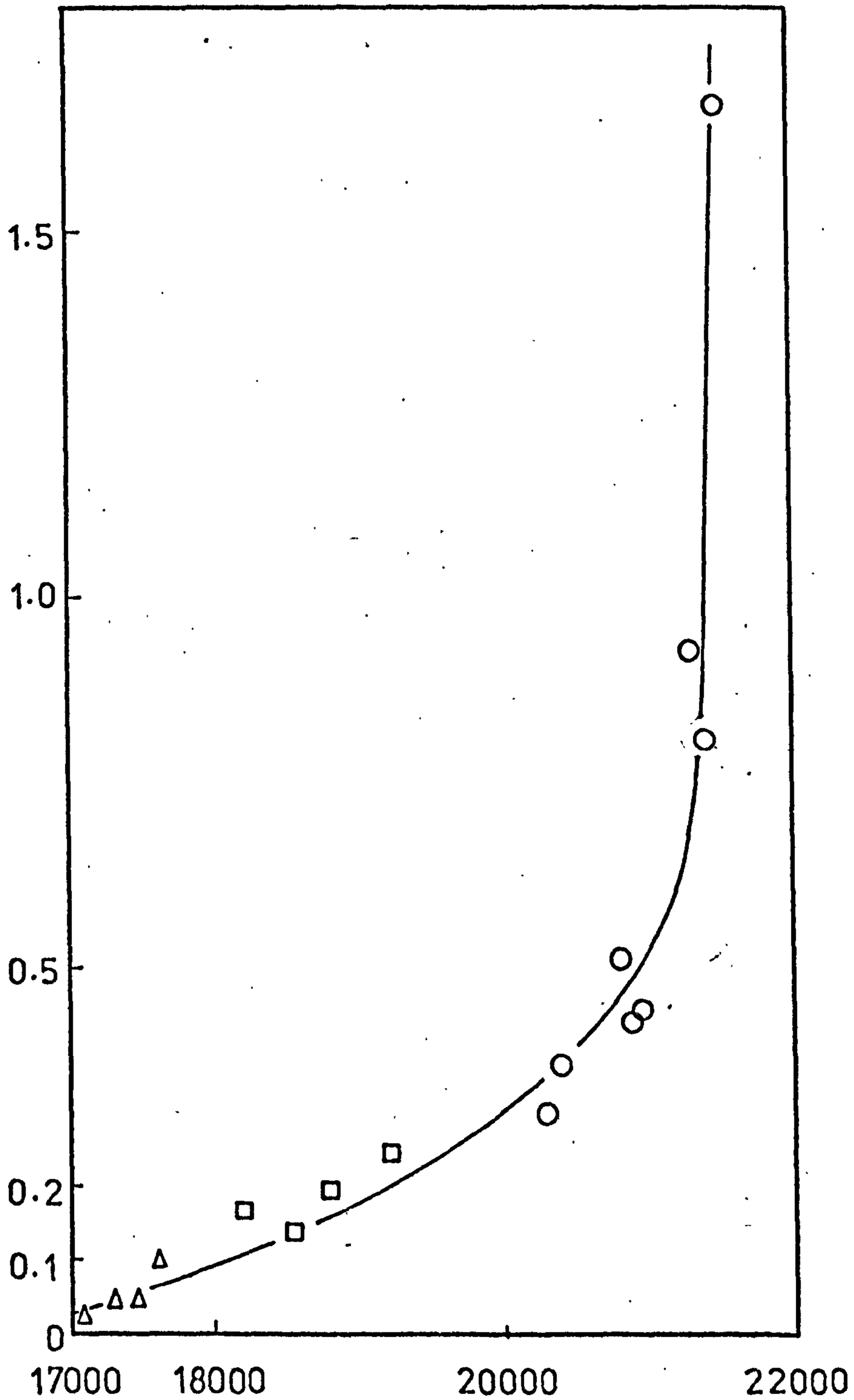

$$P_F = T(20 + \log t_F)$$

Fig. 42 Minimum creep rate plotted as a function of stress for CRMV series alloy steel.

O 963K

□ 863K

Δ 803K

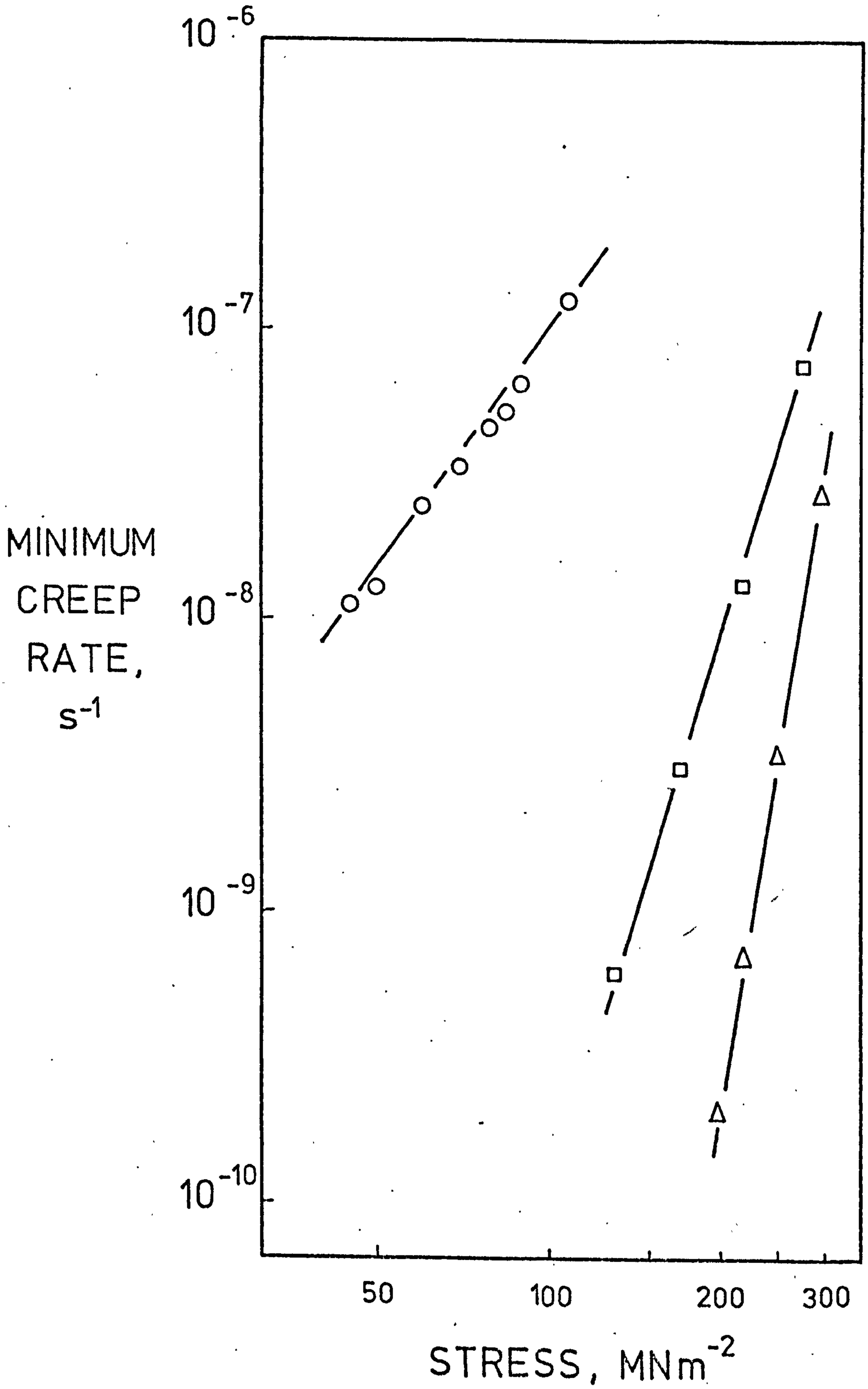
10 -6
10 -7
10 -8
10 -9
10 -10
MINIMUM CREEP RATE, s-1
50
100
200
300
STRESS, MNm-2

Fig. 43 Rupture life plotted as a function of stress for CRMV series alloy steel.

○ 963K

□ 863K

Δ 803K

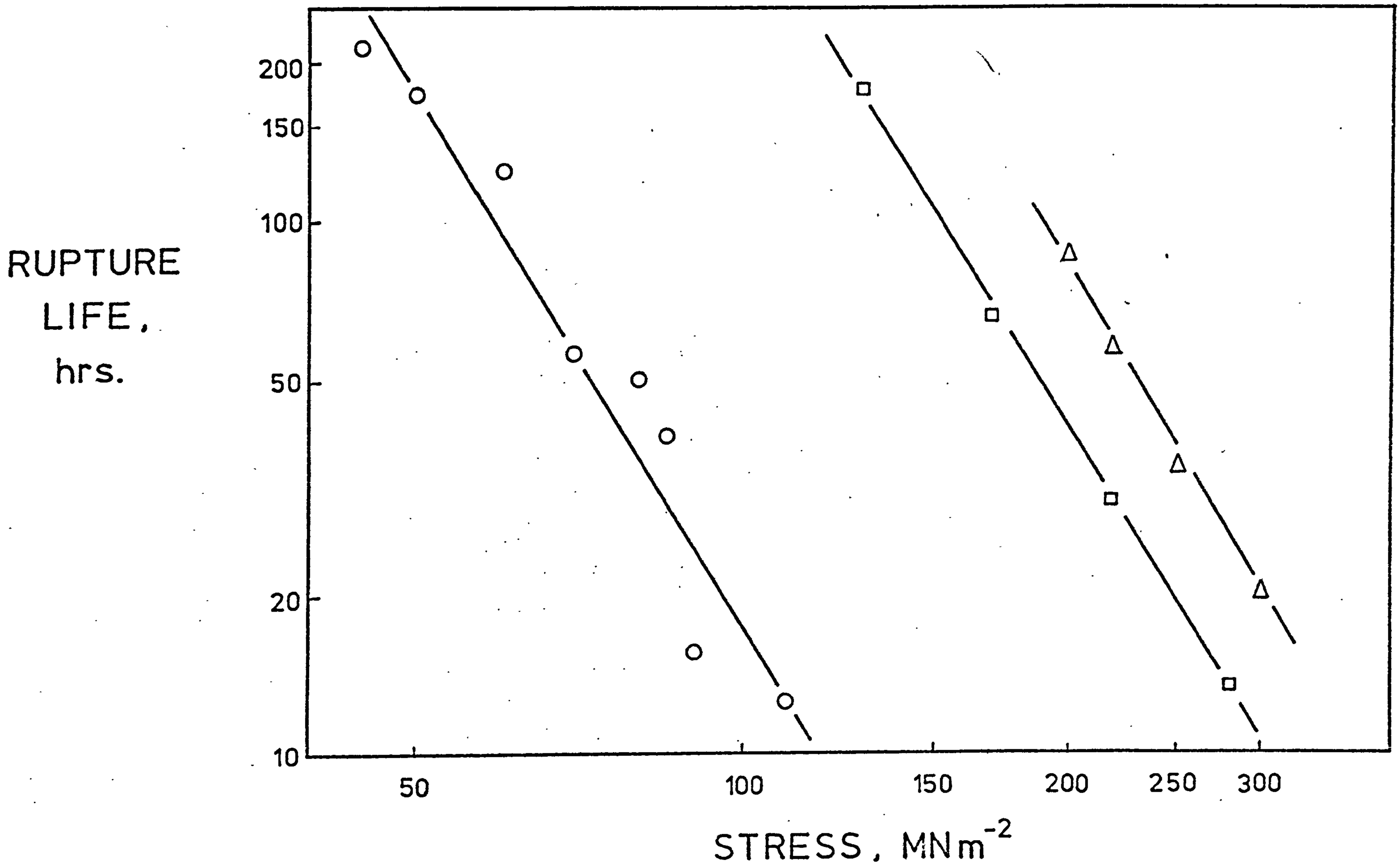
RUPTURE LIFE, hrs.
200
150
100
50
20
10
50
100
150
200
250
300
STRESS, MNm^{-2}

Fig. 44(a) Creep curve for CRMV series alloy produced by a stress of 90 MNm^{-2}, after prior deformation at a lower stress of 45 MNm^{-2}, (CRMV/R1). The curve generated by deformation at a constant stress of 90 MNm^{-2} is reproduced on the same graph, (CRMV12).

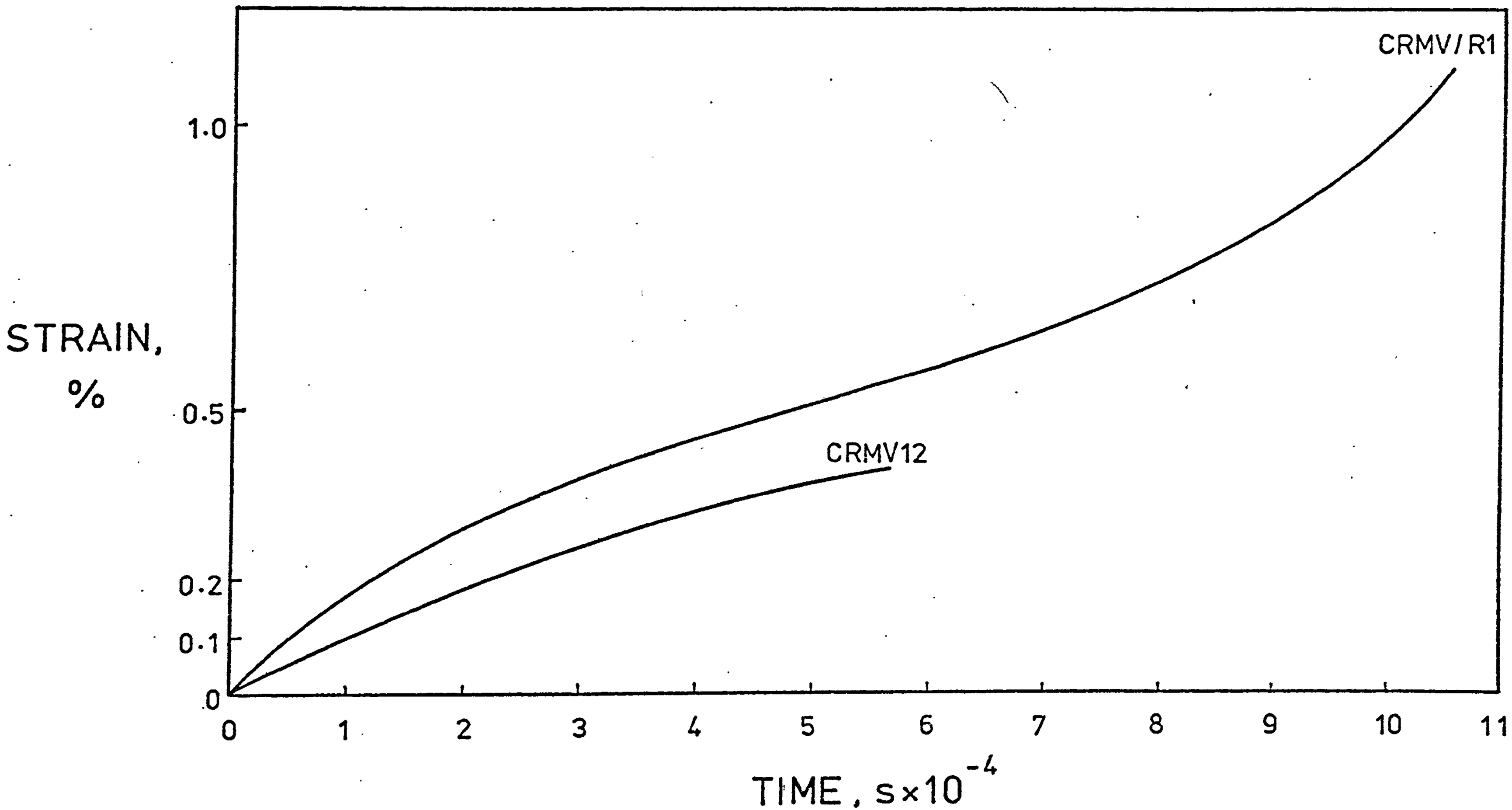
CRMV/R1
CRMV12
STRAIN, %
1.0
0.5
0.2
0.1
0
0
1
2
3
4
5
6
7
8
9
10
11
TIME, s×10^-4

Fig. 44(b) Creep curve for CRMV series alloy produced by a stress of 50 MNm^{-2}, after prior deformation at a higher stress of 110 MNm^{-2}, (CRMV/R2). The curve generated by deformation at a constant stress of 50 MNm^{-2} is reproduced on the same graph, (CRMV2)

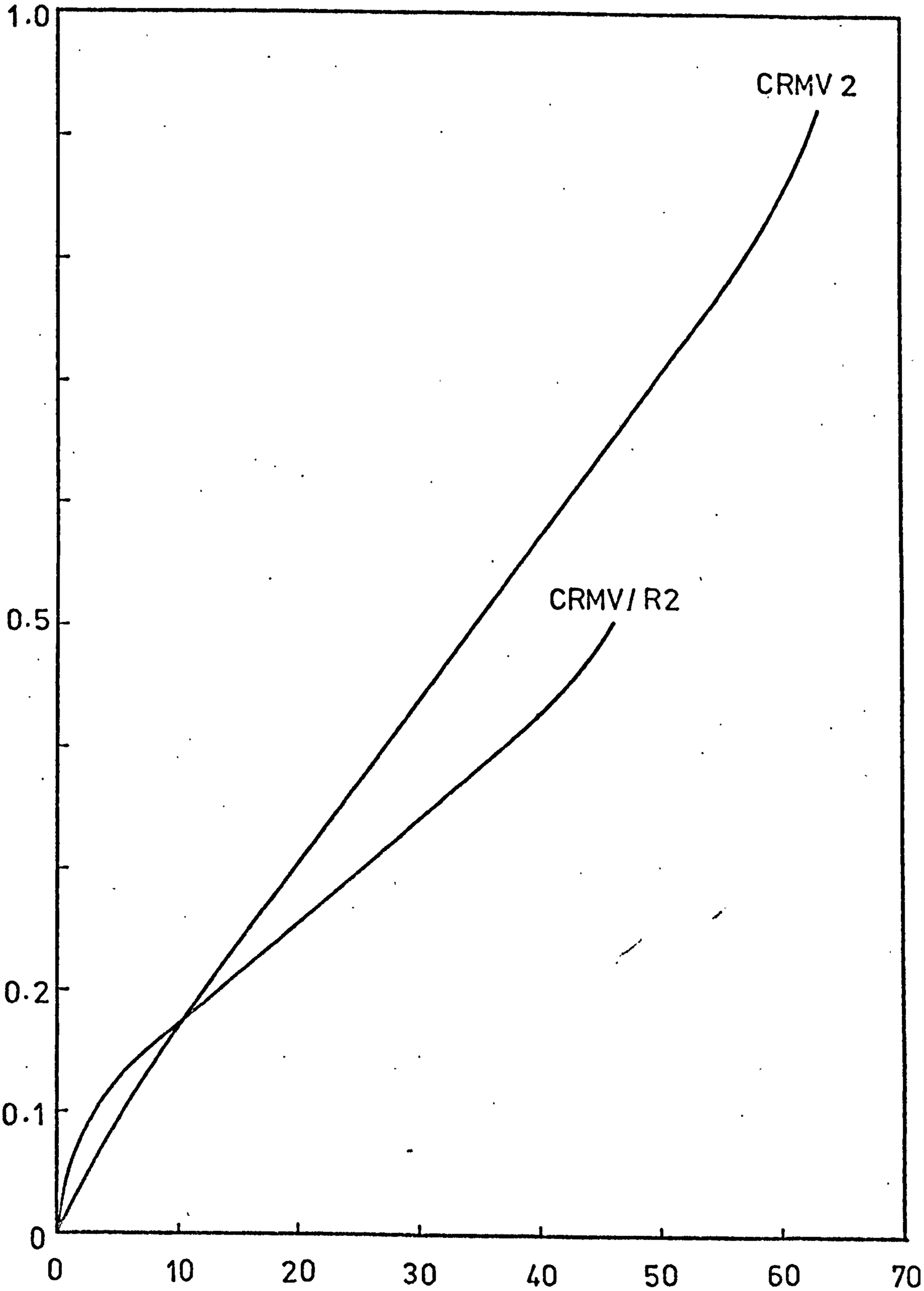
1.0
0.5
0.2
0.1
0
STRAIN
%
CRMV 2
CRMV/R2
0
10
20
30
40
50
60
70
TIME , s×10⁻⁴

Page numbering as original

Fig. 46(a) Typical fracture surface exhibited by CRMV series alloy after creep failure. The fracture has fllowed a completely intergranular path, with clearly defined grain facets. Specimen CRMV3.
X125

Fig. 46(b) Grain boundary decohesion between adjacent grains on the fracture surface after creep failure. A small ligament of material binds the two prior austenite grains shown here. Also of note is the absence of any interfacial sliding. Specimen CRMV2.
X610

Fig. 47 Grain facet topology observed after creep failure. Intricate networks produced by dense populations of creep cavities can be seen. Specimen CRMV1.

Fig. 48 The variation in cavity density and size can be seen on this grain facet exposed after creep failure. Specimen CRMV3.
X1340

Fig. 49(a) The appearance of intergranular damage on individual grain facets after failure at 50MNm^{-2}, 963K.
X1150

Fig. 49(b) Similar damage morphology observed on the intergranular fracture surface of a specimen crept to failure at 130 MNm^{-2}, 863K.
X1150

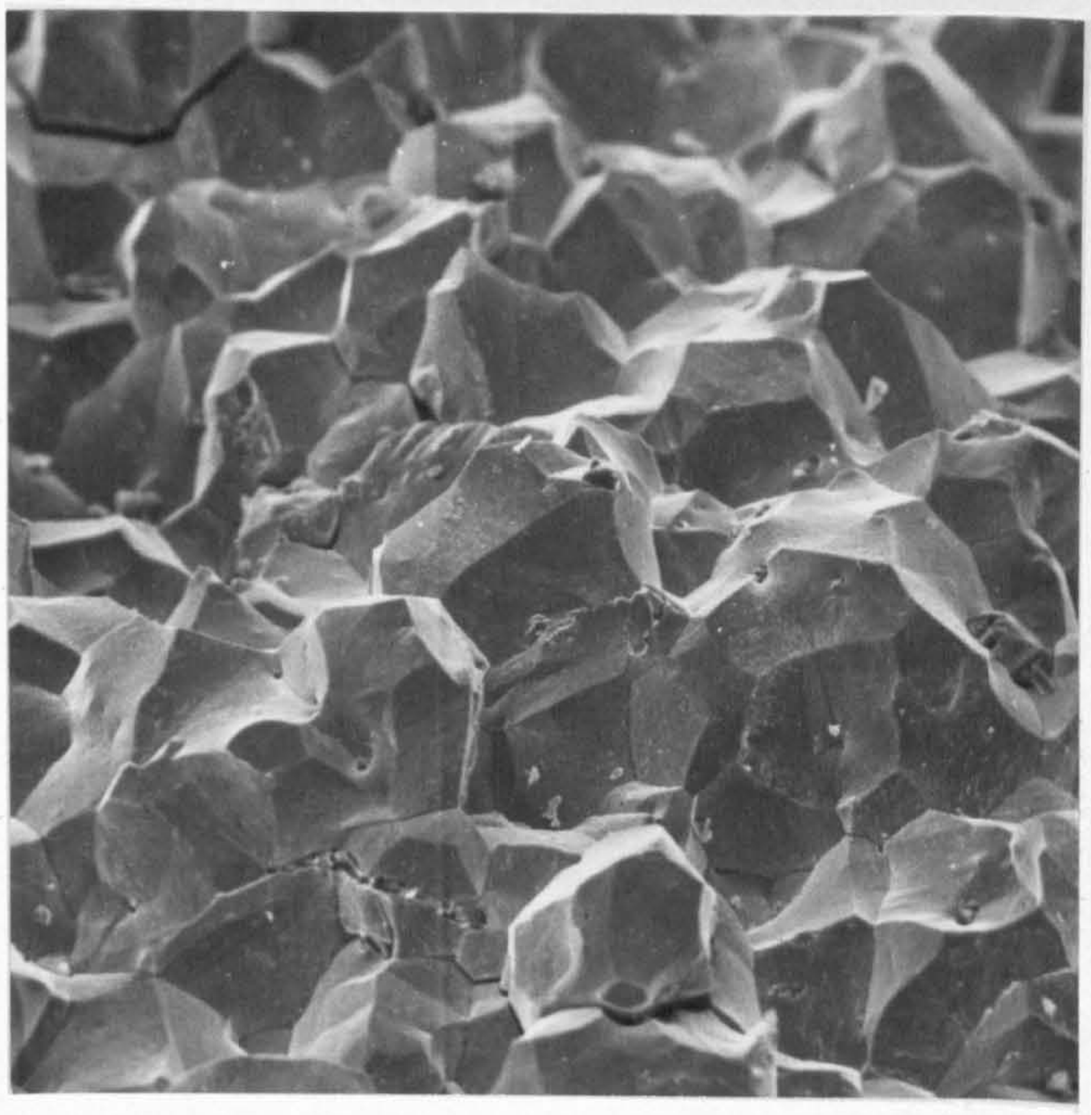

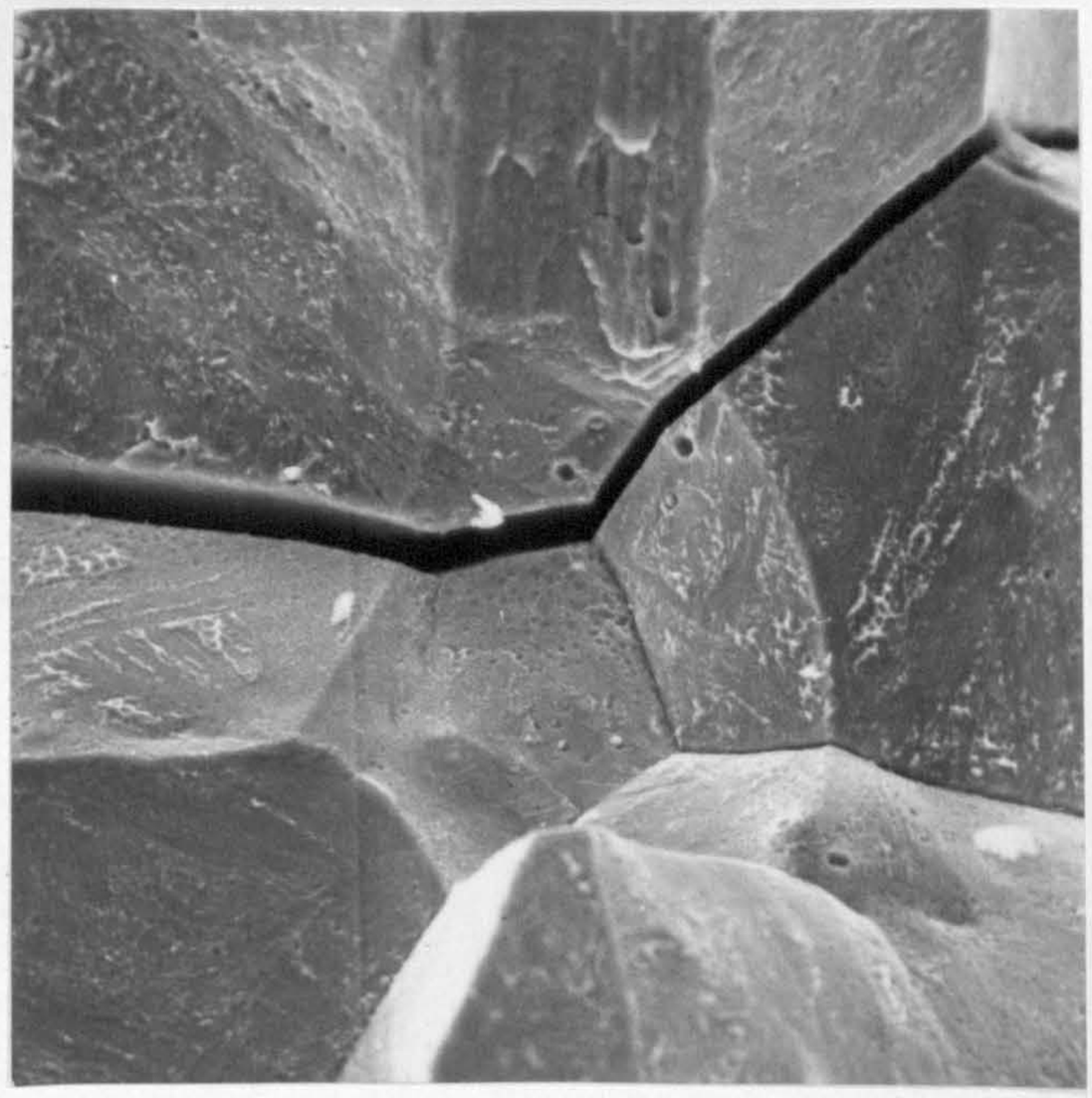

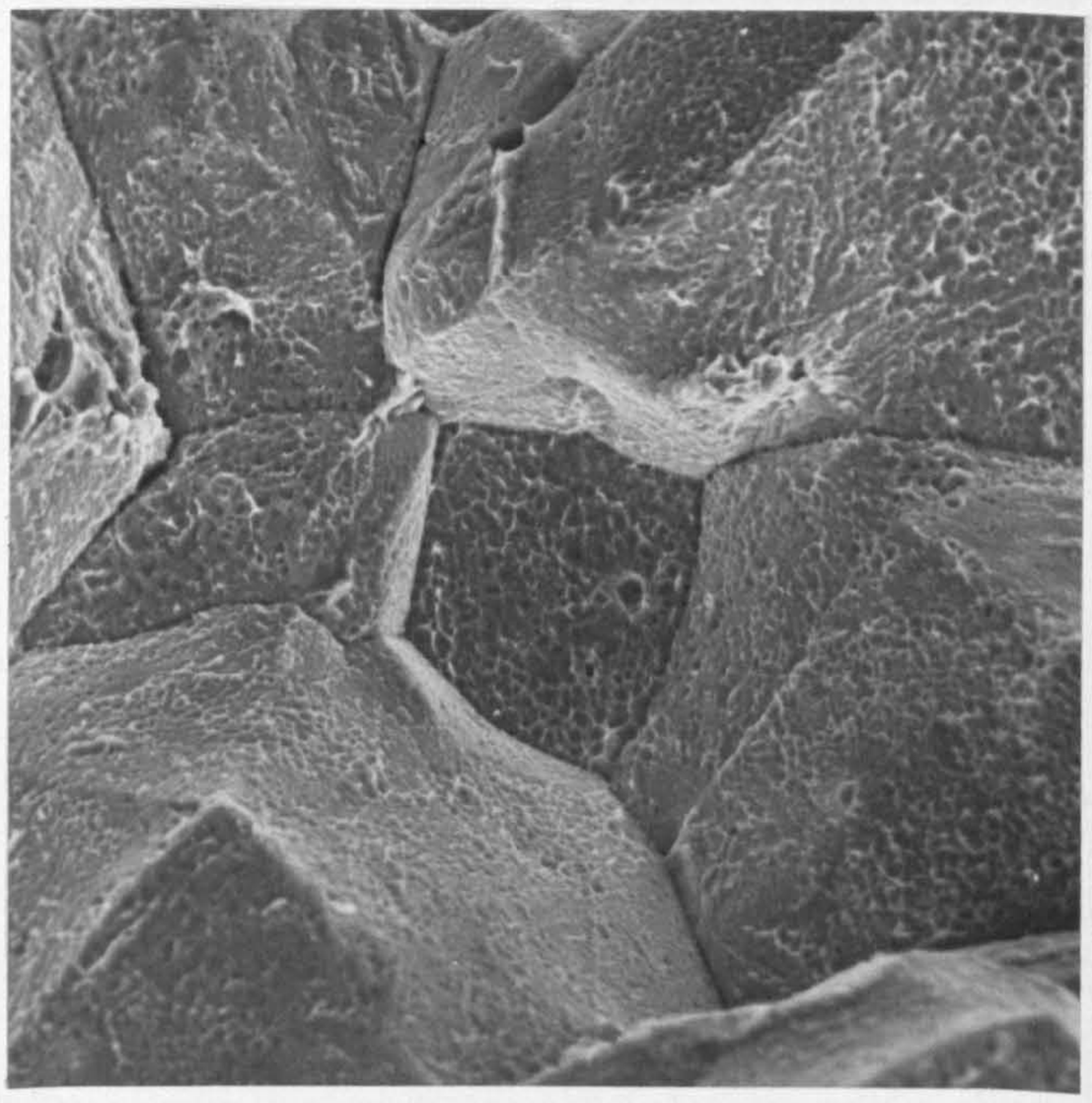

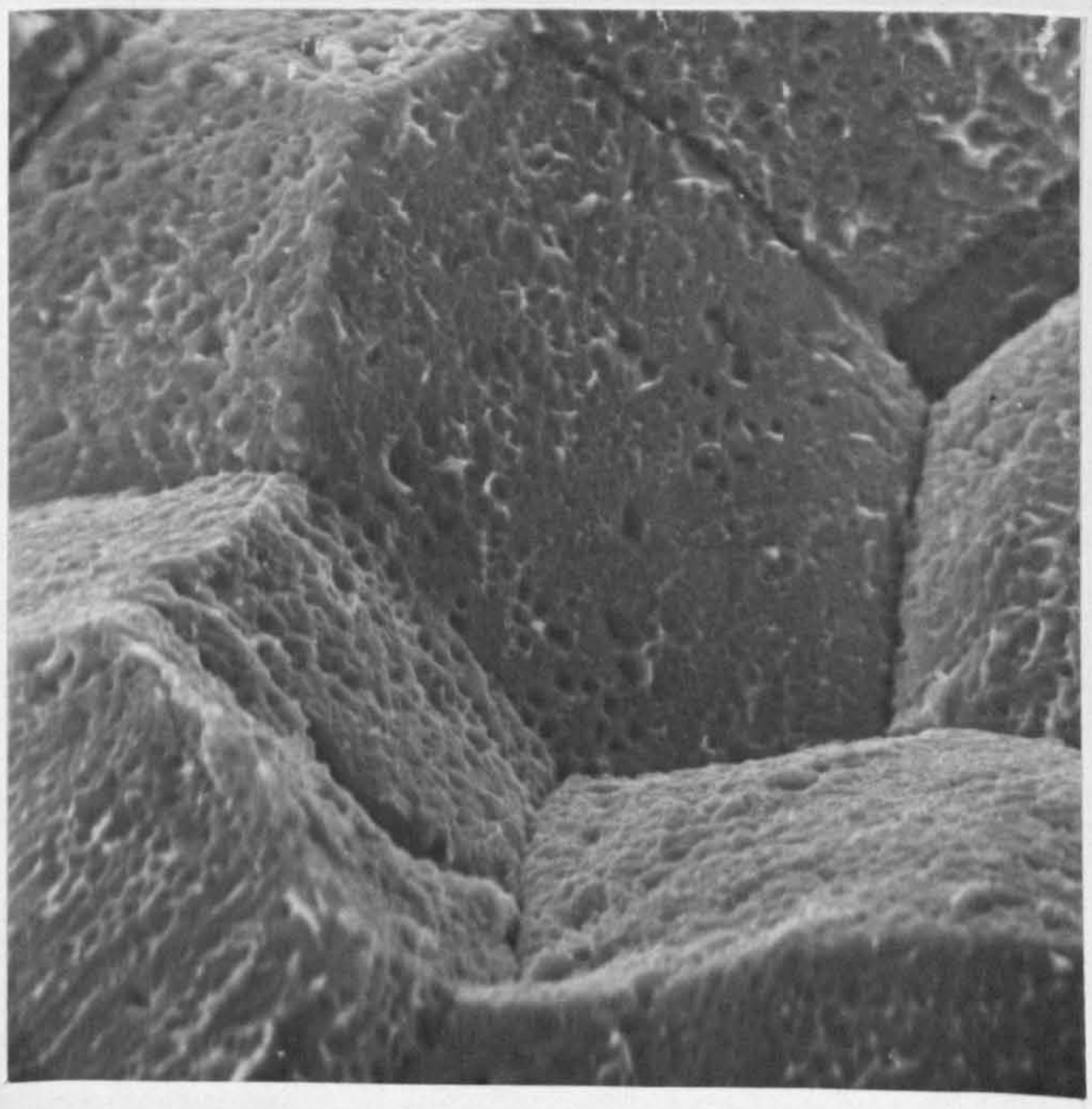

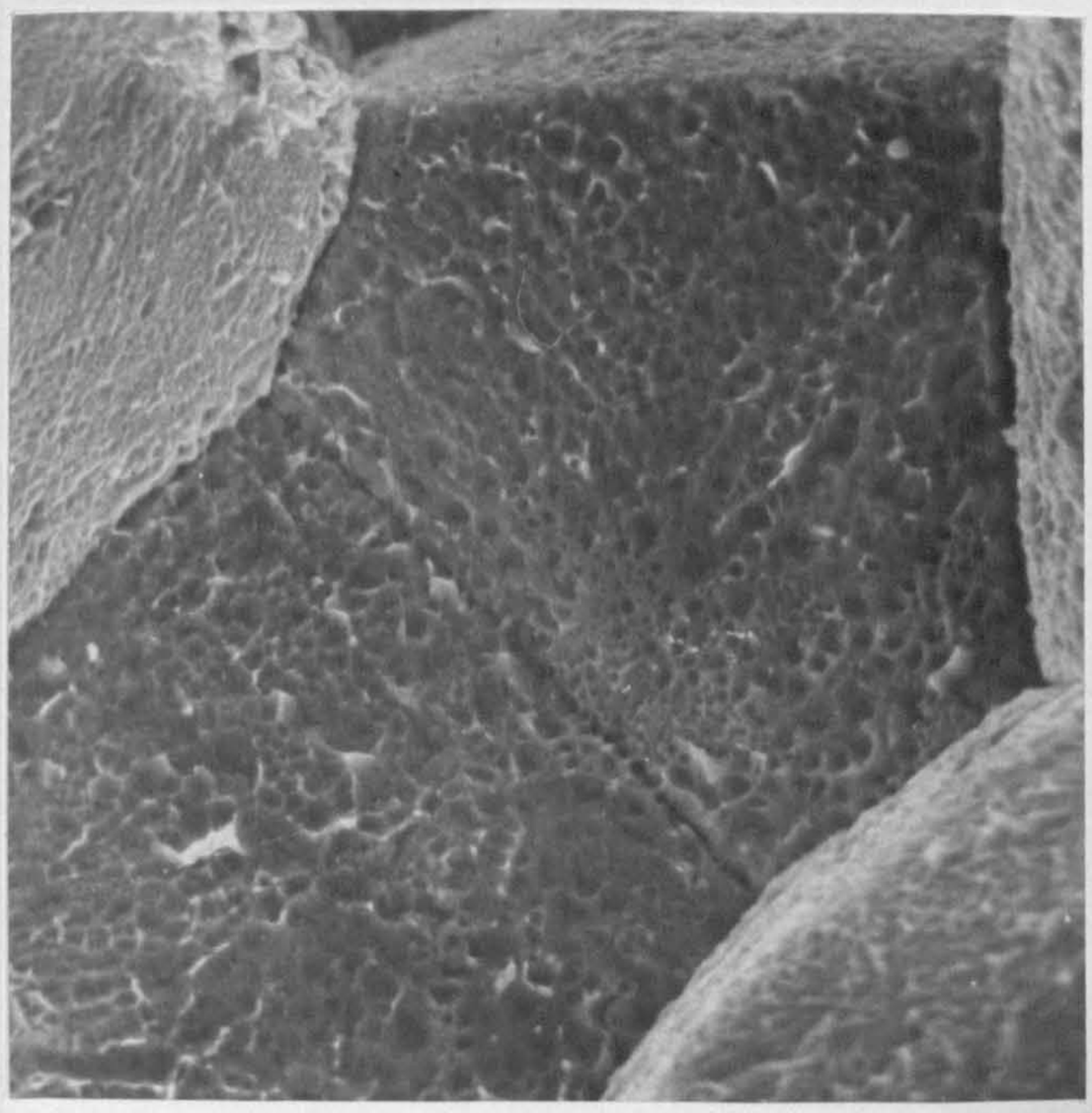

Fig. 50(a) Fracture surface of specimen CRMV1, showing the breakdown of cavity walls at a grain edge intersection. A single ligament of material remains across the boundary. Note that features of creep damage may be matched across the gap. X2270

Fig. 50(b) The interfacial decohesion at two adjacent prior austenite grains. The specimen has been tilted to reveal creep cavitation damage on one of the facets. Specimen CRMV2. X1135

Fig. 51(a) Creep fracture surface of specimen CRMV10 tested at 803K. A mixed inter- and transgranular failure has occurred (c.f. Fig.36a). X20

Fig. 51(b) Same specimen showing intergranular region. X310

Fig. 51(c) Creep cavitational damage on a grain facet in the area shown above. Note the linearity in the arrangement of cavities. X5150

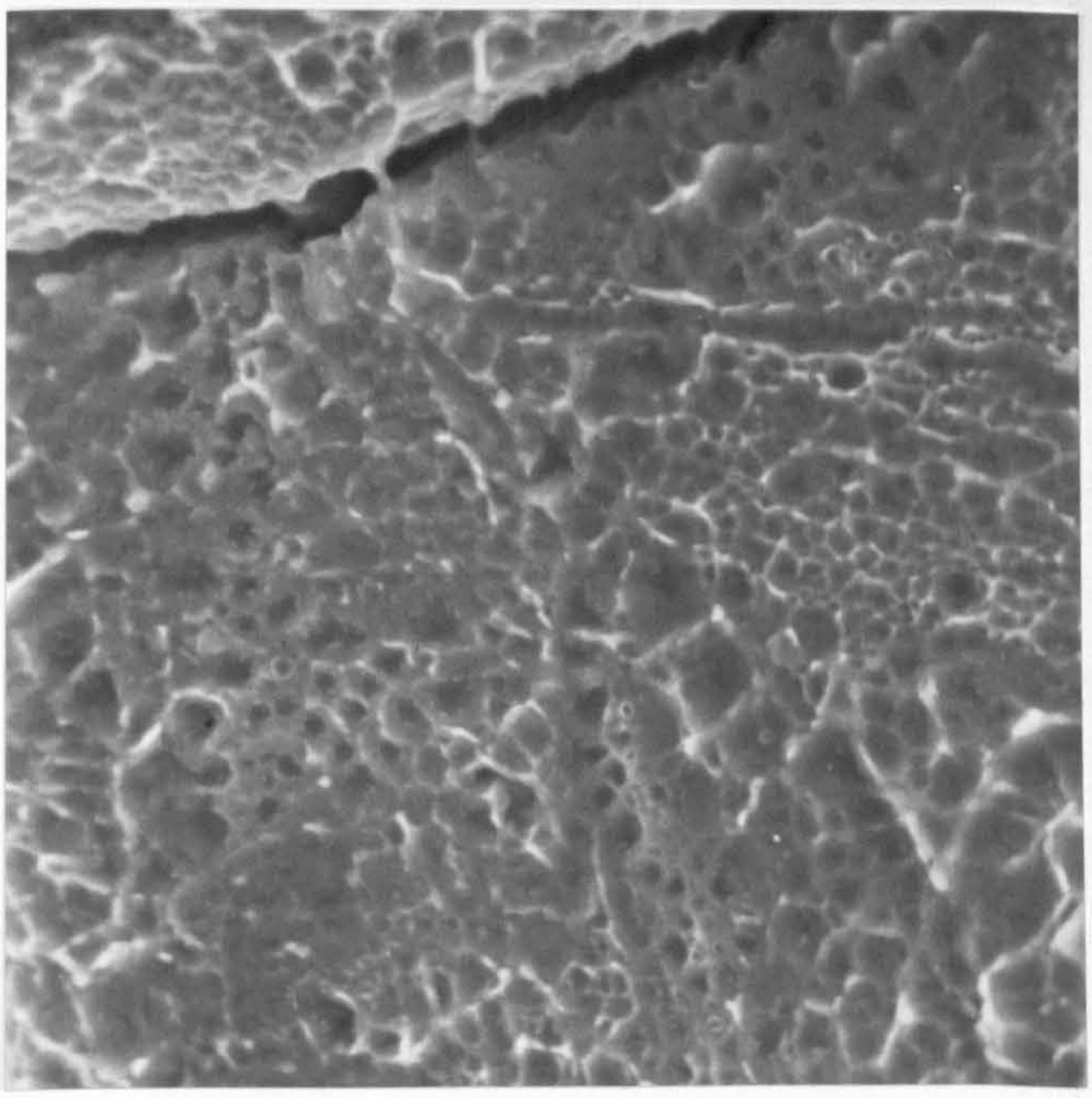

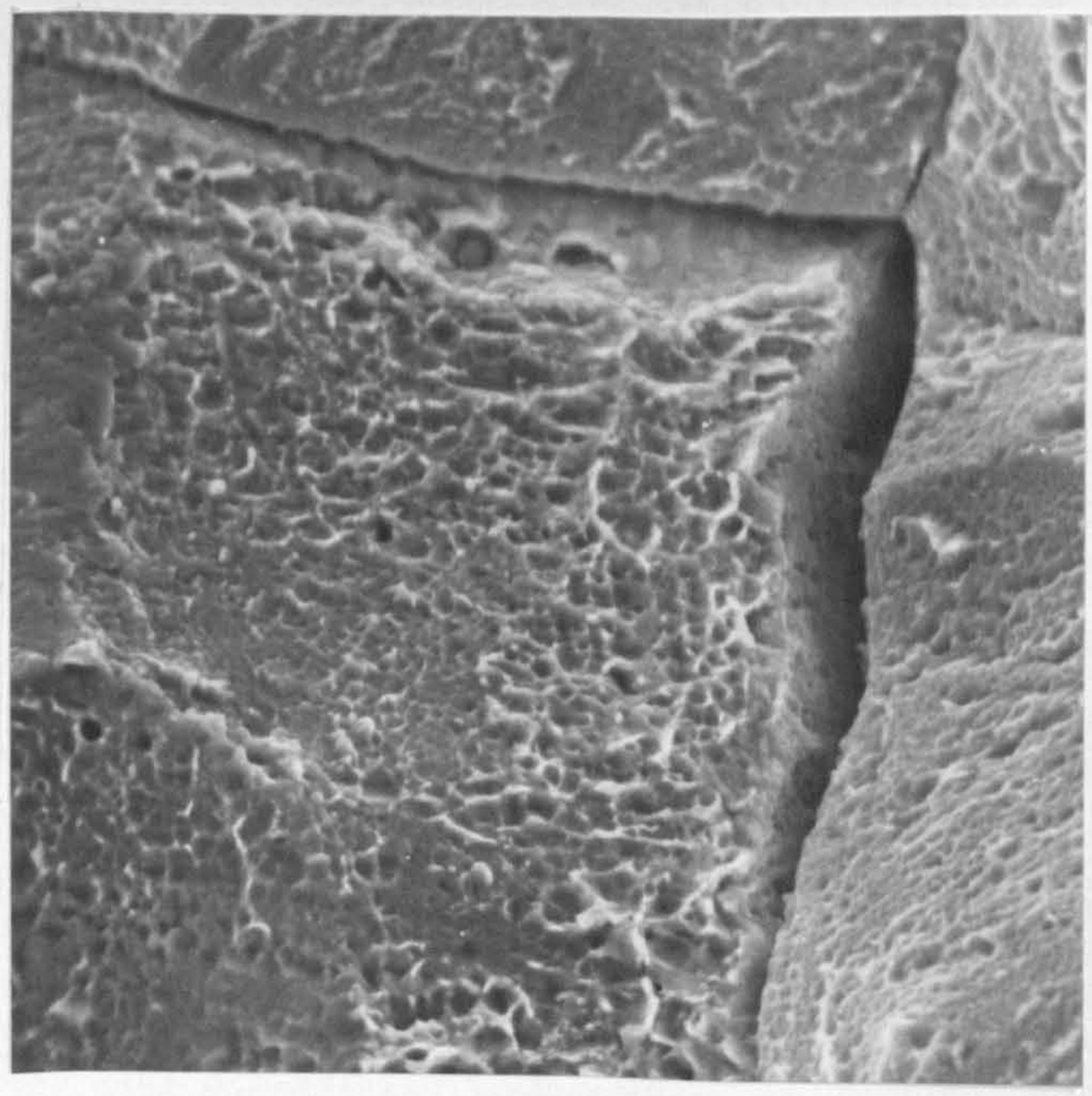

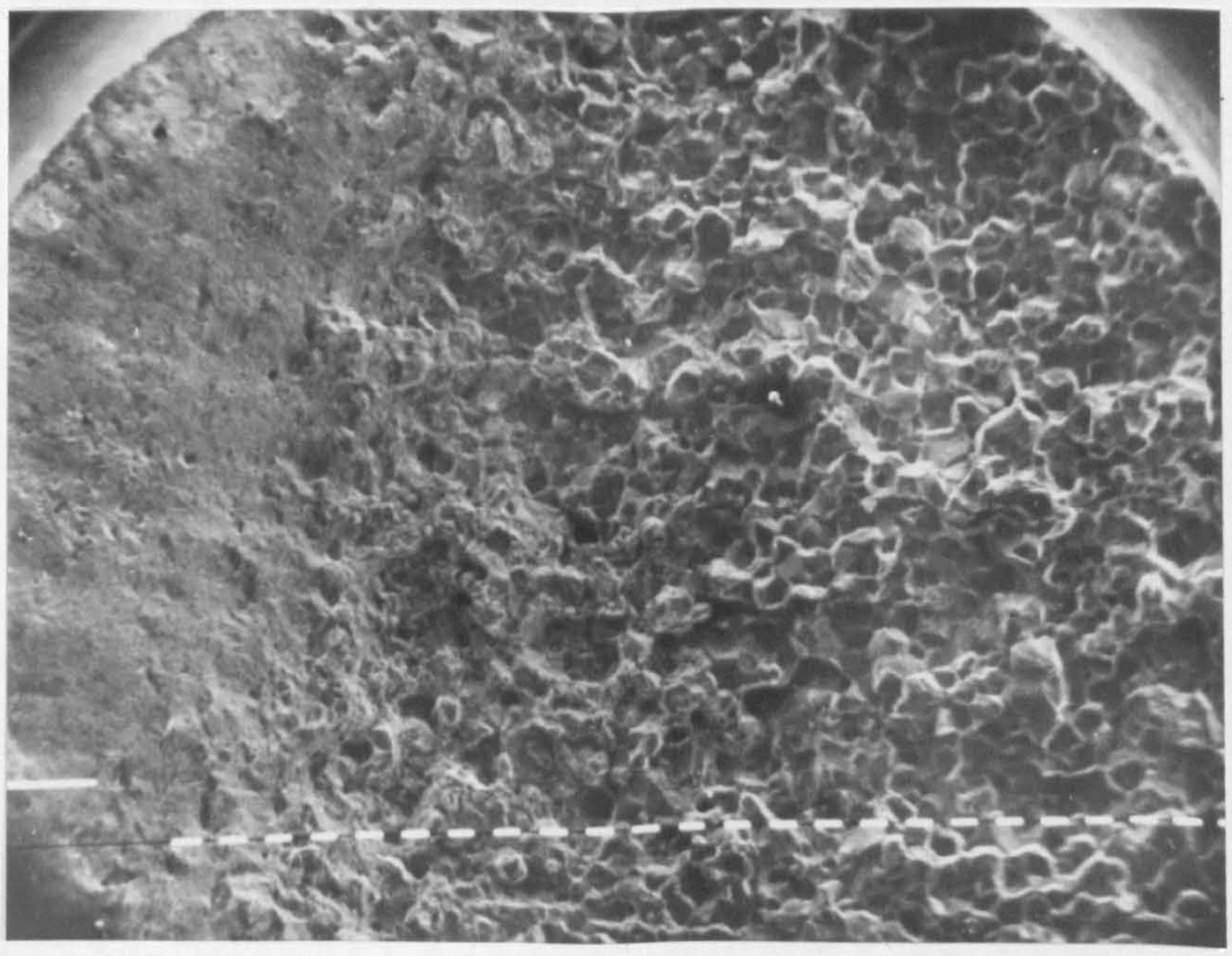

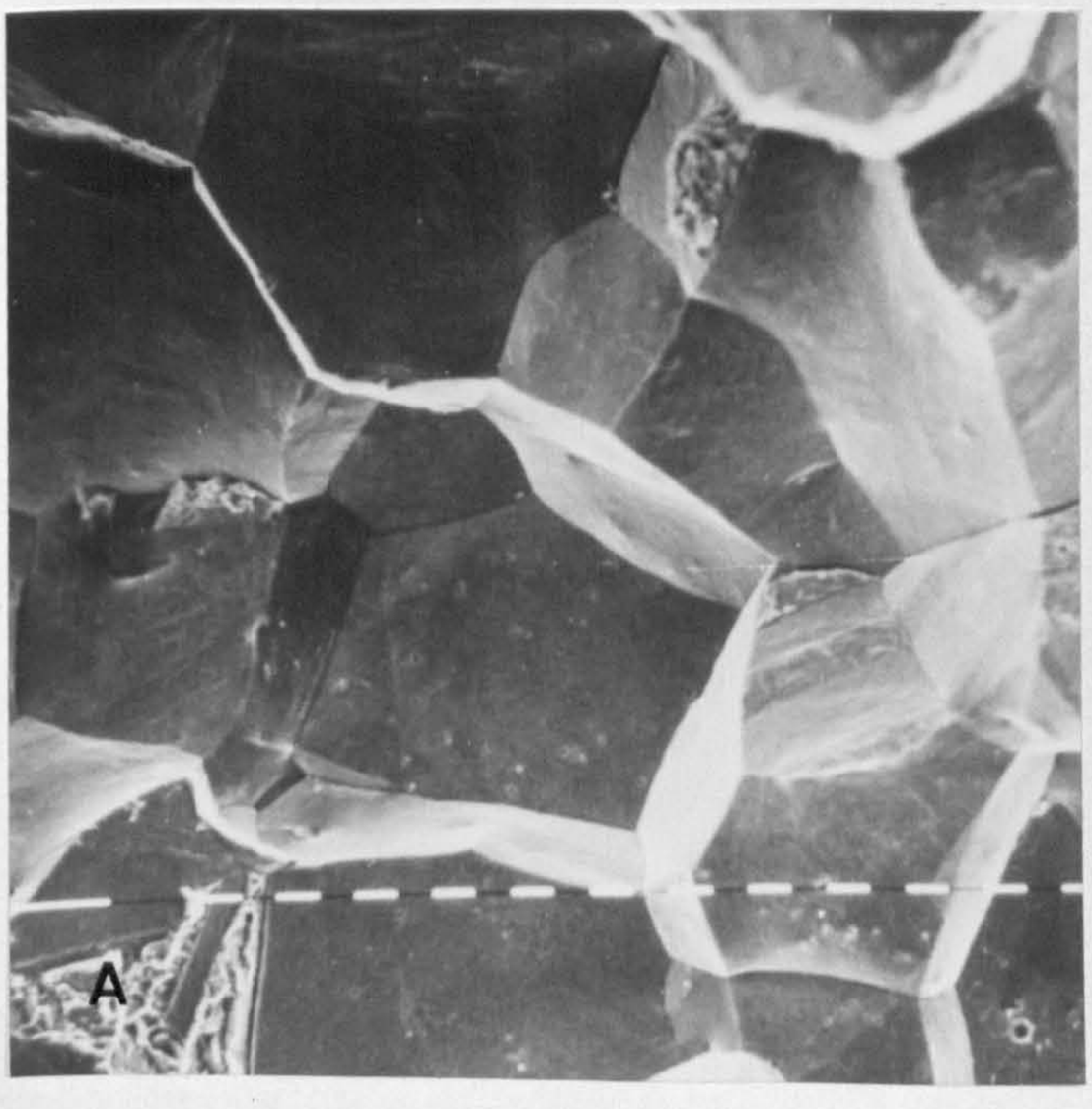
A

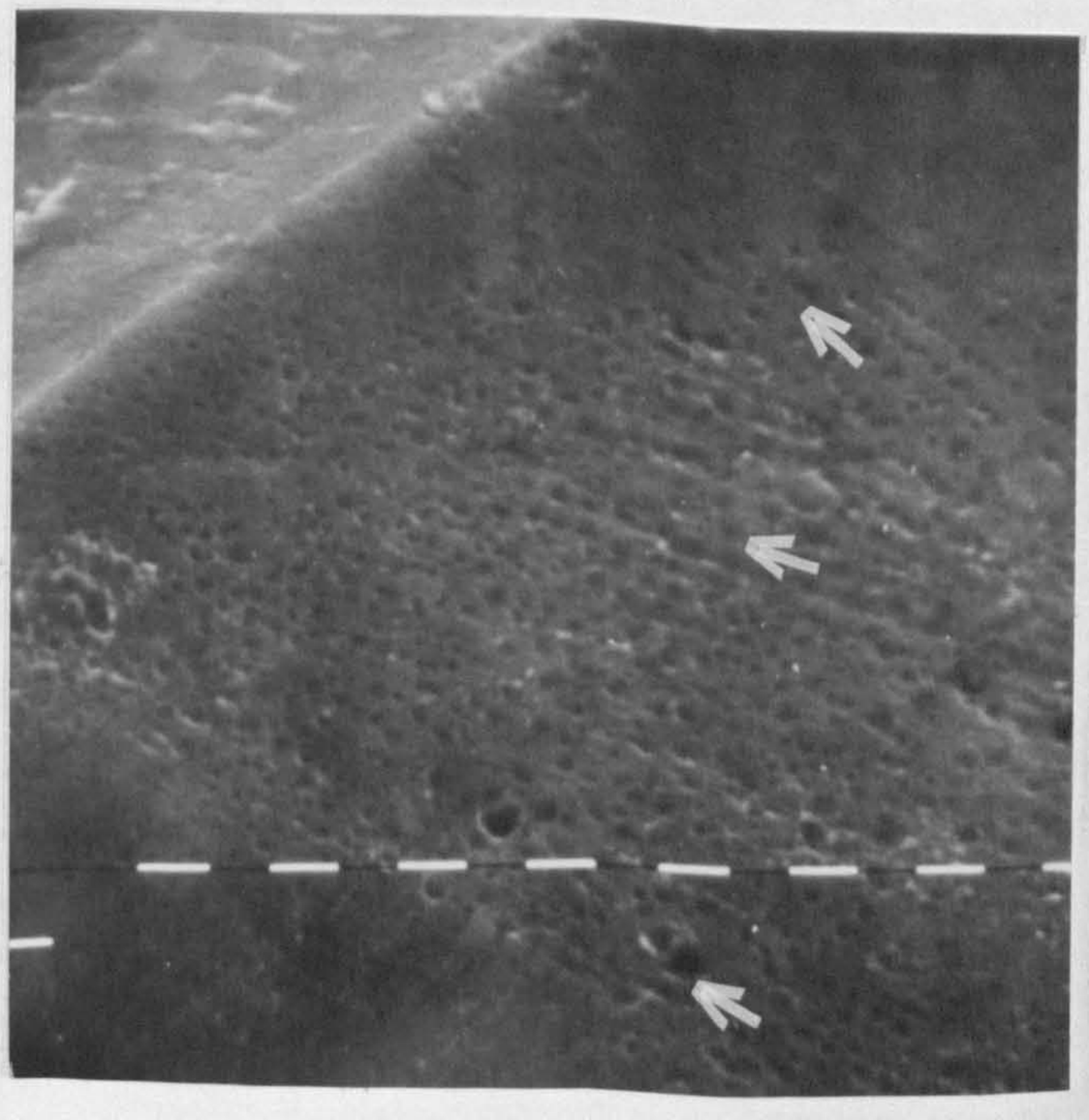

Fig. 52 Polished and etched longitudinal sections of specimen CRMV1 after creep failure. Stress axis vertical.

Fig. 52(a) The area immediately behind the fracture surface, showing grain boundary decohesion at prior austenite grain boundaries.
X250

Fig. 52(b) A prior austenite grain boundary near the fracture surface. The creep cavities are in an advanced state of coalescence.
X1500

Fig. 52(c) A less heavily cavitated boundary in an area remote from the fracture surface. The morphology of individual cavities is difficult to resolve.
X1500

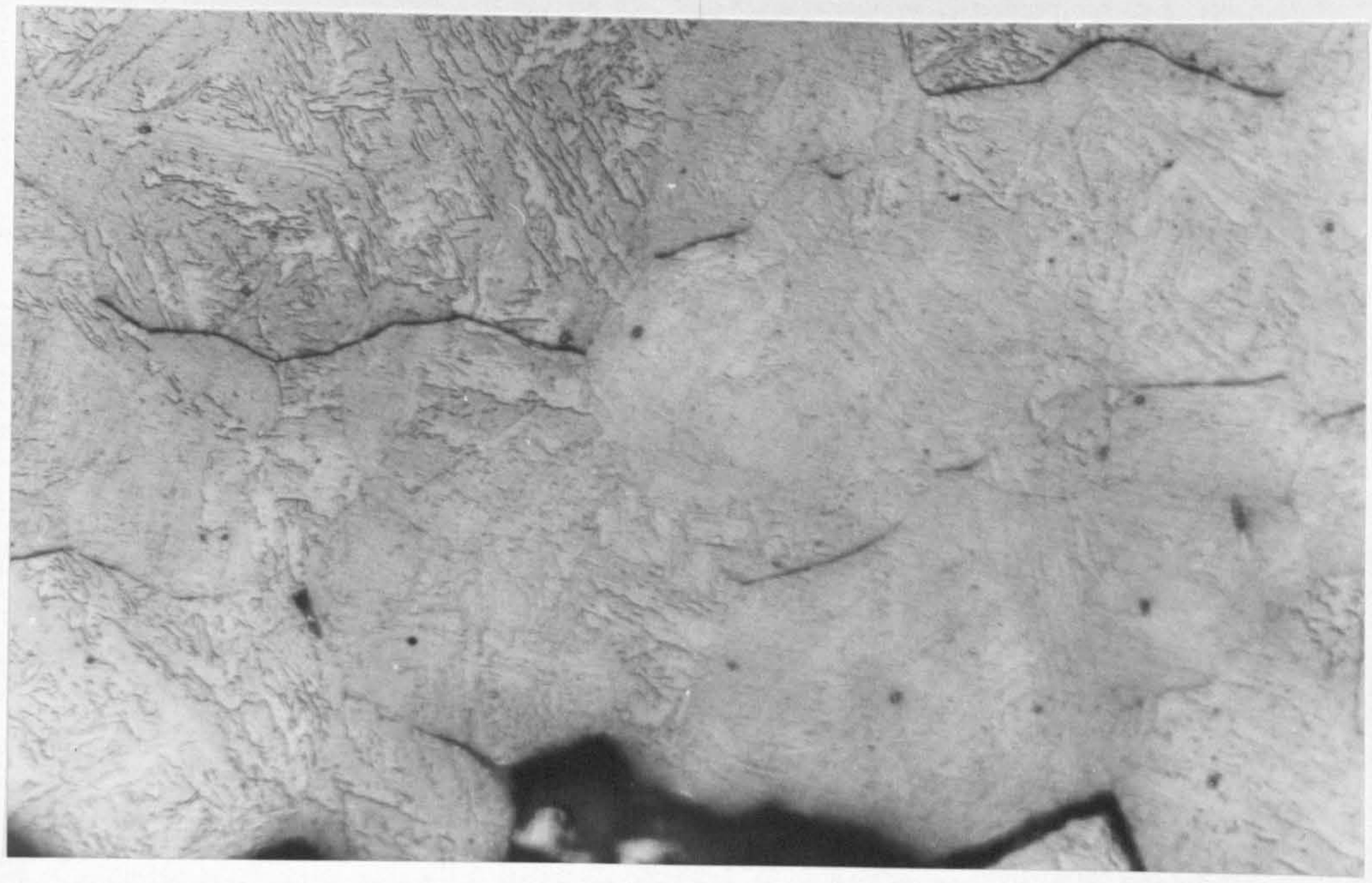

Figs. 53&54 Typical examples of longitudinal sections after ion beam etching. Stress axis vertical.

Fig. 53(a) Specimen CRMV1 after etching for 20 hrs., revealing prior austenite grain boundaries decorated with creep cavities.
X475

Fig. 53(b) High magnification view of the same area. Discrete cavities on the grain boundary can be resolved; however, their morphology remains diffuse.
X4750

Fig. 54(a) Specimen CRMV4 after etching for 10 hrs. The reduced etching time allows easier definition of grain boundary damage.
X5600

Fig. 54(b) Same specimen showing a region nearer the creep fracture surface. Complete grain boundary decohesion has occurred, of particular interest are the matching cavity "halves" across the crack.
X5600

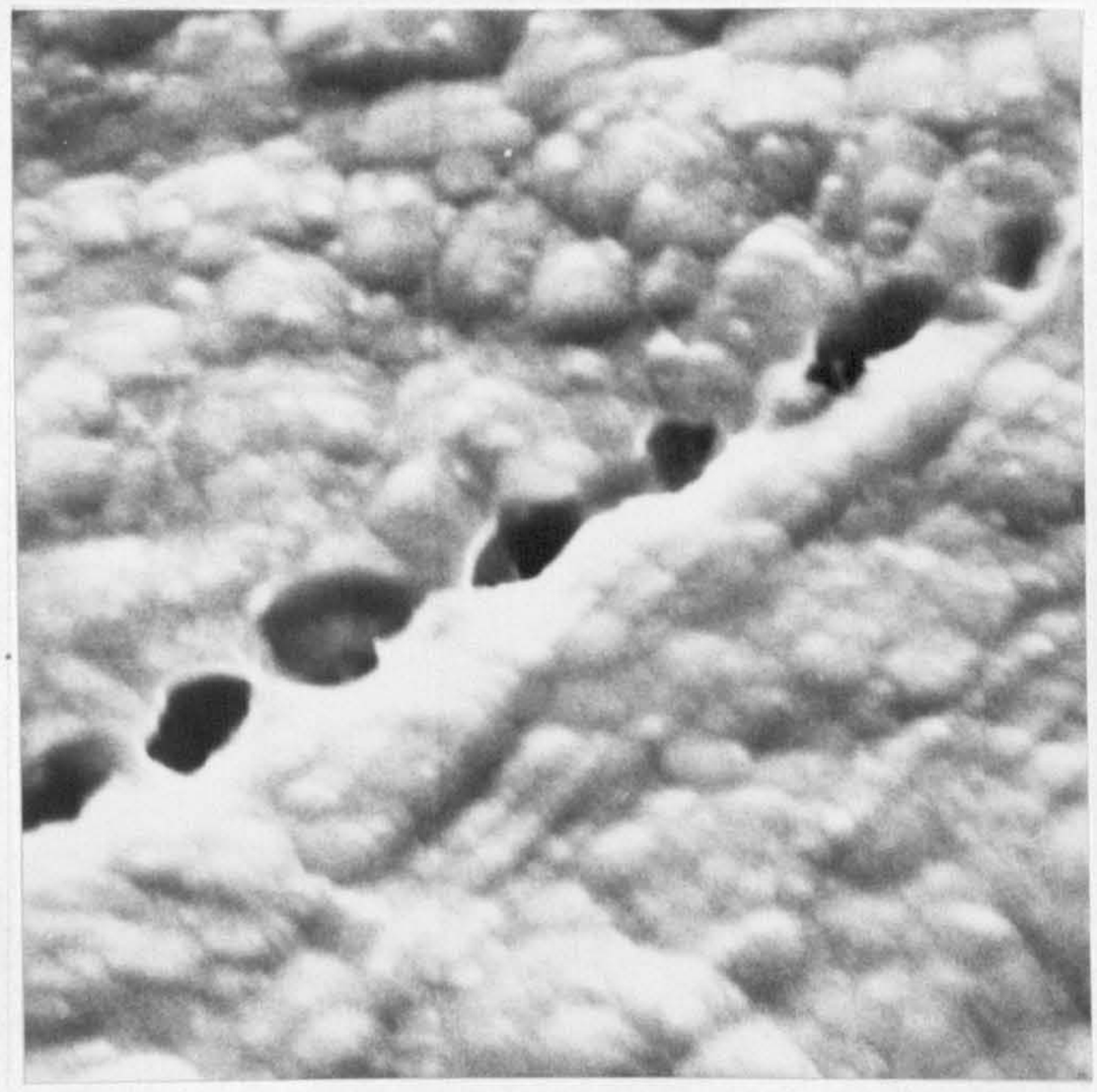

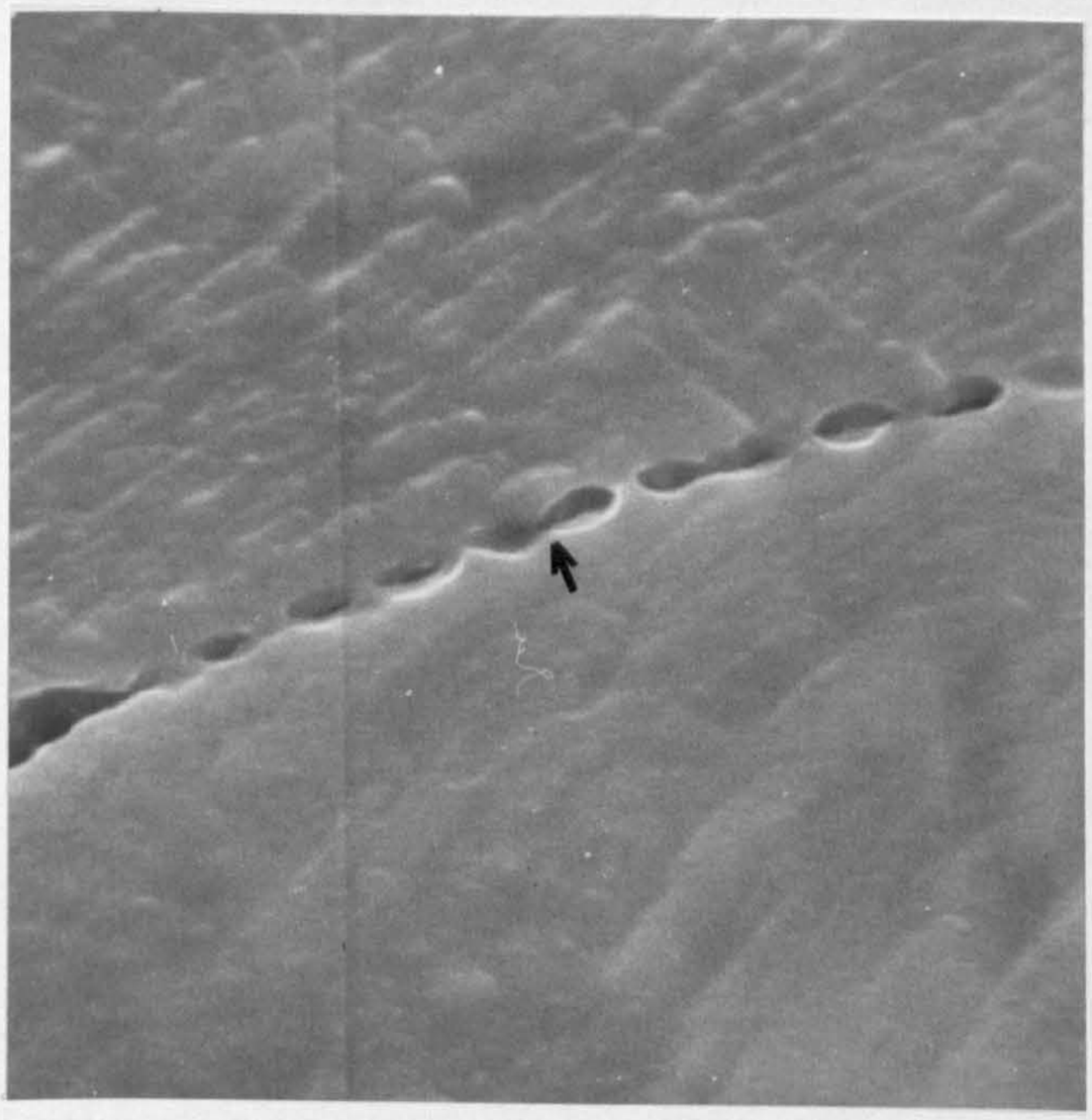

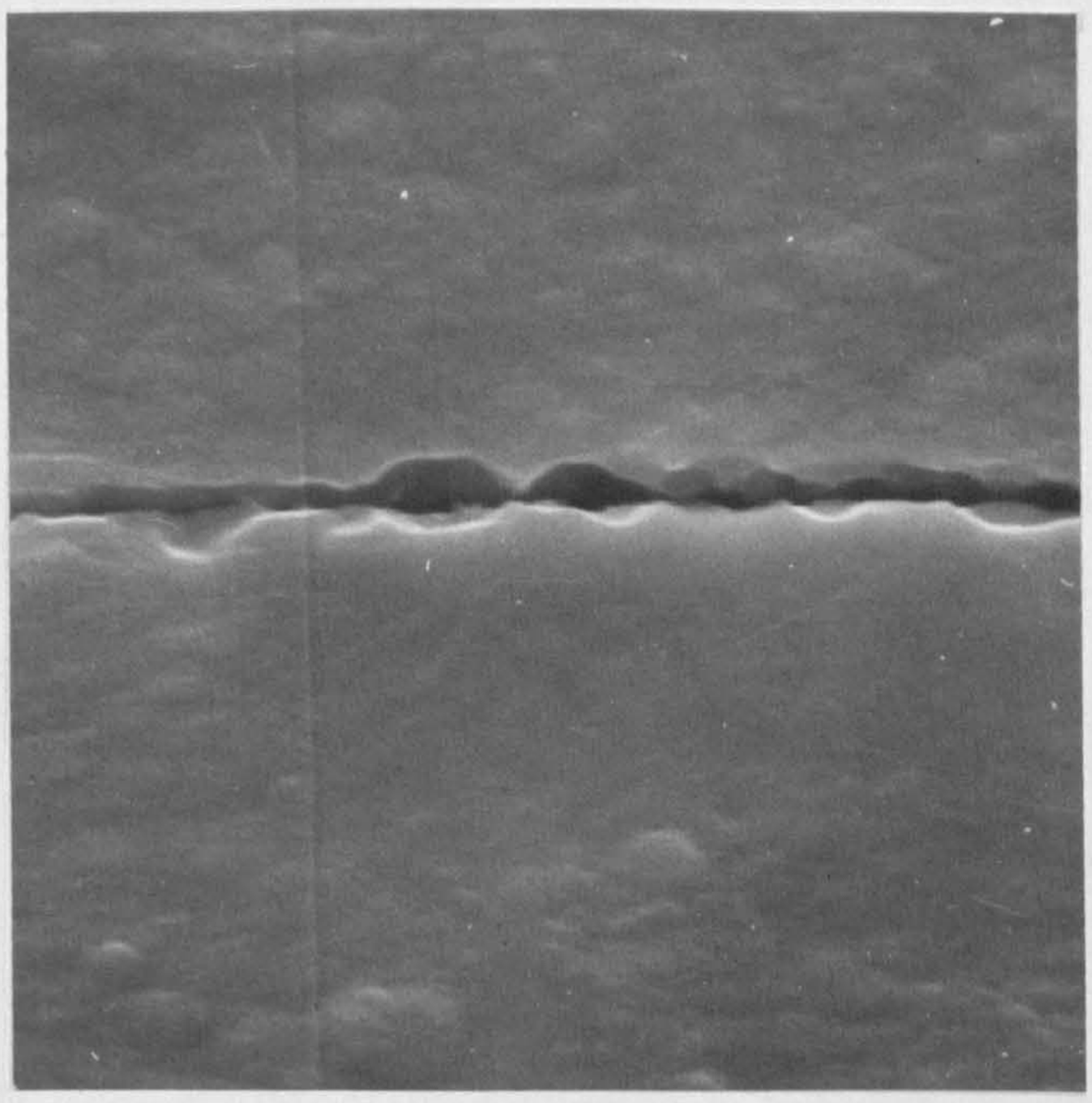

Figs. 55-57 Low temperature fractographic studies of CRMV series alloy after creep deformation.

Fig. 55(a) Specimen CRMV17, crept at 45 MNm^{-2}, 963K and interrupted after 9×10^4 s. The low density of creep damage has resulted in a high proportion of transgranular cleavage fracture.
X2500

Fig. 55(b) Specimen CRMV8 after fracture at 280 MNm^{-2}, 863K. The high density of creep damage present has resulted in more extensive regions of intergranular exposure.
X2500

Fig. 56 The completely transgranular fracture surface exhibited by the threaded region of a pre-crept specimen.
X630

Fig. 57(a) The low temperature impact fracture surface of a specimen after creep failure followed by sintering for 24 hrs. at the test temperature. The intergranular nature of the fracture is quite clear.
X220

Fig. 57(b) The morphology of the sintered creep damage on a single grain facet.
X1100

Fig. 57(c) Another region of the same specimen, showing the variation in the degree of cavity sintering on a number of prior austenite grain boundaries.
X900

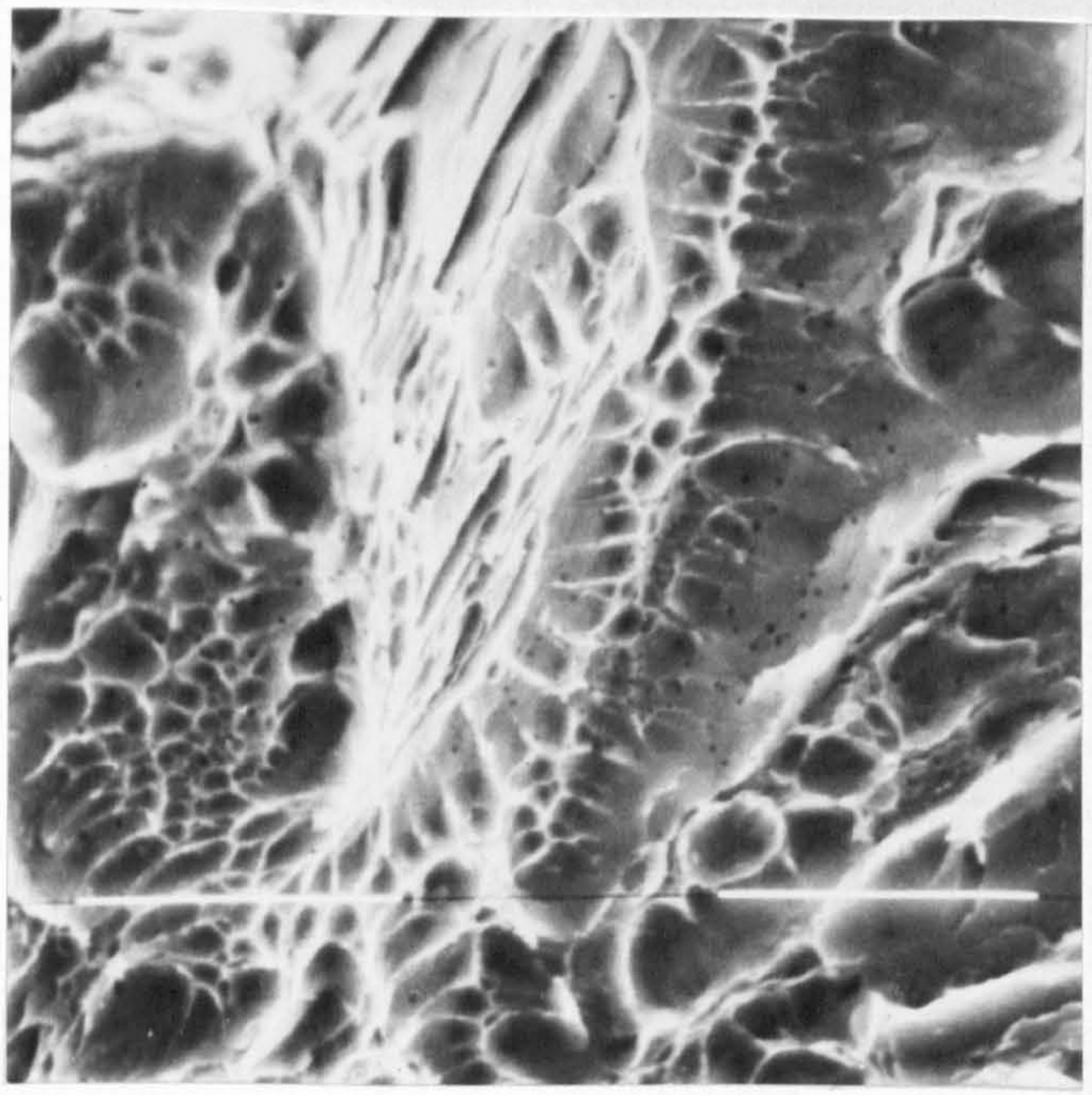

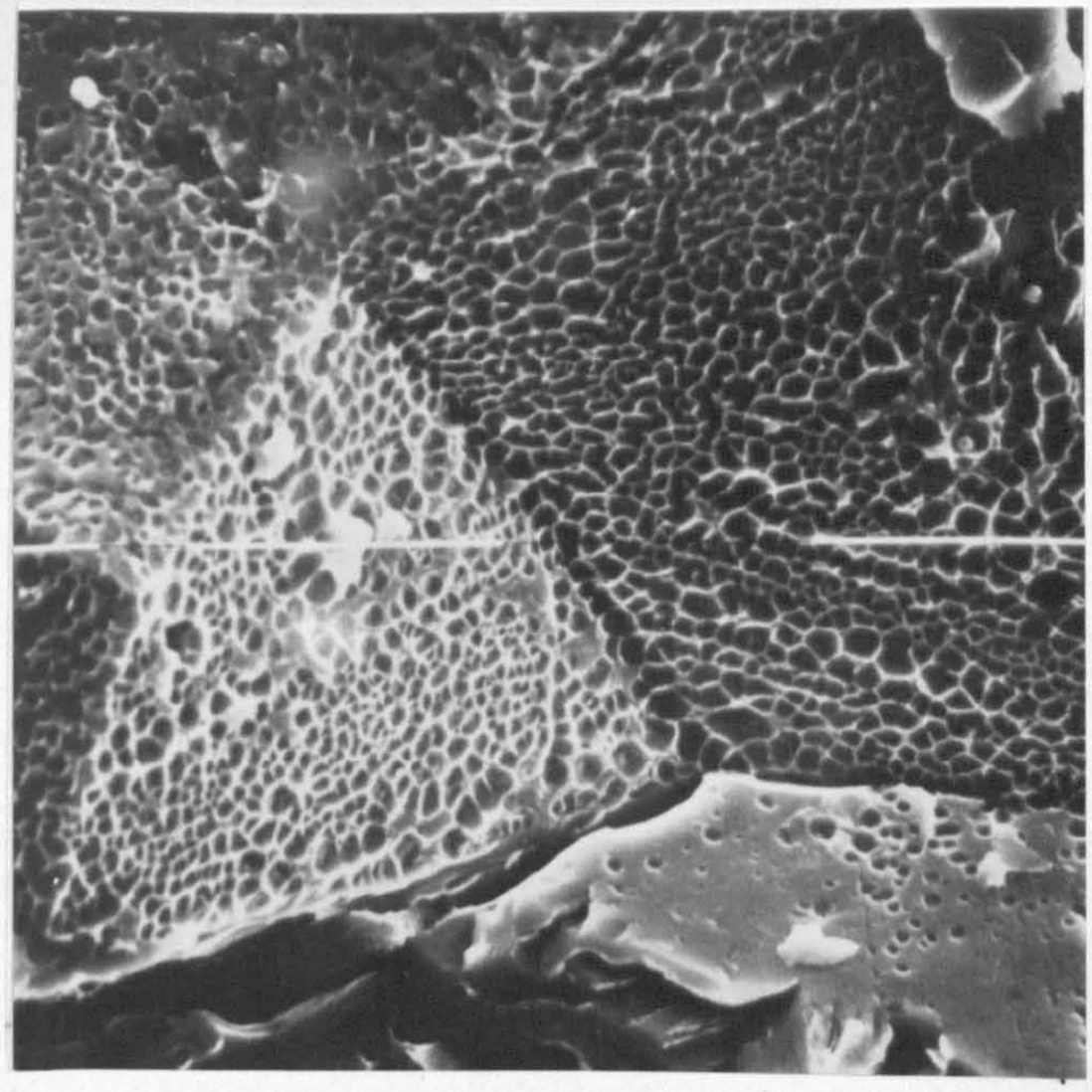

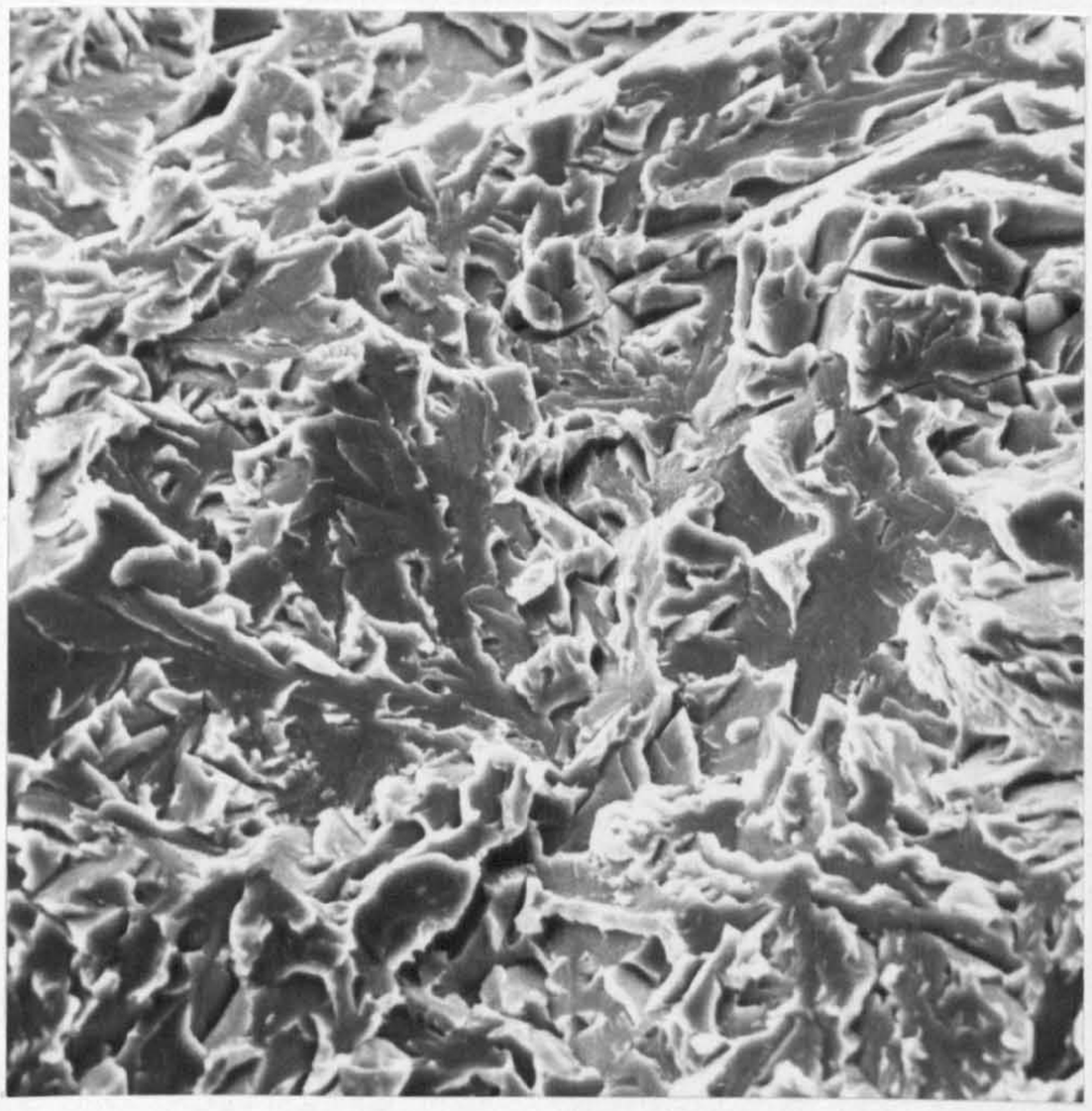

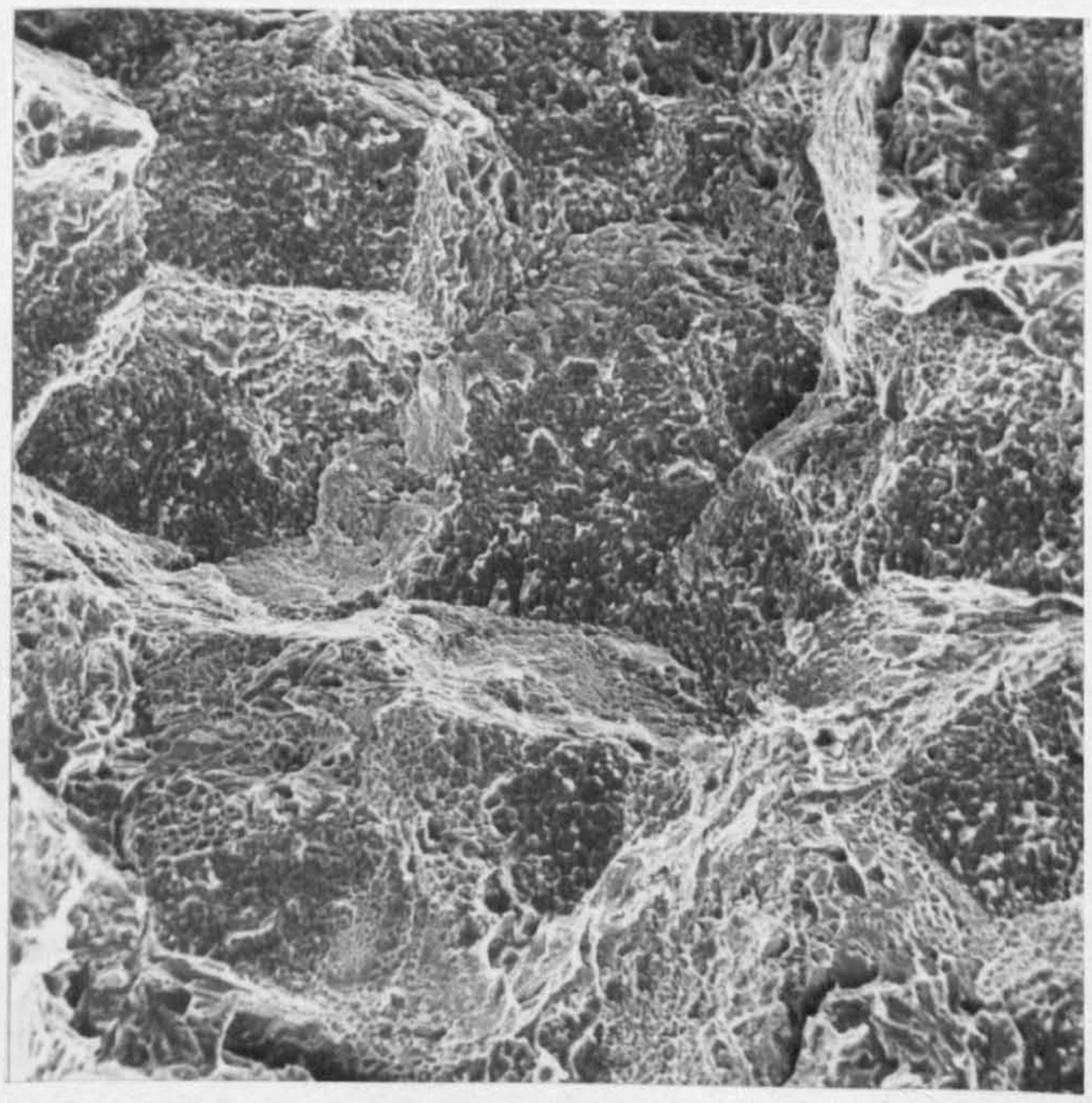

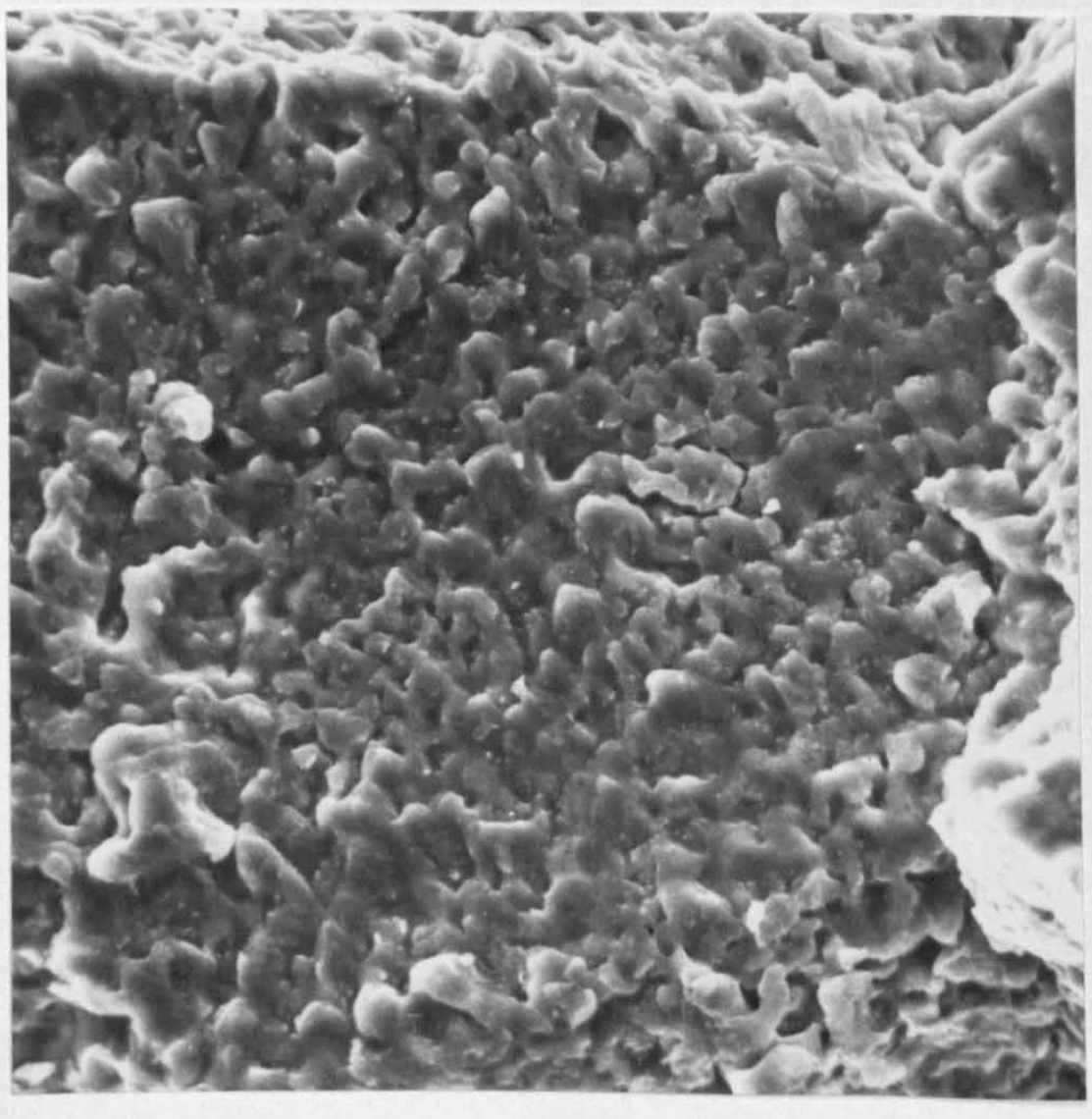

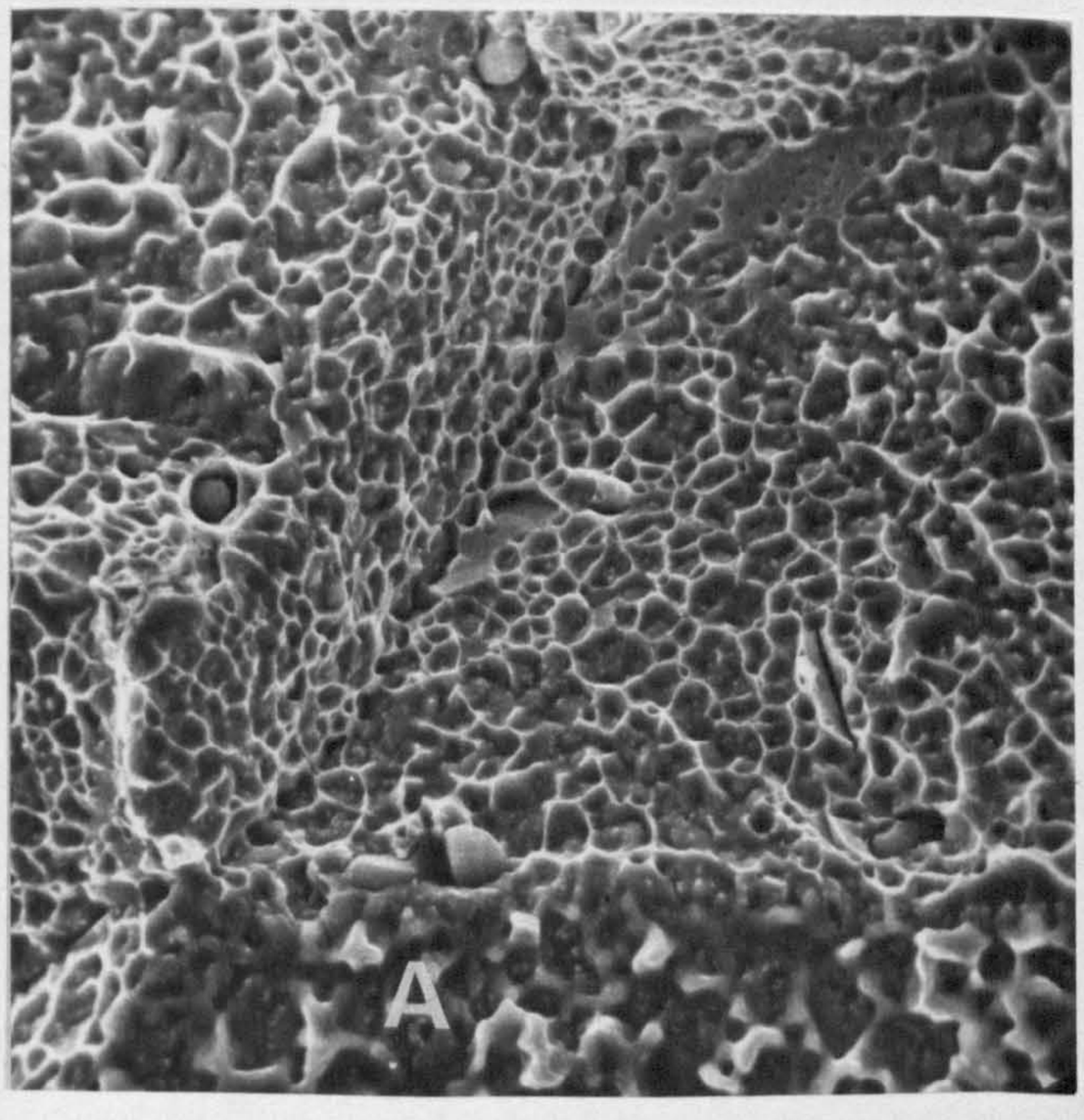
A

Fig. 58(a) Specimen CRMV27, crept at 130 MNm^{-2}, 863K and interrupted after 25.2×10^4 s. The prior austenite grain boundary exposed by low temperature impact fracture exhibits isolated colonies of creep cavities. The facet is perpendicular to the stress axis.
X860

Fig. 58(b) High magnification view of a typical cavity colony on the facet shown above. Zones of high density at the centre give way to areas of low population density on the perimeter.
X7050

Fig. 58(c) Low density zone of the colony described above. Discrete cavities exhibit a spherical morphology and there is a significant variation in size.
X13400

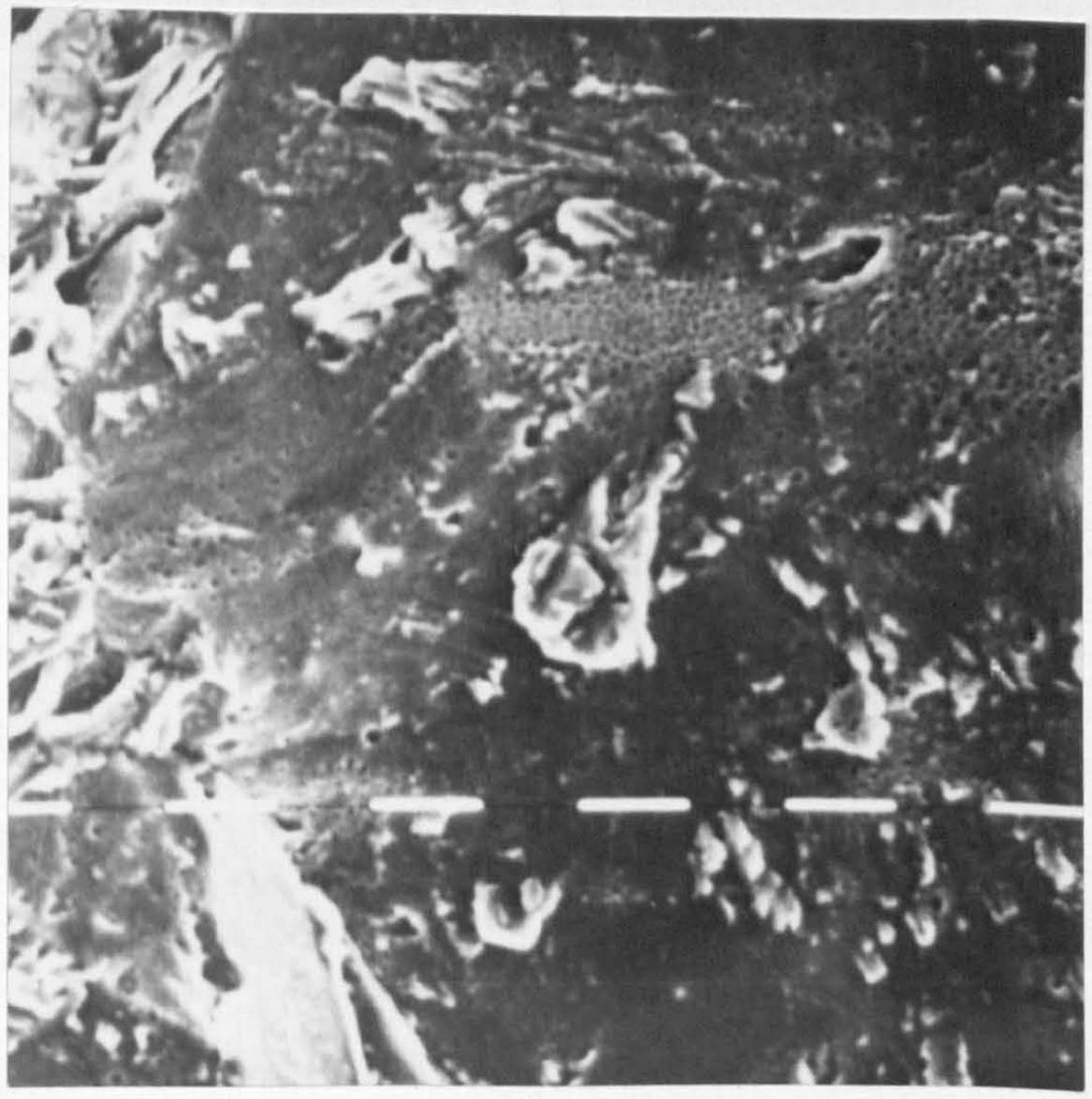

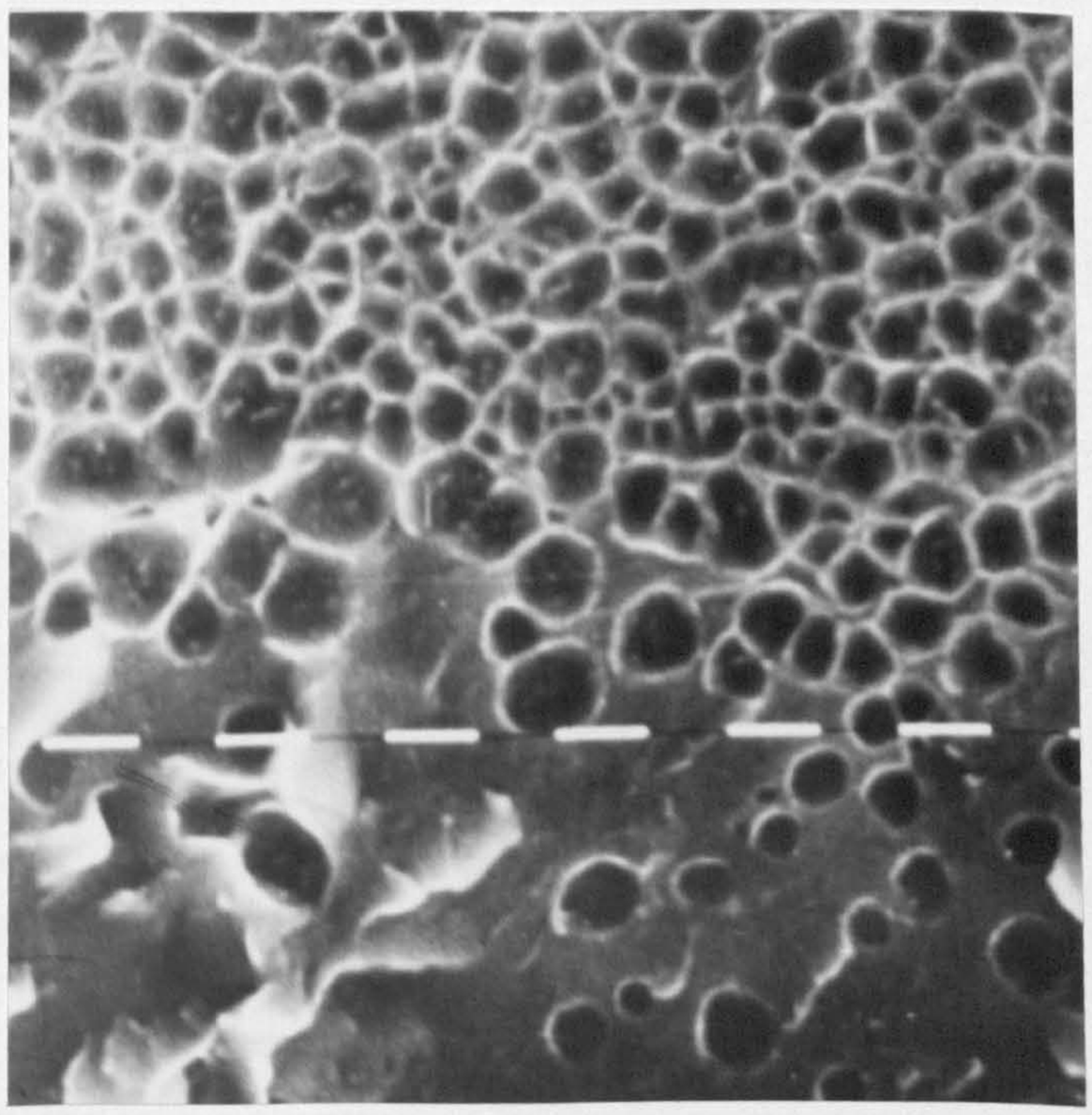

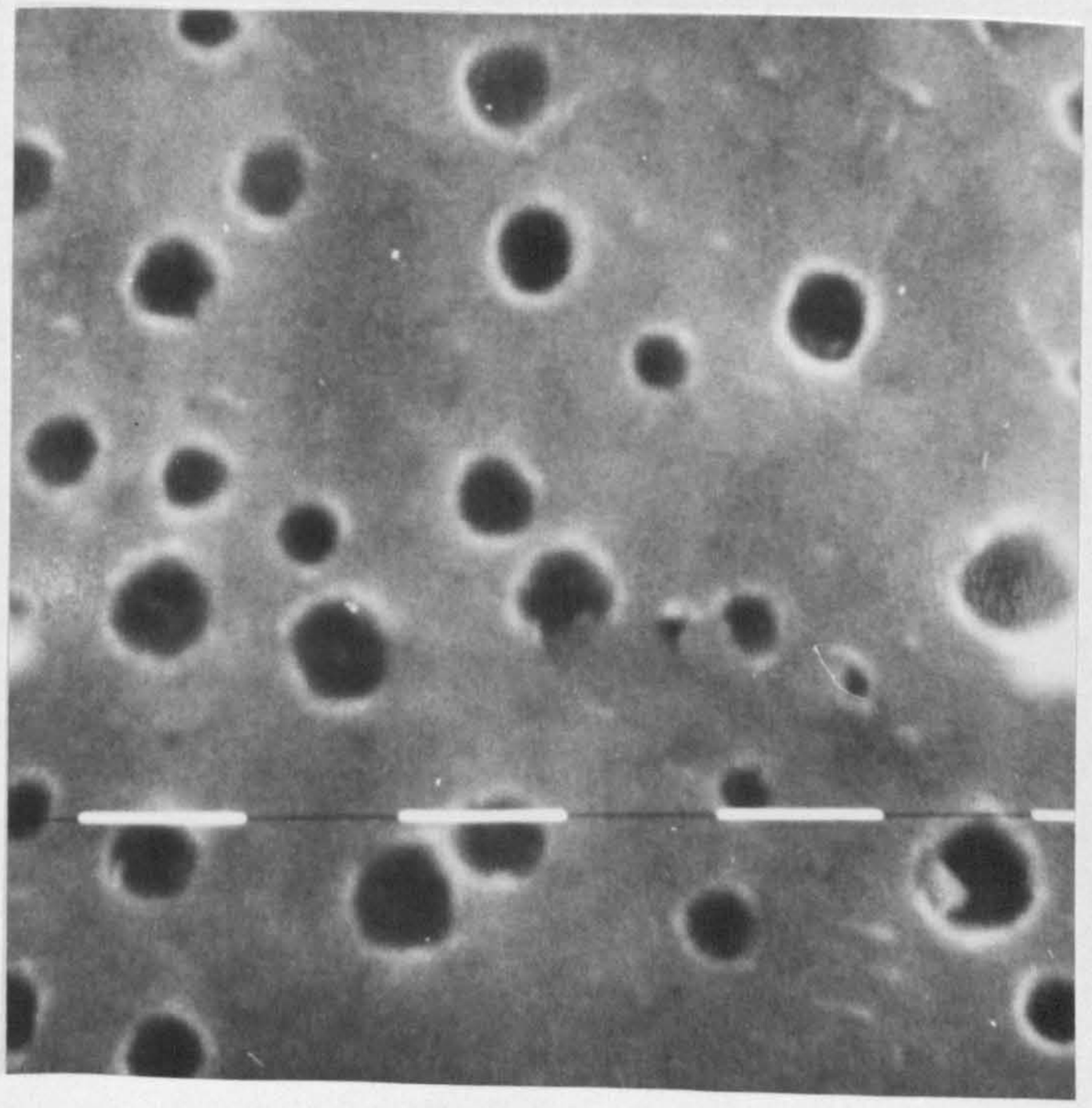

Fig. 59 Fractographic studies on the distribution of grain boundary cavities in the early stages of creep life.

Fig. 59(a) Specimen CRMV17. The grain edge, running perpendicular to the tensile axis, is heavily cavitated whilst the facets on either side are devoid of damage.
X2300

Fig. 59(b) Specimen CRMV19, showing the distribution of cavities at a triple point boundary. The stress axis runs parallel with the apex.
X2000

Fig. 59(c) An area of low population density in a zone removed from the triple-point junction shown in Fig. 59(b).
X10000

Fig. 59(d) Specimen CRMV23, showing a heavily cavitated grain facet occupying a plane normal to the stress axis; those facets at a more acute angle reveal scant evidence of creep damage. Note the band of material where cavity nucleation has been suppressed.
X625

Fig. 59(e) Another region of the same specimen illustrating the converse situation shown in Fig. 59(d). A band of material adjacent to the grain edge exhibits intense cavity nucleation.
X1225

Fig. 59(f) Specimen CRMV23, illustrating that the degree of cavity coalsence is a function of orientation with the stress axis.
X2320

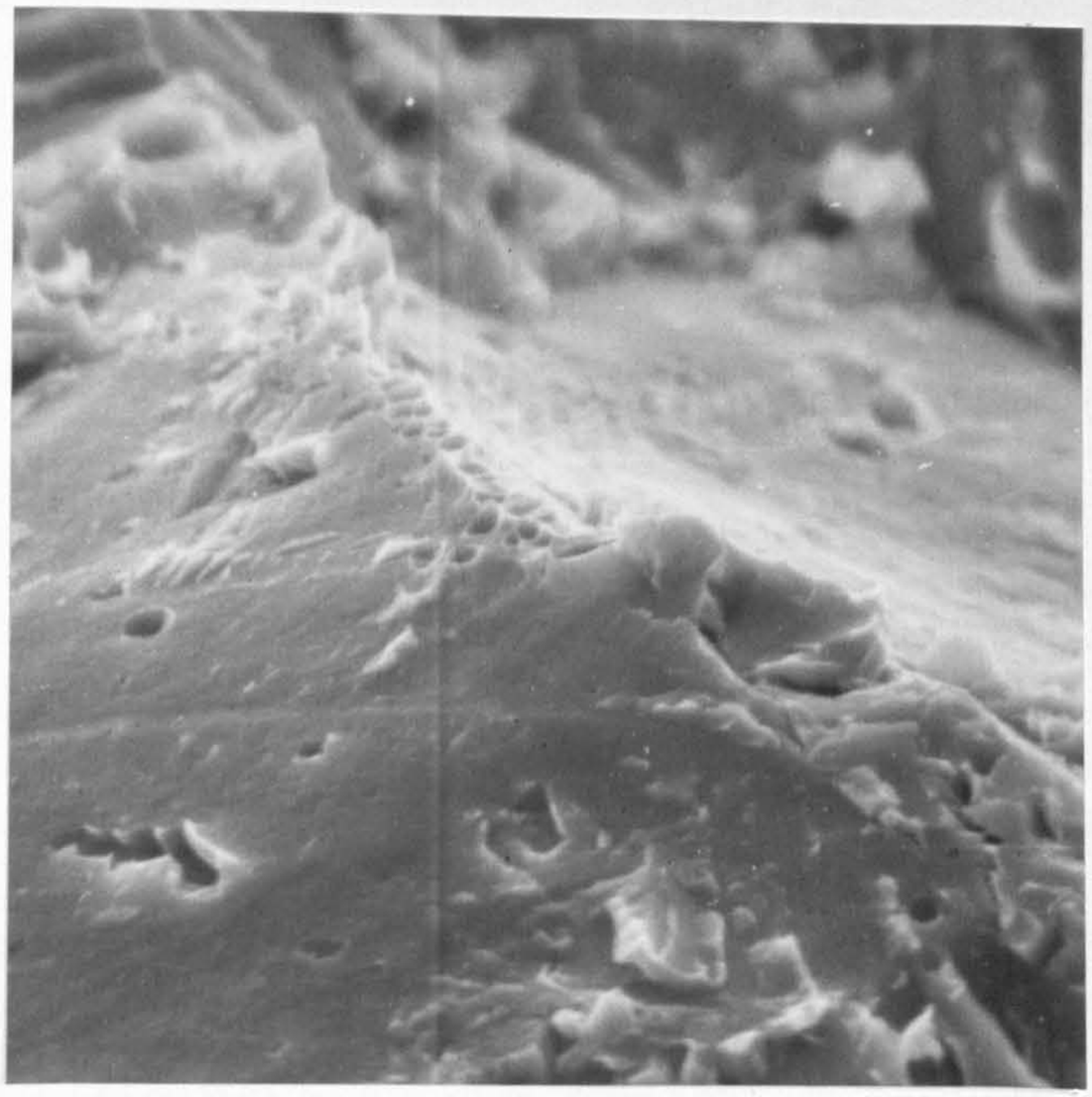

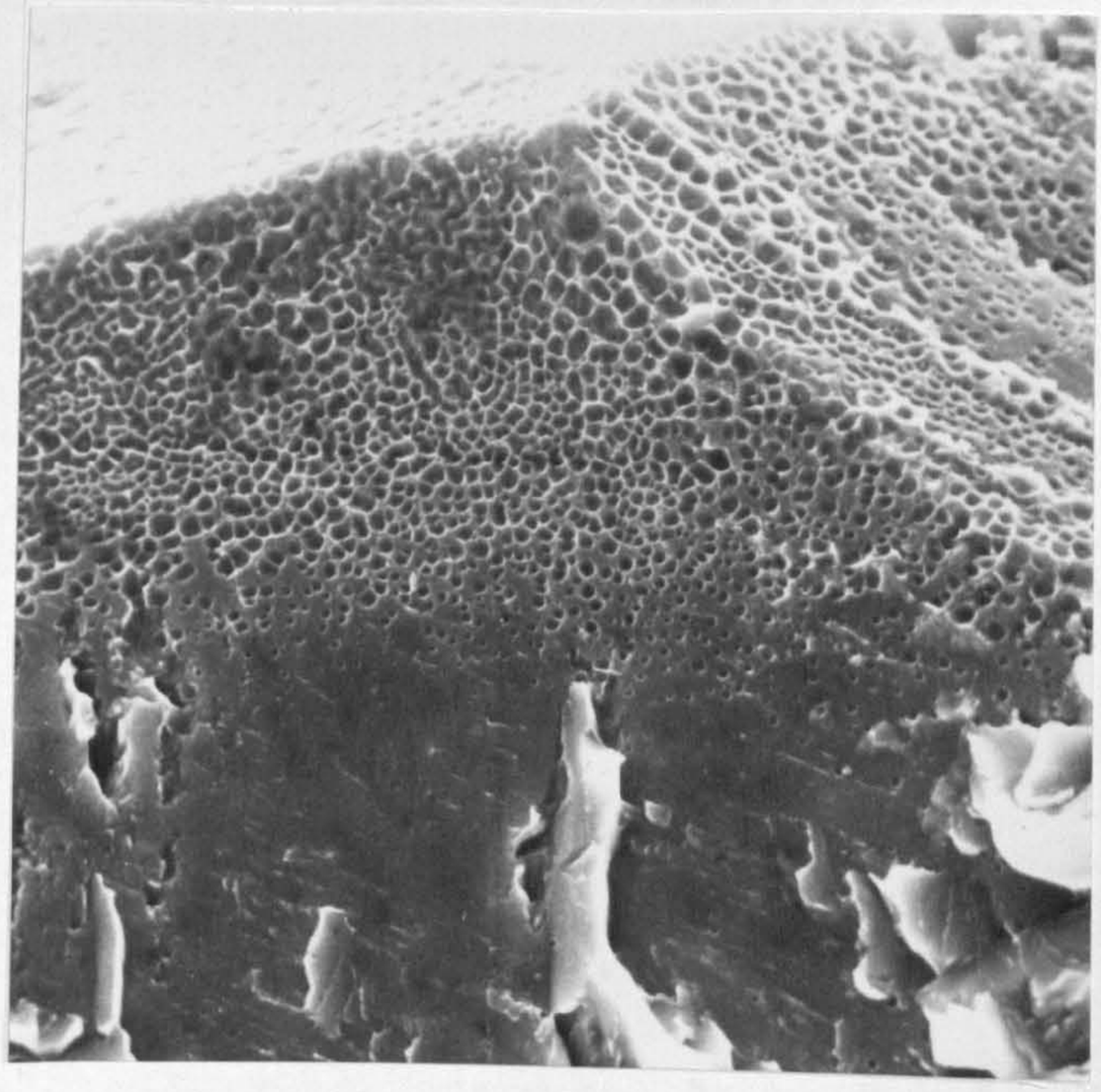

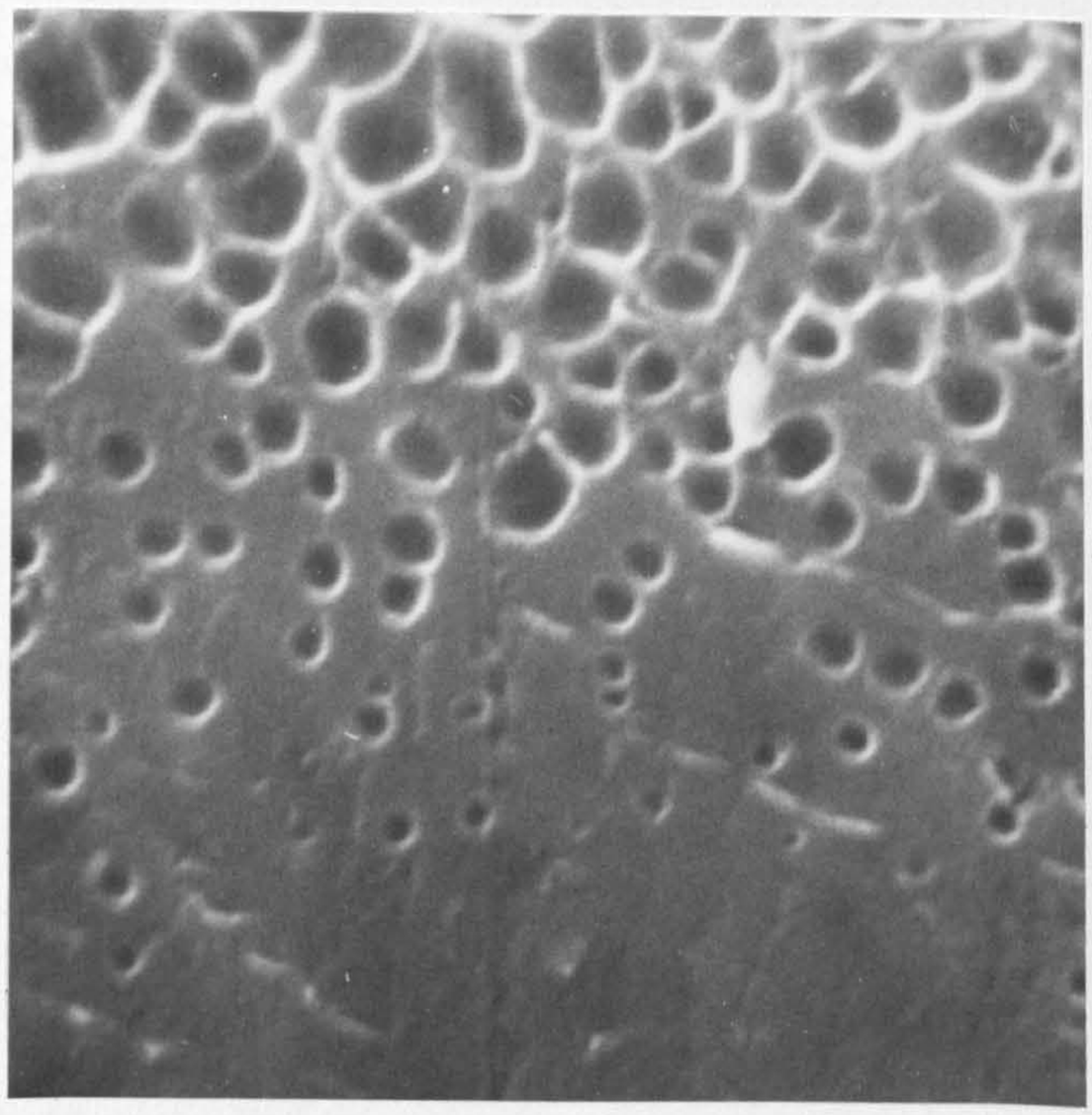

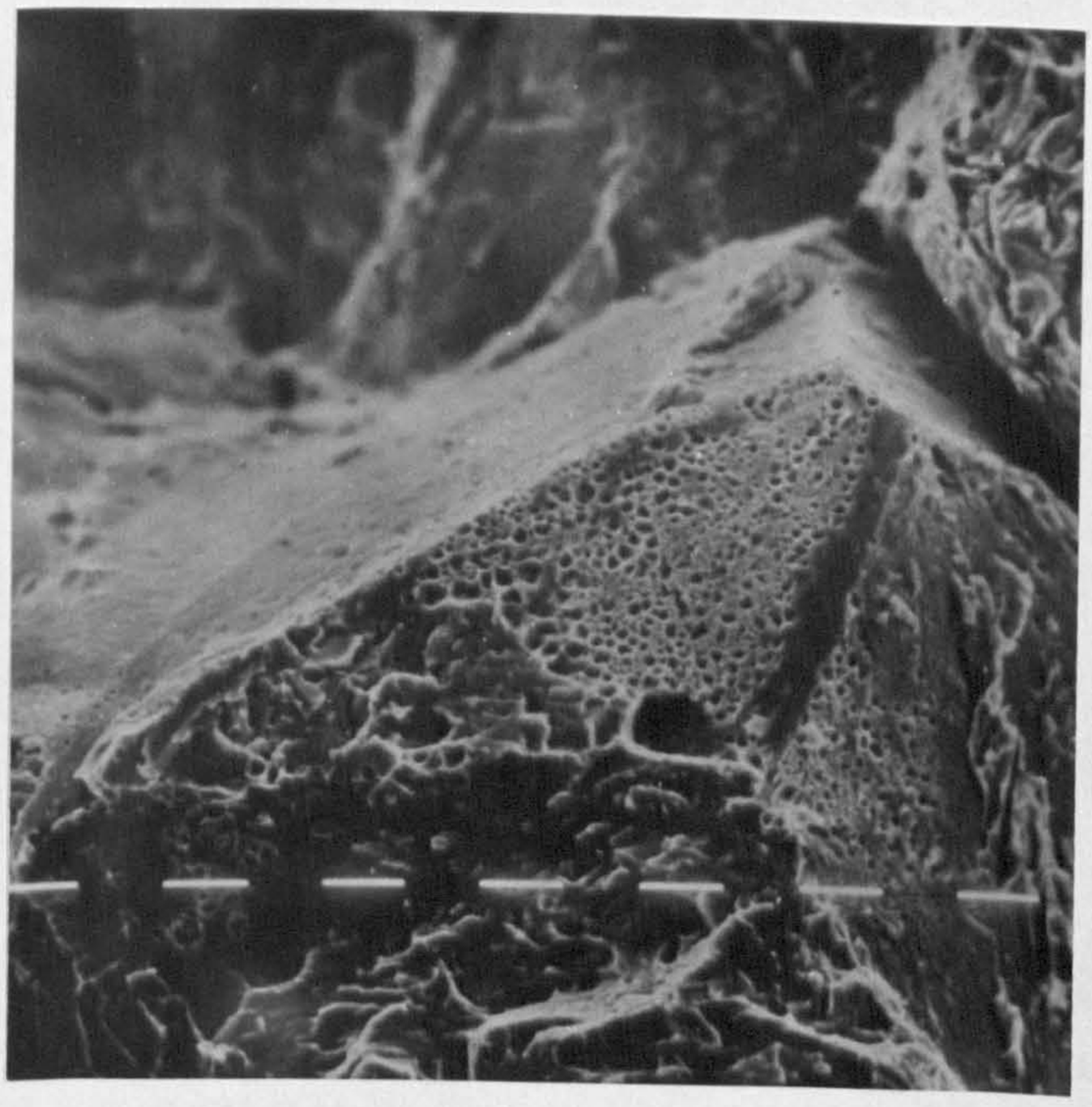

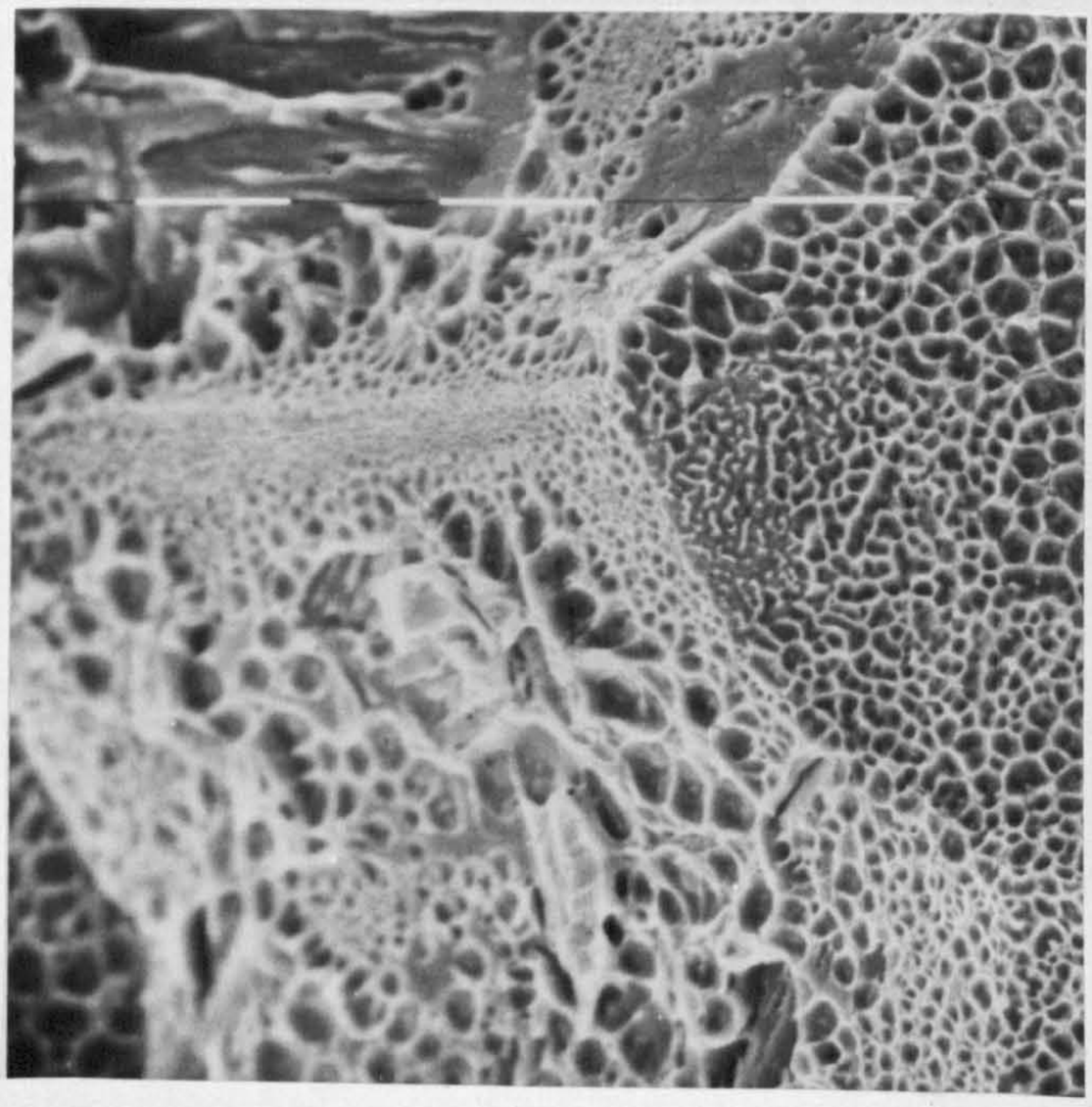

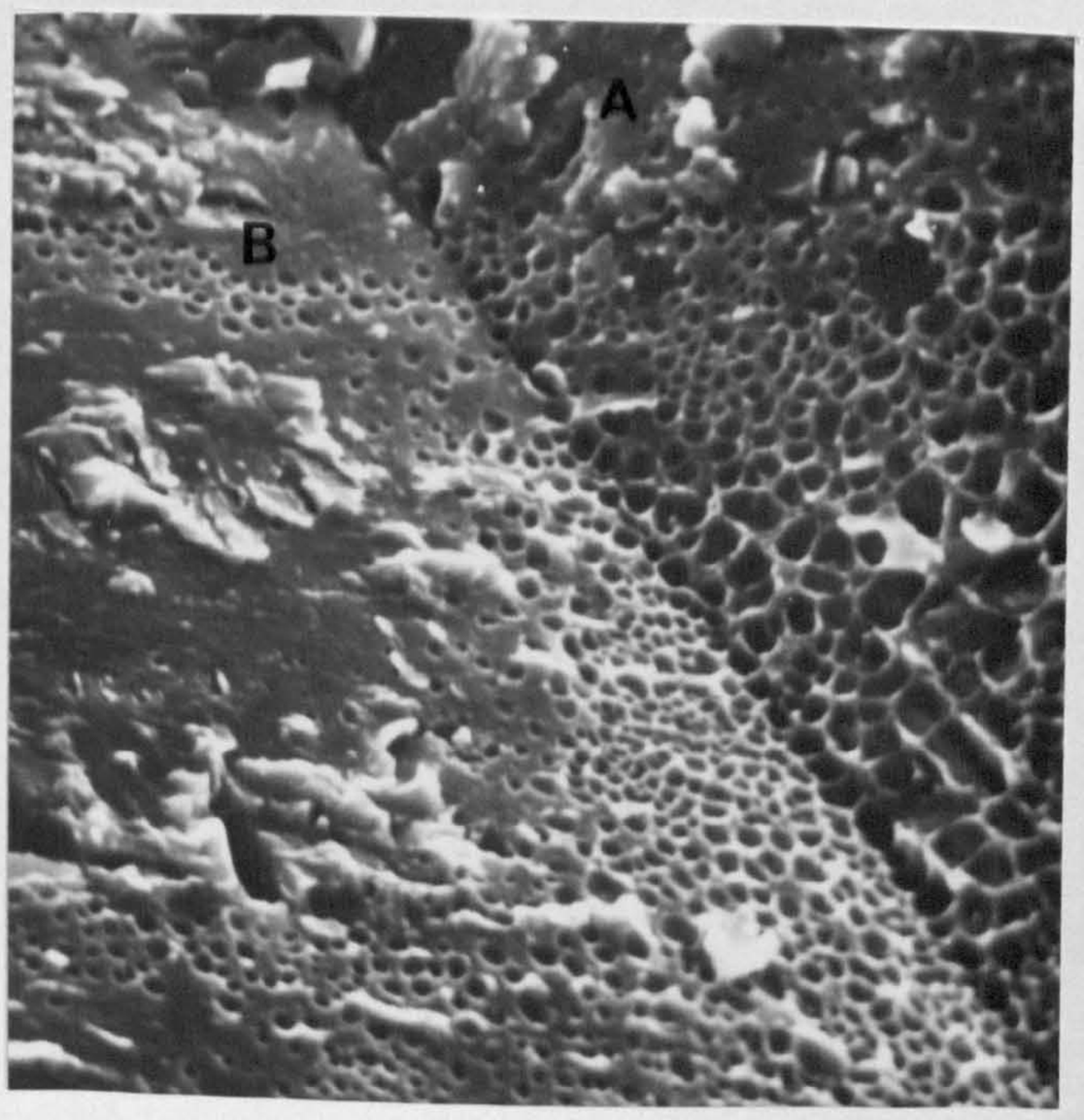
A
B

Figs. 60-63 The morphology of grain boundary damage in the later stages of creep life, as exposed by low temperature impact fracture of crept specimens.

Fig. 60 Specimen CRMV3, showing a typical completely cavitated grain facet exposed after creep failure.
X1700

Fig. 61(a) The appearance of grain boundary damage during the tertiary regime of creep deformation. Specimen CRMV29
X1000

Fig. 61(b) The cavity wall network present on a grain facet shown in Fig. 61(a).
X5750

Fig. 62(a) Specimen CRMV1, showing the coarse cavity wall structure prevailing after creep failure. The facet shown is normal to the stress axis.
X2500

Fig. 62(b) The boundary wall configuration of a cavity in the area shown in the previous micrograph. Note the presence of VC particles on the floor of the cavity.
X11100

Fig. 63 Specimen CRMV24, showing the appearance of cavities at a grain edge at the start of tertiary creep.
X11600

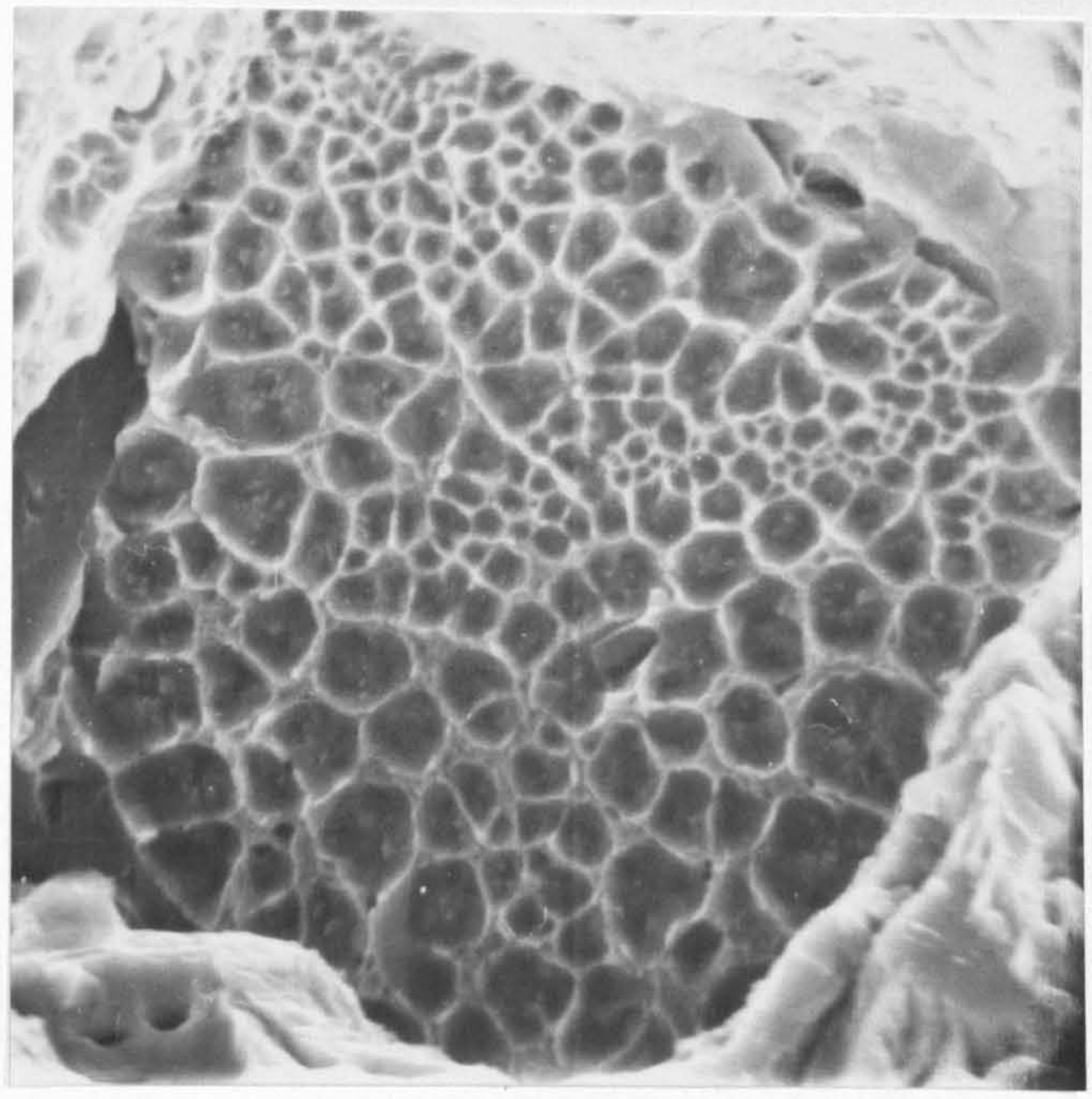

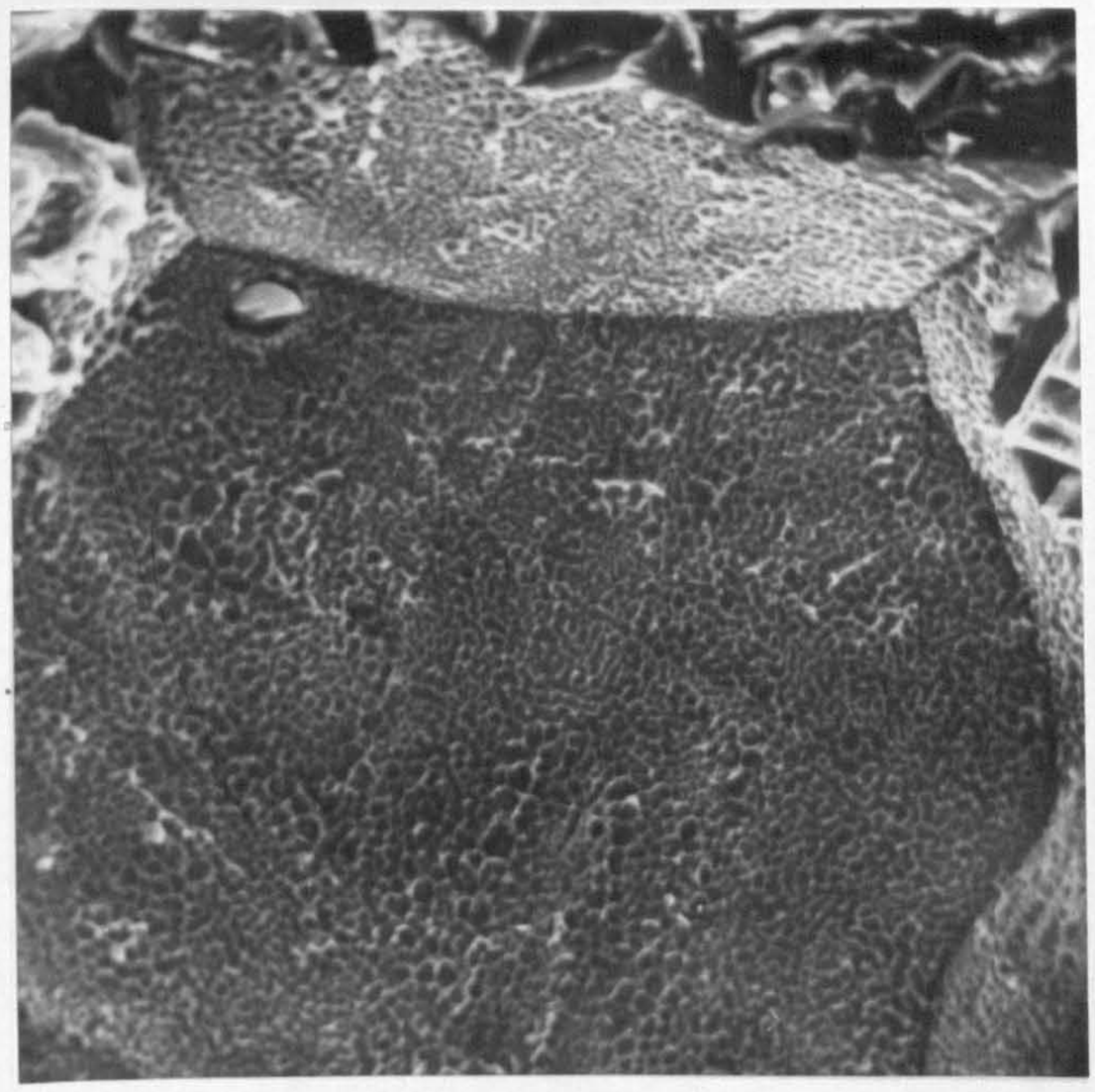

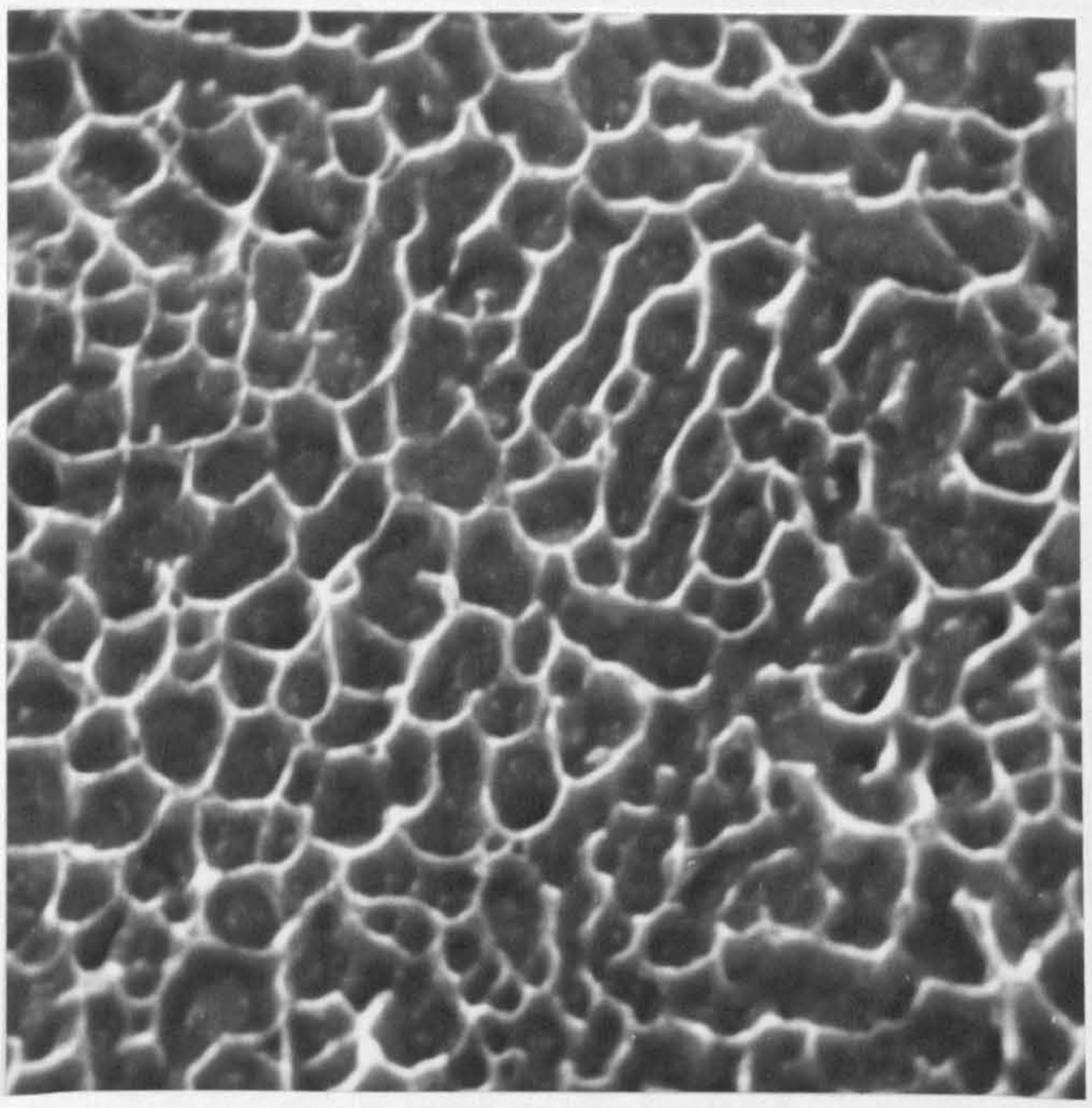

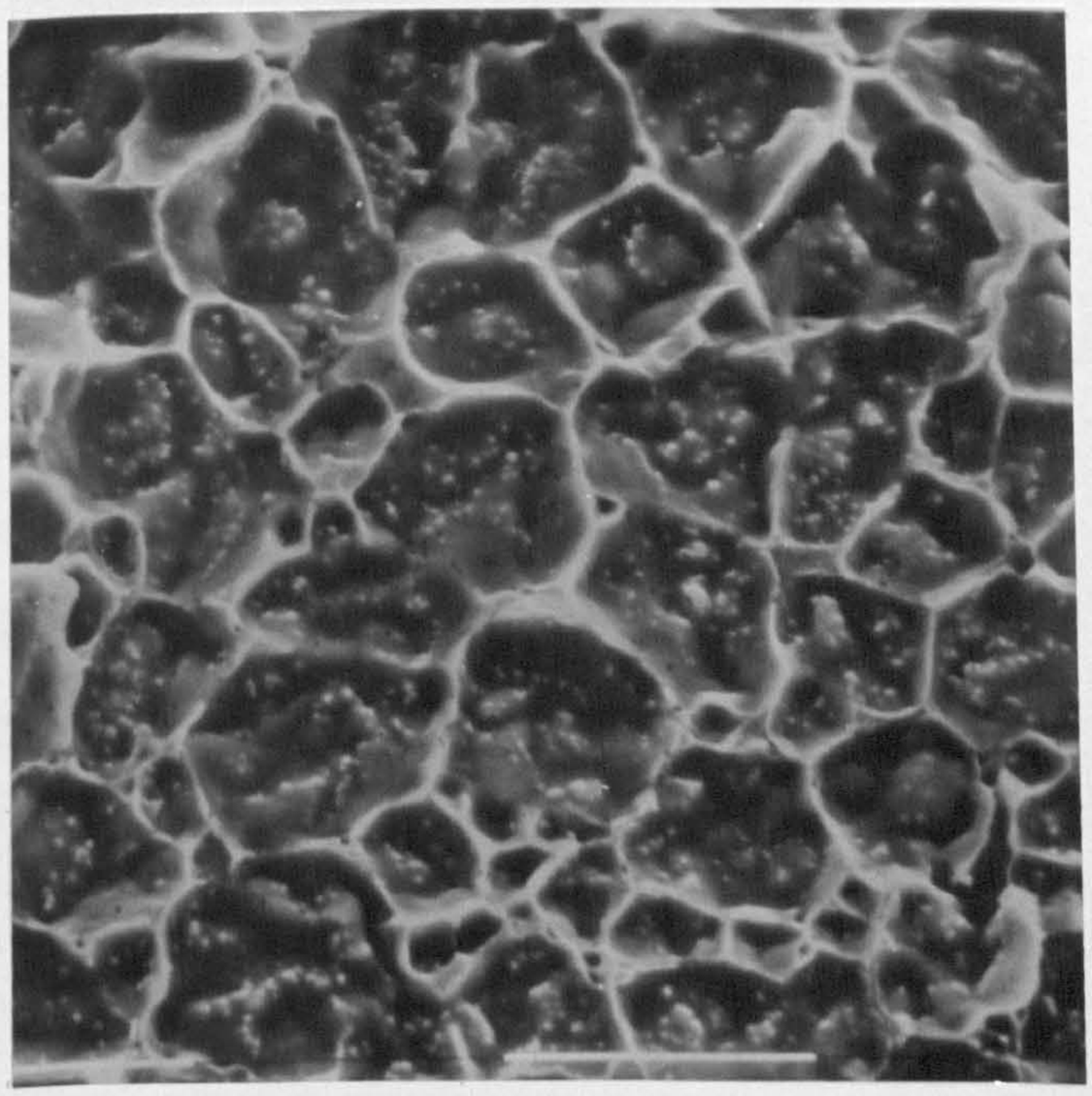

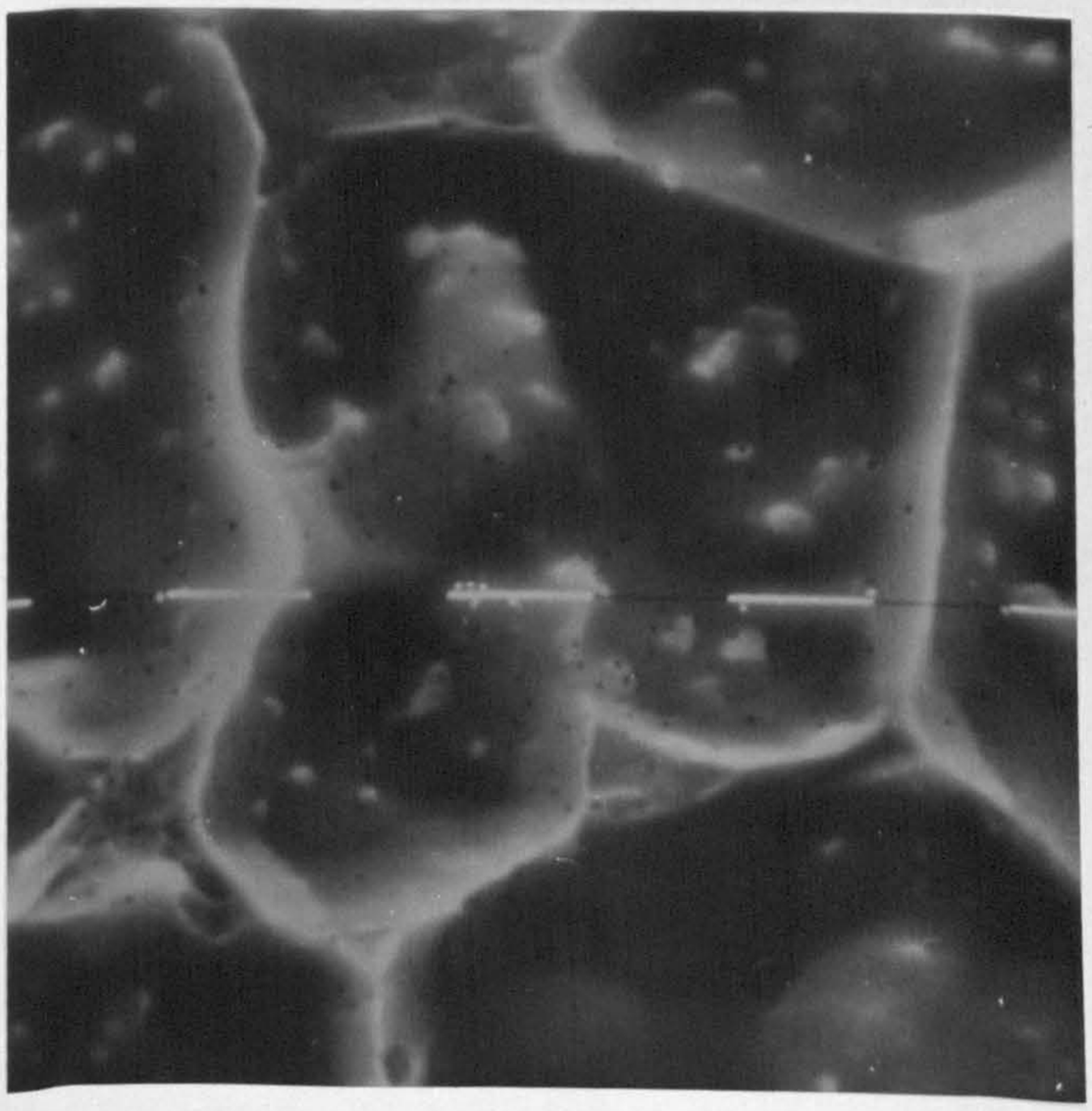

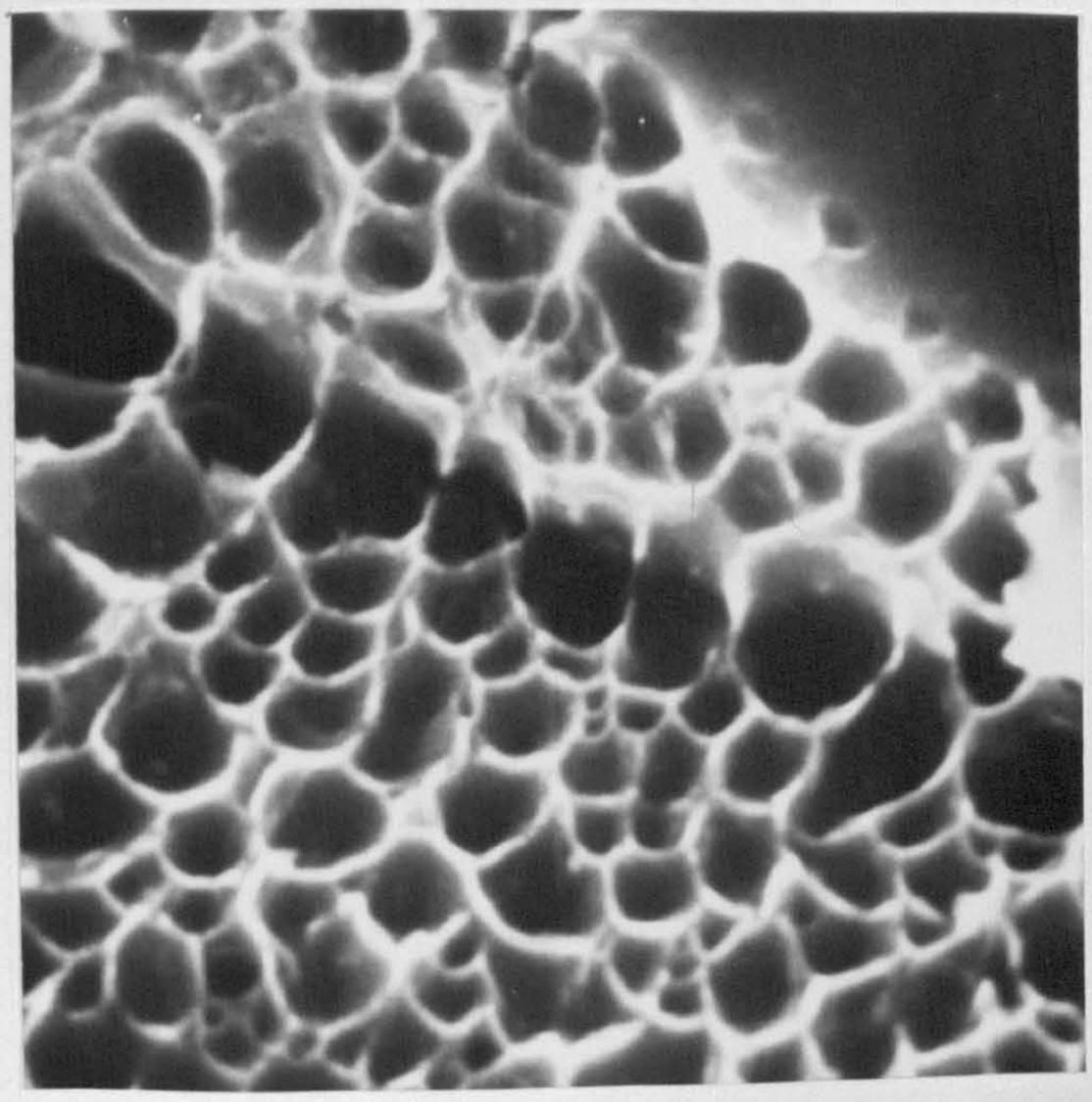

Fig. 64 Fractographic studies on the damage morphology present after creep deformation at 300 MNm^{-2}, 803K.

Fig. 64(a) Specimen CRMV21, illustrating the high density of cavities present on grain facets after limited creep deformation.
X2500

Fig. 64(b) Specimen CRMV10, the nature of cavity morphology on a single grain facet after creep failure is shown. Note the narrow size range of the population shown and the limited amount of coalescence.
X10500

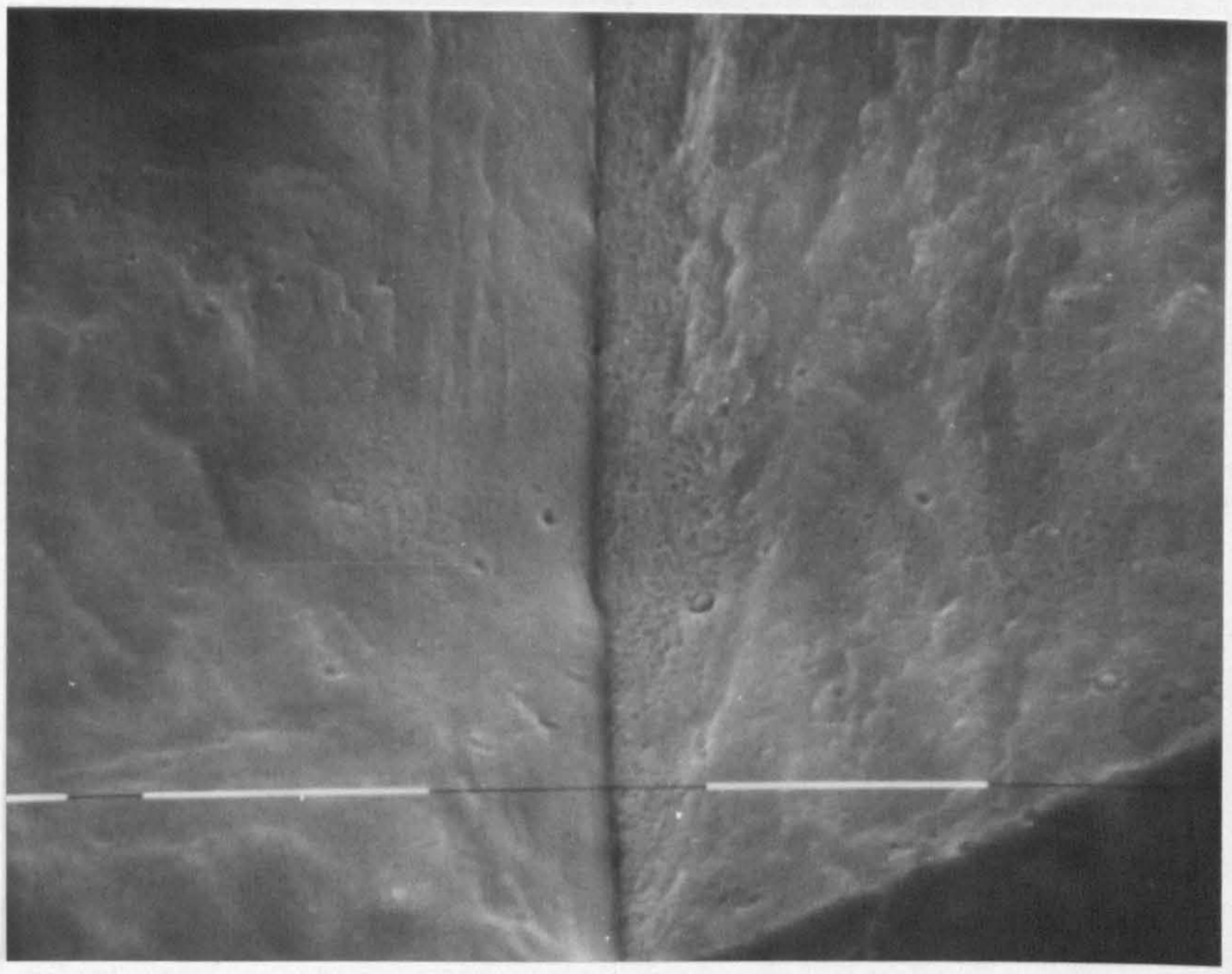

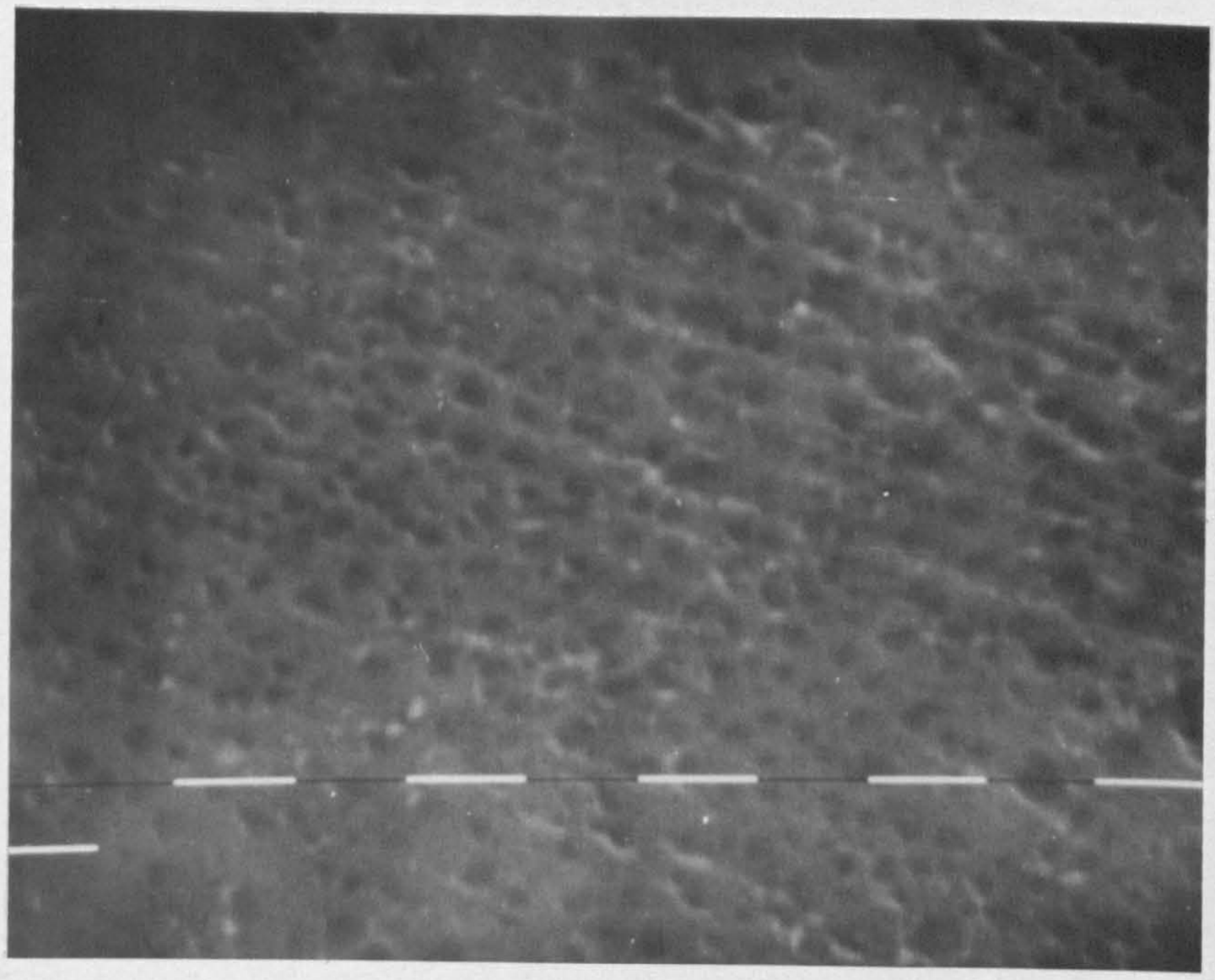

Figs. 65-68 1 MV transmission electron micrographs of thin foils of CRMV series alloy after various increments of creep deformation at 45 MNm^{-2}, 963K.

Fig. 65(a) Specimen CRMV17, revealing creep cavities on a prior austenite grain boundary after limited creep strain.
X14000

Fig. 65(b) High magnification view of the cavity marked "A" in Fig. 65(a).
X60000

Fig. 66 Specimen CRMV22, showing two adjacent cavities lying on a prior austenite grain boundary. Their internal dislocation structure can be resolved, as can the presence of fine particles on the cavity faces.
X26250

Fig. 67 Specimen CRMV22, showing a series of interference fringes emanating from the cavity/matrix interface.
X66000

Fig. 68(a) An array of creep cavities on boundaries at a triple point in specimen CRMV1 (after creep failure). Note the suppression of cavity nucleation at the boundary marked "D".
X7700

Fig. 68(b) High magnification view of a cavitated boundary in Fig. 68(a), showing cavities in their earliest stages of development.
X23750

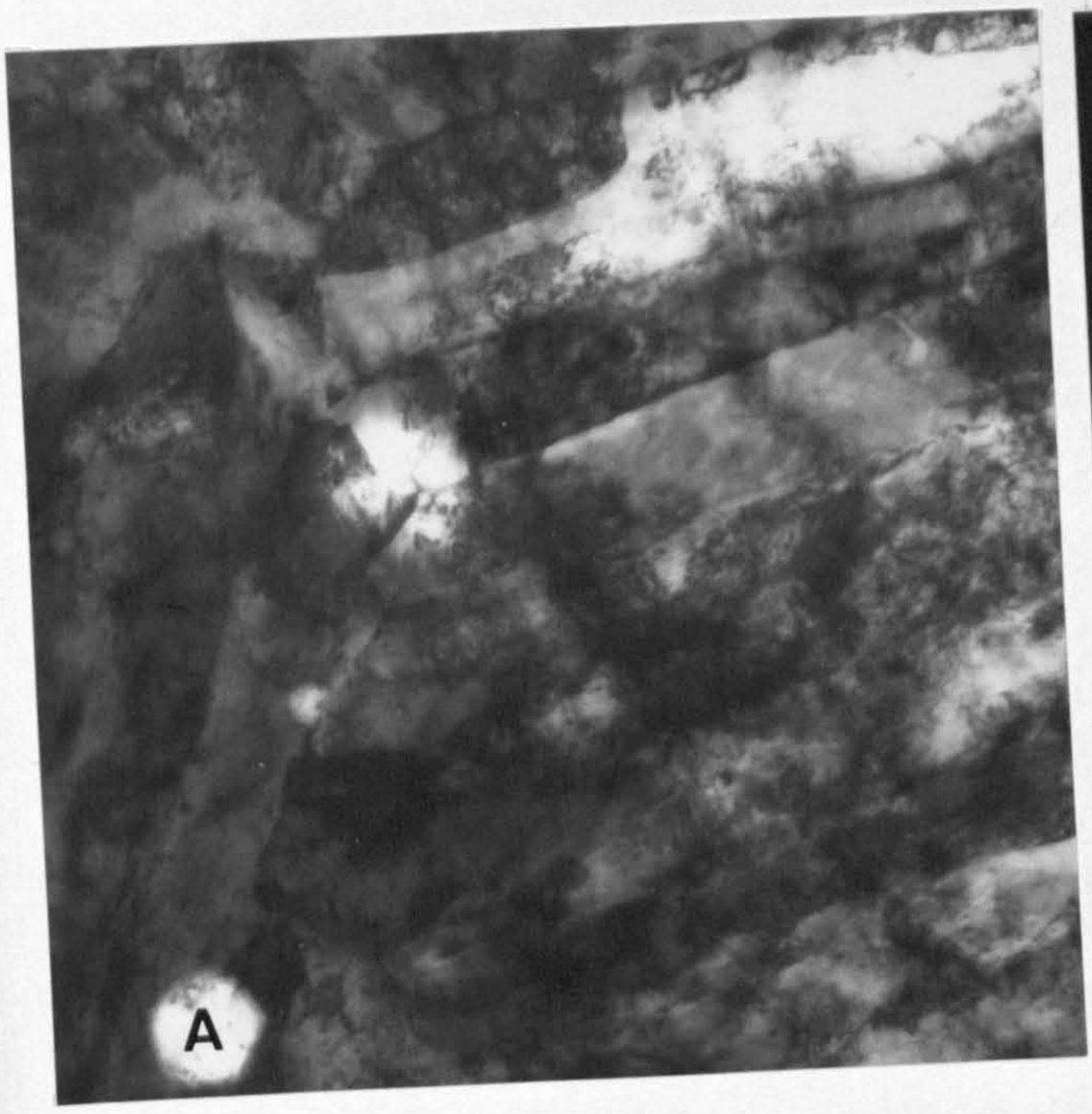
A

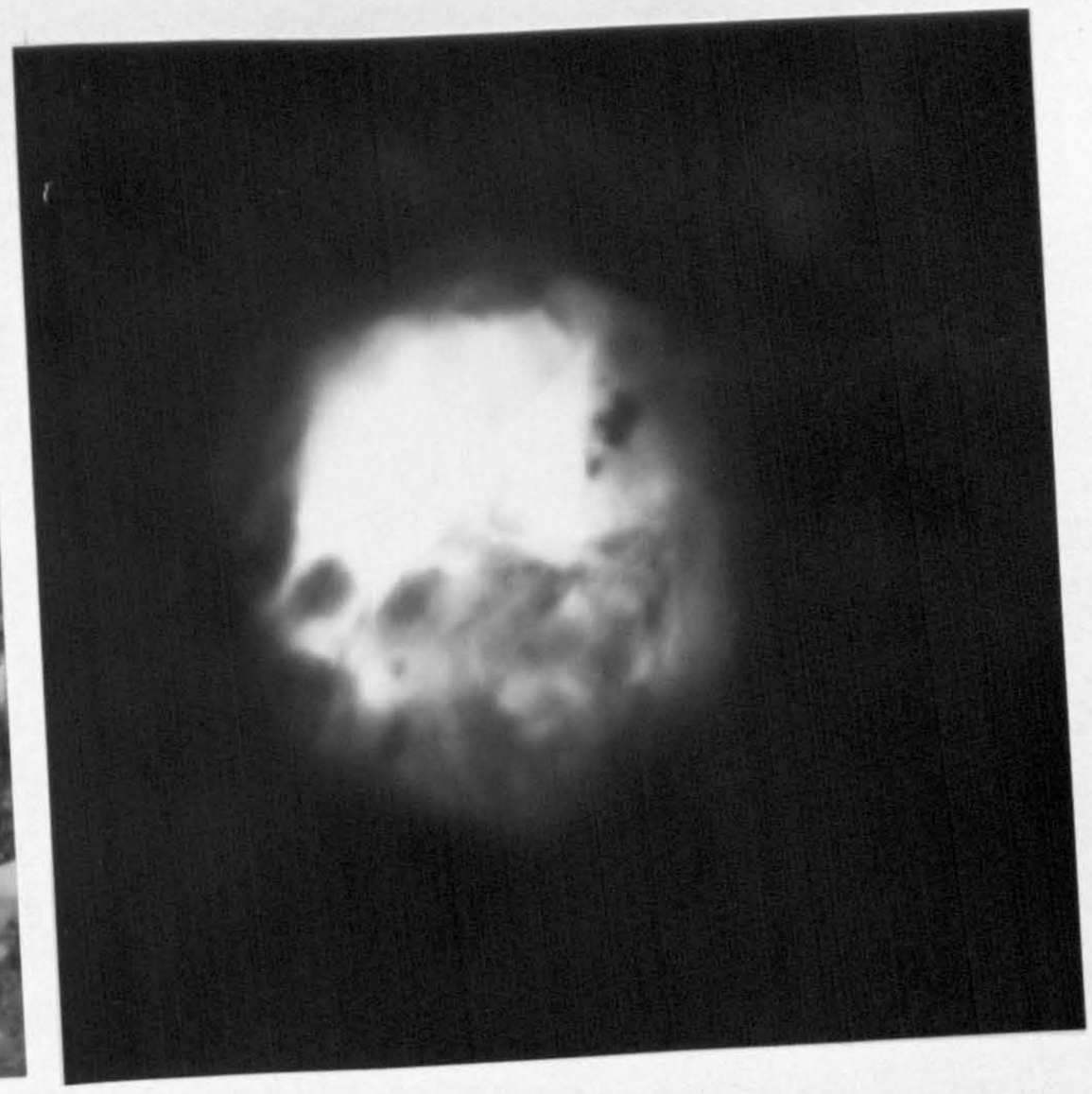

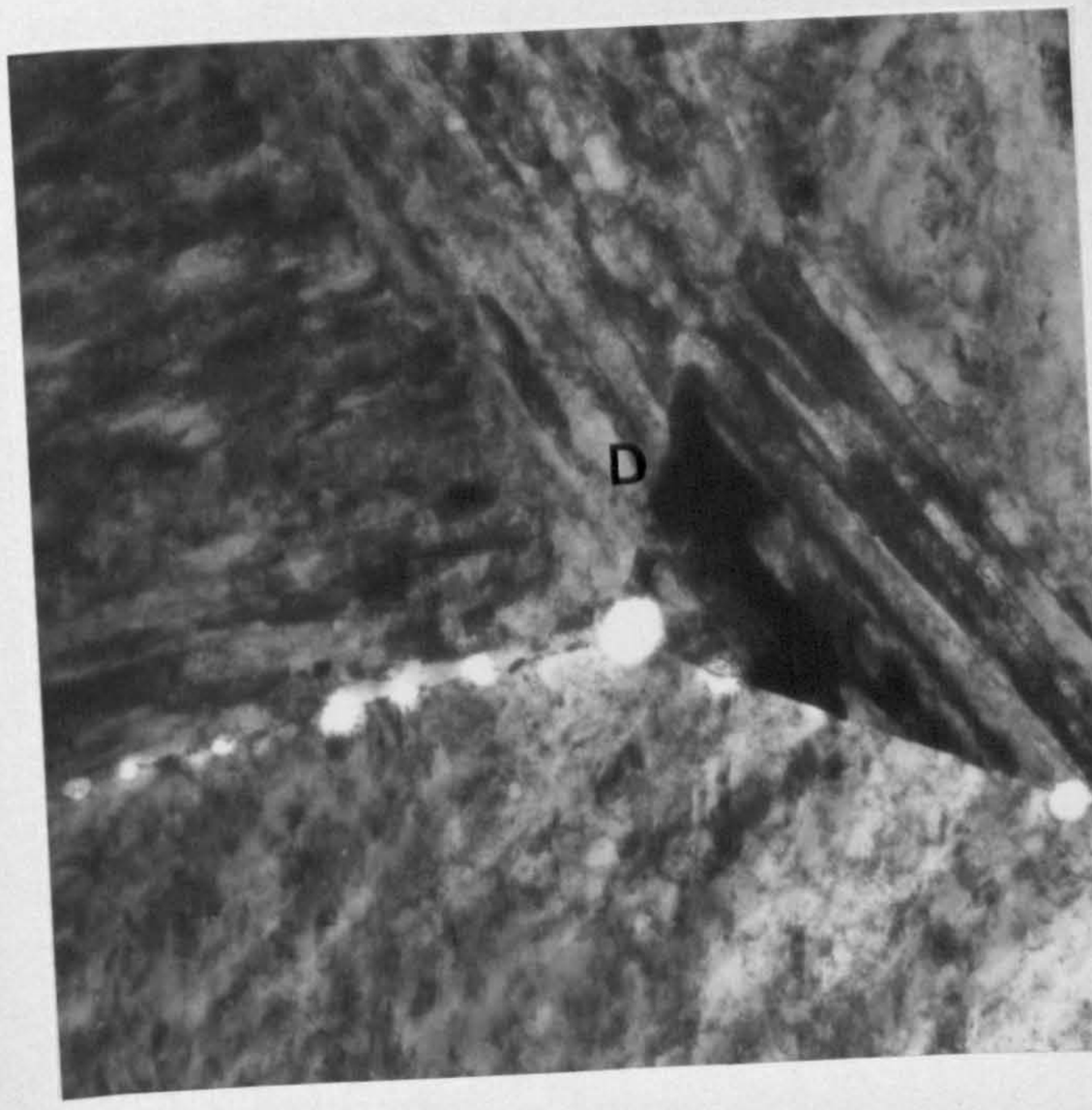
D

Fig. 69 The nature of creep damage in a notched specimen of CRMV series alloy (CRMV/N1).

Fig. 69(a) The intergranular fracture surface of the notched test piece after creep failure. Note the extensive cracking in the region of the throat.
X20

Fig. 69(b) Typical view of prior austenite grain boundaries on the fracture surface.
X1050

Fig. 69(c) High magnification view of the intergranular damage on an exposed facet in Fig. 69(b), revealing intricate cavity wall networks.
X5325

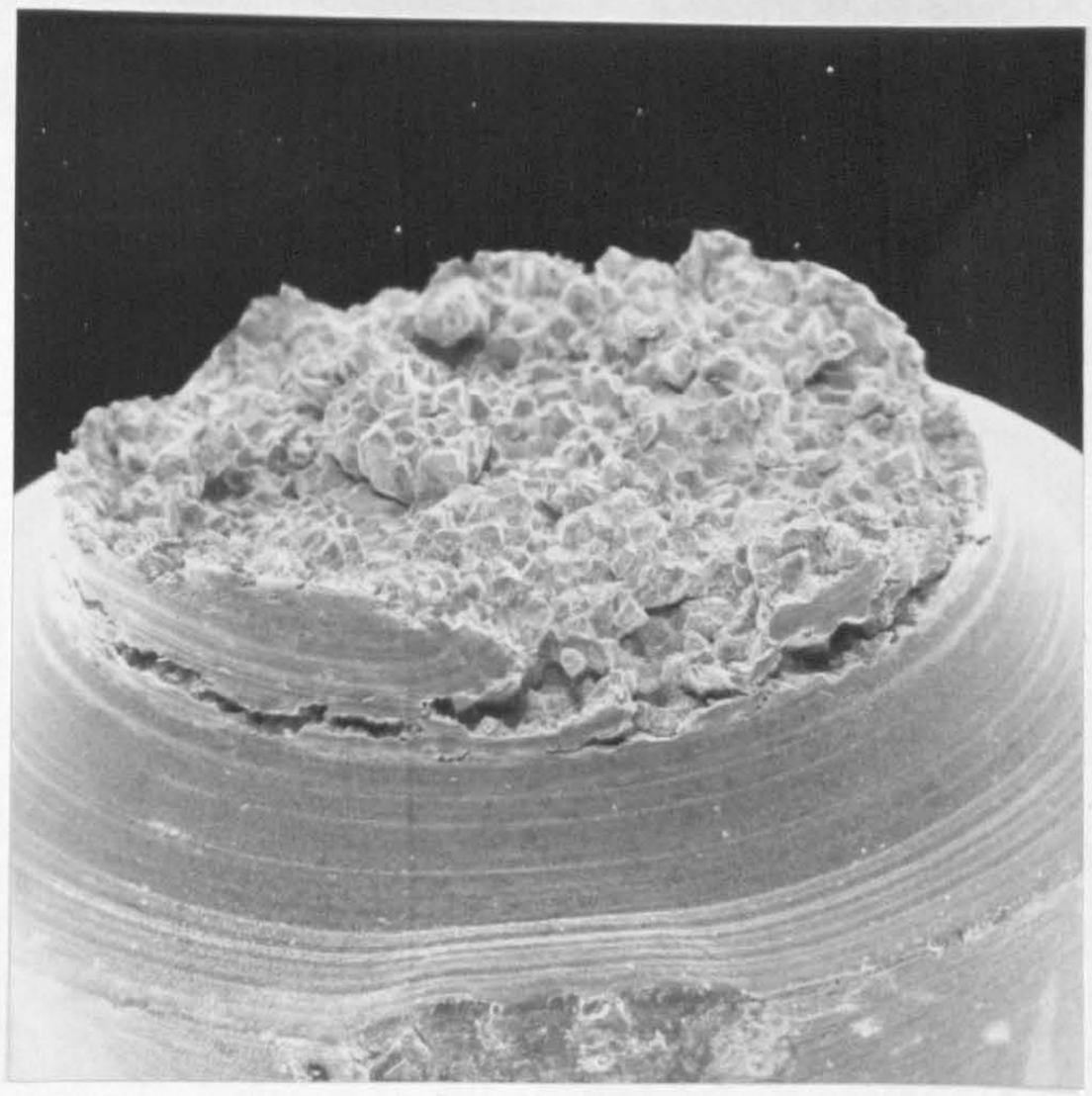

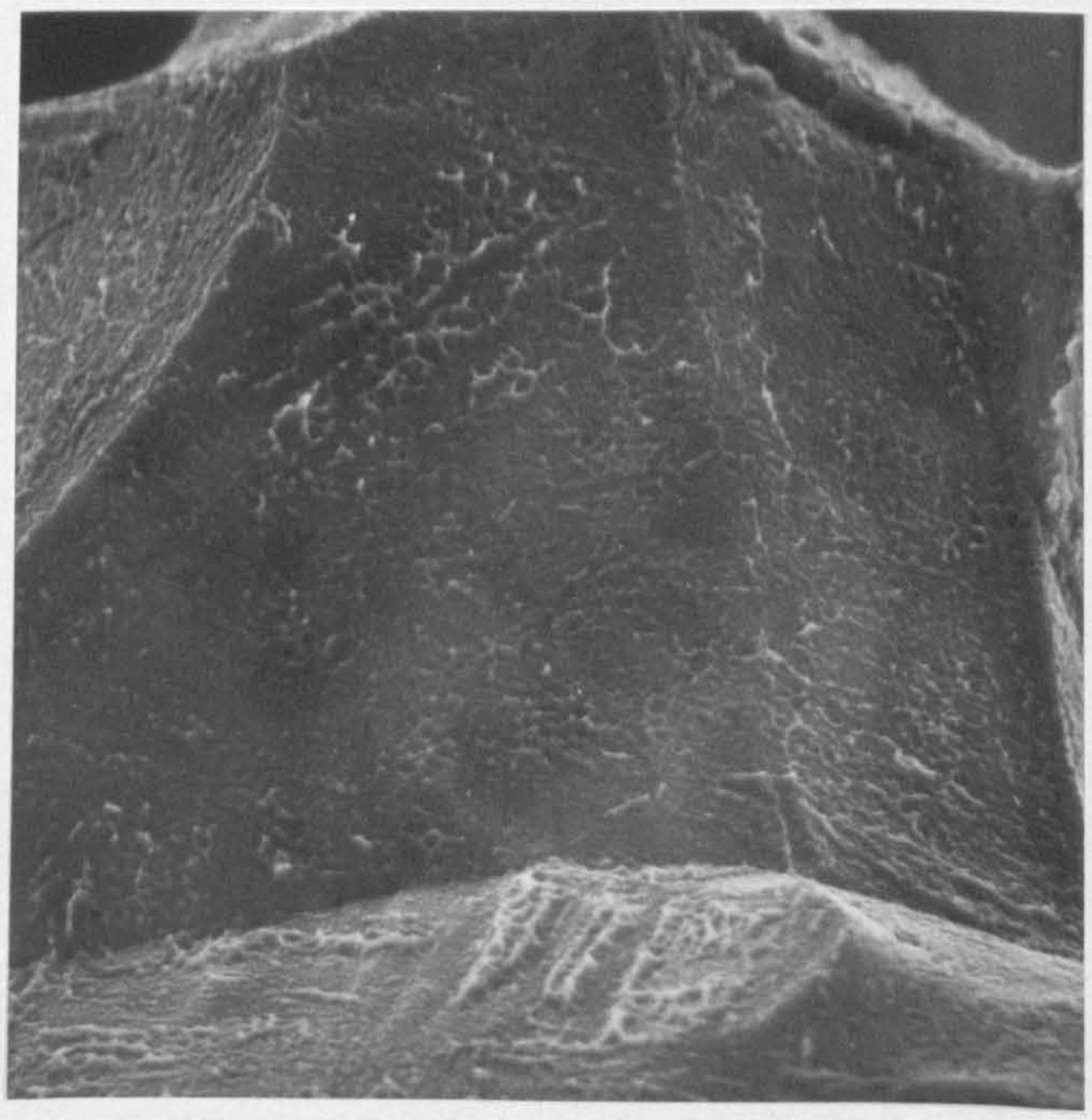

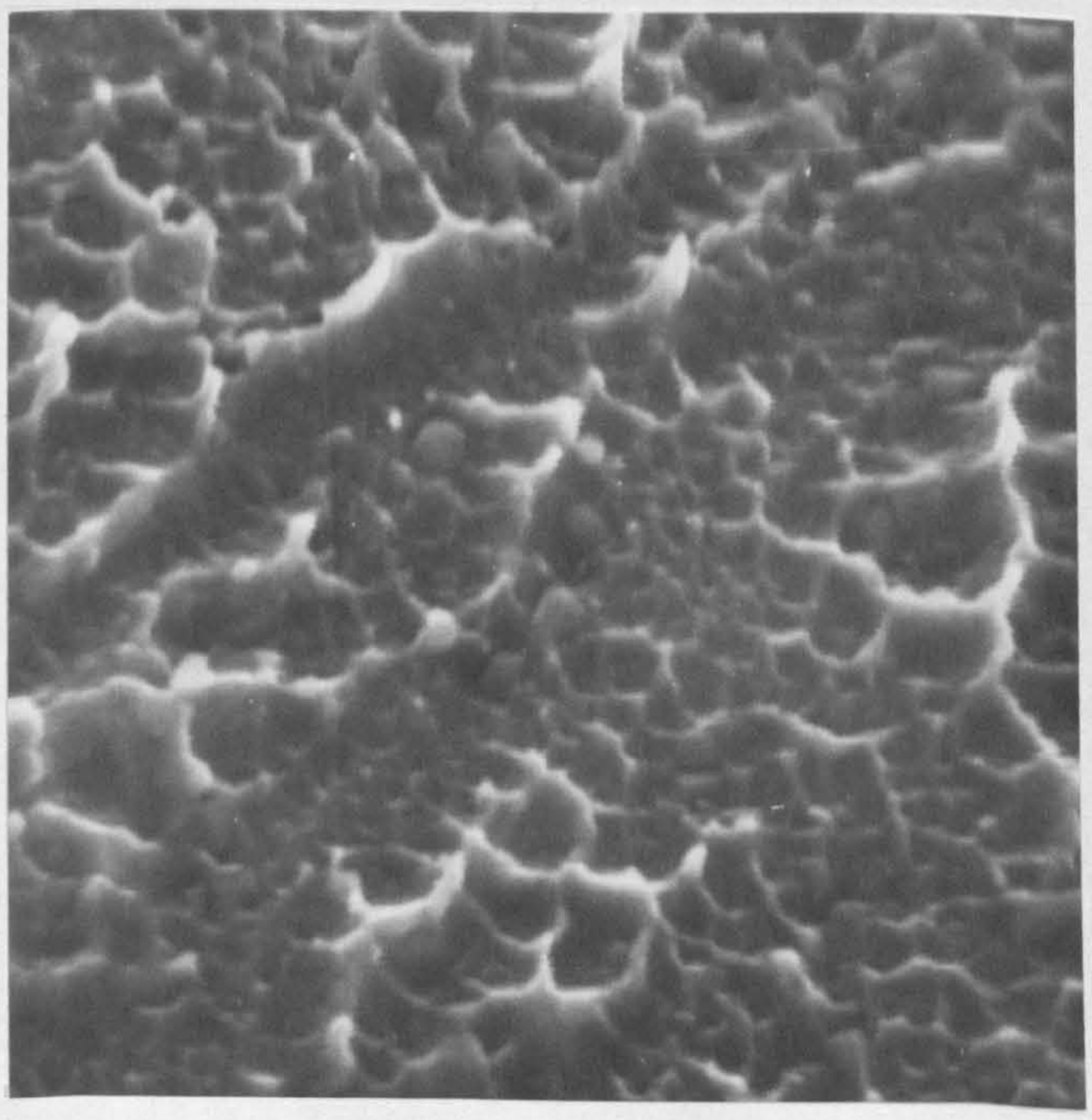

Fig. 70(a) 100kV transmission electron micrograph of a thin foil of CRMV series alloy , in the heat-treated condition. The bainite plates are bounded by massive sheets of Fe_3C.
X26000

Fig. 70(b) High magnification view of the same area, showing the complex dislocation structure present within the bainite plates.
X72000

Fig. 70(c) Diffraction pattern produced by a plate of Fe_3C.

Fig. 70(d) Analysis of diffraction pattern shown in Fig. 70(c).

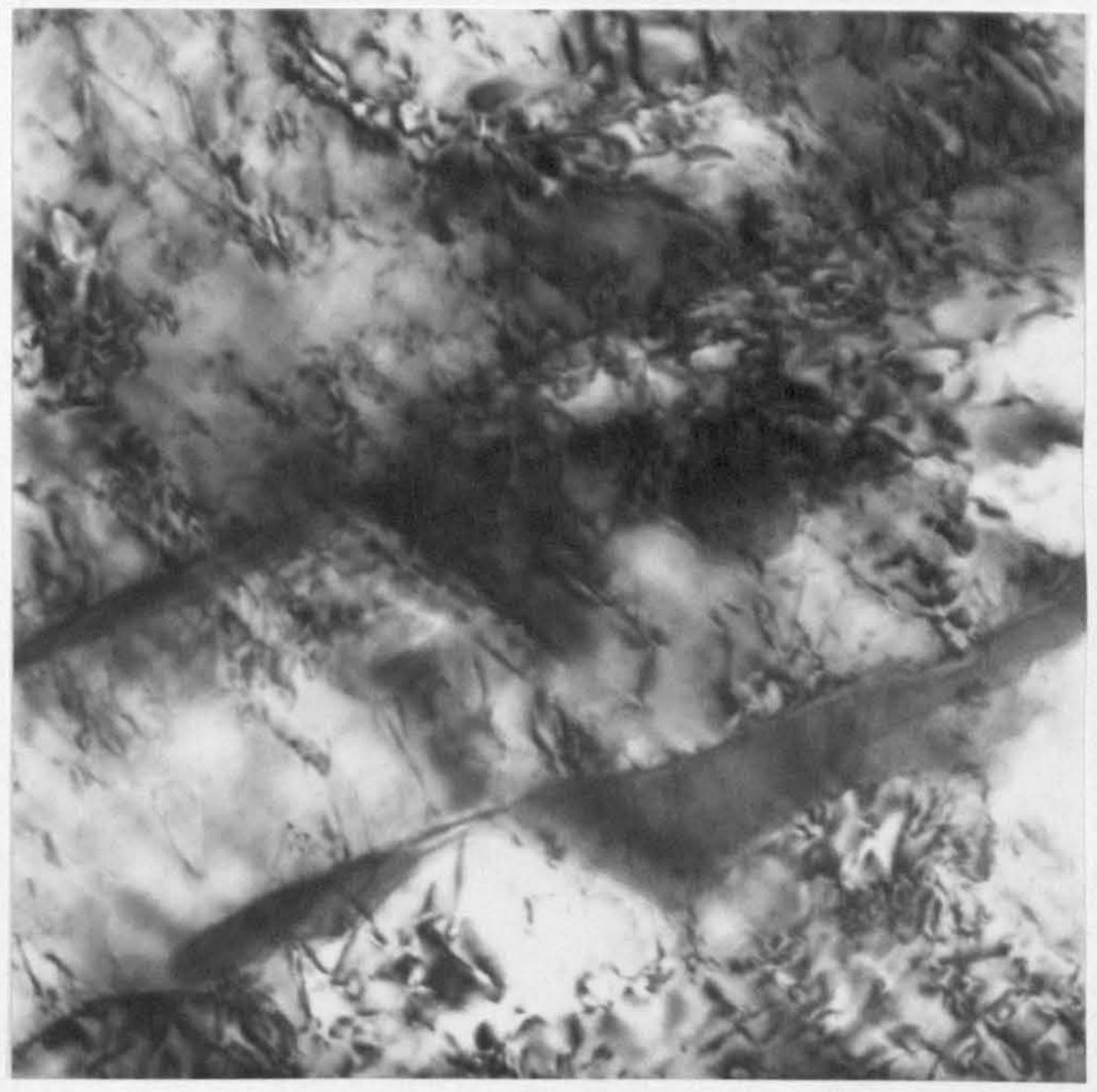

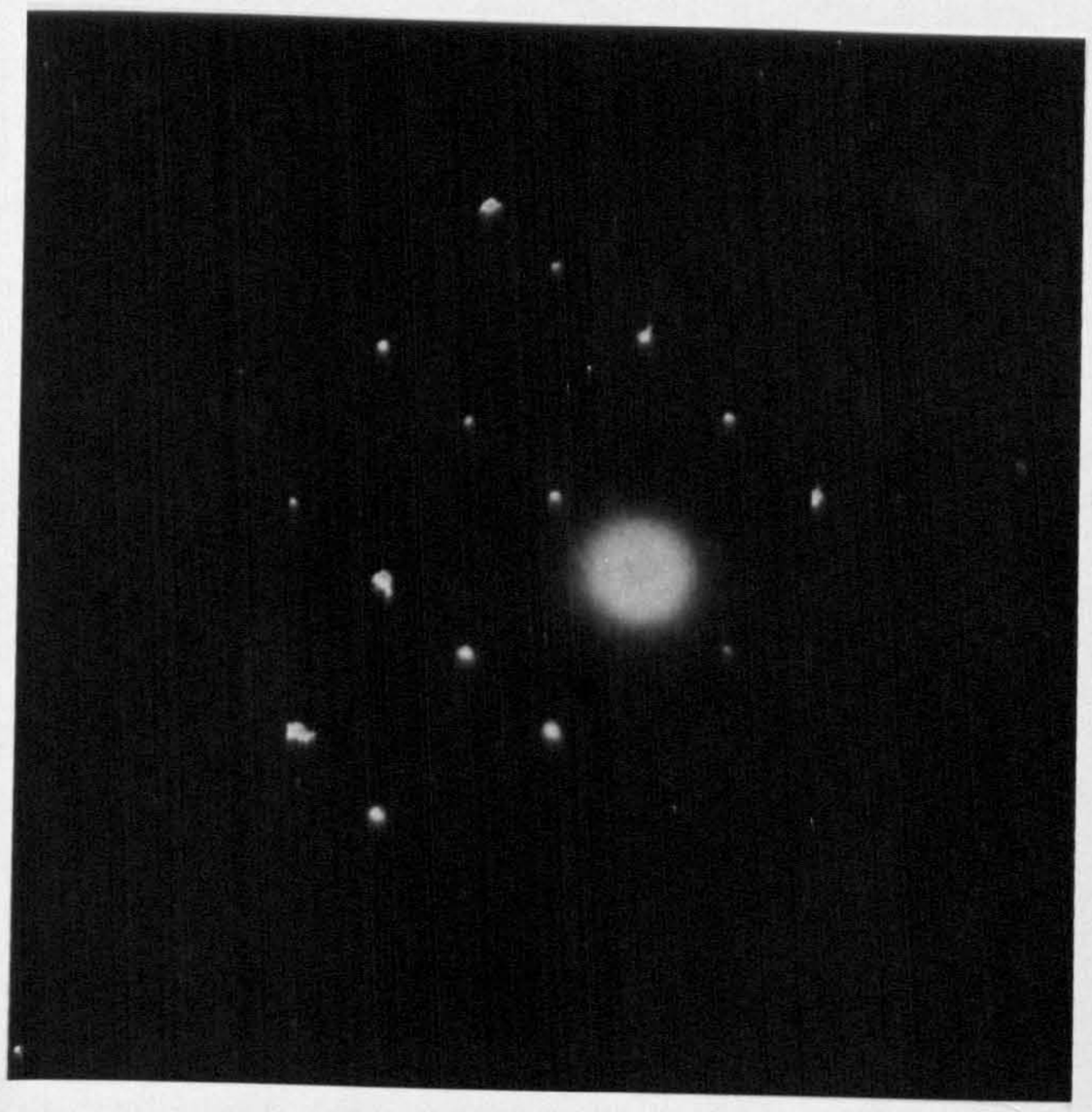

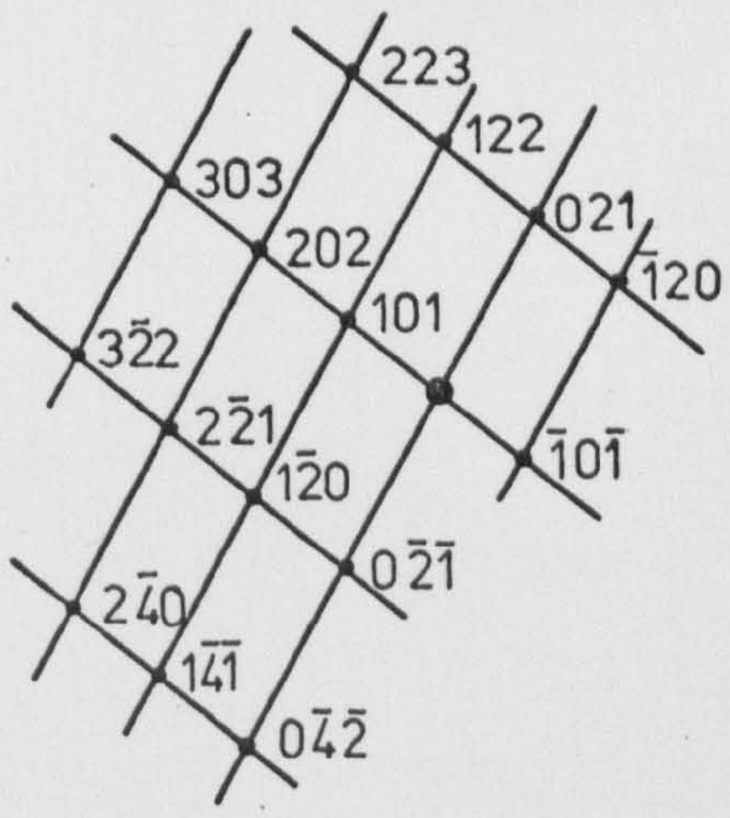

$(21\bar{2})$ ZONE, Fe_3C

Fig. 71(a) Specimen CRMV19, showing the fine scale precipitation of VC within the bainitic matrix during the early stages of creep life.
X26500

Fig. 71(b) Diffraction pattern produced by the dispersed VC phase.

Fig. 71(c) Analysis of diffraction pattern shown in Fig. 71(b), included are those reflections due to the oxide film and the ferrite matrix.

Fig. 71(d) Dark field image produced by the (002) VC reflection. Note the presence of some coarser precipitates.
X15750

Fig. 72(a) Typical region of CRMV series alloy during tertiary creep.
X15750

Fig. 72(b) Dark field image of the same area, using an Fe_3C reflection. These carbides are no longer present as massive sheets, but have shown considerable spherodisation.
X15750

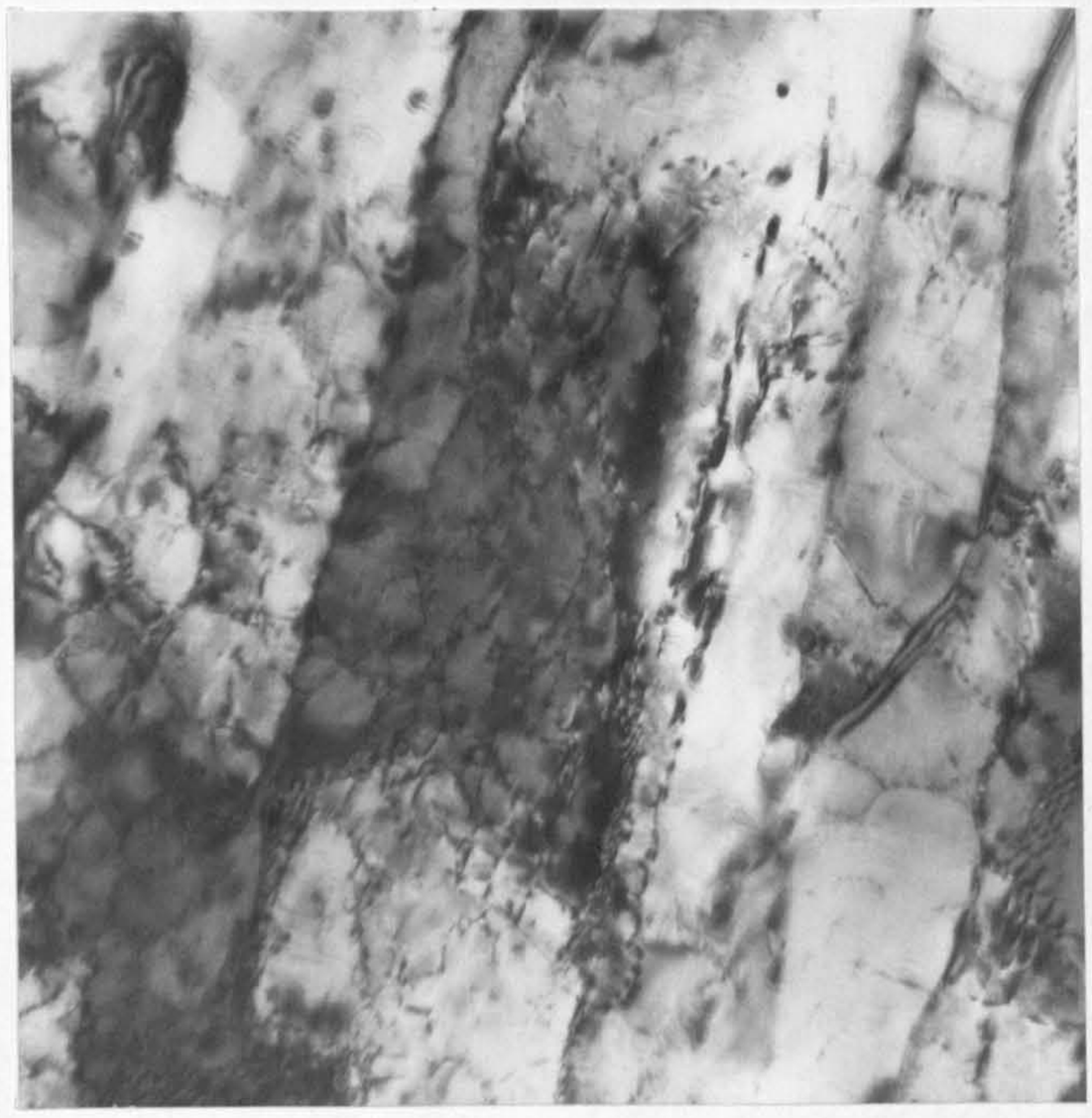

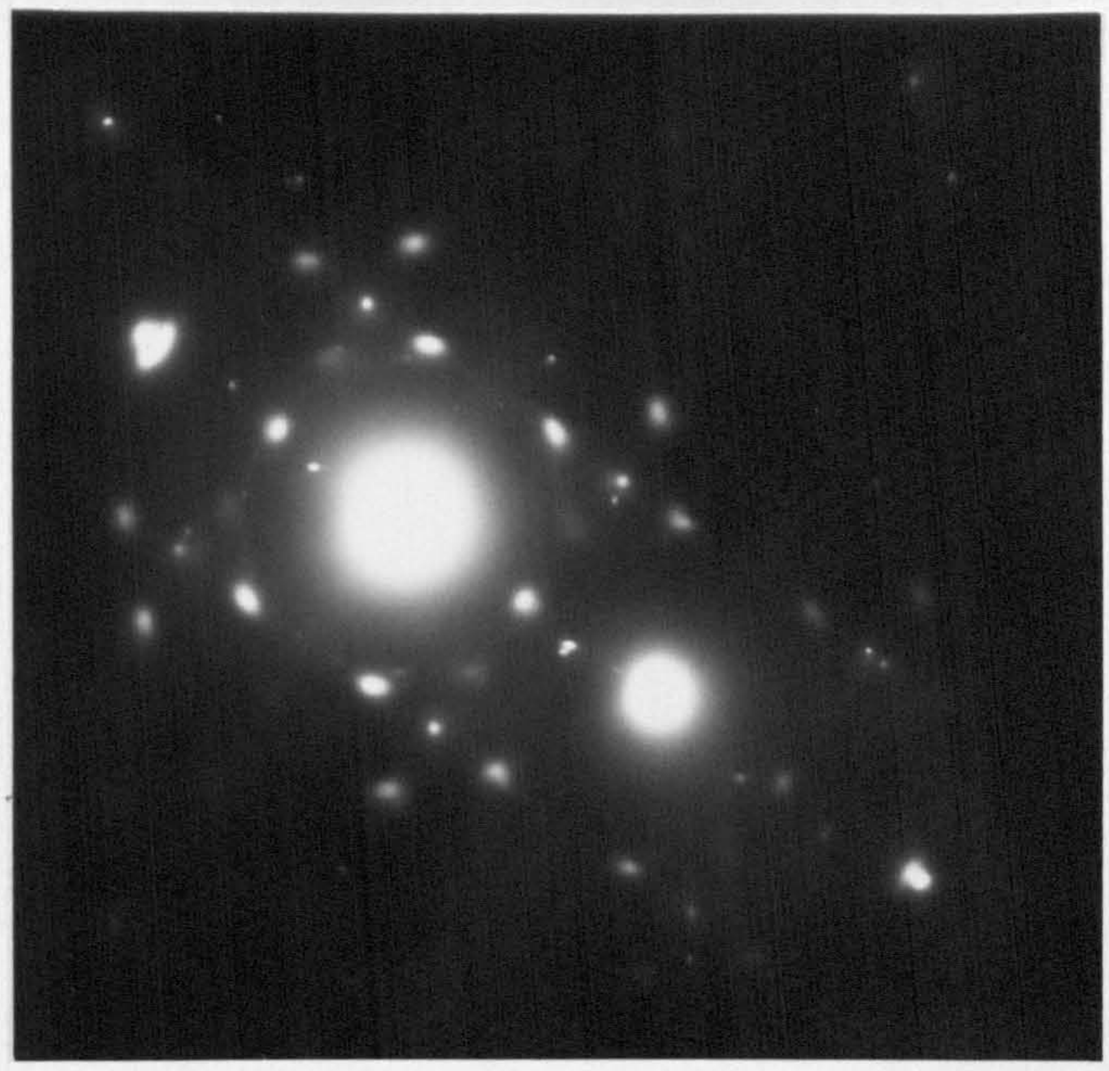

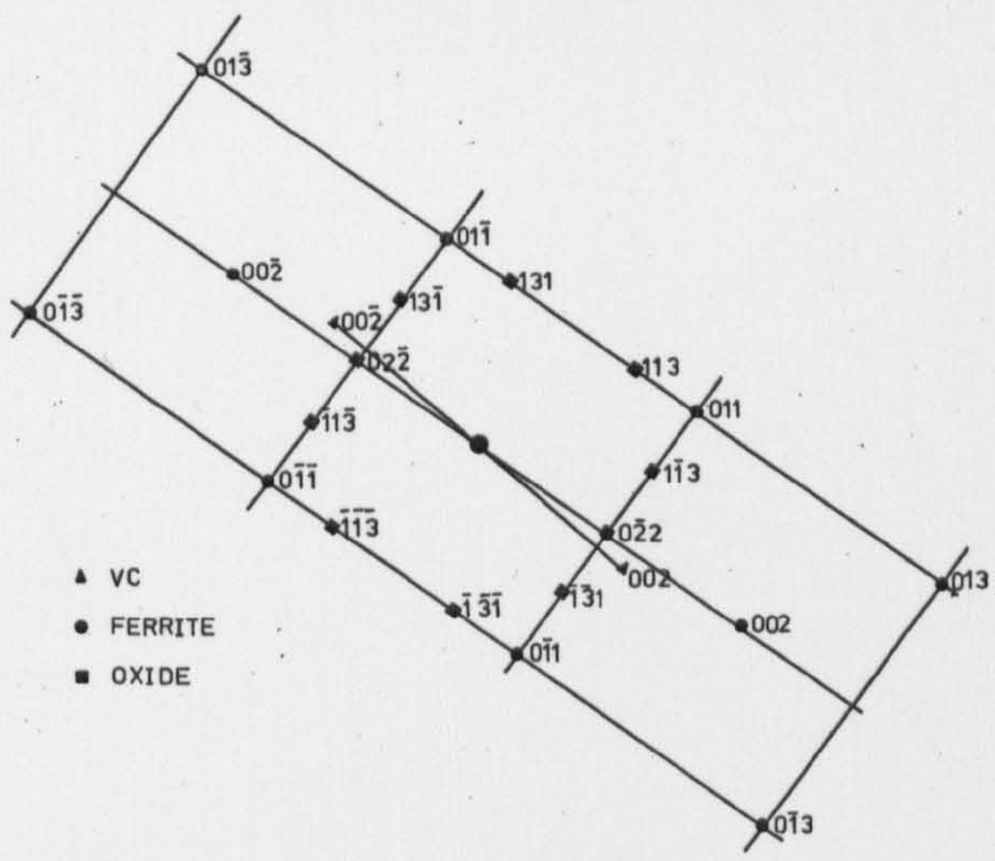

(100) ZONE, VC

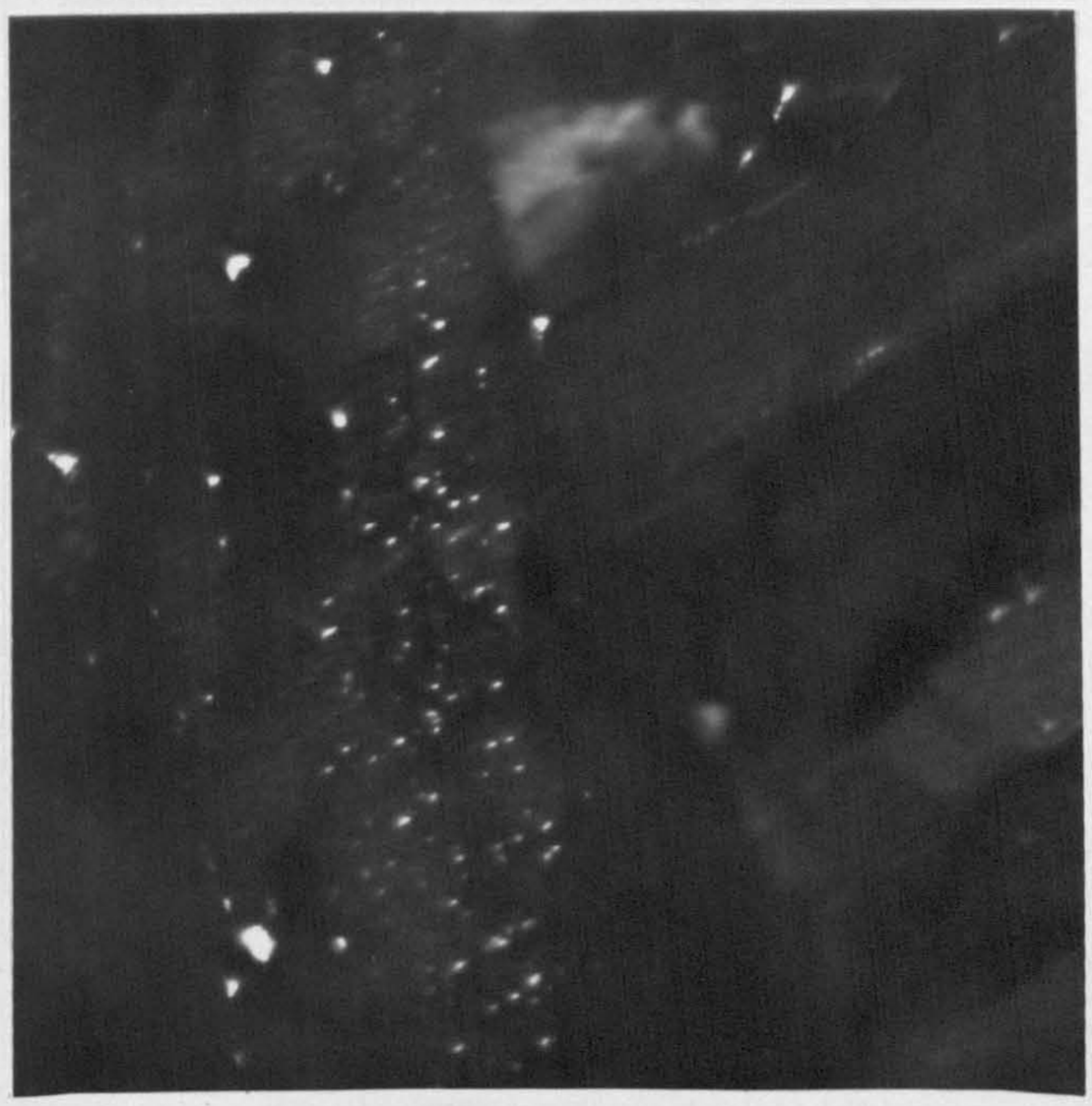

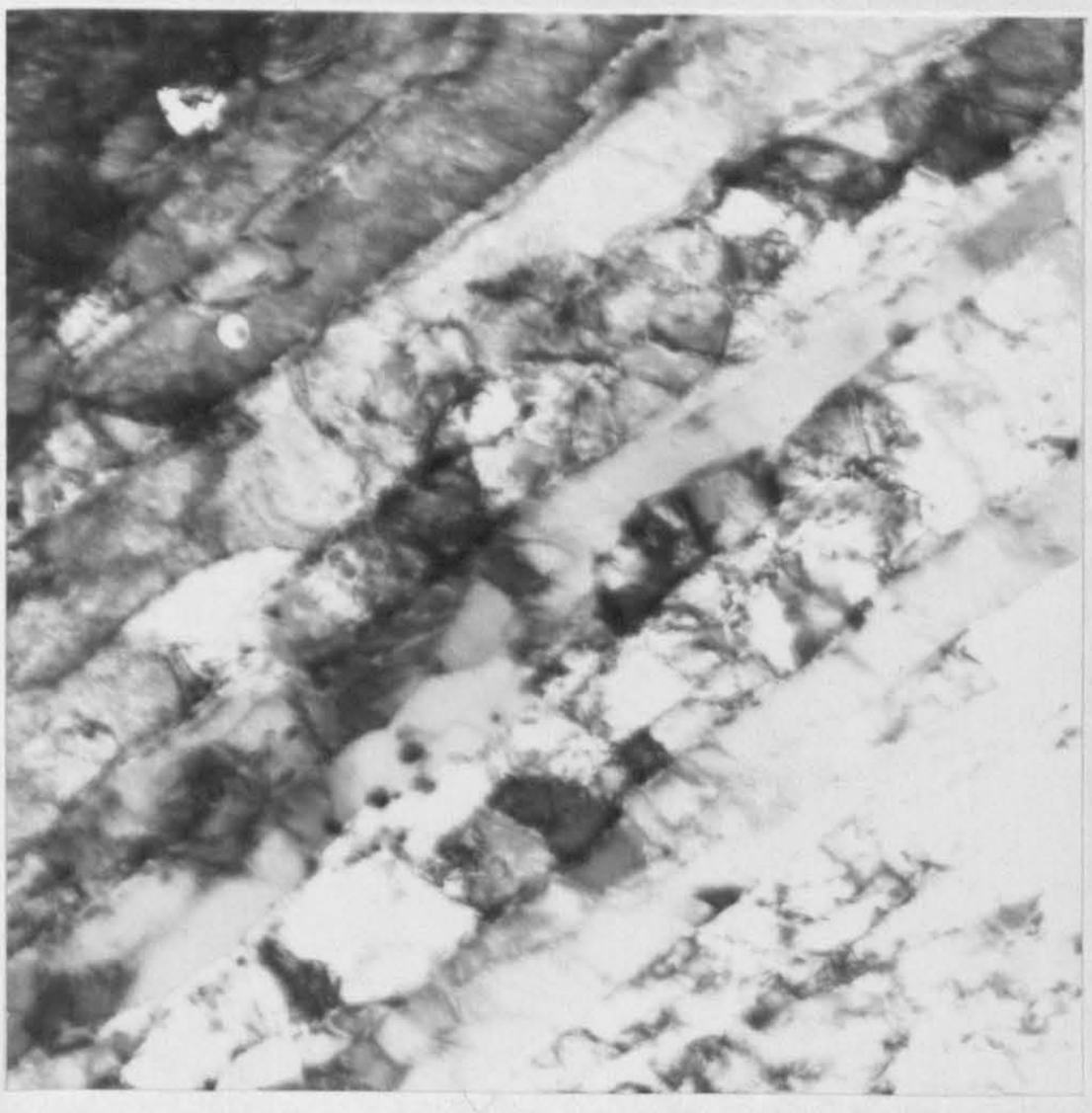

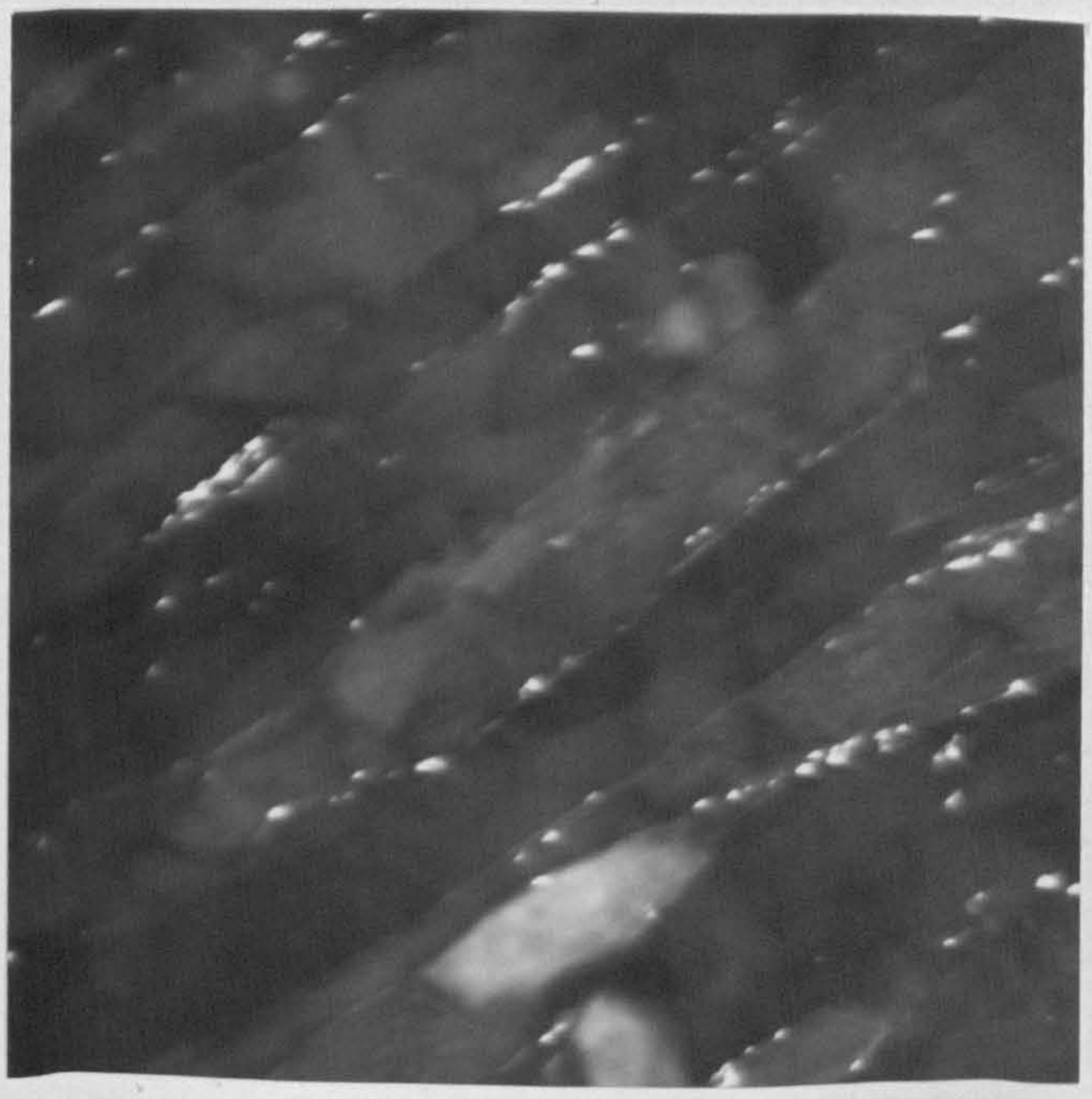

Fig. 73(a) Cavity size frequency histograms for cavity populations observed after creep deformation in the primary and secondary regimes at 45 MNm^{-2}, 963K.

-+-+-+- 9×10^4 s.

——————— 32.4×10^4 s.

_ _ _ _ _ 50.4×10^4 s.

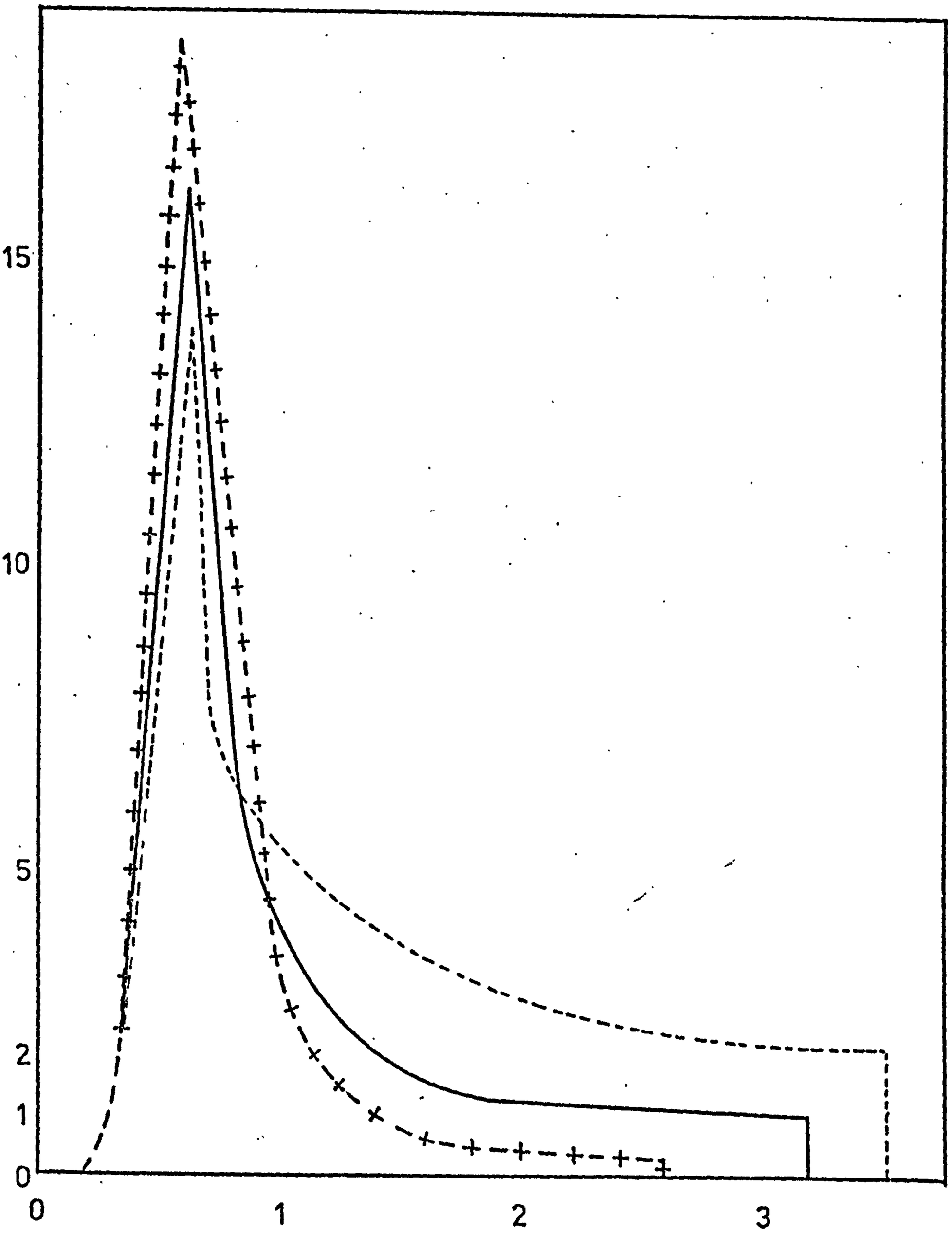
R.F. %
15
10
5
2
1
0
0
1
2
3
CAVITY WIDTH, μm.

Fig. 73(b) Cavity size frequency histograms for cavity populations observed after creep deformation in the tertiary regime and after fracture at 45 MNm^{-2}, 963K.

------- 63×10^4 s.

——— 77.5×10^4 s.

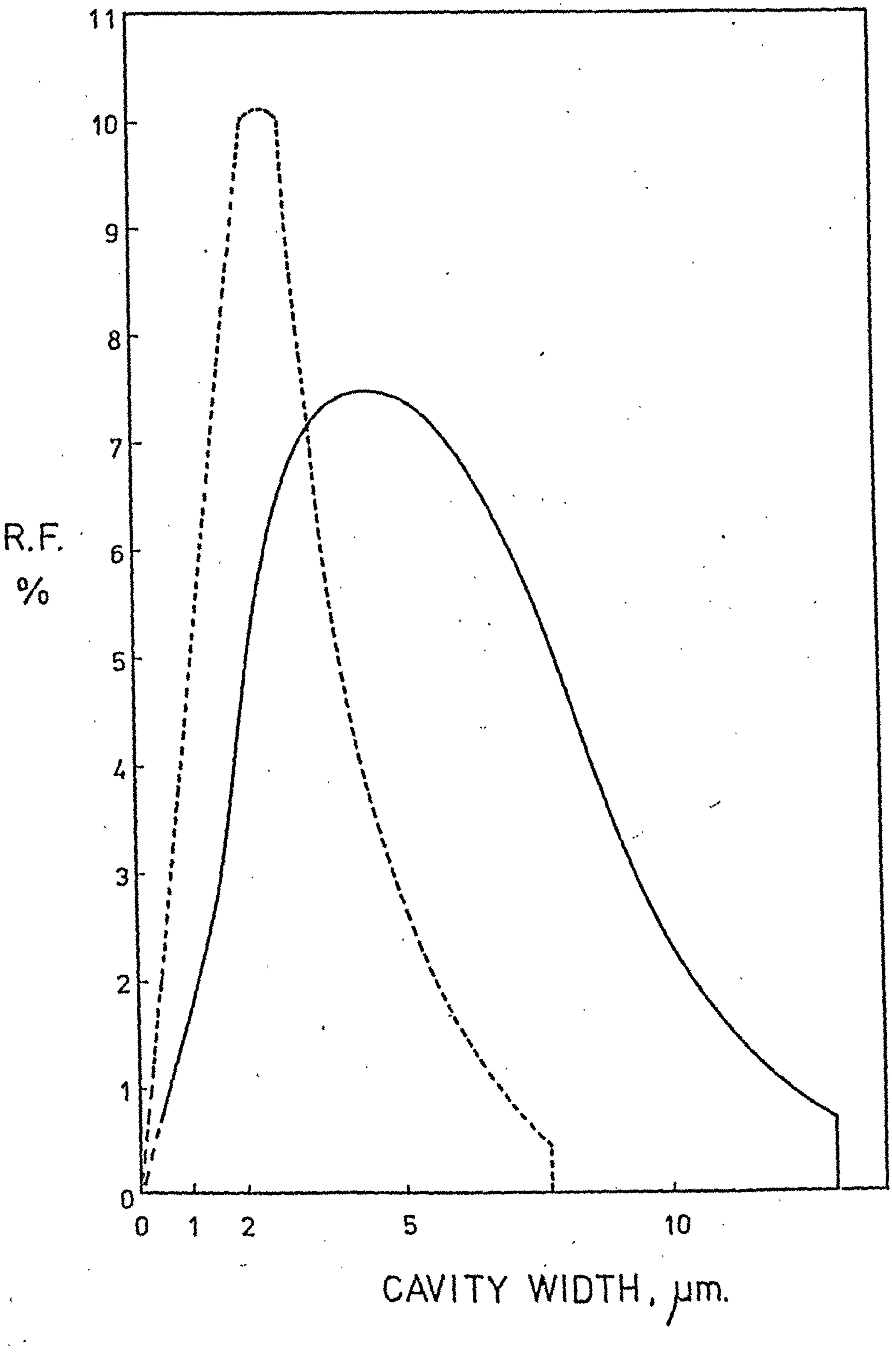
11
10
9
8
7
6
5
4
3
2
1
0
R.F.
%
0
1
2
5
10
CAVITY WIDTH, μm.

Fig. 74 Creep curve for CRMV series alloy tested at 45 MNm^{-2}, 963K with cavity growth curve superimposed (□).

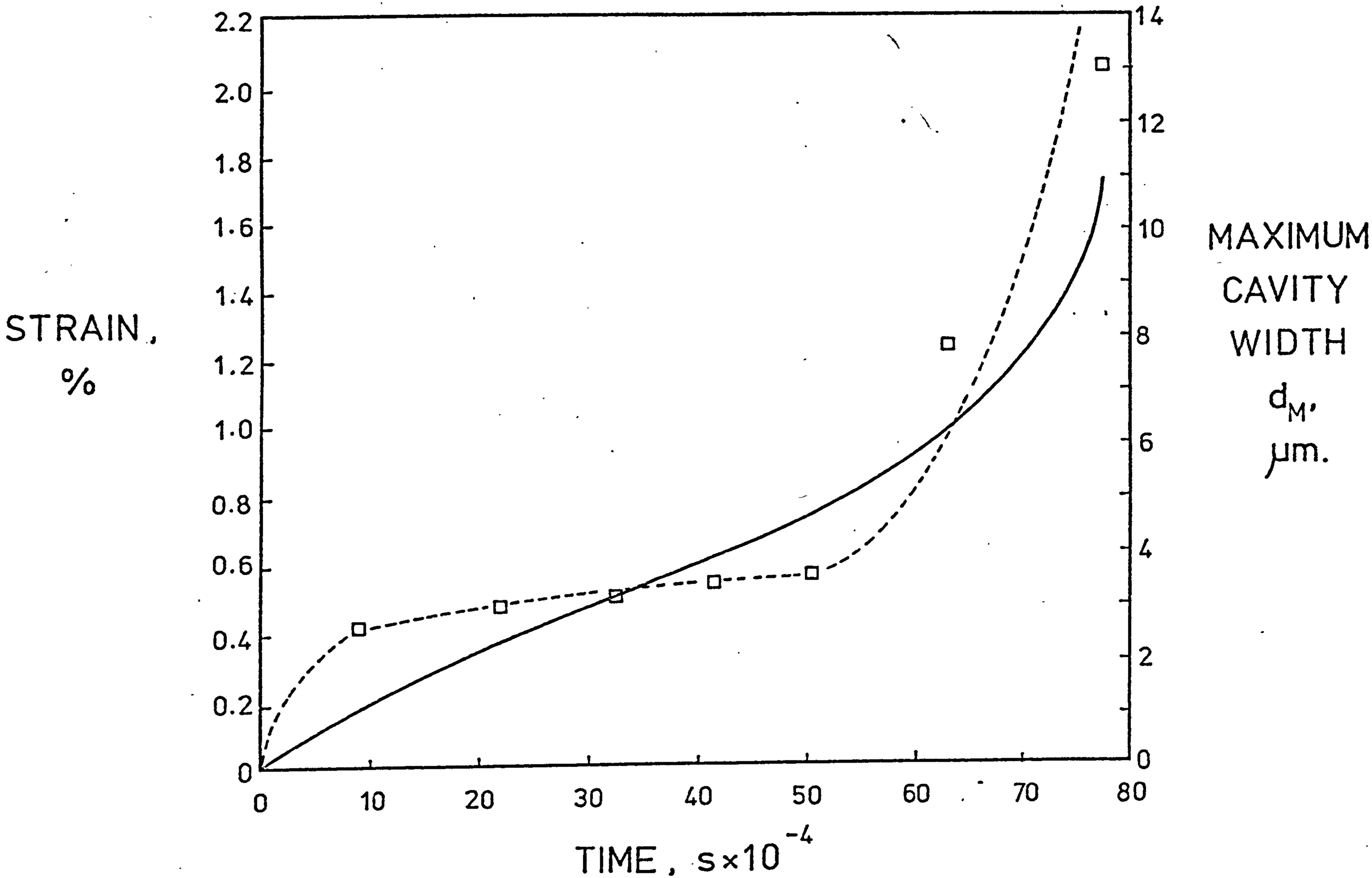
STRAIN, %
MAXIMUM CAVITY WIDTH d_M, μm.
TIME, $s \times 10^{-4}$
2.2
2.0
1.8
1.6
1.4
1.2
1.0
0.8
0.6
0.4
0.2
0
14
12
10
8
6
4
2
0
0
10
20
30
40
50
60
70
80

Fig. 75 The average cavitated area, of those grain facets normal to the tensile axis, plotted as a function of normalised creep strain.

O 45 MNm^{-2} 963K

Δ 130 MNm^{-2} 863K

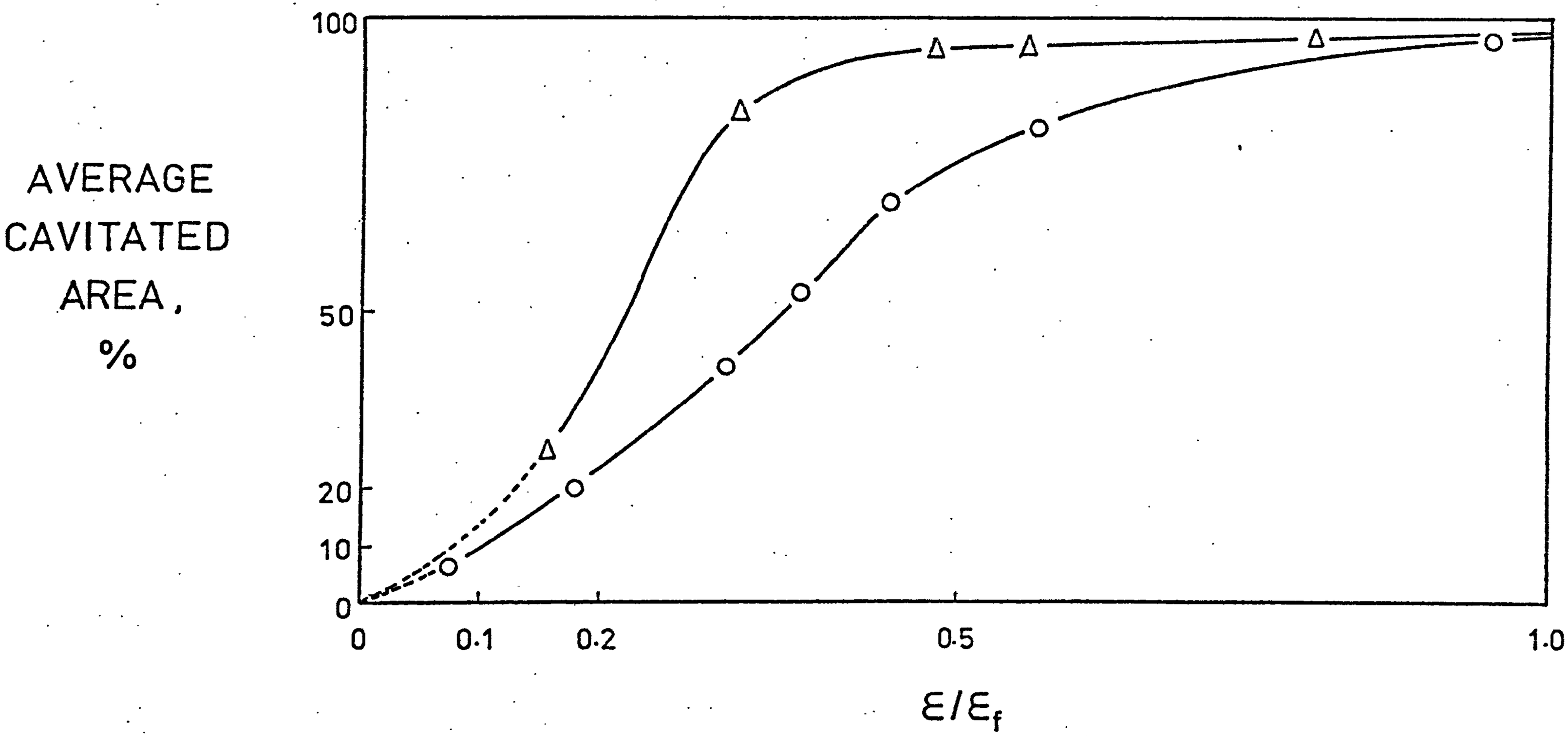
AVERAGE CAVITATED AREA, %
100
50
20
10
0
0
0.1
0.2
0.5
1.0
ε/εf

Fig. 76(a) Auger electron spectra produced by an intergranular surface of CRMV series alloy after creep failure at a stress of 60 MNm^{-2}, 963K.

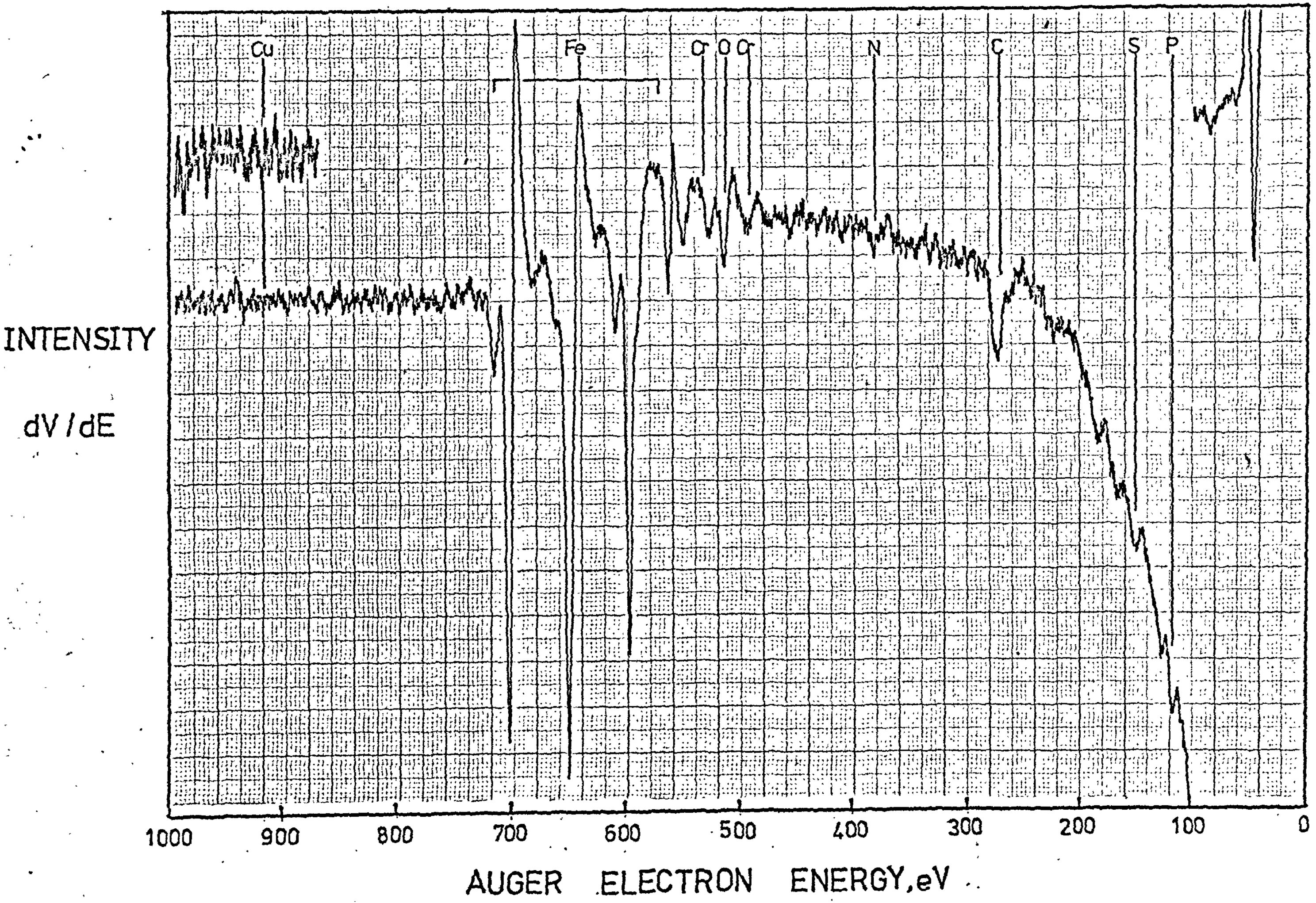
Cu
Fe
Cr
O
Cr
N
C
S
P
INTENSITY
dV/dE
1000
900
800
700
600
500
400
300
200
100
0
AUGER ELECTRON ENERGY, eV

Fig 76(b) Auger electron spectra produced by an intergranular surface of CRMV series alloy after creep failure at a stress of 90 MNm^{-2}, 963K.

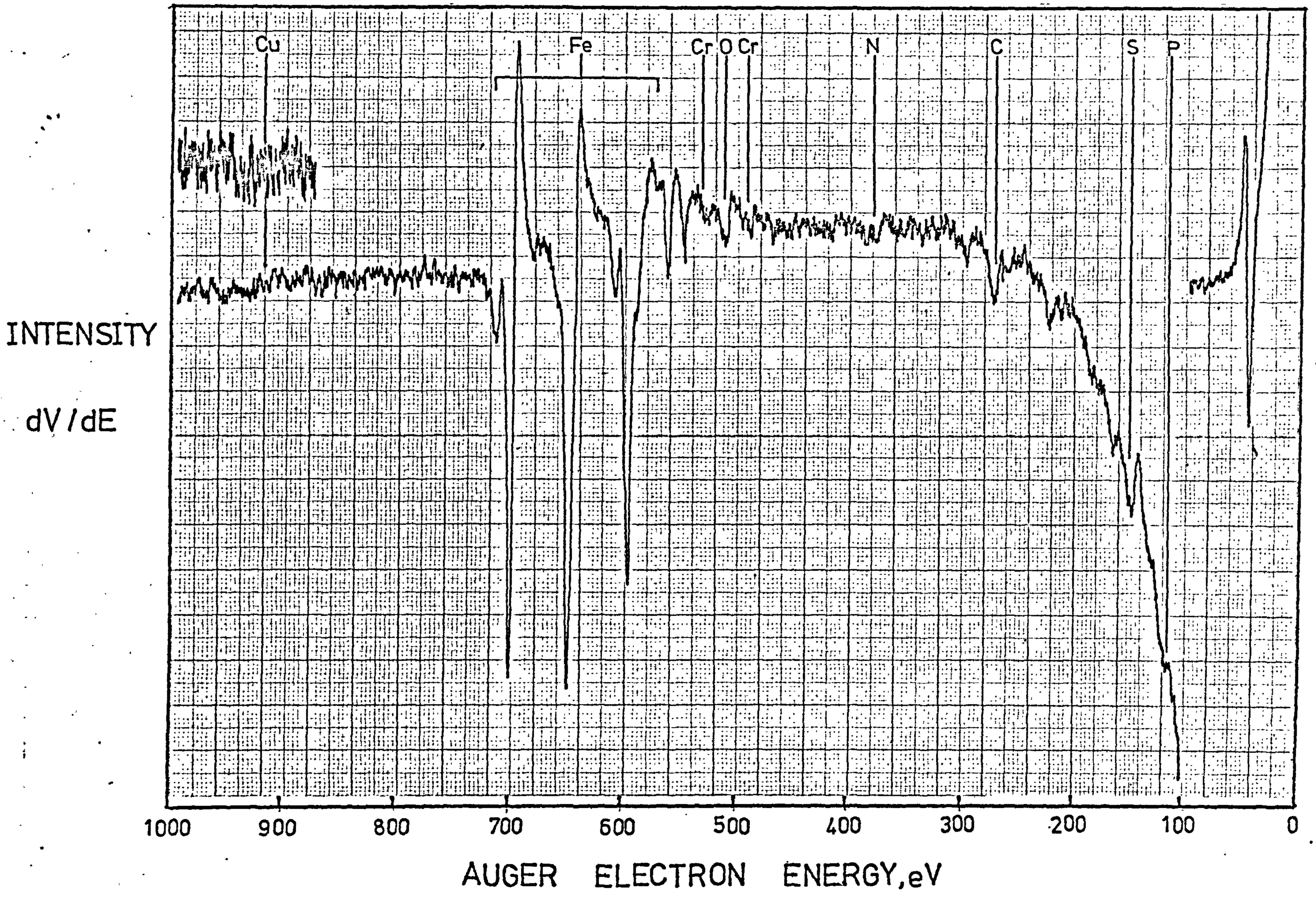
Cu
Fe
Cr
O
Cr
N
C
S
P
INTENSITY
dV/dE
1000
900
800
700
600
500
400
300
200
100
0
AUGER ELECTRON ENERGY,eV

Fig. 77 Fracture map representing the behaviour of CRMV series alloy steel over the range of stress and temperature investigated. Rupture ductility can be related to failure mode and the mechanism of damage accumulation prevalent in a particular regime of deformation stress.

——— Data obtained from tensile tests at constant strain rate.

------- Data obtained from creep tests.

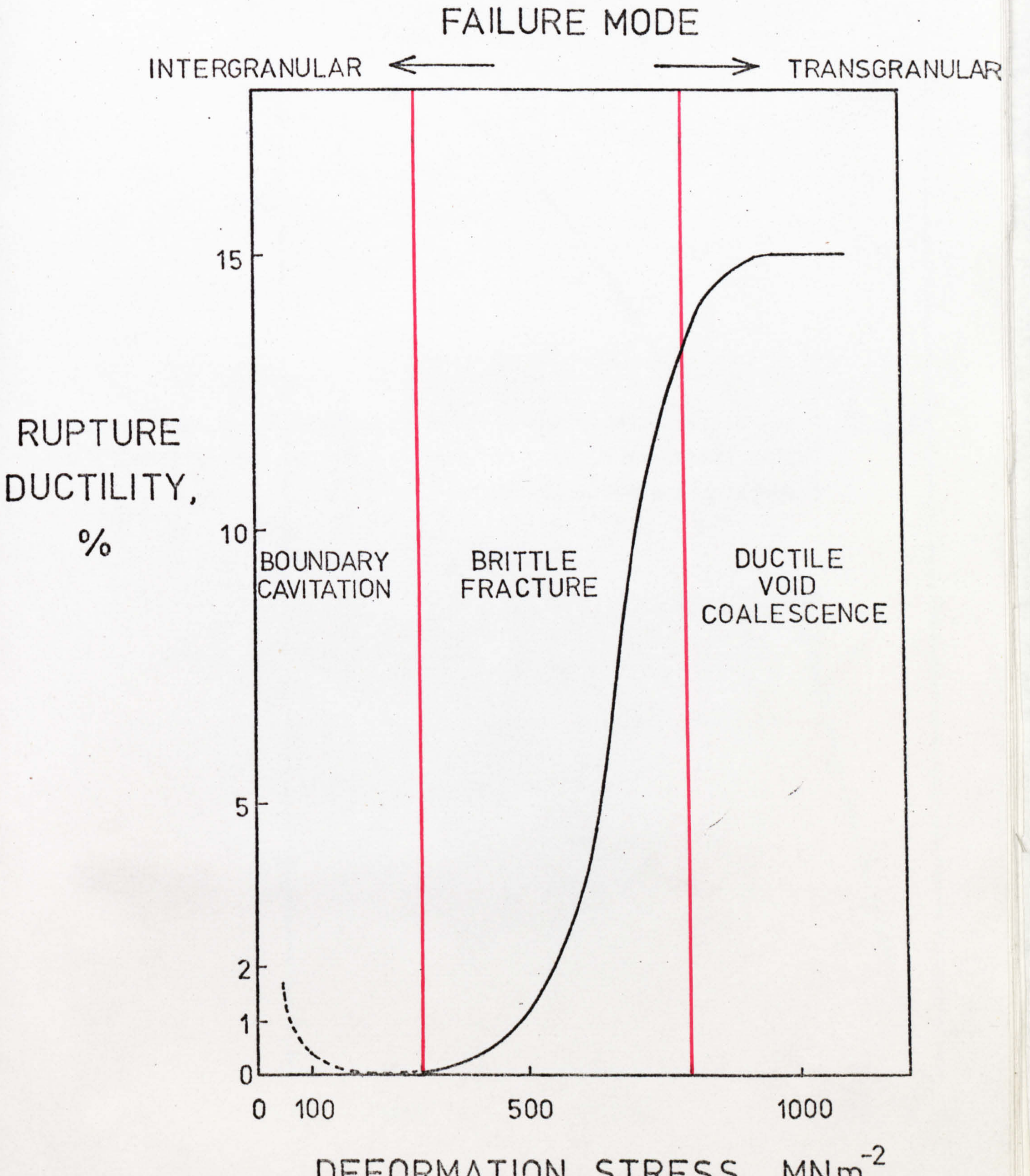
FAILURE MODE
INTERGRANULAR
TRANSGRANULAR
RUPTURE DUCTILITY, %
15
10
5
2
1
0
BOUNDARY CAVITATION
BRITTLE FRACTURE
DUCTILE VOID COALESCENCE
0
100
500
1000
DEFORMATION STRESS , MNm^{-2}

Fig. 78 Creep deformation stress plotted as a function of the Larson-Miller parameter P_R for CRMV series alloy at the various temperatures investigated.

○ 963K

□ 863K

△ 803K

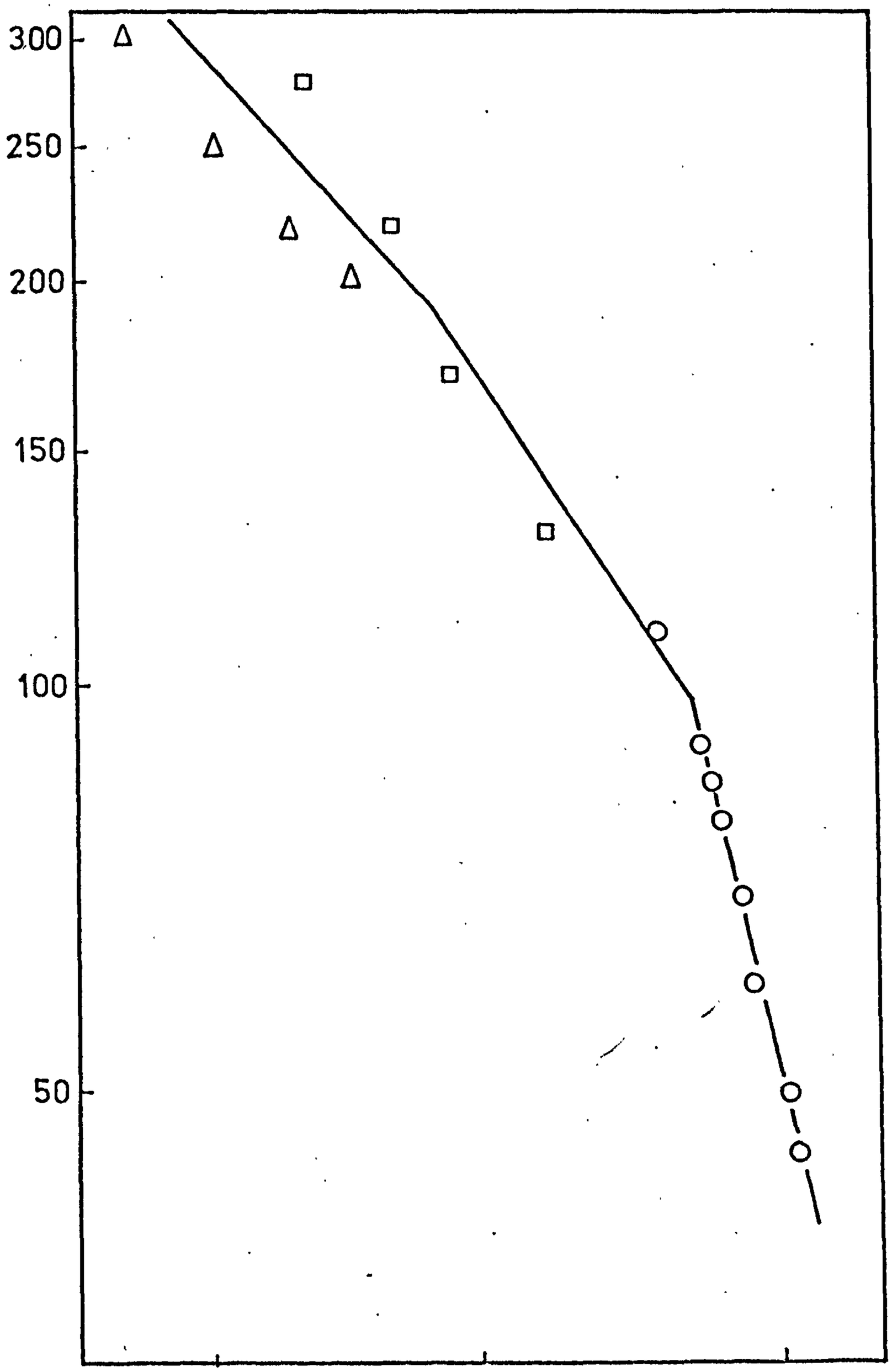

$$P_R = T(20 - \log \dot{\varepsilon}_s)$$

Fig. 79 The variation in the number of cavities per unit area of grain boundary with stress for CRMV series alloy. The mean cavity width has been plotted in the form $1/\bar{d}^2$ as a function of stress for the three temperatures investigated.

O 963K

□ 863K

Δ 803K

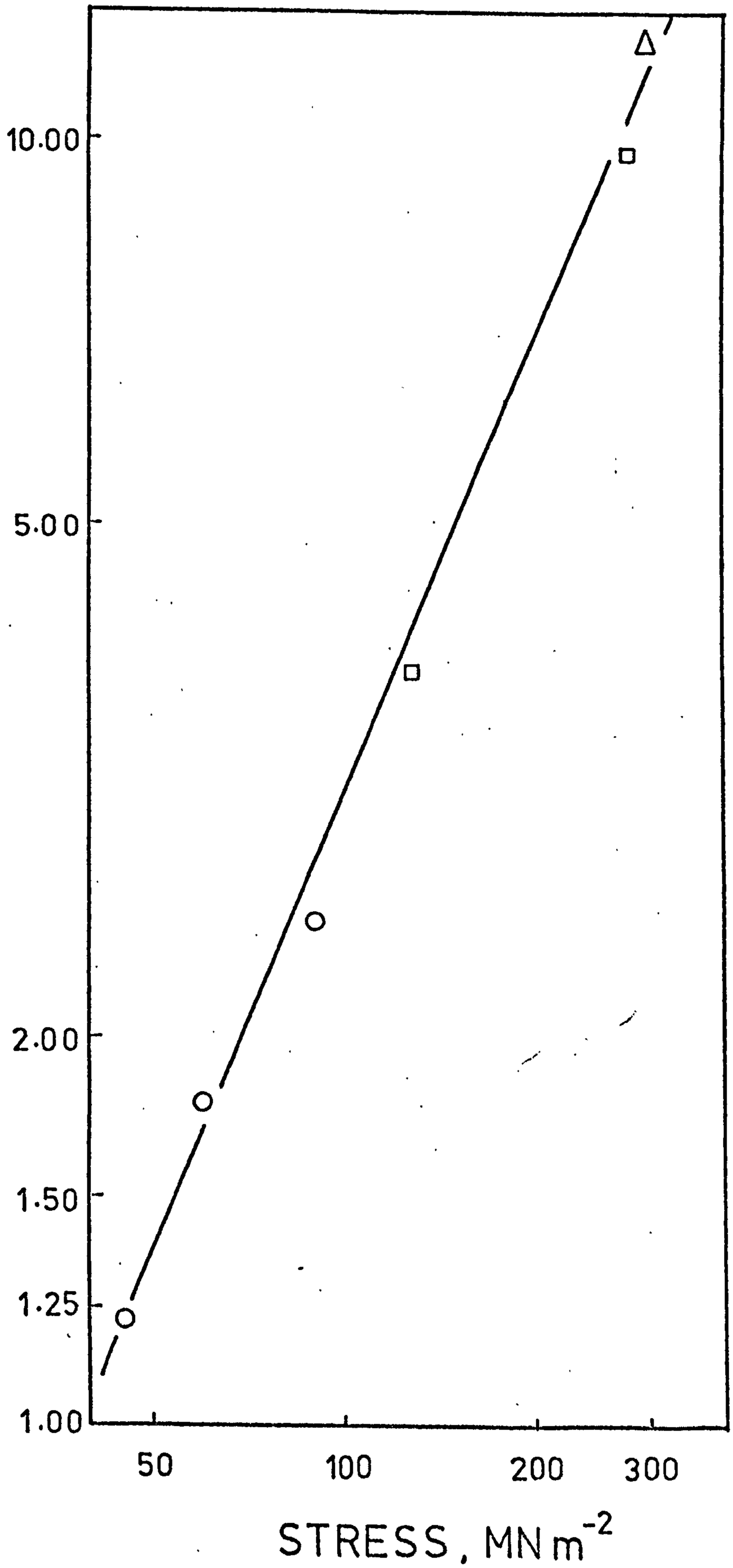
10.00
5.00
2.00
1.50
1.25
1.00
50
100
200
300
MEAN CAVITY WIDTH, $1/\bar{d}^2$, $\mu m.^{-2}$
STRESS, $MN\,m^{-2}$

Fig. 80 Schematic diagram, illustrating the position of preferred cavity nucleation sites in relation to the stress axis, the configuration of prior austenite grain boundaries and the relative orientation of bainite plates across these boundaries.

A Intense cavitation at this triple-point due to long slip planes creating large dislocation pile-ups at grain boundary discontinuities.

B A lower density of cavity nuclei is produced in this region as the slip planes impinging on the grain boundary are somewhat shorter than those at "A".

C The mismatch of bainite orientation across the prior austenite grain boundary in this region has induced a high cavity population density.

D The formation of cavity nuclei has been suppressed by the parallel alignment of bainite plates across this section of the grain boundary.

STRESS AXIS

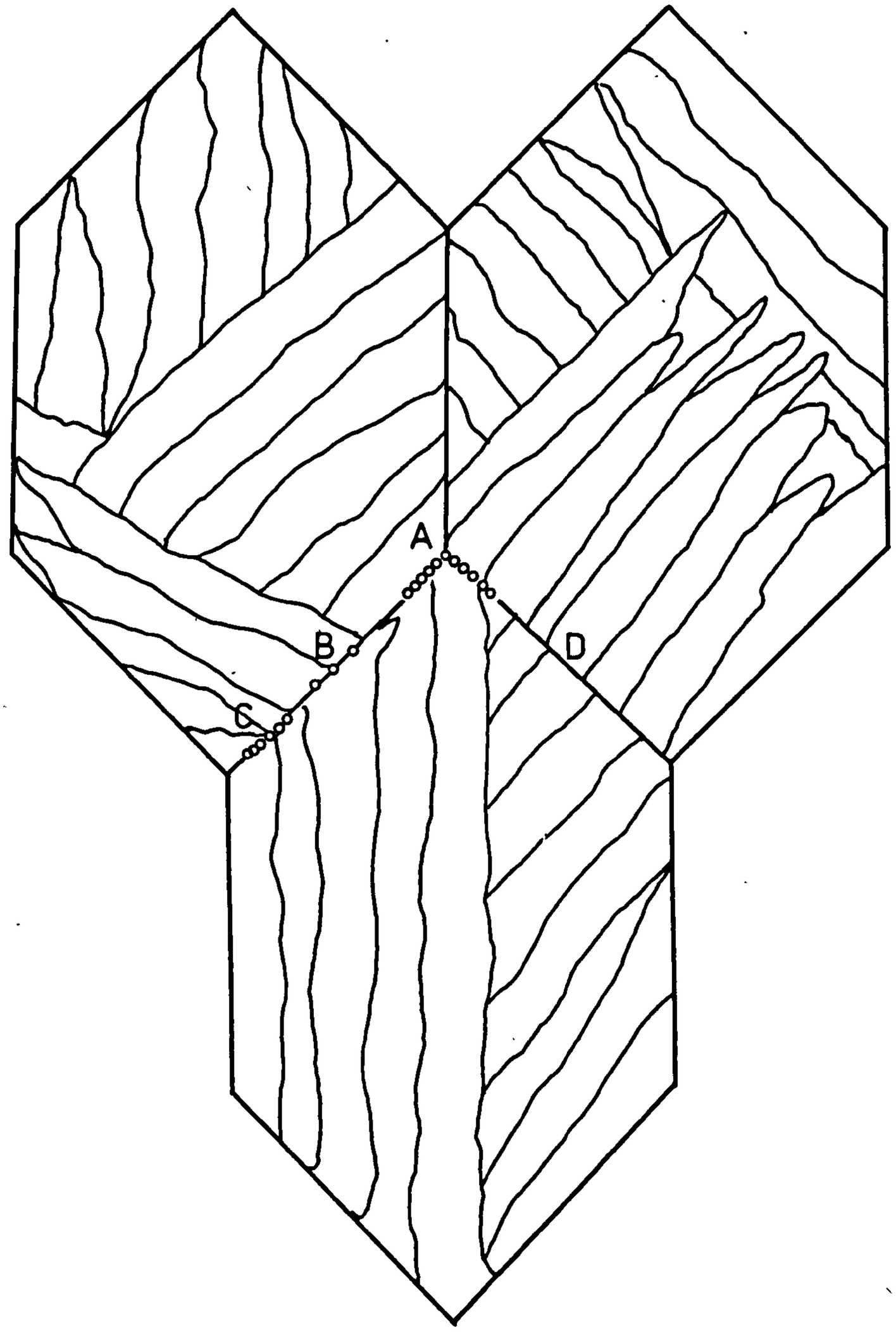

Fig. 81 Cavity growth kinetics for CRMV series alloy steel. The cube of maximum cavity width d_m is plotted as a function of creep deformation time.

O 45 MNm^{-2} 963K

Δ 130 MNm^{-2} 863K

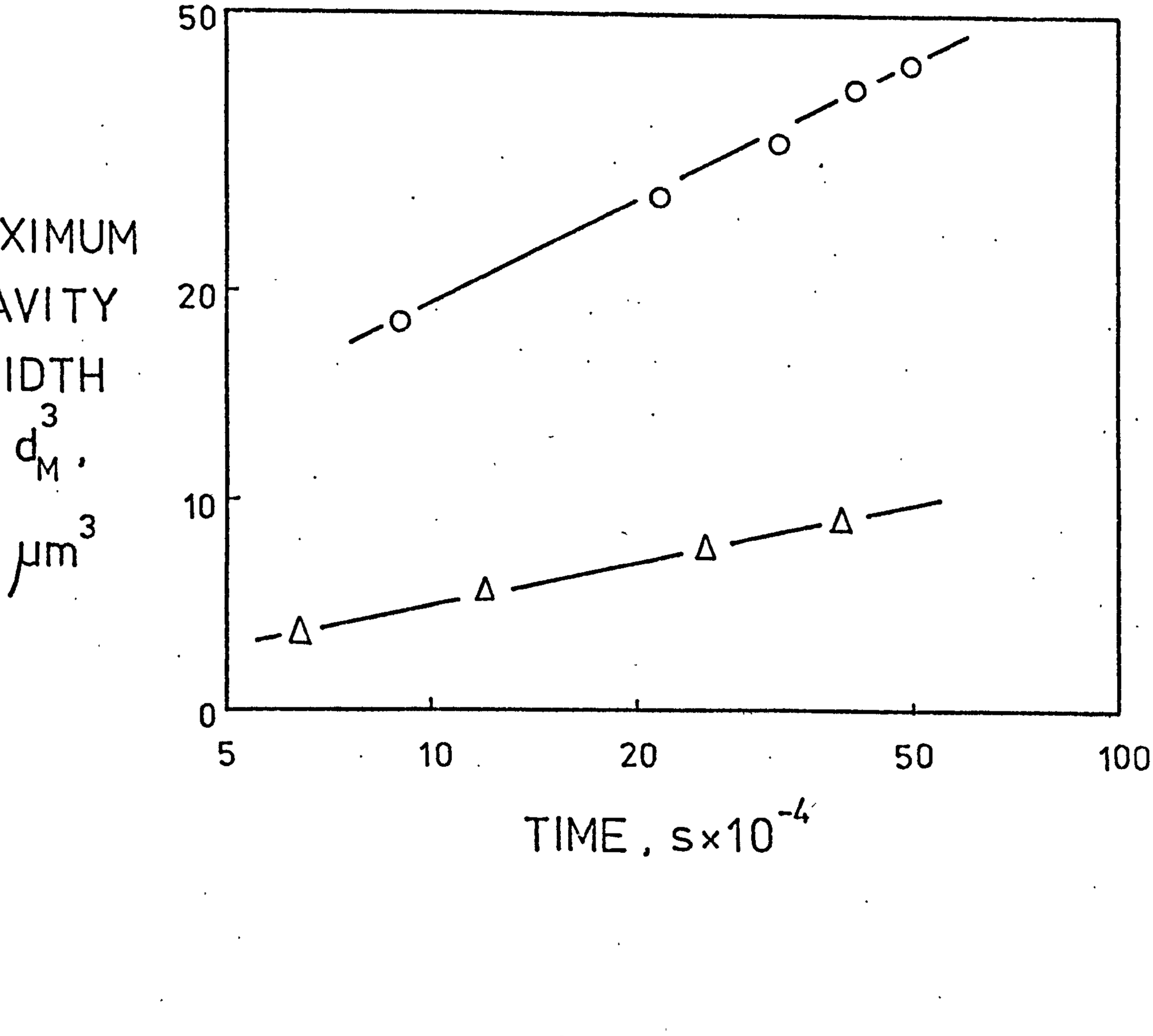
MAXIMUM CAVITY WIDTH d_M^3, μm^3
50
20
10
0
5
10
20
50
100
TIME, $s \times 10^{-4}$